U.PORTO
FEUP FACULDADE DE ENGENHARIA
UNIVERSIDADE DO PORTO

Departamento de Engenharia Mecânica

Polymer Greases: Film Thickness, Friction and Thermal Degradation

David Emanuel Pimentel Gonçalves

Porto, 2016

DAVID EMANUEL PIMENTEL GONÇALVES

POLYMER GREASES: FILM THICKNESS, FRICTION AND THERMAL DEGRADATION

A DOCTORAL THESIS SUBMITTED TO THE
FACULDADE DE ENGENHARIA DA UNIVERSIDADE DO PORTO
FOR THE *PROGRAMA DOUTORAL EM ENGENHARIA MECÂNICA*

Supervisor: Prof. Jorge H. O. Seabra
Co-supervisor: Prof. Armando J. V. Campos

DEPARTAMENTO DE ENGENHARIA MECÂNICA
FACULDADE DE ENGENHARIA
UNIVERSIDADE DO PORTO

Preface

The work presented in this thesis has been carried out at Faculty of Engineering of the University of Porto (FEUP), Department of Mechanical Engineering. I would like to acknowledge and express my sincere gratitude towards Professor Jorge Seabra, for his time, orientation and knowledge shared, but most of all for the opportunity and trust placed in me. I would also like to thank my co-supervisor Professor Armando Campos for all the help and tireless support provided during the course of this work and without whom, this work would not have been possible.

I would like to express my gratitude to FEUP and CETRIB (Tribology, Vibrations and Industrial Maintenance Unity of INEGI), for providing the laboratories and resources necessary to perform the experimental work reported in this thesis. I also wish to gratefully acknowledge the funding supported by:

- National Funds through Fundação para a Ciência e a Tecnologia (FCT), under the projects PTDC/EME-PME/122271/2010 and EXCL/SEM-PRO/0103/2012;
- COMPETE and National Funds through FCT, under the project Incentivo/EME/LA0022/2014;
- Quadro de Referência Estratégico Nacional (QREN), through Fundo Europeu de Desenvolvimento Regional (FEDER), under the project NORTE-07-0124-FEDER-000009 - Applied Mechanics and Product Development;
- FCT under the individual PHD grant SFRH/BD/111868/2015.

I also want to acknowledge Johan Leckner and René Westbroek of Axel Christiernsson International AB (Sweden), not only for providing the greases tested in this work but also for sharing all the information on the greases' formulation and manufacturing.

I wish to thank all my fellow colleagues at CETRIB for the help, friendship and incentive transmitted during the very pleasant moments shared at CETRIB: André Gama, Beatriz Graça, Carlos Fernandes, José Brandão, Jorge Castro, Luís Magalhães and Pedro Marques. I want to specially acknowledge Tiago Cousseau, for sharing his knowledge on grease lubrication and rolling bearing technology, but most importantly, for his friendship.

Finally, a very special thanks to my parents and sister for the affection and uninterrupted support, not only during this work, but also in all aspects of my life.

to my family

Abstract

Rolling bearings are expected to operate under very low friction, allowing to transmit power for extended periods of time. These requirements can only be fulfilled through effective lubrication, which is only ensured by grease lubrication in most cases. The most important functions of a lubricant are the reduction of friction and of wear, providing smooth operation and extended life. However, unlike what happens with oil lubrication, the mechanisms behind grease lubrication are not well understood and therefore it is still very hard to predict grease performance.

The present work is intended to study the mechanisms of grease lubrication in rolling bearings lubricated with greases of very different formulations. New and innovative polymer thickened greases were extensively characterized and their properties compared to those of typical multi-purpose lithium thickened greases. The influence of grease formulation on rheological properties and tribological behaviour was discussed, not only with regard to film formation but also, and specially, with regard to friction and power loss of rolling bearings. The role of the thickener and base oil in the lubrication process was studied through experimental testing performed on single rolling contacts and also on full rolling bearings. It was found that, under low entrainment speeds and fully flooded conditions, polymer greases formulated with base oils of lower viscosity generate much thicker films and lower friction when compared with lithium greases. This shows that other aspects of grease formulation should be taken into account in addition to base oil properties.

In order to investigate the different stages of grease lubrication, tests were performed both in fully flooded and in starved conditions. Furthermore, the degradation of greases when subjected to high thermal stresses was also addressed, with an emphasis on the consequent physical and chemical changes in grease properties, which can be very significant. Severe oxidation, oil loss, slower bleed rate and increased bleed-oil viscosity, associated with considerable changes in viscoelastic properties, contribute to significantly change film thickness and friction behaviour.

Resumo

Os rolamentos são órgãos de máquinas cuja função é transmitir potência com baixo atrito, durante longos períodos de tempo. Estes requisitos podem apenas ser atingidos através de uma lubrificação eficaz, que na maior parte dos casos, é garantida usando lubrificação por massa lubrificante. A função mais importante de um lubrificante é a redução do atrito e desgaste, garantindo que o mecanismo opera suavemente e com um tempo de vida longo. Contudo, e ao contrário do que acontece com lubrificação por óleo, os mecanismos que governam a lubrificação por massa são ainda desconhecidos e portanto, torna-se difícil prever com exatidão o desempenho de uma massa lubrificante.

Este trabalho pretende estudar os mecanismos que regem a lubrificação por massa em rolamentos lubrificados por massas de diferentes formulações. As massas lubrificantes de espessante polimérico são produtos recentes que foram extensivamente caracterizados neste trabalho e as suas propriedades comparadas com massas de espessante de lítio, vulgarmente denominadas como massas *multi-purpose*. A influência da formulação nas propriedades reológicas e comportamento tribológico das massas lubrificantes foi discutida, no que diz respeito não só à formação de filme lubrificante mas também no que diz respeito ao atrito e perda de potência em rolamentos. A baixas velocidades e estando o contacto abundantemente lubrificado – *fully flooded* –, as massas poliméricas formuladas com óleos base de mais baixa viscosidade geram espessuras de filme consideravelmente mais altas do que as massas de lítio, e com menor atrito. Este resultado vem provar que outros aspectos da lubrificação por massa devem ser tidos em conta além das propriedades do óleo base.

Foram realizados testes em condições *fully-flooded* e também com escassez de lubrificante – *starvation* – para investigar as diferentes fases de lubrificação por massa. Além disso, a degradação das massas quando sujeitas a elevadas temperaturas também foi estudada, dando ênfase às muito significativas alterações físicas e químicas nas propriedades das massas. Oxidação severa, perda de óleo, aumento da viscosidade do óleo libertado e alterações das propriedades reológicas contribuem consideravelmente para a alteração do comportamento tribológico das massas lubrificantes.

Résumé

Les roulements sont supposés opérer sous frottement très faible, en transmettant leurs charges durant de longues périodes. On ne peut répondre à ces exigences qu'à travers une lubrification effective, assurée dans la plupart des cas uniquement par des graisses. La fonction la plus importante d'un lubrifiant est la réduction du frottement et de l'usure, assurant ainsi un fonctionnement sans heurts et une vie prolongée. Toutefois, et au contraire de ce qui arrive avec les huiles, les mécanismes de lubrification par graisse sont mal connus et il est pour cela très difficile de prévoir la performance d'une graisse.

Le présent ouvrage se destine à étudier les mécanismes de lubrification par graisse des roulements, quand lubrifiés avec des graisses à très différentes formulations. Des nouvelles et innovantes graisses épaissies par des polymères ont étées extensivement caratctérisées, et leurs propriétés ont été comparées à celles de graisses typiques, d'usage général, épaissies au lithium. L'influence des formulations des graisses sur leurs propriétés rhéologiques et sur leur comportement tribologique a étée discutée, non seulement en ce qui concerne la formation du film lubrifiant mais aussi, et surtout, en ce qui concerne le frottement et la perte de puissance dans les roulements. Le rôle de l'épaississant et de l'huile de base dans le processus de lubrification a été étudié a travers d'expériences conduites sur des contacts roulants à un seul contact, ainsi que sur des roulements complets. Il a été déterminé que, sous faible vitesse d'entrainement et alimentation complète, les graisses polymériques formulées avec des huiles de base à basse viscosité génèrent une épaisseur de film plus élevée que ne le font les graisses à lithium, et avec plus faible frottement. Cela prouve que d'autres aspects de la formulation des graisses que les propriétés des huiles de base devraient être pris en compte.

Des expériences ont été conduites tant sous conditions de sous-alimentation comme d'alimentation complète, dans le but d'étudier les différentes phases de la lubrification par graisse. De surcroit, la détérioration des graisses quand soumises à de grandes sollicitations thermales a étée étudiée, soulignant en particulier les très sensibles changements de leurs propriétés physiques et chimiques. L'oxydation sévère, la perte d'huile, le ralentissement du taux de purge (bleed rate) et la hausse de viscosité de l'huile de purge, associées à de considérables altérations des propriétés viscoélastiques, contribuent à modifier radicalement l'épaisseur de film e le comportement de frottement.

Contents

List of Figures

List of Tables

List of Symbols

Symbol	Unit	Designation
a	μm	Hertzian half-width
b	m	roller length for film thickness calculation
B	-	constant for film thickness calculation
C	N	dynamic load rating
C_0	N	static load rating
C_0	-	influence of ellipticity: $C_0 = 1 - 0.61 \cdot e^{(-0.752 \cdot (R_x/R_y)^{0.64})}$
d	mm	rolling bearing inner diameter
d_m	mm	rolling bearing mean diameter
D	mm	rolling bearing outer diameter
E	Pa	modulus of elasticity
E^*	Pa	effective modulus of elasticity: $1/E^* = (1 - {\nu_1}^2)/E1 + (1 - {\nu_2}^2)/E2$
E_k^*	Pa	effective modulus of elasticity: $1/E_k^* = 0.5 \cdot (1 - {\nu_1}^2)/E1 + (1 - {\nu_2}^2)/E2$
F	N	normal force
F_a	N	axial force
F_r	N	radial force
F_N	N	normal force
G	-	dimensionless material parameter - $G = 2 \cdot \alpha \cdot E^*$
G_k	-	dimensionless material parameter - $G_k = \alpha \cdot E_k^*$
G_{cr}	Pa	critical stress (Newtonian limit)
$\bar{G}_{cr}$	-	$\bar{G}_{cr} = G_{cr}/E^*$
$G_{rr,sl}$	-	factor that depends on the bearing type, geometry and load (SKF)
G'	Pa	storage/elastic modulus
G''	Pa	loss/viscous modulus
h_G	nm	grease central film thickness
h_{bo}	nm	base oil central film thickness
h_{bl}	nm	bleed-oil central film thickness
h_{exp}	nm	experimentally measured central film thickness
h_m	nm	minimum film thickness
h_{pl}	nm	central film thickness in the low speeds region

Symbol	Unit	Designation
h_R	nm	residual or zero speed central film thickness
$\bar{h}_{st}$	nm	average central film thickness in starved conditions
h_{0c}	nm	central film thickness with inlet shear heating correction
h_{0c}^k	nm	central film thickness with inlet shear heating and shear thinning corrections
K_{rs}	-	replenishment/starvation constant
K_z	-	bearing type related geometry constant
k	Pa·s^n	consistency index
k	-	viscosity ratio (SKF)
k_{ISO}	-	viscosity ratio (ISO 281)
M_{drag}	N.mm	lubricant churning friction torque (SKF)
M_{exp}	N.mm	rolling bearing friction torque measured experimentally
M'_{rr}	N.mm	corrected rolling friction torque (SKF)
M_{seal}	N.mm	seals losses friction torque (SKF)
M_{sl}	N.mm	sliding friction torque (SKF)
M_t	N.mm	total rolling bearing friction torque
M_0	N.mm	load independent friction torque (Palmgren)
M_1	N.mm	load dependent friction torque (Palmgren)
$f_{0,1}$	-	geometry constants for friction torque model (Palmgren)
n	-	flow/ shear-thinning index
m	-	flow/ shear-thinning index (Cross)
n	rpm	rotational speed
p	Pa	pressure
p_0	Pa	maximum Hertzian pressure
P	N	load
R_a	nm	average surface roughness
R_x	m	equivalent radius of contact in the X direction: $1/R_x = 1/2 \cdot (1/R_{x1} + 1/R_{x2})$
R_{xk}	m	equivalent radius of contact in the X direction: $1/R_{xk} = 1/R_{x1} + 1/R_{x2}$
R_1	-	geometry constant for rolling frictional moment
$\bar{R}$	-	shear thinning factor: $\bar{R} = \left[1 + 1.325280 \cdot \frac{U_k^{0.69} \cdot W_k^{0.264}}{G_k^{0.77} \cdot \bar{G_{cr}}^{1.92}}\right]^{\frac{-1.2}{(1-n)^2}}$
S_1	-	geometry constant for sliding frictional moment
S	1/m	original Hersey parameter
S_p	-	modified Hersey parameter
SRR	-	slide-to-roll ratio

Symbol	Unit	Designation
T	°C	temperature
T_0	°C	reference temperature
$tan(\delta)$	-	phase angle
u_{tr}	m/s	transition speed at which the film thickness changes its behaviour
$\bar{U}$	-	dimensionless speed parameter: $\bar{U} = \eta_0 \cdot (U_1 + U_2)/(2 \cdot R_x \cdot E^*)$
U	m/s	entrainment speed
U_k	-	dimensionless speed parameter: $U_k = \eta_0 \cdot (U_1 + U_2)/(R_{xk} \cdot E_k^*)$
$U_{1,2}$	m/s	tangential speed of the body contacts 1 and 2
u_{ball}	m/s	tangential speed of the ball
u_{disc}	m/s	tangential speed of the disc
W	-	dimensionless load parameter, point contacts: $W = 2 \cdot F_N/({R_x}^2 \cdot E^*)$
W	-	dimensionless load parameter, linear contacts: $W = 2 \cdot F_N/(R_x \cdot b \cdot E^*)$
W_k	-	dimensionless load parameter - $W_k = F_N/(R_{xk}^2 \cdot E_k^*)$
α	Pa^{-1}	pressure-viscosity coefficient
α_{Gold}	Pa^{-1}	pressure-viscosity coefficient according to Gold *et al.*
δ	-	loss factor
Δh	%	relative film thickness between grease and base oil
ΔU	m/s	sliding speed
ϕ_{bl}	-	weighting factor for the sliding friction coefficient
ϕ_{ish}	-	inlet shear heating reduction factor
ϕ_{rs}	-	kinematic replenishment / starvation reduction factor
Φ	-	thickener content
$\dot{\gamma}$	s^{-1}	shear rate
γ	%	strain
η	Pa.s	dynamic viscosity
η_0	Pa.s	dynamic viscosity at very low shear rate
η_0	Pa.s	dynamic viscosity at reference temperature T_0
η_{ap}^*	Pa.s	apparent viscosity
η_∞	Pa.s	dynamic viscosity at very high shear rate
η_{bo}	Pa.s	base oil's dynamic viscosity
η_{bl}	Pa.s	bleed-oil's dynamic viscosity
Λ	-	specific film thickness
μ	-	coefficient of friction
μ	-	traction friction
μ_{bl}	-	boundary coefficient of friction
μ_{ehd}	-	friction coefficient in full film conditions
μ_{sl}	-	sliding friction coefficient

Symbol	Unit	Designation
μ_1	-	coefficient of friction (Palmgren)
ν	mm^2/s	kinematic viscosity
ν_1	mm^2/s	required kinematic viscosity for $\Lambda = 1$
ρ	g/cm^3	density
$\sigma_{1,2}$	m	surface roughness - arithmetic average
σ	m	composite surface roughness
σ	-	standard deviation
τ	Pa	shear stress
τ_{co}	Pa	cross over shear stress
τ_y	Pa	yield stress

Acronyms	Meaning
AFM	Atomic Force Microscopy
$AGED$	lubricant sample obtained after thermal aging
ATR	Attenuated Total Reflectance
COF	Coefficient of Friction
E	ester oil nature
EHD	elasto-hydrodynamic
FF	fully flooded conditions
$FRESH$	lubricant sample before being submitted to any kind of stress
$FTIR$	Fourier Transform Infra-red Spectroscopy
LiX	lithium complex
LVE	linear viscoelastic
MIN	mineral oil nature
$NLGI$	National Lubricating Grease Institute
PAO	poly-alpha-olefin oil nature
PP	polypropylene
SEM	Scanning Electron Microscopy
TBB	Thrust ball bearing
TRB	Thrust roller bearing

1 Introduction

1.1 Problem statement

Due to economic and environmental concerns, the reduction of friction in mechanical transmissions is of the utmost importance. Since a large part of the power losses in mechanical transmissions are related to friction in rolling bearings, the most effective way to reduce it is through lubrication. This study is amply justified by the fact that the vast majority of rolling bearings are grease lubricated [1,2]. However, in the past fifty years, the research effort of the industry in improving the manufacturing procedures and increasing the knowledge on grease lubrication has been small. Not only due to the complexity of the subject but mainly because the market of grease manufacturers is relatively small, not justifying large research programs [3].

The main advantages of grease over other forms of lubrication are related to the fact that grease is easy to use and confine, it operates under very low friction if the operating conditions are adequate and the rolling bearing is properly filled, it seals and protect the bearing against contaminations and it stays in place not easily leaking out. Lubricating greases are expected to operate over a wide range of conditions and through extended periods of time, but the main disadvantage of using grease is its limited life and the fact that there is no reliable way to predict its life or performance [3], based only on the bulk properties of the fresh grease. Hence, the grease life and consequently, the rolling bearings' re-lubrication intervals are predicted statistically. Therefore, any study which contributes to understand how grease ages and the phenomena which might contribute to premature end of grease life, is very important.

For many years the purpose of grease manufacturers was to produce multi-purpose greases which could be used in any application. However, there was no scientific basis for choosing a specific grease formulation (thickener type, base oil nature, etc) for any particular application [1], as long as the correct consistency was selected (NLGI number). The lack of knowledge on the grease lubrication mechanisms associated with the unknown role/influence of the base oil and thickener properties in the lubrication process, greatly impeded the development of new grease formulations

and also bearing technology. Still, it was during this period that new products like the polymer greases were created, expected to show extended grease life, low operation temperature, low noise and excellent oil bleeding capability at both low and high temperatures. However, even now, these polymer greases are still poorly studied.

In the last twenty years, intensive academic research associated with the growing interest of the bearing industry in increasing grease and rolling bearings life, has allowed to greatly increase the knowledge on grease lubrication, specially concerning film formation. Nevertheless, there is still a lack of work regarding friction in grease lubrication. During these years, significant advances were made and it is now accepted that, after the initial churning phase, the grease lubricated bearings operate mainly in starved conditions, where the active lubricant is base oil slowly bleeding from the grease into the contact. Subsequently, most of the analytical tools developed to predict grease film thickness [4–6] and rolling bearing friction torque [7, 8] only take into account the properties of the grease's base oil and neglect the interaction between thickener, additives and base oil. However, such assumptions often lead to incorrect predictions. Not only because additives might considerably change the original base oil properties, but also because the thickener might also play an important role in the lubrication process depending on the operating conditions. Thus, further testing to investigate the thickener role is needed, firstly with respect to film formation and friction behaviour, but also in what concerns bleed-rate, low and high temperature behaviour, oxidation resistance, and how the thickener might promote or delay the additives' interaction with the rolling surfaces. Therefore, rather than finding multi-purpose greases, the goal for the manufacturers and researchers should be to select the right combination of base oil, thickener and additives for each specific application, alongside with the development of new predictive tools, that take into account other aspects of grease formulation.

1.2 Aim and thesis outline

The purpose of this work was to study the influence of grease formulation on the rheological properties and tribological behaviour of lubricating greases. Not only by analysing the film formation but also investigating how friction is affected, this work intends to contribute to the understanding of the grease lubrication mechanisms in fully flooded and starved grease lubricated contacts in the early stages of grease life. The aim of the experimental work performed was to investigate the thickener role in the lubrication process and determine if the base oil is indeed representative of the active lubricant inside the EHD contact for different operating conditions, specially in

what concerns the development of tools for the prediction of lubricant film thickness and rolling bearings friction torque. Besides all these objectives, this work also intends to be one of the first and very extensive studies on the recent and fairly unknown polymer thickened greases, comparing them with typical multi-purpose greases in the market.

Finally, alongside with all the other objectives, this work also intends to investigate the thermal degradation of lubricating greases, increasing the knowledge on the mechanisms behind the degradation process and how they affect film formation and friction behaviour under controlled fully flooded conditions.

These objectives were approached in different phases. The first phase included research on the current literature knowledge regarding grease lubrication, thermal degradation and the experimental methods available to characterize lubricating greases. In the second phase, each grease and its corresponding base oil and bleed-oil were characterized by the selected methods in order to obtain the maximum information from these products. Samples of each lubricating grease were also artificially aged and characterized in this phase. Then, single contact tests were conducted to analyse the film formation and friction behaviour of each product, looking into the grease lubrication mechanisms in fully flooded conditions and investigating the roles of base oil and thickener in the lubrication process, specially relevant for the early stages of grease life.

Since rolling bearings generally operate under starvation for the largest part of grease life, the third phase of this work was focused on starved grease lubricated contacts, exploring the film formation and friction generation of fresh greases under starvation. Furthermore, full bearing tests of different geometries were also carried out at different operating conditions in order to evaluate the friction torque generated by the lubricating greases, their base oils and bleed-oils and also thermally degraded grease samples. These measurements, coupled with the application of the SKF's friction torque model to the experimental results, allowed to understand the different sources of friction at the light of the results achieved in other parts of this work.

This thesis is composed of 9 chapters, including this **1 - Introduction** chapter where the purpose of this work is explained and contextualized at the light of the current knowledge on grease lubrication.

Chapter **2 - State of Scientific Research** briefly summarizes the history of lubrication contextualizing the grease developments in the last century. A definition of grease and the major remarks about this lubricant type are presented here alongside with a quick description on the advantages of grease versus oil lubrication in suitable applications, and vice-versa. Then, the grease lubrication mechanisms are presented according to the current literature. Finally, a general description of lubri-

cating greases and their components is also reported, emphasizing the role of the base oil and thickener, and their importance for the grease's final characteristics.

Chapter **3 - Experimental characterization** presents the main experimental techniques used to chemically and physically characterize the tested greases and their components. The characterization results are shown and discussed regarding the different grease formulations.

Chapter **4 - Film thickness of fully flooded grease and oil lubricated contacts** presents the results of the film thickness measurements performed in a ball-on-disc machine under different operating conditions. The grease lubrication mechanisms are discussed here, analysing the film thickness measurements performed with different grease formulations and their corresponding base oils and bleed-oils. The role of the thickener and of the base oil in the lubrication process is discussed in this chapter, supported by the experimental results measured in fully flooded conditions. Background on the film thickness predictions of Newtonian and Non-Newtonian fluids is reported and applied to the experimental results.

Chapter **5 - Friction coefficient in fully flooded grease and oil lubricated contacts** presents the results obtained when measuring traction and friction coefficients in a ball-on-disc device. The friction behaviour is analysed at the light of the results presented in previous chapters. Traction and Stribeck curves are shown, measured under different operating conditions whilst crossing different lubrication regimes. Again, the roles of the thickener and base oil in the lubrication process are analysed and discussed regarding its effect on friction.

In Chapter **6 - Starved grease lubricated contacts**, the phenomenon of starvation is approached. Experimental tests were performed in a ball-on-disc device without forced replenishment, measuring film thickness and coefficient of friction over time. The results were discussed regarding different grease properties.

Chapter **7 - Rolling bearings friction torque** presents the friction torque measurements performed with rolling bearings lubricated not only with grease, but also with its base oil and bleed-oil. The friction torque measurements were performed with two different geometries at constant operating temperature and constant load, while varying the entrainment speed to identify the main sources of friction and correlate them with the properties of each grease formulation. The grease lubrication mechanisms are discussed once more and the SKF friction torque model is applied to the experimental results.

In Chapter **8 - Thermal degradation of lubricating greases**, the degradation of lubricating greases subjected to very high thermal stresses is described. All the techniques and measurement procedures described in the previous chapters 3, 4, 5 and 7 were also performed in this chapter, now applied to the thermally aged

greases. A comparison between fresh and aged greases is presented and the results discussed based on current literature on the subject.

Finally, Chapter **9 - Conclusions and future work** presents the main conclusions of this work. Comments on what was left to do or what could be done better in future work are also discussed in this final chapter.

1.3 Research approach

The research presented in this thesis is based mainly on experimental work. Although some numerical work was also performed, it was only to apply existing film thickness and friction torque models to the experimental results.

Several different equipments were used to obtained the experimental data. From tribological testing to rheological measurements, FTIR, SEM, AFM, etc, many hours of experimental work were necessary to obtain the results reported here. Besides that, of all the tested greases only a few were selected and their results effectively analysed here. Furthermore, the hardest and most time consuming part of the experimental work is the exploratory part, where the operating conditions are being defined in order to achieve the best results and repeatability. Therefore, much of the performed experimental work is not even reported here because it is slightly out of the purpose of the thesis or because it was not performed for all the grease samples.

1.3.1 Scientific publications

Part of the work presented in this document has already been published on scientific journals or conference proceedings, whilst part of it is still under a peer-review process. Those already published are highlighted here:

Paper I Gonçalves, D.; Graça, B.; Campos, A.; Seabra, J. H. O.; Leckner, J. & Westbroek, R.
Formulation, rheology and thermal aging of polymer greases Part I: Influence of the thickener content
Tribology International, Elsevier, 2015, 87, 160-170
doi : 10.1016/j.triboint.2015.02.018

Paper II Gonçalves, D.; Marques, R.; Graça, B.; Campos, A.; Seabra, J. H.; Leckner, J. & Westbroek, R.
Formulation, rheology and thermal aging of polymer greases Part II: Influence of the co-thickener content
Tribology International, 2015, 87, 171-177
doi : 10.1016/j.triboint.2015.01.012

Paper III Gonçalves, D.; Graça, B.; Campos, A.; Seabra, J. H. O.; Leckner, J. & Westbroek, R.
On the film thickness behaviour of polymer greases at low and high speeds
Tribology International, 2015
doi : 10.1016/j.triboint.2015.05.007

Paper IV Gonçalves, D.; Graça, B.; Campos, A. & Seabra, J.
On the friction behaviour of polymer greases
Tribology International, Elsevier, 2015, 93, 399-410
doi : 10.1016/j.triboint.2015.09.027

Paper V Gonçalves, D.; Pinho, S.; Graça, B.; Campos, A. V. & Seabra, J. H.
Friction torque in thrust ball bearings lubricated with polymer greases of different thickener content
Tribology International, Elsevier, 2016, 96, 87-96
doi : 10.1016/j.triboint.2015.12.017

Paper VI Gonçalves, D.; Graça, B.; Campos, A. & Seabra, J.
Film thickness and friction behaviour of thermally aged lubricating greases
Tribology International, Elsevier, 2016, 1-11
doi : 10.1016/j.triboint.2016.01.044

2 State of scientific research

2.1 Brief history of tribology and lubrication

The word tribology is derived from the Greek word *tribos* which means rubbing. The term was first reported in a landmark report by Jost (1966) and its often referred to as the science of lubrication, friction and wear. Tribology is therefore treated as the science which studies the interaction between surfaces in relative motion in the presence or absence of lubricant. This interaction can be quite complex and involves several disciplines including physics, chemistry, applied mathematics, solid and fluid mechanics, heat transfer and thermodynamics, materials science, lubrication and rheology, machine design, performance and reliability.

Although the word tribology is relatively recent, the interest in this area is quite old. In fact, the technology of tribology and lubrication has been used for thousands of years. From lighting fire with dry wood and a stick, or generating a spark to initiate fire by striking pyrites of flint, up to the invention of the wheel and the primordial rolling bearings (in the form of wooden rollers) used to help move large and heavy objects, the basic principles of tribology have been used since the beginning of recorded history.

Evidence dated around 3500 to 2500 b.C. report our ancestors' concerns with reducing friction in translational motion. Ancient inscriptions and drawings show people using some kind of lubricant, such as water or oil, to reduce friction during the transportation of massive rock slabs, which points out the early knowledge of frictional devices and lubrication [9, 10]. Records also show that the Sumerian used grease-like lubricants on the wheels of chariots and early wagons [9, 11]. Furthermore, as early as 1400 b.C., the Egyptians used grease-like lubricants made from olive oil or tallow (animal fat), quartz, iron and lime, to lubricate the chariot wheel axles [12]. The efforts to reduce friction were therefore, very dependent on the relatively abundant animal and vegetable-based oils. Moreover, the earliest recovered example of a rolling element bearing is a wooden ball bearing supporting a rotation table, obtained from the remains of Roman ships, dated to 40 A.D.

It was during the Renaissance, that Leonardo da Vinci first postulated a scien-

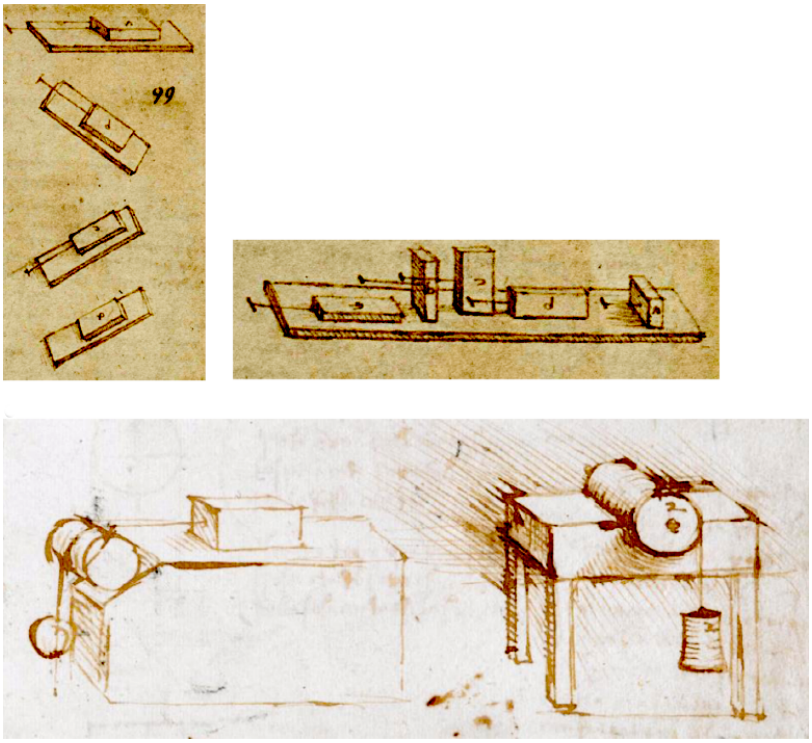

Figure 2.1: Leonardo da Vinci's drawings relating the motion of a rectangular block sliding over a flat surface. Reproduced from [14].

tific approach to friction deducting the rules governing the motion of a rectangular block sliding over a flat surface (as shown in Figure 2.1), relating the ratio between the frictional force and the normal load to the coefficient of friction [13, 14]. Da Vinci also made a few drawings of a primordial ball bearing mechanism in his design for a helicopter. Later on, Agostino Ramelli published sketches of roller and thrust bearings for the first time and in the 17th century Galileo described a caged ball bearing design.

During the Middle Ages (450-1450 A.D.) there was a steady development in the use of lubricants, but it was not until 1600-1850 A.D. (particularly during the industrial revolution in 1750-1850 A.D.) that the value of lubricants in decreasing friction and wear was recognized. The thirst for animal-based products as lubes and fuels demanded the search for other sources, specially petroleum. The first grease of the industrial age, a calcium grease made from olive oil or tallow, was probably patented by Partridge [15] in 1835. About 10 years later, greases based on mineral oils and thickened with soaps were probably first proposed by Raecz [16]. In 1849, William Little [17] patented a sodium grease made from tallow and from then on, many other grease types were developed. By the end of 1860, petroleum oil based products became popular as lubricants.

It was also during that time (1600-1850 A.D.), that the scientific approach to

friction was revisited. Guillaume Amontons rediscovered the rules of friction after he studied dry sliding between two flat surfaces (1699). Amontons stated that the friction force that resists sliding at an interface is directly proportional to the normal load and he also found out that the amount of friction force does not depend on the apparent area of contact. Some years later, Euler gave an important contribution to the distinction between static and kinetic friction, concluding that the value of the kinetic coefficient of friction should be much smaller than that of the static coefficient of friction. Later on, in 1785, Charles-Augustin Coulomb verified these rules and added a third one, clearly distinguishing between static and kinetic friction by stating that the friction force is independent of the velocity once motion starts. Coulomb also verified that friction depends upon the nature of the materials in contact and their coating and theorized that at least part of the frictional force must be due to cohesion between molecules of the interacting surfaces.

It was in 1822 that the word viscosity was first used after Claude Louis Navier described its concept. A few years later (1845), together with G. G. Stokes, Navier defined the equations of motion which would later form the basis of hydrodynamic theory. In the late 1800s, work on the nature of sliding and rolling friction continued to be published, enhanced by the development of a number of analytical tools for solid contact proposed by Hertz (1881) who developed the foundation of present-day contact stress calculations for elastic bodies in rolling friction [18]. Around 1866-1869, Osborne Reynolds studied the theory and application of lubricants, producing a classic paper on hydrodynamic lubrication [19] and proving that the lubricating film generated through the hydrodynamic effect of the pressurized fluid entrained between sliding surfaces, was sufficient to prevent contact between surfaces even at low sliding speeds.

In the end of the ninetieth century and following years, Richard Stribeck published a series of papers making an important contribution to the relationship between friction and liquid lubrication [20]. In one of the papers, the concept of the "Stribeck curve" was established, a plot which relates the coefficient of friction with the lubrication regime through the lubricants's viscosity, the speed of the sliding surfaces and the contact load applied, as represented in Figure 2.2.

In the beginning of the twentieth century, Sommerfeld made some refinements to the theory of hydrodynamic lubrication proposing an analytical solution of the Reynold's equation.

Friction studies in the 1900s benefited from the development of new technologies to study and characterize new surfaces at macro and micro level, which lead to important publications on solid friction and the relation between friction, lubrication and wear, with the works of Hölm [21] and later with Bowden and Tabor [22]. In

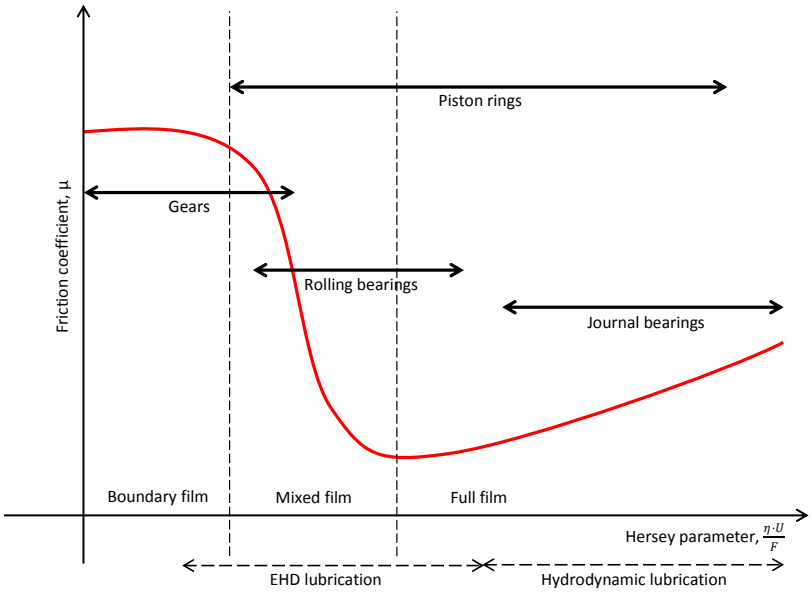

Figure 2.2: Stribeck curve scheme.

1949, Grubin proposed the first realistic model to solve the elasto-hydrodynamic film problem, combining the hydrodynamics, the elastic deformation of the metal surfaces and the changes in the lubricant's rheology with extreme pressure.

Regarding lubricants manufacturing, during the 1930s and 1940s a large amount of work was done with the introduction of synthetic lubricants and additives. It was also around this time that calcium, lithium and barium thickened greases were developed as multi-purpose lubricants. The 1950s was the age of aluminium complex greases and the 1960s, that of lithium complex thickened greases. Later, the 1980s saw the first use of polyurea and in the 1990s, the development of polypropylene greases [23, 24].

2.2 General remarks and definition of greases

Greases are generally defined as "a solid to semi fluid product of a thickening agent in a liquid lubricant", as proposed by the American Society for Testing and Materials (ASTM D288). A note is also added to allow the inclusion of "other ingredients imparting special properties", also known as additives [25]. Hence, a lubricating grease can be treated as a thickened oil where both the base oil and the thickener agent plays an important role in the grease lubrication mechanisms at micro and macro level. Such composition provides the grease with a certain consistency and viscoelastic properties. Each influences the grease's tribological behaviour and therefore, their effectiveness depends on their interaction and on the manufacturing process.

Greases are non-Newtonian fluids known to exhibit solid and liquid state properties under different operating conditions. The physical interaction between the thickener and the base oil is responsible for this behaviour, creating a three-dimensional structure with the inherent ability to regain its solid structure after mechanical stress. Lubricating greases present several advantages including the ability to seal and prevent the entrance of water and other contaminants to the tribological contact, the ability to remain in spot and slowly releasing oil to the contact, showing a solid behaviour when no mechanical stress is being applied (as it happens in the rolling bearing's cage pockets) and on the other hand, the ability to show very interesting flow properties when subjected to rolling or sliding shear, creating an elasto-hydrodynamic film capable of fully separating the contact surfaces in relative motion to each other.

The mechanical work is also responsible for the deterioration of the grease structure over time. Associated with high operating temperature, the mechanical work accelerates the oxidation, leading to severe starvation and eventually to bearing premature failure. Generally, this phenomenon happens much sooner than the bearing failure by fatigue [2]. This implies that the rolling bearing expected life is determined by the life of the grease.

Therefore, further developments in grease lubrication are expected due to ever-increasing demands for long life, higher speed, higher running temperatures, higher performance in different types of materials (steel, aluminium, composites, etc.) and also due to the ever-demanding environmental restrictions. According to specialists from the European Lubricating Grease Institute (ELGI), fundamental research able to describe the basic principles of grease lubrication is still just in its infancy and presents a major challenge for current and future researchers and grease manufacturers [26], as well as the development of predictive tools and numerical models capable of fully describing the grease behaviour.

2.2.1 Grease lubrication versus oil lubrication

The main role of any lubricant in a rolling bearing is to promote the separation of the contacting surfaces, minimizing friction and ensuring that the bearing has a long life [27]. There are certain applications where only one type of lubrication can be employed and it is not possible to choose between oil or grease to lubricate a given mechanism. However, for general purposes where both types of lubrication could be used, there are both advantages and disadvantages in using grease over oil.

One of the most interesting things about grease is its ability to stay in place and act as a sealant, stopping contaminants and water from entering the contact. Moreover, unless the grease is operating at very high temperatures (lower consistency)

or if it is severely worked up, it will not flow out of the bearing, preventing premature starvation and protecting the metal surfaces from corrosion [2, 27]. In fact, rolling bearings "sealed-for-life" (see Figure 2.3) are lubricated with grease and operate for many years with no need for maintenance or refill. Even if the seals are worn, they are much more prone to retain grease than oil, lowering the risk of leakage and lubricant loss or even contamination of the work product (food industry, newspapers, textile, etc.). Additionally, grease is generally more environment friendly since it is easier to use and to contain than oil and there are also a few biodegradable products as it happens with oils. Regarding maintenance, it is quite easy to get a representative sample of oil for laboratory analysis of wear metals and contaminants. On the other hand, it is significantly more difficult to get an in-service grease sample.

Since the grease is much more viscous than the generality of oils, its resistance to motion is also higher. Hence, grease lubrication has the disadvantage of not being appropriate for low torque/high speed operations. However, given its ability to stay in place, grease promotes a better start/stop performance, since it will not flow back to sump when the mechanism is stopped, as it happens with oil. On the other hand, grease generally operates at higher temperatures than oil. Due to its high consistency, grease is unable to dissipate the generated heat like a circulating oil would, and therefore increases the risk of premature oxidation of surfaces, additive depletion and lubricant degradation. Still, when properly selected for a given application, the operating temperature of the grease will remain reasonably low. This means that with the right amount of grease and the correct consistency for a given application, the churning losses are negligible after the start up period and the mechanism will work at low friction.

Figure 2.3: Example of sealed rolling bearings' technology.
Reproduced from SKF's product catalogue.

2.3 Grease lubrication mechanisms

The grease lubrication mechanisms have been the focus of many recent works. Although there is still no consensus on the topic, a few general guidelines have been accepted. One of them is the fact that generally, the grease lubricated bearings run under starved lubrication over the largest part of the rolling bearing life, as shown by Poon [28] in 1972 and Wilson [29] in 1979 in full bearing tests. Wilson measured the film thickness in cylindrical and spherical roller bearings to find out that the lubricant film initially exceeds 20 to 25 % the value of fully flooded oil lubrication but quickly decreases below this value after a few hours. Figure 2.4 illustrates this behaviour for spherical and cylindrical roller bearings, reproduced from [29].

In the beginning of operation, assuming that the amount of grease available in this phase is large enough to provide a fully flooded lubricant film (approximately 30% of the free volume of the bearing), excessive grease churning takes place and it is common to observe a high temperature peak at this time, due to increased friction caused by the churning of the "high viscosity grease" [2, 27].

This first phase of grease lubrication is called the churning phase and generally lasts from a few hours up to 24 hours, depending on the operating speed and grease quantity. During this phase, the flow behaviour is governed by the rheological properties of the grease and by the design of the bearing and housing. Part of the grease flows to the boarder of the running tracks, where it stays given its consistency, and part of it goes inside the bearing, under the cage pockets [2], forming grease reservoirs. The film thickness may change rapidly in this phase due to the changes on the rheological properties of degraded grease, which is under very high shear rates in the running tracks. Furthermore, thickener lumps enter the contact very frequently, instantaneously increasing the film thickness as it was optically observed by several

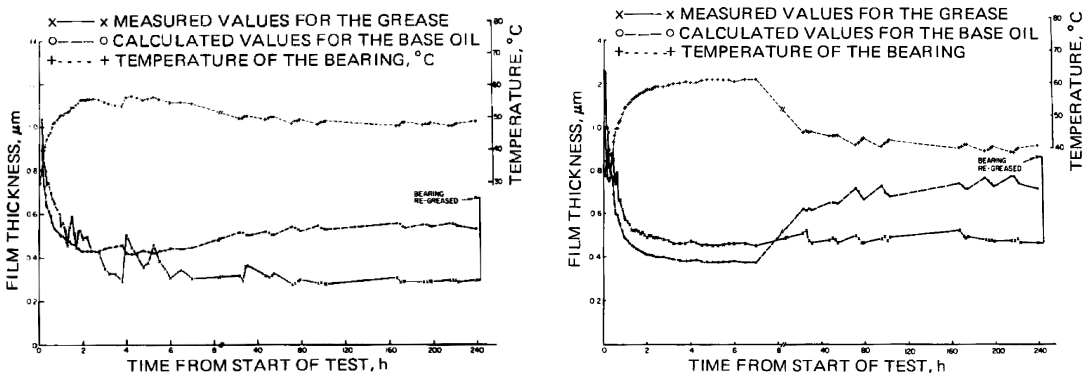

Figure 2.4: Film thickness evolution with time in grease lubricated spherical roller (left picture) and cylindrical roller (right picture) bearings, running at 1200 rpm. Reproduced from [29].

authors [30–32] in single contact experimental measurements, using a scoop to ensure fully flooded conditions. It is only in the initial churning phase that a fully flooded situation exists. After some time, the side flow in the inlet and in the Hertzian contact itself will cause starvation due to the reduction of the volume of lubricant on the running tracks.

The next phase in grease lubrication is designated as the to the bleeding period, where the grease reservoirs are consumed either by bleed, shear or even shear-induced bleeding. Booser and Wilcock [33] proposed a model to describe grease lubrication where the grease acts has a reservoir, slowly releasing oil into the running track. More recently, other authors observed a residual thickener layer deposited on the surfaces of a ball-on-disc machine [6, 34], proposing a model where a thin layer of soap is covering the surfaces and the film is formed by base oil thickened with broken thickener fibres. Cann and Hurley [35] attributed the release of oil not to bleeding, but to the progressive destruction of the soap matrix by over-rolling, providing free lubricant for replenishment. In 1996, Cann measured the grease film thickness in a ball-on-flat disc machine showing that the lubricant film was composed of a part of elasto-hydrodynamic action and a part formed by a residual layer [36].

There is no consensus regarding the mechanism which controls the bleeding phase. However, the bleeding properties of the greases are known to be very important. A few authors found correlation between the grease bleeding properties and its life. Other authors found the properties of the oil released from the grease (bleed-oil) to be significantly different from the base oil's, carrying information on the thickener-additives-base oil interaction [37–39]. Moreover, Cousseau *et al.* [39], measured the film thickness of both grease and bleed-oil, in a ball-on-disc apparatus, and found that their film thickness is very close and higher than the base oil's, as shown in Figure 2.5. He also found that the friction torque behaviour of a rolling bearing lubricated with grease depends mainly on the bleed-oil viscosity, for early stages of grease lubrication [40].

Despite this, most analytical tools to predict film thickness [4–6, 41] and rolling bearing friction torque [8, 42] in grease lubrication, only take into account the base oil properties and generally disregard the grease formulation, i.e., the type of thickener, its content or its interaction with the base oil, the additive package, etc.

During this bleeding phase, the film thickness should be determined by the mass balance between the oil replenishment and the oil loss to the contacts. In the model proposed by Wilkström and Jacobsson [43], the lubricant replenishment is due to oil bleeding, shear, centrifugal forces and capillary forces. Inside the EHD contact, the pressure gradient is responsible for pushing the lubricant out of the contact. In the case of rolling bearings, the lubricant fraction that leaves the contact

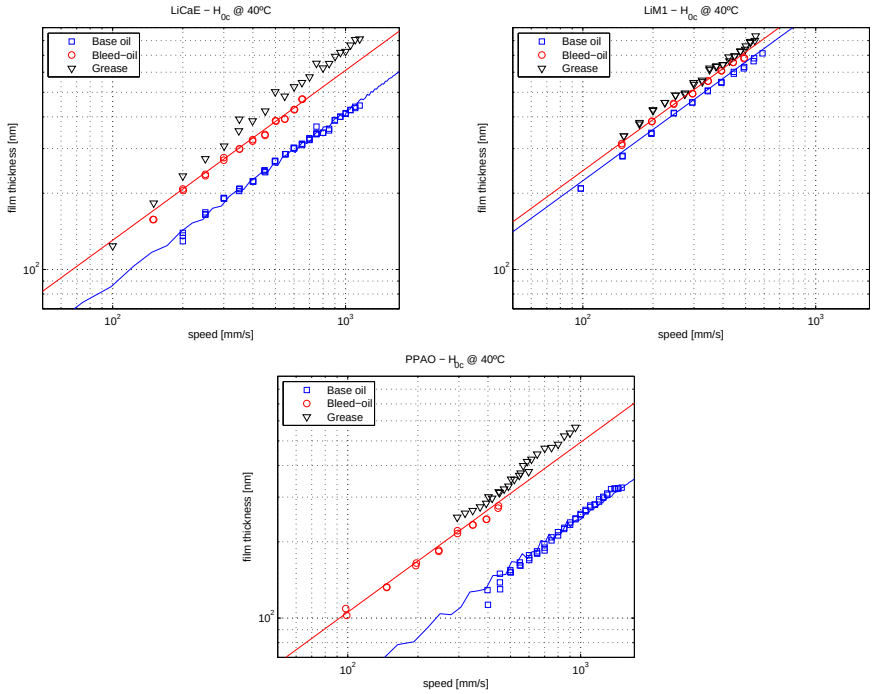

Figure 2.5: Film thickness measurements of three differently formulated greases. The film thickness of their base oils and bleed-oils is also shown. Courtesy of Cousseau *et al.* [39].

in the running direction will feed the next contact, being successively over-rolled in the running track. Another fraction flows out of the track and it stays outside, not flowing back inside easily. This grease fraction, along with the grease located in the bearing shoulders and cage pockets is slowly sheared by the cage and may be scrapped off or redistributed. The centrifugal forces, if sufficiently high, can induce grease flow towards the contact or away from it, being both a feed and loss mechanism [2]. In the same way, capillary forces might contribute to the replenishment of the contact, particularly during start/stop operations.

On the other hand, the changes in the lubricant properties due to oxidation and polymerization processes may also contribute to the replenishment or loss mechanisms. While the evaporation is a loss mechanism which causes the loss of free oil in the rolling bearing, the oxidation and consequent polymerization processes might work either way to increase or decrease the replenishment depending on the alterations produced in the lubricant.

Finally, reaching the end of grease life, severe film breakdown may occur, with consequent severe wear and premature failure of the rolling bearing.

2.4 Composition of lubricating greases

Lubricating grease is a three component system of base oil, thickener and additives. Typically, the base oil content is about 65 to 95 w/w % of the grease, while the thickener content may vary between 5 and 35 w/w %. The additives can be liquid or solid and their content is generally up to 10 w/w % [44].

2.4.1 Base oils

The base oil is extremely important for the behaviour of the finished grease and should be chosen specifically for a given application. One of the main guidelines is that base oil viscosity should provide full film lubrication over the range of operating speeds and temperature.

Therefore, in grease formulation, the following oil properties should be taken into account when choosing the base oil:

- viscosity;
- solubility;
- low temperature properties;
- oxidation stability;
- evaporation loss;
- environmental and health restrictions.

The base oils can be of different nature: mineral, triglyceride and synthetic. The first two are commonly used but synthetic oils are becoming more and more frequent. One of the reasons is that these oils are required for many applications since it is possible to manufacture them with specific properties not achievable with conventional mineral products. The most common synthetic oils are poly-alpha-olefins (PAO) and synthetic esters. Many of these are incompatible with soap thickeners and hence, the greases produced with these base oils are formulated with unconventional thickeners such as clay, polyurea, teflon and other polymers.

The greases to be tested in this work were formulated with poly-alpha-olefin (PAO) and mineral (MIN) base oils. However, in this section, the properties of three different nature base oils will be stated, given its very common applicability.

2.4.1.1 Mineral

A mineral oil is a product which has undergone a series of processes during the refining of the crude. This type of oil contains a wide variety of chemical components and, depending on the carbon bond type of its molecules, the oil nature will be different and so will its properties. Although most hydrocarbons are paraffinic, they also contain naphthenic and aromatic groups. Depending on the amount of these groups, the oils might have different properties:

- Aromatic based oils show excellent solubility;
- Naphthenic based oils show good low temperature properties;
- Paraffinic based oils generally show high viscosity index, low sulphur content and inherent good oxidative stability.

Mineral oils are generally grouped based on the refining process, according to the American Petroleum Institute (API):

- Group I: These are the least refined oils, mixing different hydrocarbon chains of different sizes and lengths; They are cheaper and generally used in less demanding applications;
- Group II: These base oils are more refined than those of the previous group. Therefore, they show less impurities, have less sulphur content, are more inert and less prone to oxidation. They show better thermal stability and should provide longer service life. Since they are more pure, they have almost no colour;
- Group III: The difference between the oils of group II and II is related to the viscosity index only. The oils on this group show unconventional values of viscosity index (>120).

2.4.1.2 Poly-alpha-olefins (PAO)

PAO's are available in a wide variety of viscosity grades. Although they are significantly more expensive than mineral oils, these synthetic oils are and can be used in any lifetime application. These base oils belong to Group IV of the API classification.

High oxidation and thermal stability, high viscosity index, low evaporation rates (under 160 °C) and very low pour point are the main characteristics of PAO's. Although their low polarity leads to poorer additive solvency, their response to some

additives is actually better than for mineral oils. Due to their total paraffinic structure, these oils tend to shrink seals. To avoid this, they are commonly blended with a small amount of polar oil, for instance an ester. The addition of this ester content can also be important to promote the saponification reaction during the grease processing with metallic soaps.

2.4.1.3 Diesters and polyesters

Esters show very good aging properties, excellent low temperature behaviour and viscosity index, favourable evaporation behaviour and good solubility, therefore being miscible with mineral and PAO oils. Some of them are also rapidly biodegradable which is a very interesting advantage for certain applications.

However, careful selection of sealing materials is necessary, and care must be taken with paint coatings. These oils are also significantly more expensive than mineral oils. These base oils are generally grouped into Group V of the API classification.

2.4.2 Thickeners

The thickener system is a key factor in providing a mechanically stable grease matrix, both over time and under the operating shear within the mechanical components. The thickener is the element responsible to give the grease its semi-solid structure. The thickener should provide a mechanically stable matrix, capable of retaining the oil and showing a solid-like behaviour until shear, load and/or temperature initiate a viscoelastic response in the grease. When subjected to very high shear rates, the grease will show excellent flow and lubrication properties due to its shear-thinning behaviour.

Water resistance, surface adhesion/tackiness, dropping point and compatibility with other grease are all properties where the thickener plays an important role. Besides, as with all other grease components, human toxicology, eco-toxicology and the biodegradability of lubricating greases are also thickener-related and have become important issues.

The thickener structure holds the base oil by mechanical entrapment and a combination of Van der Waals and capillary forces [45]. Interaction between thickener molecules are dipole-dipole, including hydrogen bonding [46] or ionic and Van der Waals forces. Although this is true for most of soap thickeners, in the case of non-soap thickeners like Polypropylene (PP), these interact through Van der Waals forces only, and their interaction with the oil should also be different. The effectiveness of these forces depends on how these fibres contact each other [2].

When all their properties are taken into consideration, none of the commercially important thickeners stand out from the others. They are comparably competitive and suited for their tasks. The differences mainly lie in the most special demands that are made on them [47]. The thickener itself, although it provides several characteristics to the greases, it is not believed to influence the grease performance so far. However, for the same application, a certain type of thickener can be better or worse than others in terms of efficiency (power loss and wear), depending on its interaction with the base oil and additives, but also on the manufacturing process.

When comparing different thickeners or different thickener content, the following grease properties should be taken into account:

- high and low temperature properties;
- water resistance;
- tackiness and surface adhesion;
- compatibility and toxicity;
- dropping point;
- oil loss.

Generally, the thickener types can be divided in metal soap and non-metal soap thickeners. In this work only two types of thickeners were analysed based on the greases to be tested: Lithium complex as the metal soap and Polypropylene (PP) as the non soap-thickener.

2.4.2.1 Lithium complex

The greases formulated with Lithium complex are the most common greases. Its popularity is due to its excellent properties, being very often classified as a multi-purpose greases.

The most common version of lithium complex grease is based on 12-hydroxy stearic acid and dibasic acid. As a general guideline, these greases have a dropping point around 300 °C and can be continuously used at temperatures over 150 °C depending on the base oil. The excellent high temperature performance results from the very dense fibre structure of the soap matrix associated with the high melting point. The polar nature of the fibres link to the base oil, trapping it in the matrix and therefore, offering an increased protection against oxidation. Associated with the wide temperature range, the mechanical stability of these greases make them suitable

for several different applications where high temperatures are involved. Its excellent pump ability led to its common use on cold climate applications.

2.4.2.2 Polypropylene

This new ground-breaking polymer thickener consists of combinations of different polypropylene chains and rubber resulting in a polymer compound with an optimized crystalline-amorphous balance. The grease formulated with this thickener are non-ionic products with controlled oil separation.

By changing certain parameters in the grease formulation and production process, it is possible to control the amount of oil released or even the amount of additives. This property allows the reduction of the risk of starvation and modify the temperature dependence of the oil release, providing excellent low temperature properties to these greases.

The non-ionic thickener matrix brings several advantages, one of the most important is the fact it allows the active components in the additives to reach and react with the metal surfaces more easily. While the typical metal soap thickeners will react with the surface and compete with the additives, this polymer system will promote the additives-surface reaction by not interfering with it.

The greases formulated with this technology provide a higher film thickness, reduced wear and an increased load carrying capacity. Moreover, given the high adhesion and low solubility, the polymer thickeners show good resistance against water and aggressive chemicals, while being able to protect the surfaces against corrosion. The polymer systems are generally more resistant to oxidation, degradation and centrifugal forces than the metal soap products. All these properties should contribute to a longer grease life.

Finally, the inert nature of PP allows full compatibility with most existing greases. Furthermore, the non-toxic nature of the polymer might prove these greases to be suitable for the food industry and environmentally acceptable applications.

Regarding cost, the polymer thickener material costs about the same as the lithium complex thickener. However, the manufacturing process of these polymer greases is slightly more expensive than the typical soap greases [1].

2.4.3 Bleed-oil

The oil effectively released by the grease under static (storage) or dynamic (mechanical and/or thermal stresses) conditions is often called “bled oil” or “bleed-oil”. In this work, the designation “bleed-oil” is used to refer to this oil.

[1] Personal communication with Johan Leckner and René Westbroek from Axel Christiernsson.

During storage, oil bleeding occurs naturally, either by room temperature variations, vibrations or just very long storage time. Promoted by gravity, long storage time originates thickener deposition and oil release through the free surface of the grease. Sometimes, during manufacturing, insufficient mixing might also lead to oil separation when the grease is stored.

Under dynamic conditions the bleed rate is affected by operating and environmental conditions. Mechanical and thermal work are the most important promoters of oil bleeding/loss, while water contamination might retard the oil bleeding.

The oil bleed rate of the grease can be adjusted by optimizing the composition (thickener type/content, base oil viscosity/nature, etc.) or even during the manufacturing process. Manufacturing process plays a key role in determining the distribution of the thickener matrix within the lubricating fluid and, consequently, the bleed characteristics of the finished lubricating grease.

Different oil bleed rates are targeted depending on the end application of the lubricating greases. For very high speed or high temperature applications, where centrifugal forces are greatly important, greases are formulated to present a minimum separation of oil. On the other hand, for applications operating at low speeds or with a reciprocal motion of small amplitude there is a little churning of the grease, which requires grease design to be sensitive to mechanical shear and to release oil under the effect of small stresses. High temperatures increase bleed rate, leading to rapid loss of oil (leakage, evaporation) and premature grease aging. On the other hand, greases with low, although sufficient oil bleed at high temperatures, may under-perform at ambient temperatures because of oil starvation.

2.5 Grease manufacturing

The manufacturing of lubricating greases is a complicated and still experimental process requiring a high level of investment in terms of capital, manpower and know-how. Different greases require different manufacturing methods and each grease plant has its own particular detailed technology. According to some grease manufacturers, if formulations are regarded as proprietary and confidential, then the manufacturing processes must be classified as top secret. The properties of the greases depend not only on their composition, but also on the way in which the thickeners are prepared, the temperatures used and so on. That is why very often different batches of the same grease formulation show different properties.

Delgado *et al.* [48] manufactured lubricating greases, generating the soap thickener in situ and with online viscosity and torque measurements. He also collected

grease samples at different processing stages showing that the rheological properties of the grease, the morphology of the thickener structure and its distribution changed considerably at different stages of grease production. This means that lubricating greases with the same formulation but different manufacturing processes can have significantly different properties. However, it is still very hard to evaluate their differences in terms of performance with the current technology, using short duration rolling bearing tests.

Still, grease performance should not be evaluated solely by its base oil, or thickener, or additive package. Their interaction plus the micro-structural characteristics achieved during processing might be determinant to the grease properties and eventually, to their performance. For instance, the grease replenishment mechanisms depend on the flow properties of the grease, its ability to release oil and its interaction with lubricated surfaces. In fact, all grease properties are related to the micro-structural characteristics achieved during processing coupled with their composition, both of which are generally not shared by the manufacturers to public domain.

2.6 Closure and objectives

In this chapter, the current knowledge on the grease lubrication mechanisms was reported. The advantages and disadvantages of using grease over oil in lubrication were addressed and the most relevant remarks on grease lubrication were presented.

A quick description of grease and their different components is also presented and how they can change grease properties. Emphasis was given on the base oils and thickener types which will be tested later on.

With the conclusion of this chapter, the main objectives of this work can be established more clearly and with more detail. Those objectives are:

a) study the influence of formulation (thickener type/content, base oil nature/viscosity) in the grease performance: film thickness and friction behaviour, and the mechanisms behind it, in both fully flooded and starved contacts;

b) fully characterize the new polymer thickened greases regarding their rheological properties and tribological behaviour, correlating them;

c) analyse the mechanisms which lead to grease aging by thermal stresses and their influence on the tribological behaviour.

3 Experimental Characterization

3.1 Introduction

As stated before, lubricating greases consist of mineral or synthetic oils which have been thickened by a thickener agent, typically a metallic soap, guaranteeing that it remains in place and in contact with the moving surfaces when needed. Although metallic soaps are the most common grease thickeners (specially lithium soaps), new and innovative polymer based greases have been slowly introduced to the market.

Polymers have been used in oil/grease formulation not only as thickeners [23,24, 49–51] but also, and primarily, as Viscosity Index improvers and as dispersants [52,53]. A good review on different polymer types used in grease formulations and their effects can be seen in [54]. When used as thickener, the polymers form short and thick elements connected to each other, which trap the oil and modify its rheology, giving consistency to the mixture. On the other hand, when used as additives, the polymers are added to improve the Viscosity Index, to promote the adhesion and cohesion characteristics of lubricating greases and also to improve mechanical and chemical stability at high and low temperatures [53].

These polymer greases, expected to perform with high efficiency and reliability, are quite recent. Thus, their characterization and tribological performance have yet to be thoroughly investigated. However, there are already a few works which describe these greases' rheological behaviour regarding formulation, thermal behaviour and base oil interaction [53, 55–58].

In this chapter the main properties of lubricating greases and how they were measured will be described. Of the many grease properties one can evaluate, only some might effectively allow a better understanding of the grease lubrication mechanisms under certain specific operating conditions. The rheological parameters of lubricating greases (G', G", τ_y, τ_{co}, n, G_{cr}, etc.) were measured/calculated to understand how grease flows, while trying to correlate the viscoelastic characteristics to their tribological behaviour and performance. The characterization of the base oil and bleed-oil properties is also very important since the largest phase of grease life is the bleeding phase, where the bled oil plays a major role. Furthermore, they are

often required for the prediction of film thickness and rolling bearing friction torque, hence its importance.

3.2 Tested Greases

During the course of this work, several different polymer greases were tested as well as a few lithium thickened greases. However, for the purpose of showing the most relevant results, only six different formulations are presented. These greases' main properties are shown in Table 3.1.

Experimental batches of polymer greases were specifically manufactured for this work. These batches were processed so they should reflect the differences in their composition. The first phase in the manufacturing of the polymer grease is the melting of the polypropylene in the oil. This was carried out in a round flask with a mantle heater with a batch size of 2 kg. The polymer/oil solution was then quench cooled to a temperature far below the melting point of the polymers. In the second phase four batches of quenched material were transferred to a mixing vessel where the material was deaerated and worked into the desired consistency. The milling has been done in a colloidal mill where each grease has passed through the mill exactly the same number of times with decreasing gap size. The process is kept as uniform as possible.

Four polymer greases were tested in this work: M1, M2, M3 and M5. All the polymer greases were formulated with the same poly-alpha-olefin (PAO) base oil and thickened with Polypropylene (PP). Greases M1, M2 and M3 were formulated with different PP content, respectively, 11, 13 and 15 %, while grease M5 was formulated with 13 % of PP and 2.6 % of an elastomer, as co-thickener. These greases are not additized and were all formulated with the same base oil, which means that their differences rely only on the thickener and elastomer content.

Two lithium thickened greases were also tested: MLi and MLiM, both formulated with Lithium Complex (LiX). Since lithium thickened greases are the most common lubricating greases in the market, greases MLi and MLiM were tested as benchmarks for multi-purpose greases. Regarding the base oil, grease MLi was formulated with a mixture of two different grades of PAO and some ester to facilitate the "saponification" reaction. Grease MLi was retrieved from a production batch prior to the addition of additives and therefore, it has no polymer or additives in its formulation.

Table 3.1: Tested greases' properties, according to manufacturer's information.

Grease Reference		M1 ⋆	M2 □	M3 △	M5 ○	MLi ◇	MLiM △	Units
Thickener type		Polypropylene				Lithium complex		—
Thickener content		11	13	15	13	17.5	10.6	%
Elastomer content		0	0	0	2.60	0	0	%
Polyisobutylene (PIB) content		0	0	0	0	0	1.7	%
Worked penetration (ISO 2137)		290	269	249	276	288	279	10^{-1} mm
NLGI		2	2	3	2	2	2	—
Shell Roll Stability 80 °C /50h (mod. ASTM D1831)	Before	286	264	256	282	284	n.a.	10^{-1} mm
	After	318	323	281	289	324	n.a.	
	Difference	32	59	25	7	40	n.a.	
Flow pressure at -25 °C (DIN 51805)		320	390	670	1865	370	n.a.	hPa
Oil separation 100 °C /30h (ASTM D6184)		7.2	5.3	3.0	5.6	1.8	n.a.	%
Oil separation 40 °C /168h (IP121)		7.3	5.3	5.9	4.0	2.8	n.a.	
Oil evaporation 100 °C /30h (ASTM D6184)		0.2	0.9	0.8	0.2	0.5	n.a.	
Base oil viscosity (ASTM D445)	40 °C		48		48^a	179	153^b	mm^2/s
	100 °C		8		8^a	21	16^b	

[a] base oil without elastomer.
[b] blend oil with PIB.

On the other hand, grease MLiM was also formulated with a mixture of mineral based oils of different viscosity, but Polyisobutylene (PIB) was also added to increase the viscosity of the blend. The approximate composition of the mineral oil blend is: 11 % aromatic, 51 % paraffinic and 38 % naphtenic.

The production of the lithium complex greases was done in a pilot reactor with a batch size of 8 kg. The manufacturing procedure followed a standard protocol and the soap was synthesized in around 40 % of the total oil volume. The first saponification using 12-hydroxystearic acid was performed at 90 °C with a hold time of 30 minutes. The temperature was then increased to around 115 °C and kept there for two hours after which the second saponification using azelaic acid took place. The grease was then kept at 115 °C for 30 minutes before the temperature was increased to the top temperature of 205 °C. The cooling was performed by adding portions of 5% of oil, with a hold time of 15 minutes between each addition. The grease was finally milled and deaerated for 1 hour to achieve the desired consistency.

All tested greases are NLGI 2, except grease M3 which is NLGI 3. These greases are designed for ball or roller bearings, under moderately loaded and medium speed applications.

3.3 Oil/thickener separation

In order to separate the thickener and the oil of each grease and therefore be able to study them separately, a sample of each grease was dissolved in petroleum ether by means of an ultrasonic device. The obtained solution was filtered through an 8 μm mesh paper filter by the action of a vacuum pump and then kept in the oven at 50 °C for at least 24 h, in order to ensure the evaporation of the residual ether from the filter. In the end, solid thickener material is obtained on the filter which can be observed by Scanning Electron Microscopy (SEM) and its chemical signature obtained from FTIR spectroscopy.

Not only this is not a standard method, but also it is not optimal since the thickener matrix might get destroyed/collapsed in the process [2]. Still, since it is not possible to observe wet grease samples using SEM operating under high vacuum environment, this solution was used to investigate the thickener morphology only.

Nonetheless, this method has the advantage of requiring a very small grease sample and of being fairly quick to perform. The method is also important to study grease degradation since it allows to quantify the oil lost in an aged grease sample.

3.4 Scanning electron microscopy (SEM)

The analysis of the grease micro-structure was performed with a scanning electron microscope (FEI Quanta 400FEG ESEM - high vacuum), using the secondary electrons beam. Secondary electrons are emitted from the atoms occupying the top surface of the sample, after being excited through the primary electrons beam. This method allows to quickly produce an interpretable image of the surface's topography. A high resolution image can be obtained because of the small diameter of the primary electron beam, while the contrast of the image is mainly determined by the sample's morphology. In order to improve the resolution and to avoid the melting of the polymer thickener given the high energy of the beam, all samples were covered with a very thin carbon film. With this process, an electron beam of higher energy can be used, highly improving the image quality.

In Figure 3.1, the thickener morphology of greases M2, M5, MLi and MLiM is shown. Pictures of the thickener obtained from the other polymer greases were also taken but given the similarities with greases M2 and M5, they will not be shown here.

The PP thickener morphology shows short and thick polymer elements randomly distributed in a dense matrix. Despite being hard to measure the diameter of such elements, their dimensions vary from ≈0.2 up to 1.2 μm. This structure was found for all the polymer thickened greases independently of its formulation.

On the other hand, the morphology of the LiX thickener is quite different. The typical fibre entanglement of the lithium thickened greases is observed where long and relatively thin fibres are entangled with each other in a porous matrix. In most of the soap based greases, the soap is presented as fibres or ribbons varying in size and length, from a few microns up to one hundred [59]. In the case of the greases tested here (MLi and MLiM) the fibre/ribbons diameter vary from ≈0.05 to 0.2 μm.

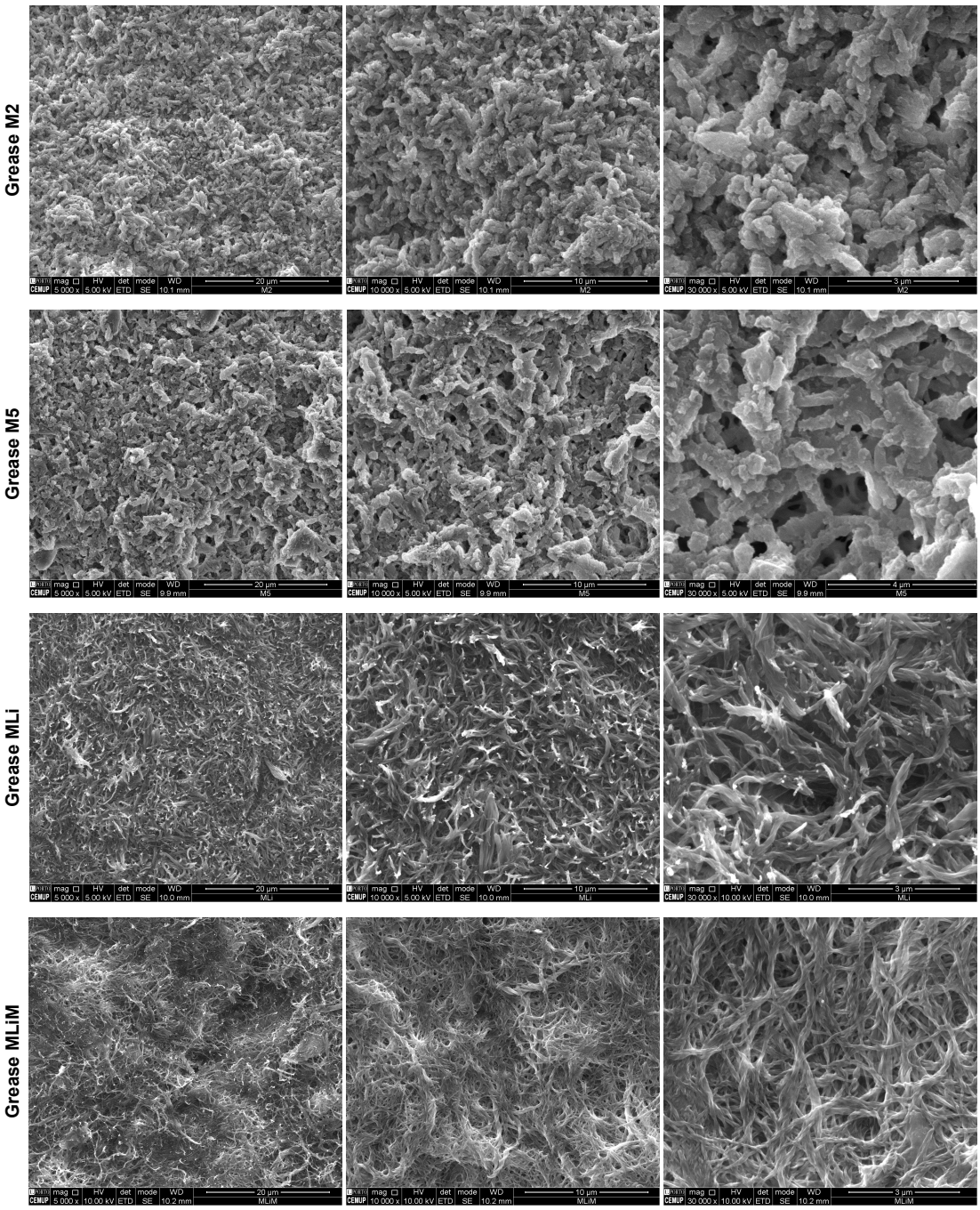

Figure 3.1: SEM images of the thickener morphology of greases M2, M5, MLi and MLiM.

3.5 Atomic Force Microscopy (AFM)

In order to study the grease structure without washing out the oil from the sample, it is necessary to use a different microscopy technique. Atomic force microscopy (AFM) is a very high resolution technique which scans the sample surface to obtain its topography (among other properties) at the atomic scale. A piezoelectric element oscillates the cantilever very precisely and, as the cantilever is displaced via its inter-

action with the surface, the reflection of the laser beam will also be displaced on the detector, registering the deflection and motion of the cantilever. The reaction of the mechanical probe to the forces that the sample imposes on it, at the atomic level, can be used to form a high resolution image of the three-dimensional topography of the sample's surface.

Samples for micro-structural characterization using AFM were prepared by carefully scraping the grease on a steel disk. AFM measurements were taken using a Multimode AFM (Veeco Metrology, Santa Barbara, CA, USA) with a Nanoscope IVA controller. Tapping mode AFM images were collected with commercially available silicon cantilevers (Bruker TESP-SS). These super sharp silicon cantilevers (tip size: 2 nm) had to be used because of the very high adhesion and viscosity of the oil on the surface of the grease. These special tips get ruined very often, for the same reason. The measuring process is also very difficult since it is frequent to find a lot of oil on the surface, while the embedded thickener elements are below the surface and therefore, very hard for the tip to interact with them.

The resulting 2D images ($5 \times 5\ \mu m$) of the topography of greases M2, M5, MLi and MLiM are shown in Figure 3.2. At least two pictures were taken in different areas of the same sample to assure that each picture was representative of the sample's surface. For each measurement the system scans the surface in two different directions but only the one which showed the less amount of artefacts will be presented here.

Although these AFM pictures allow to observe the thickener elements embedded in the oil and somehow quantify the volume fraction of thickener within the oil for a certain sample, the difficulty to achieve these images with the current technology and the information effectively drawn from them is difficult to justify. When comparing these images to those obtained through SEM it is possible to see that not only the resolution is worse, but also the thickener morphology is much harder to analyse.

Still, it is possible to confirm that both LiX thickener greases show twisted fibres entangled with each other. The volume fraction of fibres seems higher for grease MLi, although the fibres are thinner than grease MLiM. On the other hand, the thickener's structure of grease MLiM is coarser when compared to MLi. The average diameter of the fibres is similar to what was found in the pictures from SEM. It is also not possible to infer on the fibres' length since it is clearly impossible to identify the beginning and ending of a single fibre embedded in the oil.

Regarding the polymer greases it is even harder to conclude anything. Although the results of grease M2 look very different from those of grease M5, its structure should in fact be very similar. However, for grease M2 it was very hard to reach a zone were thickener material was close to surface and even when it was, its morphology was very hard to understand.

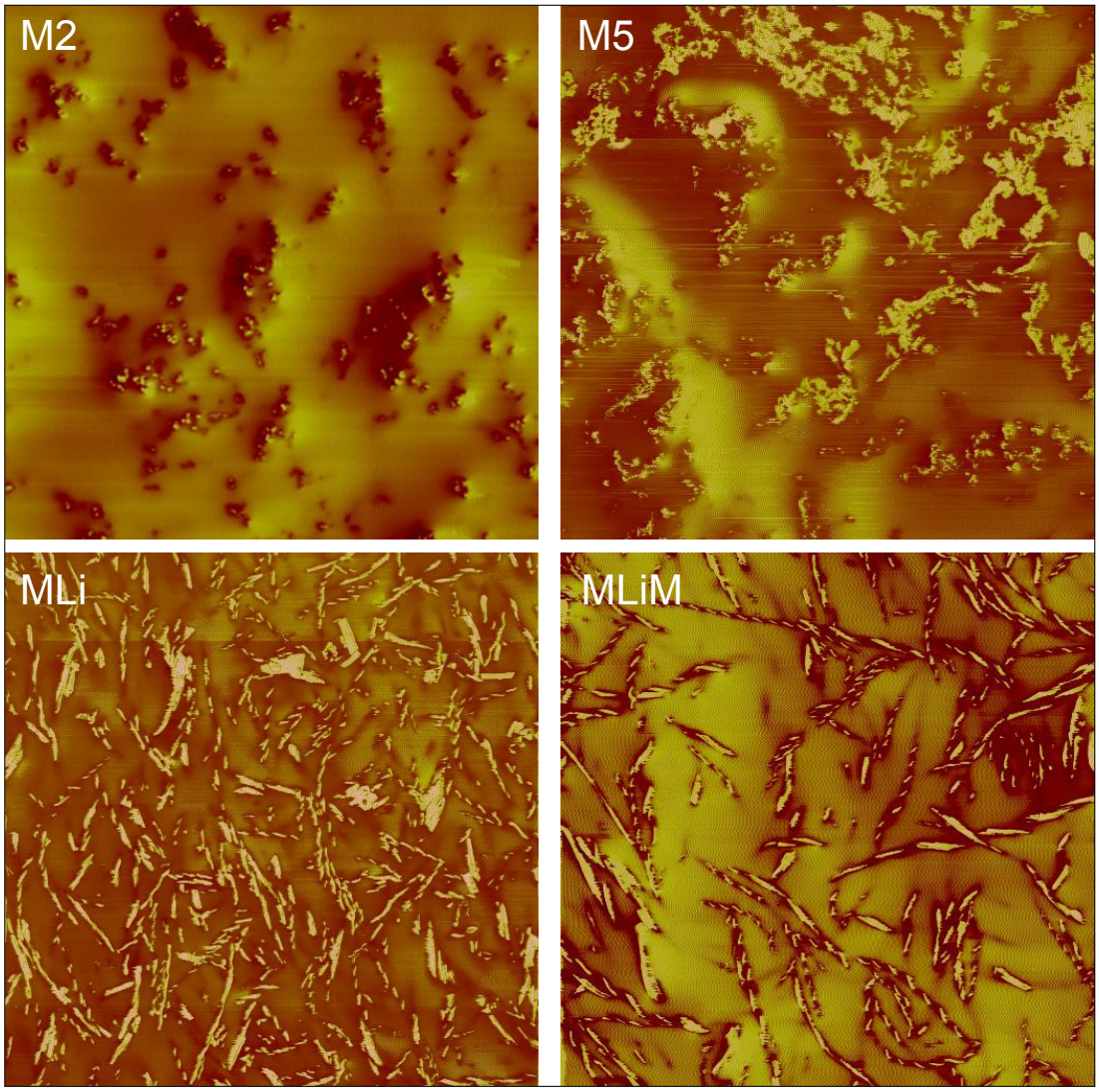

Figure 3.2: AFM images of the surface of a greases M2, M5, MLi and MLiM. Each picture shows a 5×5 μm resolution.

3.6 Oil bleeding rate

Several oil bleed tests were developed in order to determine the oil bleeding characteristics of lubricating greases. ASTM D1742 pressure bleed, ASTM D6184 cone bleed and IP 121 are static bleed tests that can be used for quality control in grease production. They determine the amount of oil separation from the grease, which can be related to the situation of the grease in its container during storage or in the pre-greased equipment when not in service - storage or static bleeding. They are referred to as static tests because they operate on undisturbed grease exposed to relatively low stresses.

Dynamic bleed tests such as M1066 CGOR (Churned Grease Oil Release, in-house proprietary test), ASTM D4425 Centrifugal Oil Bleed and Trabon (Method

905A) determine the amount of oil separation after the grease is mechanically sheared, as would occur in rolling element bearings, or exposed to high levels of centrifugal stress, as typically found in shaft couplings and universal joints.

In this work, the bleed-oil of each grease was extracted using a non-standard dynamic bleeding process, similar to the ASTM D4425 standard method. This process consists in pressurizing an amount of grease (5 ml) through centrifugal forces. The grease is pushed against an 8 μm paper filter supported by a metallic net on a centrifuge cup, while rotating at 1000 rpm (v_t=20.9 m/s) and at ambient temperature (≈27±1 °C), as represented in Figure 3.3.

The bleed-oil obtained through this non-standard dynamic method shows the same viscosity than the bleed-oil obtained through the static ASTM D6184 method, while the FTIR spectra revealed that the bleed-oils are chemically similar. Given that the non-standard method is much faster, it was preferred for this work.

This dynamic method was used to calculate the oil bleed rate of each grease. At a given time, the extraction process was stopped and the oil mass on the container was measured from 2 to 100 hours at different time steps. The amount of oil separated was calculated relative to the initial mass of the sample. Similar bleed rate mechanism was used by Baart *et al.* [60].

The bleed-rate results of grease M1, M2 and M3 are shown in Figure 3.4. These greases were formulated with the same base oil but different thickener content. According to this figure, the thickener content influences the bleed rate: the higher it is, the smaller is the oil bleeding rate. With higher thickener content, the matrix

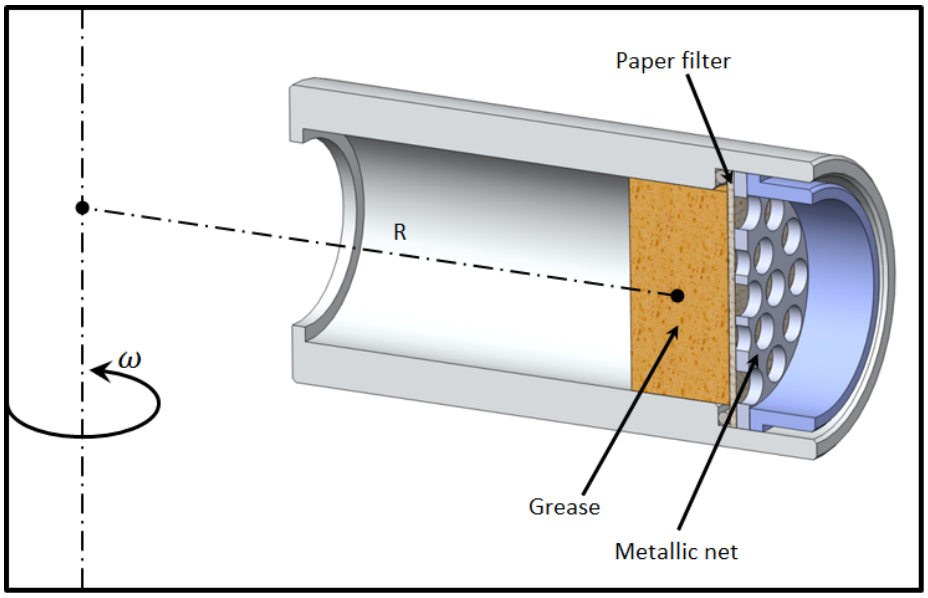

Figure 3.3: Bleed-oil extraction mechanism scheme.
Note: the bleed-oil container is not represented.

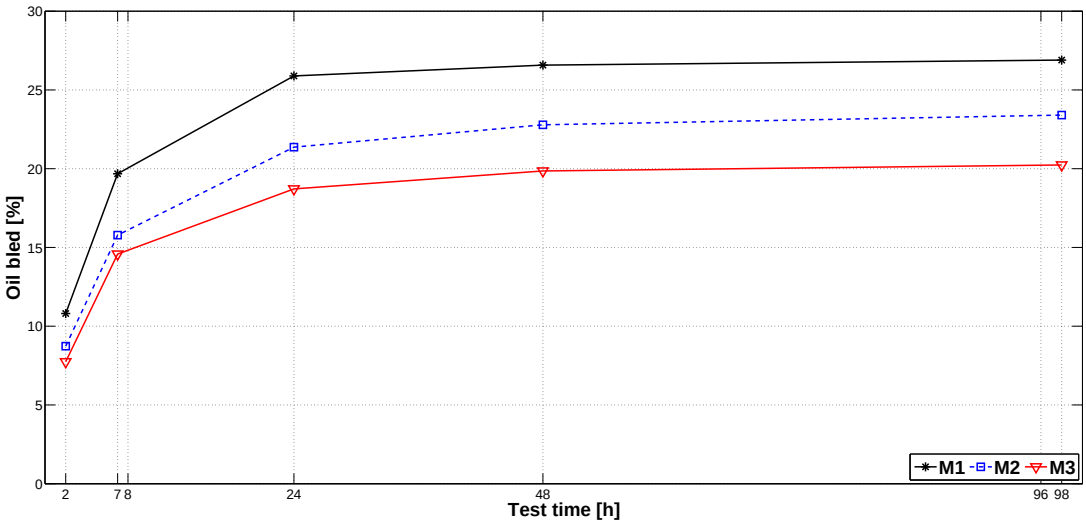

Figure 3.4: Bleed-rate results of greases M1, M2 and M3, obtained at ambient temperature using a non-standard dynamic method.

is much denser and therefore, the oil is more easily trapped.

In fact, this phenomenon is also what happens during the tests, independently of the grease formulation: as soon as the oil starts to be released, the grease permeability starts to decrease due not only to the increase of the thickener fraction but also to micro-structural changes [60]. Hence, the oil bleeding rate decreases with the test duration up to the point where little or no oil can escape.

In Figure 3.5, the oil bleeding results of greases M2, M5 and MLi are shown. Greases M2 and M5 were formulated with the same PP thickener content but different elastomer content. Elastomers are known to act as viscosity improvers and, as it will be shown in a following section, they contribute to increase the viscosity of the oil released from the grease during service - bleed-oil. This increased viscosity is also responsible for slowing the oil bleeding. Grease M5, formulated with 2.6 % of elastomer shows a slower bleed rate than any of the other polymer greases. This does not mean that the total amount of oil bled will be smaller, but only that the higher is its viscosity, the slower is the oil bleeding.

This can also be confirmed by the results of grease MLi. Formulated not only with higher thickener content than any of the other greases, but also with a base oil of higher viscosity, grease MLi also shows a slower oil bleeding rate than the other greases, very similar to the result of grease M5.

Unfortunately, the bleed-rate of grease MLiM was not measured.

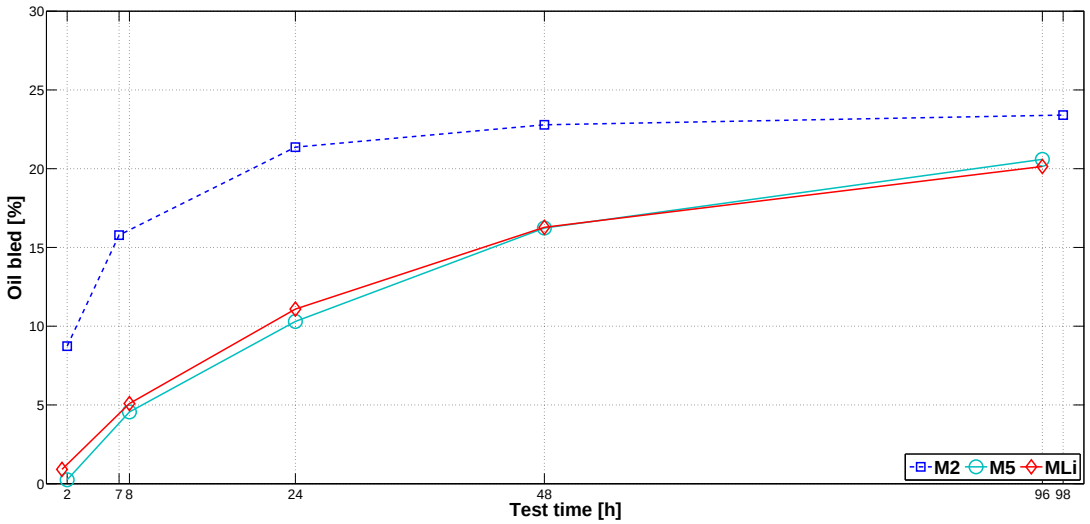

Figure 3.5: Bleed-rate results of greases M2, M5 and MLi, obtained at ambient temperature using a non-standard dynamic method.

3.7 Fourier transform infra-red spectroscopy (FTIR)

In Fourier Transform Infra-red spectroscopy, infra-red radiation is passed through a sample. Some of the emitted IR radiation is absorbed by the sample and some of it is transmitted/reflected back to the detector. The resulting spectrum represents the molecular absorption and transmission, creating a molecular fingerprint of the sample. Since two unique molecular structures cannot produce the same infra-red spectrum, FTIR is very useful to identify unknown materials, determine the quality or consistency of a batch and, in the particular case of lubrication, is commonly used to:

- study the composition of lubricating greases and distinguish different thickeners, base oil natures and additives [35, 61–63].
- evaluate additive consumption, lubricant contamination (water, etc.) and the formation of oxidation/nitration products during service [64–71].

The first item is addressed in this section. FTIR spectra were obtained to study the grease composition and to obtain the spectra of each grease, base oil and thickener, identifying the peaks which are characteristic of the different thickener and base oil natures. The second item was also studied and the results are presented later on, in Chapter 8, were fresh and severely aged greases are analysed with respect to grease degradation.

All spectra were obtained on an Agilent® Cary 630 FTIR device, using an Attenuated Total Reflectance (ATR) accessory. Before each measurement, the crystal

was cleaned with petroleum ether and 16 scans were performed to assure the crystal was clean. After that, the background spectrum is obtained and then the sample is applied over the crystal. A total of 64 backgrounds scans and 128 sample scans were performed at a resolution of 4 cm^{-1}. The procedure is repeated twice for each sample, with a spectral range from 4000 to 650 cm^{-1}. All spectra were normalized to the same peak's height at 1460 cm^{-1} [72], allowing an easier comparison between samples. Slight baseline corrections were also performed, when required. Other than that, all spectra shown in this work were taken directly from the device's software without curve smoothing and a very good reproducibility was found.

In Figure 3.6, the spectra of greases M2, MLi and MLiM are shown, as well as their respective base oils and thickeners. Despite all spectra were obtained over the range of 4000 to 650 cm^{-1}, only the fingerprint region is shown. This region is of the utmost importance, since it is where most of the material's characteristic peaks are located.

Regarding the spectra of grease M2, its PAO base oil and the PP thickener, the following aspects were found:

- There are several similarities between the spectra of PAO and PP, given their also similar nature. Some peaks were found in both spectra despite being located at slightly different wavelengths. However, the thickener content is much smaller in relation with the base oil and therefore, some of its peaks cannot be observed seperatly in the grease's spectrum;

- The peaks mainly attributed to the PP thickener are found at: 1453, 1437, 1359, 1256, 1216, 1167, 1102, 1044, 997.7, 927.8, 939.6, 841 and 809.1 cm^{-1};

- Two peak were found to be mainly attributed to the PAO base oil: 1461 and 721.5;

- The peaks at 1461 cm^{-1} for the base oil and 1453 cm^{-1} for the thickener are due to the CH_2 deformation vibration;

- The peaks at 1378 cm^{-1} for the base oil and 1376 cm^{-1} for the thickener are due to the CH_3 deformation vibration;

- The ratio of the peaks' height at 1378/1491 (base oil) and 1376/1453 (thickener), is much higher for the thickener.

Grease MLi is substantially different from grease M2, specially because the thickener is of very different nature. Moreover, the base oil used in the formulation of grease MLi is a blend of different grades of PAOs with 5% of Ester to help in the

saponification reaction of the LiX thickener. Based on this information, the most important observations regarding this grease and its base oil and thickener are:

- The PAO base oil of grease M2 shows a very similar spectrum to the blend base oil of grease MLi. The main differences are related to the peaks at 1742, 1170, 1142 and 1077 cm^{-1}. The 5% content of ester should be responsible for these differences, specially in the peaks at 1742 and 1142 cm^{-1};
- The peaks attributed to the blend base oil are: 1742, 1460, 1378, 1170, 1142 and 891.5 cm^{-1};
- There are several strong peaks clearly attributed to the LiX thickener at 1578, 1557, 1443, 1409, 1133, 1076, 1027, 996.5, 920, 861.1, 835.3, 776.9 and 710 cm^{-1}. A few others are less clear and are not even observed in the grease's spectrum;
- The peak around 721 shown in the spectrum of both base oil and thickener, is higher and more well defined for the base oil.

On the other hand, grease MLiM shows a very similar spectrum to grease MLi. In this case, the main differences are related to the different nature of the base oils:

- The blend oil of mineral nature shows a quite different spectrum from the other base oils. The peaks attributed only to the mineral base oil are: 1458, 1377, 1366, 1168, 814.1 and 764.2 cm^{-1};
- The spectrum of the LiX thickener is almost equal to the one found for grease MLi and the same peaks were found for both spectra. This was already expected since the thickener used in their formulation was the same. The amplitude of certain peaks however, is different which might be related to the different thickener content;
- The peaks previously attributed to the Ester used in the blend oil of grease MLi (1742, 1170, 1142 and 1077 cm^{-1}) are absent here. Besides those peaks, the region around 720 cm^{-1} is also quite different since the amplitude of this peak is much smaller for the mineral based oil.

Despite other polymer greases were tested in this work (M1, M3 and M5, among others), their spectra are very similar to the spectra of grease M2. Formulated with the same base oil, the differences in their composition are very small and therefore it was not possible to distinguish the different thickener content of greases M1, M2 and M3. Moreover, since greases M2 and M5 were all formulated with the same PP content, their spectra is also very close and not even the elastomer characteristic peaks could be identified since its nature is very similar to the PP thickener nature.

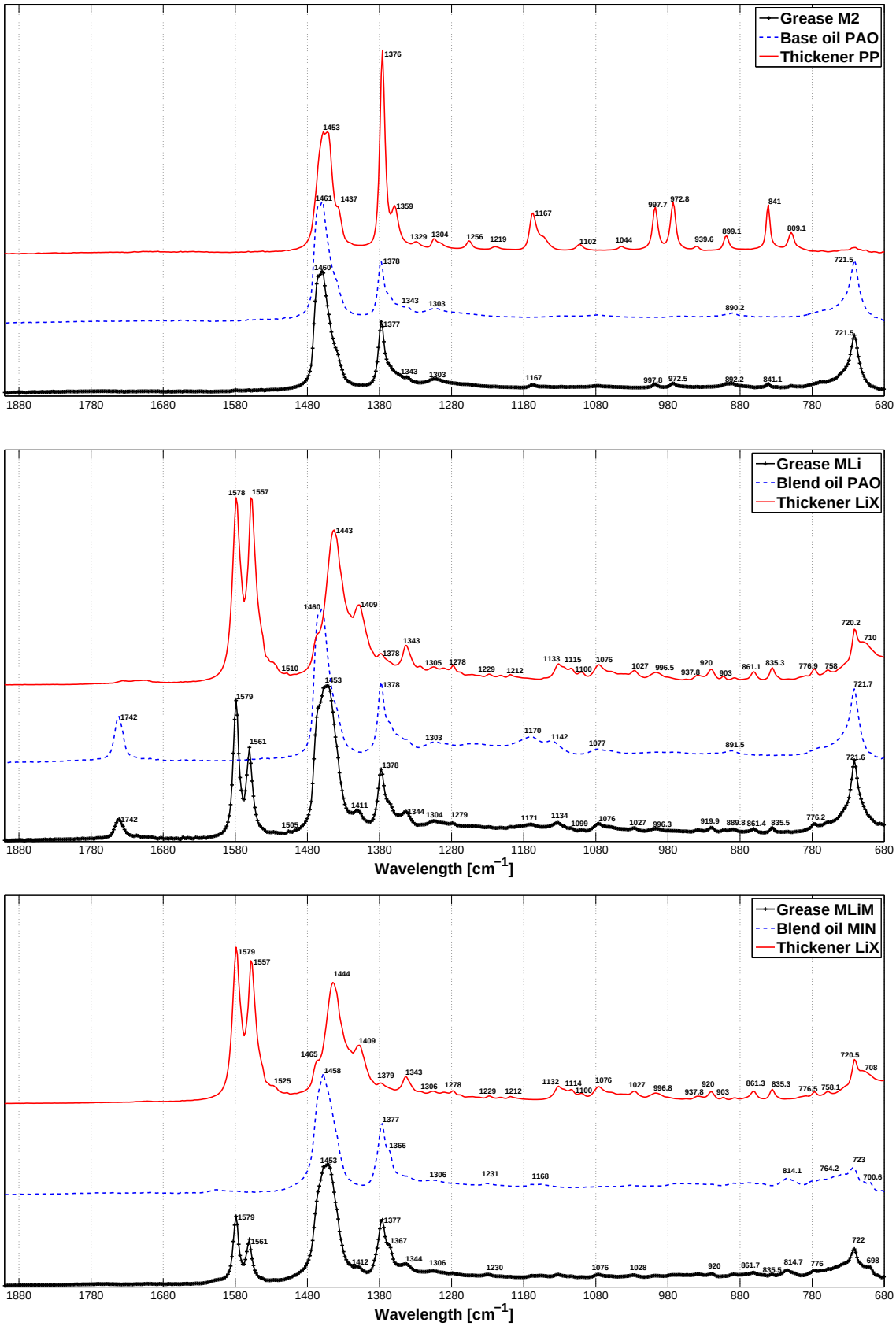

Figure 3.6: FTIR spectra of grease M2, MLi and MLiM, and their respective base oils and thickeners.

3.8 Viscosity of base and bleed-oils

The dynamic viscosity of the base and bleed-oils was measured on a Physica® MCR 301 rheometer, using a smooth plate-plate geometry PP50 (ϕ = 49.998 mm). A gap of ±100 μm between plates was chosen in order to obtain the highest shear-rate possible. After applying the oil sample in the lower plate, the upper plate is pressed against the sample until a gap of ±100 μm is reached. The sample excess is trimmed and then the upper plate rotates from 10^{-4} to 3300 rpm at constant operating temperature. The procedure was repeated at 20, 40, 60, 80 and 110 °C.

The measured viscosity curves are shown in Figure 3.7 showing the base and bleed-oils of greases M2, M5, MLi and MLiM at 60, 80 and 110 °C. The points measured at a temperature which deviated more than 0.5 °C from the desired operating temperature were removed from the plot and not considered in any calculation. The viscosity points measured at a shear rate lower than 1 s^{-1} were also disregarded since a few curves showed artefacts resulting from measurement errors.

In the absence of additives or viscosity changing elements, the bleed-oil should generally show a very similar behaviour to the base oil. For some of the greases tested in this work (M1, M2, M3 and MLiM), the dynamic viscosity curves of base oils and bleed-oils are very close but generally the bleed-oil shows slightly higher viscosity.

An exception to this behaviour was found for greases M5 and MLi. The bleed-oil of grease MLi which shows smaller viscosity than the base oil. The reason behind this is unclear since there is no additives or other components which might change the viscosity of the bleed-oil, but it should be related to the manufacturing process or eventually, to the thickener/base oil interaction.

The bleed-oil of grease M5 is a whole different case. The elastomer used in the formulation of grease M5 acts as a viscosity improver and therefore, the bleed-oil of this grease shows a much higher dynamic viscosity than its base oil, at least under low shear rates. As soon as the shear rate gets higher than 10^3 s^{-1}, the dynamic viscosity starts to quickly drop. However, it is not possible to measure the viscosity above 10^5 s^{-1} and thus, it is also impossible to understand if the dynamic viscosity would continue to drop until the base oil viscosity was reached. In Figure 3.8, the measured dynamic viscosity of the bleed-oil of grease M5 is represented as well as its prediction using the Carreau viscosity model, shown here by Equation 3.1.

$$\eta = \eta_\infty + (\eta_0 - \eta_\infty) \cdot \left[1 + \left(\frac{\eta_0 \cdot \dot{\gamma}}{G_{cr}}\right)^2\right]^{(n-1)/2} \tag{3.1}$$

In Equation 3.1, η_0 is the first Newtonian viscosity at low shear rates while η_∞ is the second Newtonian viscosity at very high shear rates. G_{cr} is the bleed-oil critical

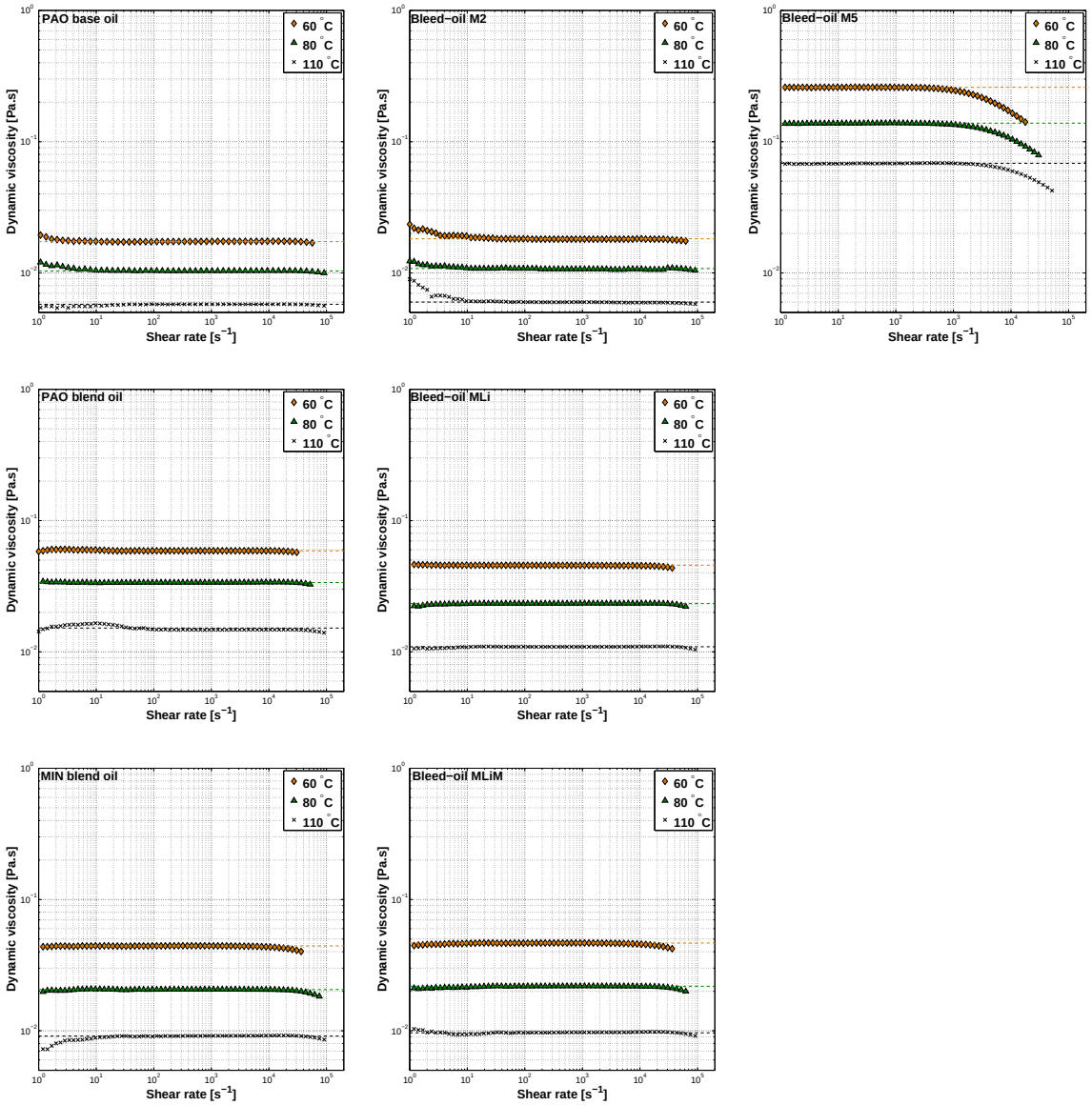

Figure 3.7: Measured dynamic viscosities of all the base oils and bleed-oils.

stress[1], while n is the power-law or flow index.

The viscosity was calculated assuming that when the shear rate tends to infinity, the value of η approaches either the base oil viscosity (η_{bo}) or zero. However, according to Figure 3.8, the difference between these predictions can be quite significant. Moreover, both predictions are very far from the base oil viscosity under the typical shear rate range of the film thickness measurements performed in this work (between 10^5 to 10^7 s^{-1}). Since the rheometer is not capable of measuring at shear rates above 10^5 s^{-1}, it is not possible to know which assumption is more correct, but the fitting shows a better correlation to the experimental points when $\eta_\infty = 0$. Furthermore,

[1]Equivalent to the yield stress, this parameter is referred to the stress at which the dynamic viscosity starts to drop from the first Newtonian plateau.

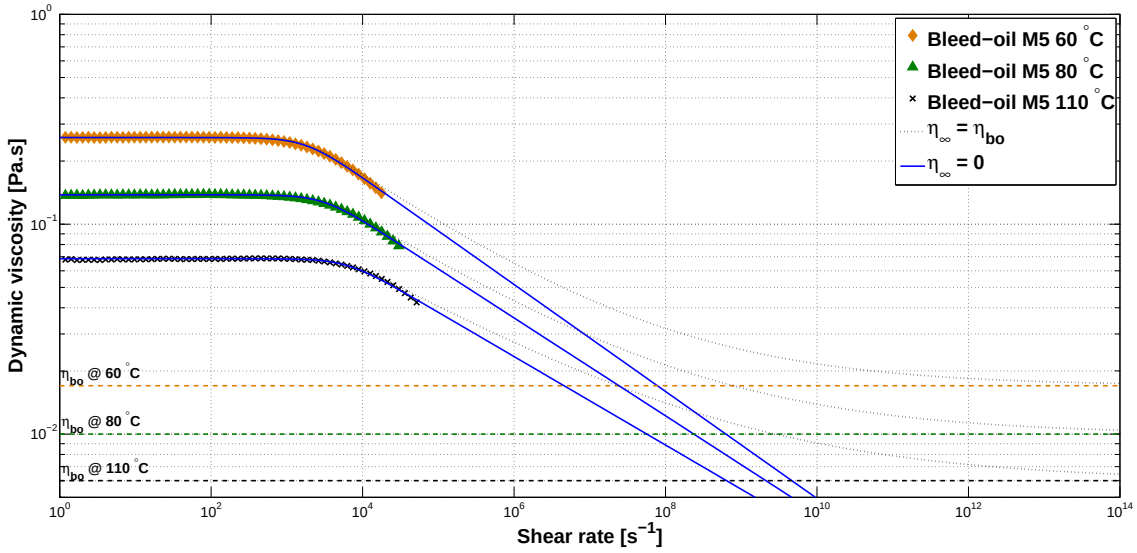

Figure 3.8: Dynamic viscosity of the bleed-oil of grease M5. The prediction using the Carreau viscosity model is also shown, calculated considering that η approaches i) η_{bo} or ii) zero.

Katyal and Kumar [73] stated that when the film thickness of shear-thinning fluids is being predicted using this rheological model to calculate the viscosity, η_∞ can be set as zero without considerably changing the final result.

The ratio between dynamic viscosity and density, shown in Equation 3.2, is called kinematic viscosity. Its value at different temperatures is often used as input in the most common friction torque models. Besides, it generally easy to measure this property, since it does not require expensive equipment.

$$\nu = \frac{\eta}{\rho} \tag{3.2}$$

In the case of this work, the kinematic viscosity was calculated using Equation 3.2. The dynamic viscosity was calculated from an average of 20 points in the linear region - first Newtonian plateau - of the dynamic viscosity curves shown in Figure 3.7. The bleed-oil density was considered to be equal to that of base oil and to decrease with temperature at a factor of $6.24{\times}10^{-4}$ $(g/cm^3)/°C$ (measured according to ASTM D1250). Table 3.2 shows the calculated kinematic viscosity values at 60, 80 and 110 °C. For all curves shown in Figure 3.7 besides the ones of the bleed-oil of grease M5, the calculated kinematic viscosity should be representative of the true kinematic viscosity under the shear rate range tested.

Table 3.2: Kinematic viscosities [cSt] calculated from the low shear dynamic viscosity values.

	60 °C	80 °C	110 °C
PAO base oil	22	13	7
Bleed-oil M2	23	13	7
Bleed-oil M5	322	174	88
PAO blend oil	78	43	21
Bleed-oil MLi	57	29	14
MIN blend oil	55	26	12
Bleed-oil MLiM	58	27	13

Depending on which oil's viscosity is being compared, the following relationships can be established:

$$\text{Base oil: } \nu_{MLi} > \nu_{MLiM} > \nu_{M2} = \nu_{M5};$$
$$\text{Bleed-oil: } \nu_{M5} > \nu_{MLiM} \geq \nu_{MLi} > \nu_{M2}.$$

3.9 Pressure-viscosity coefficient

The viscosity dependency on pressure is generally described by piezoviscosity or pressure-viscosity coefficient. This coefficient is hard to measure since it requires very specific and expensive equipment. In EHD contacts, pressures are typically higher than 1 GPa. Under these conditions, the prediction of the film thickness and friction conditions are highly dependent on how viscosity changes with pressure [47, 74].

In 1893, Barus [75] proposed Equation (3.3) for isothermal pressure-viscosity dependence of liquids, where η_0 is the viscosity at ambient pressure and α_p is the pressure-viscosity coefficient.

$$\eta = \eta_0 \cdot e^{(\alpha_p \cdot p)} \tag{3.3}$$

However, it was found that Barus' equation overestimates the viscosity at high pressures [74,76]. Since then, several isothermal viscosity-pressure formulas have been proposed that usually fit experimental data better than that suggested by Equation (3.3). One of the most accurate approaches was introduced by Roelands in 1966, and is presented in Equation (3.4).

$$\eta(p,T) = \eta_0 \cdot e^{\left[\{ln(\eta_0)+9.67\}\left\{\left(1+\frac{p}{0.1962}\right)^z\left(\frac{T_0-138}{T-138}\right)^{S_0}-1\right\}\right]} \tag{3.4}$$

More recently, Gold *et al.* [77] performed measurements with a high pressure viscometer. Gold *et al.* used the "Modulus-Equation" (Equation (3.5)), which is based on Barus' equation, to obtain a mathematical expression relating the pressure-viscosity coefficient with the high pressure rheology data.

$$\eta(p,T) = \eta_0 \cdot e^{\left(\frac{p}{a_1+a_2\cdot T+(b_1+b_2\cdot T)\cdot p}\right)} \tag{3.5}$$

The a_1 a_2, b_1 and b_2 represent the fluid behaviour and are calculated from the experimental results. The pressure-viscosity coefficient can be calculated from the same parameters, using Equation (3.6).

$$\alpha(p,T) = \frac{ln\ \eta - ln\ \eta_0}{p - p_0} = \frac{1}{a_1 + a_2\cdot T + (b_1 + b_2\cdot T)\cdot p} \tag{3.6}$$

Assuming a relation with kinematic viscosity at atmospheric pressure, Gold *et al.* established Equation 3.7, providing an interesting estimation of the pressure-viscosity coefficient at 0.2 GPa (typical pressure at the contact inlet [78]), which can easily be calculated without high pressure rheology measurements.

$$\alpha = s\cdot\nu^t\cdot 10^{-9} \tag{3.7}$$

The s and t parameters are specific of different natures of base oils [77] and are shown for poly-alpha-olefin and mineral based oils, in Table 3.3.

Table 3.3: Parameters for the calculation of the pressure-viscosity coefficient according to Gold *et al.* [77], valid for 0.2 GPa and temperature range from 45 to 80 °C.

	s	t
Ester	6.605	0.1360
MIN paraf.	9.904	0.1390
MIN naph.	12.517	0.1803
PAO	7.382	1.335

In elasto-hydrodynamic lubrication, the formation of the lubricating film is strongly dependent on the pressure-viscosity behaviour of the lubricant [78], hence its importance. In this work, the pressure-viscosity coefficient of base oils and bleed-oils was calculated to predict film thickness, according to Equation 3.7.

Although this subject was already extensively studied for oils and liquids in general, it was not discussed for greases so far. One of the reasons for this should surely be related to the fact that only the oil released by the grease is expected inside the contact.

3.10 Rheometry

This section is dedicated to the techniques used to study the flow and determine the rheological properties of materials - rheometry. These techniques are specially important for the characterization of non-Newtonian fluids and semi-solids in order to understand the relationship between deformation and stress. Hence, its importance for grease lubrication. Although it is still extremely hard to correlate the rheological properties of the greases to their tribological performance, it is quite common for researchers to characterize different grease samples at least to obtain parameters which enable them to do a qualitative analysis of the grease properties. There are many different techniques to measure such parameters, but unfortunately, they often lead to different results. Due to the lack of standards for obtaining some rheological parameters, the measured results should always be preceded by a full description of the methodology and operating conditions used.

Of the available equipments used to measure the rheological properties of non-Newtonian fluids, the shear rheometer is the most common, working under controlled strain or controlled shear stress methods. Although there are several different configurations and geometries available, the most commonly used are the parallel plates and the cone-plate configurations. Different surface finishing of the plates is also available, varying from smooth to very rough surfaces. Further description of different shear rheometer characteristics can be found in [2, 26].

For grease characterization a large range of shear rates ($10^{-6} - 10^{7}$ s^{-1}) is very important. Still, many errors can be found when performing measurements at such extreme values of that shear rate range. Wall slip is frequently observed at very low shear rates (below 1 s^{-1}) whilst grease leakage, edge effects and viscous heating occur at very high shear rates (above 10^{4} s^{-1}). The selection of the appropriate shear rheometer, geometry type, surface finishing and operating conditions depends on the desired outputs and the sample characteristics. As to the geometries, parallel plates have some advantages over others: they are less sensitive to grease leakage and edge effects due to their geometry and they are the only ones that allow gap-height control and hence, a larger range of shear rates. Regarding the surface finishing of the geometry, rough surfaces are preferred over smooth ones as they are less susceptible to wall slip [79–82]. Extremely rough surfaces, however, may be less reliable [83].

The minimum possible gap size is usually set in order to minimise artefacts from the walls while trying to achieve the highest shear rate possible. However, according to some authors [82, 84], the gap should be at least one order of magnitude above the thickener elements' size. Additionally, the small gaps and high speeds required to reach high shear rates may introduce several errors due to a non-constant shear rate

distribution, inertia of the grease sample, errors in gap settings, viscous heating of the sample and edge fracture [82]. Viscous shear heating was not taken into account since Davies and Stokes [82] showed that the heat generated in the sample is rapidly dissipated into the plates due to the small gap height and therefore, no significant temperature gradients in the rheometer sample are expected.

In this work, a shear rheometer under controlled stress was used. Two different types of tests were performed to analyse the rheological behaviour of the tested greases: oscillatory and rotational. The tests were performed at 60, 80 and 110 °C on a Physica® MCR 301 rheometer, using a smooth plate-plate geometry PP50 (ϕ = 49.998 mm). Although the smooth plate-plate geometry is not ideal, no sand-blasted or rough discs were available. Despite not being the usual temperatures at which rheological measurements are performed, these test temperatures were chosen because many of the tribological testing was also performed at these temperatures. The main test procedures are summarized in Table 3.4.

The same pre-shear procedure was applied to each sample independently of the test type. The pre-shear should not reach too high speeds or last too long to prevent unintended grease loss from the edges, edge fracture or excessive shear degradation [85], which was the case. Nevertheless, it should last long enough to overlap sample history. Each sample was applied on the lower plate with a spoon, without spreading, and then the upper plate was lowered to the desired gap. Following the sample trimming, it was let to recover for 10 minutes at the test temperature, until strain stabilization. Afterwards, an oscillatory movement at a constant strain of 0.1 % and constant angular frequency of 1 rad/s was maintained for 1 min (oscillation in the LVE region for all the samples), followed by another recovery time of 3 minutes without stress applied, after which the main test was conducted. This pre-shear procedure was intended to "reset" the previous history of the grease, clearing internal stresses and reducing the handling differences between samples. All measurements were performed at least twice and a very satisfying reproducibility was achieved using this method.

The oscillatory tests were performed with a gap of 1 mm, since sample leakage by centrifugal forces is not a problem with these tests in which the amplitude and

Table 3.4: Test procedures for rheology measurements.

Type of test	1^{st} stage	2^{nd} stage
Oscillatory	Pre-shear	γ = 0.01 to 200 % ω = 1 rad/s
Rotational	Pre-shear	n = 10^{-4} to 3300 rpm

frequency of the upper plate movement was small. On the other hand, the rotational tests were performed with a 0.2 mm gap to reach the highest possible shear rates (around 10^5 s^{-1}) without sample leakage. However, the occurrence of wall slip at low shear rates was found for these tests due to the plates used being smooth. When visually identifiable on the flow curves, the wall slip effects where taken into account and the corresponding data disregarded.

3.10.1 Oscillatory tests - Storage and Loss moduli

Small-amplitude oscillatory shear (SAOS) was used to study the linear viscoelastic properties of the lubricating greases. An oscillatory shear rate of increasing amplitude at constant frequency is applied at different temperatures while the storage (G') and loss (G") moduli are measured. The storage modulus is related to the elastic properties of grease; the highest is the G'/G" ratio, the highest is the grease stiffness. For fluids showing Newtonian behaviour (as the majority of the base oils), the storage modulus (G') is insignificant. The loss modulus is related to the viscous properties of the grease; the highest is the G"/G' ratio, the highest is the fluidity of the grease.

In the linear viscoelastic region (LVE), the storage and loss moduli are independent of the magnitude of the applied stress/strain and a plateau zone is observed. In this region, the loss modulus is generally much smaller than storage modulus and the grease behaviour is mostly elastic, depending on the type and content of the grease components (mainly thickener and base oil) and their interaction [37]. As amplitude increases, a rapid decay of G' is observed, reflecting the breakdown of grease structure. The grease's elastic behaviour ends and the dissipated energy becomes more important as it reacts to the stress imposed on the internal structure.

The G"/G' ratio is also called phase angle $tan(\delta)$ and expresses the balance between elastic and viscous behaviour. The crossover stress τ_{co} or "flow point", reflects the shear stress at which the storage and loss moduli intersect, $\tan(\delta) = 1$, from which the loss modulus overcomes the storage modulus, indicating flow [86].

This parameter, τ_{co}, is often associated with the yield stress, although they should actually refer to different stress values. The yield stress can be interpreted as an engineering concept referred to as the minimum stress needed for the grease to flow. Its physical interpretation is difficult since there is no consensus on how to effectively measure it and, on the other hand, because it was already observed that flow occurs even before this stress is reached - creep flow [87, 88]. The yield stress τ_y will be defined in this section as the oscillatory stress at which the LVE region ends, considered to be the point at which the complex modulus drops 10% from the

plateau value. However, there are also other ways to address the yield stress as it will be shown in the next section of this chapter.

The Storage and Loss moduli of grease M1, M2 and M3, measured at 60, 80 and 110 °C, are shown in Figure 3.9 as function of the applied shear stress. The temperature increase is responsible for decreasing the grease's viscosity (and consistency). As a consequence, also the storage and loss moduli slightly decrease with it. The storage modulus decreases faster than the loss modulus and therefore, it is also common for the phase angle $tan(\delta)$ to increase with increasing temperature, as the viscous behaviour of the grease becomes more relevant. This behaviour was generally found for all greases, although a few exceptions were found.

Table 3.5 reports the viscoelastic properties of greases M1, M2 and M3 measured at different operating temperatures. As the storage modulus decreases at higher temperatures, it becomes easier for the grease to be deformed (the consistency drops) and the necessary stress to overcome the elastic forces is smaller which means that the yield stress is reached at smaller oscillatory stresses. A few authors reported a much stronger dependence on the temperature [27] than the one reported here, but for tests performed at lower temperatures. A correlation between the yield stress and penetration can be found in [89]. The same behaviour was found for the crossover stress, which generally decreases with the increasing temperature.

According to Table 3.5, is possible to verify that generally the storage and loss moduli increase with the thickener content at any of the tested temperatures, as seen before by other authors [85, 86, 90]. In fact, it seems that all the previously mentioned rheological properties increase for higher thickener content, if the greases are formulated with the same base oil. Since there is more thickener material, the

Table 3.5: Rheological properties of grease M1, M2 and M3 for different operating temperatures, calculated at the linear viscoelastic (LVE) region. The values in bold are referred to exceptions found on the expected behaviour of the viscoelastic properties with increasing temperature.

Grease	M1 (11 % PP)			M2 (13 % PP)			M3 (15 % PP)		
Temp. [°C]	60	80	110	60	80	110	60	80	110
G' [Pa]	16970	12153	**13410**	29279	23170	21122	47709	30560	19880
G" [Pa]	3226	2444	**3756**	5611	4884	3946	8490	5620	3869
$\eta_{ap}{}^*$ [Pa.s]	17035	12305	**13480**	29702	23735	22103	47482	31330	20415
tan(δ)	0.190	0.201	0.280	0.192	0.211	**0.187**	0.178	0.184	0.195
τ_{co} [Pa]	179	114	33	208	187	**189**	302	196	107
τ_y [Pa]	89	71	24	105	**112**	**142**	124	109	79

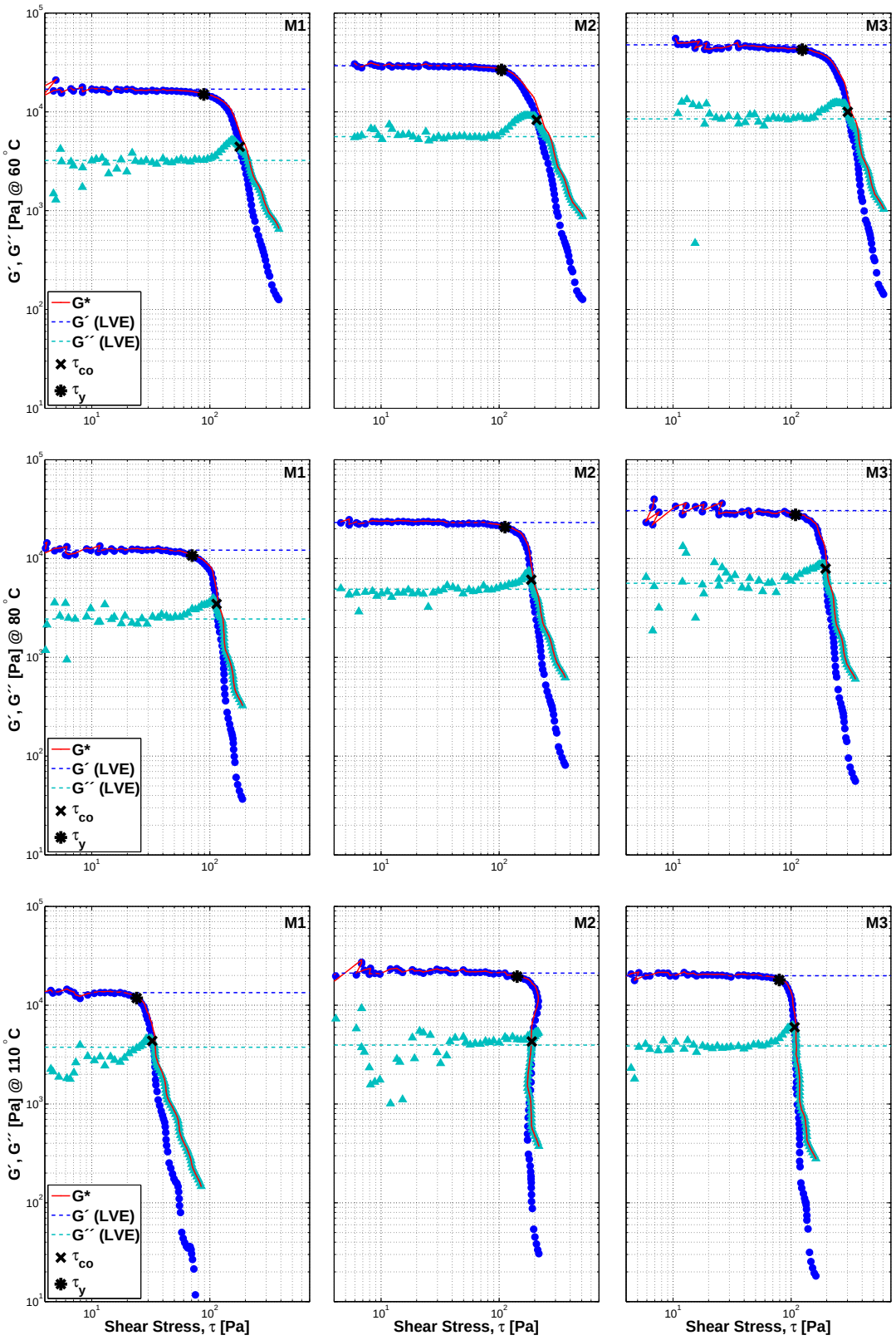

Figure 3.9: Viscoelastic properties of greases M1, M2 and M3.
Note: ● - Storage modulus G', ▲ - Loss modulus G".

elastic properties of the grease are higher. This relationship seems to indicate a stronger gel network with increasing thickener content. Alongside this, the crossover stress τ_{co} and the low shear viscosity η_0^*, also increased with the thickener content, supporting this stronger network theory. However, this might also be related to the fact that, as the thickener content increases, the higher polymer viscosity becomes more relevant to the mixture, therefore increasing the viscoelastic properties.

Figure 3.10 shows the viscoelastic properties of grease M2, M5, MLi and MLiM measured at 60, 80 and 110 °C, as function of the applied shear stress. From this figure it is possible to build Table 3.6 with the calculated values of storage and loss moduli obtained from the LVE region, as well as the yield stress and crossover stress.

Although it does not seem to exit a clear relationship between the results of different formulated greases, as a general rule the storage and loss moduli follow this order:

$$\text{MLi} > \text{M2} > \text{M5} > \text{MLiM}.$$

While it is true that grease MLi is the grease formulated with higher thickener content (17.5 % of LiX) and MLiM the one formulated with the less amount (10.6 % of LiX), the fact that G' and G" also show this relationship might be misleading. No other properties could be correlated with either the base oil viscosity or thickener content when comparing greases of different formulation. The yield and cross over stresses, other than decreasing with temperature, showed no relationship to the thickener content or type.

All the observations reported for greases M1, M2 and M3 regarding the temperature effect on the viscoelastic properties also apply to greases M5, MLi and MLiM.

Table 3.6: Rheological properties of grease M5, MLi and MLiM for different operating temperatures, calculated at the linear viscoelastic (LVE) region. The values in bold are referred to exceptions found on the expected behaviour of the viscoelastic properties with increasing temperature.

Grease	M5			MLi			MLiM		
Temp. [°C]	60	80	110	60	80	110	60	80	110
G' [Pa]	26120	16950	11960	40050	28120	16620	18180	16840	13390
G" [Pa]	5183	4905	3419	6754	6047	4996	1643	**1844**	1578
$\eta_{ap}{}^*$ [Pa.s]	26635	17840	12440	39630	27820	16730	17990	16730	13235
$\tan(\delta)$	0.198	0.289	**0.286**	0.169	0.215	0.301	0.090	0.110	0.118
τ_{co} [Pa]	339	92	67	115	64	50	141	**163**	104
τ_y [Pa]	76	31	43	51	33	12	32	**37**	23

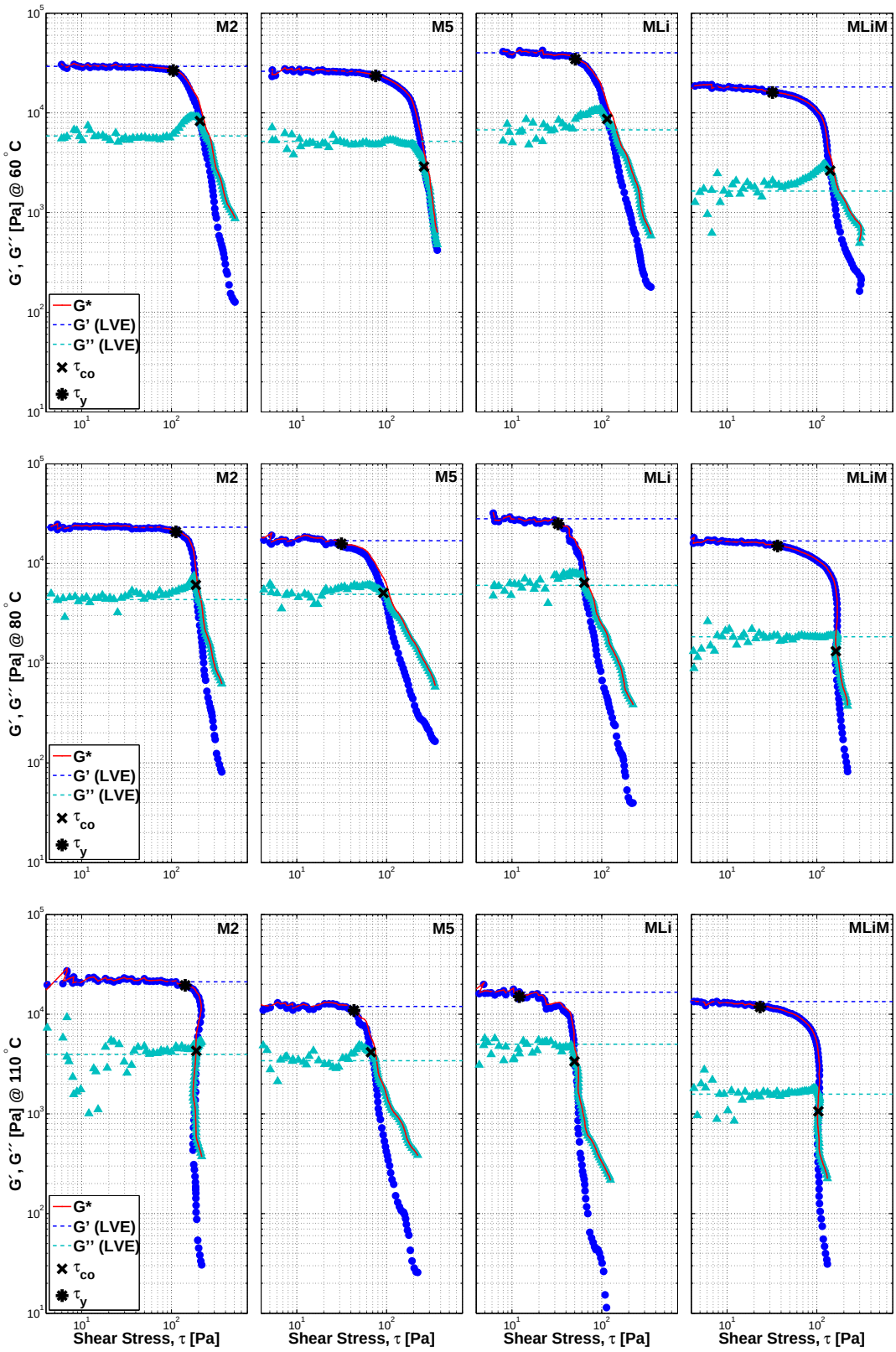

Figure 3.10: Viscoelastic properties of greases M2, M5, MLi and MLiM.
Note: ● - Storage modulus G', ▲ - Loss modulus G".

Apart from a few exceptions, the viscoelastic properties decrease for higher temperature independently of the thickener type/content or base oil viscosity/nature.

3.10.2 Rotational tests - Flow curves

Flow curves usually describe the shear stress and the apparent viscosity behaviour within a large range of shear rates (10^{-6} - 10^{5} s^{-1}) and temperature at atmospheric pressure. Under these operating conditions, Newtonian fluids (such as the majority of the base and bleed-oils shown in Figure 3.7) present a linear increase of the shear stress with shear rate in a logarithmic scale, while the viscosity shows a constant value independently of the applied shear rate.

In the case of lubricating greases and other non-Newtonian fluids/semi-solids, the increasing shear-rate is responsible for a non-linear increase of the shear stress. Furthermore, the apparent viscosity shows "shear thinning" behaviour, greatly decreasing its value as the shear rate grows. This shear-thinning may occur for many reasons as the shear rate increases: alignment of the fibres/elements, loss of junctions between them or even the reduction in width and length due to the break off and rearrangement of the thickener elements.

The flow curves of grease M2, measured at 60 °C, is shown in Figure 3.11. The viscosity curves of the base oil and bleed-oil are also represented, as shown before in Figure 3.7. Although the complete flow curve of grease M2 is represented (circles in grey), only the points represented with a blue square were considered. All the other points were disregarded given the occurrence of wall slip under shear rates below ≈1 s^{-1}. Wall slip is a measurement error characterized by providing an inaccurate value of viscosity, generally by defect, occurring specially under low shear-rate values and hence, easily identifiable in the viscosity curve. The problem with wall slip is that it is extremely dependent on the grease characteristics, which means that it does not occur under the same shear rate range for all the greases and even that range is not equal for the same grease under different operating temperatures.

The viscosity values of the base oil (black star) and bleed-oil (green triangle) under shear rates below 1 s^{-1} were also disregarded. Although the mechanism might not be the same as wall slip, the viscosity values of these oils in this region is not representative of their behaviour and thus, only the plateau region was considered.

The flow curves are often coupled with rheology models, used to extrapolate the shear stress and viscosity values at both low and very high shear rates, at which the rheometers are not capable of accurately measure these properties. The application of these models allows to obtain numerical parameters which can be used not only to compare different grease formulations, but also as tools to model the tribological

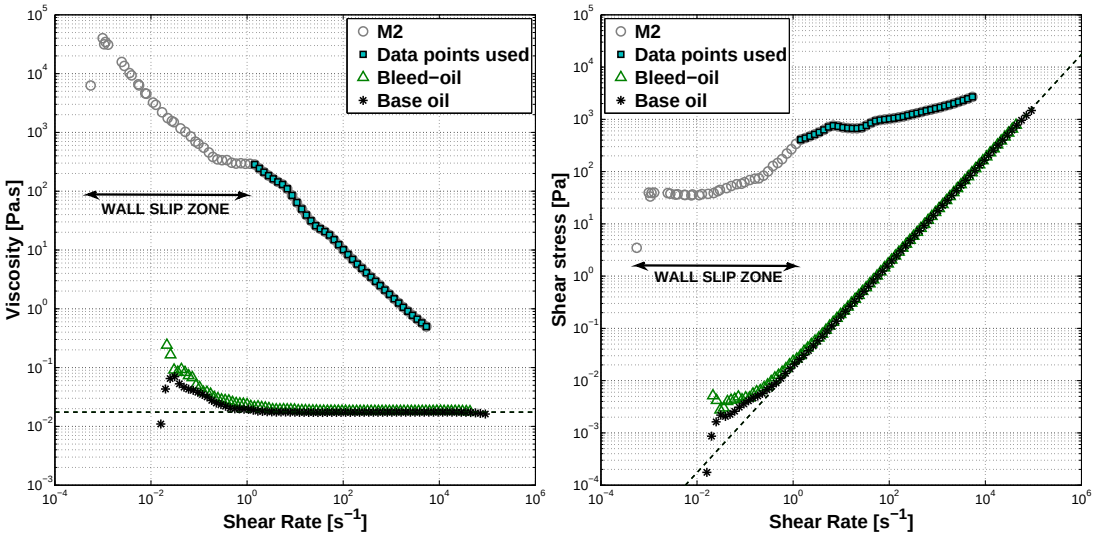

Figure 3.11: Flow curves of grease M2, measured at 60 °C.

behaviour of the grease, e.g., predicting the grease viscosity in the EHD contact. All these models require the optimization of a number of parameters to match the experimental results.

In this work, the measured flow curves were numerically adjusted using three different rheological models. A non-linear least squares algorithm was used to minimize the relative error between the experimental data and the calculated models.

The first method used was the Herschel-Buckley rheological model, corrected to include the base oil viscosity limit when the shear rate tends to infinity - also known as Palacios & Palacios model [91]. The shear stress curve was numerically adjusted using Equation 3.8 [91], where the yield stress τ_y and both k and n factors, were used as optimization parameters. The factor k is usually referred to as consistency index, while the parameter n is the power law or shear-thinning index of the fluid. For greases, the value of n is generally between 0 and 1, indicating a shear-thinning effect, i.e., the viscosity η decreases with the applied shear rate $\dot{\gamma}$. The higher the n, the less shear-thinning the grease is.

$$\tau = \tau_y + k \cdot \dot{\gamma}^n + \eta_\infty \cdot \dot{\gamma} \tag{3.8}$$

The viscosity curve was calculated afterwards, using the same optimized parameters, through Equation 3.9. In this equation, the yield stress τ_y will only be relevant for the low shear rate region.

$$\eta = \frac{\tau_y}{\dot{\gamma}} + k \cdot \dot{\gamma}^{(n-1)} + \eta_\infty \tag{3.9}$$

Following the previous equations, it is possible to observe that the model re-

quires the knowledge of the grease viscosity at very high shear rates, η_∞. Very frequently, it is assumed that this viscosity is equal to that of the base oil. In this very high shear rate zone, the shear-thinning effect slows down as the thickener is completely broken into very small thickener material and therefore, the grease response at this stage should be governed by the base oil with little thickener material dispersed in it [92]. Such assumptions are well accepted since grease typically consists of 80-90 % base oil. However, for some grease formulations, the oil bled by the grease shows quite different properties from the base oil and hence, this bleed-oil should also be taken into consideration. In the case of fresh greases, if the viscosities of the base and bleed-oil are very similar, to consider one or the other for η_∞ has very little influence in the numerical adjustment. However, the same might not be true for grease M5.

Even though some authors consider the existence of a first Newtonian plateau at very low shear rates [93], this plateau could not be observed in the rotational tests. In this region, the grease viscosity should be very high and show Newtonian behaviour. With the increasing shear stress, creep flow starts to occur, up to the point where the shear-thinning behaviour begins. There are a few rheological models which take into account this first Newtonian plateau [94, 95]. One of them is the Carreau model, previously described in section 3.8, regarding the viscosity of the bleed-oil of grease M5. The equation which represents this model is repeated here in Equation 3.10.

$$\eta = \eta_\infty + (\eta_0 - \eta_\infty) \cdot \left[1 + \left(\frac{\eta_0 \cdot \dot{\gamma}}{G_{cr}}\right)^2\right]^{(n-1)/2} \tag{3.10}$$

The advantage of using the Carreau's model is the fact that it requires the optimization of only G_{cr} and n to predict the complete viscosity curve under low and high shear rates. The value of G_{cr} can be interpreted here at the light of the yield stress concept and n is the power-law index: the higher its value, the less shear-thinning the fluid is. This model requires the knowledge not only of the high shear viscosity η_∞, but also the zero shear viscosity η_0. Since the viscosity of the grease was measured in both oscillatory tests (from low to medium shear rates) and rotational tests (from medium to high shear rates), it is possible combine both measurements and produce a complete flow curve for each temperature and evaluate the value of η_0 directly from the results of the oscillatory tests. This concept of zero shear viscosity and first Newtonian plateau, is not widely accepted. Moreover, the procedure in which the oscillatory curves are combined with the flow curves from the rotational tests is also open to discussion since there might be a few errors associated with it.

The Cross model is a rheological model very similar to the previously discussed

Carreau model. This model describes the viscosity according to Equation 3.11.

$$\eta = \eta_\infty + (\eta_0 - \eta_\infty) \cdot \left[1 + (k \cdot \dot{\gamma})^m\right]^{-1} \tag{3.11}$$

where k is the consistency index and m is also the shear-thinning index, similar to n of the previous models. However, in the Cross model, the higher the value of m, the more shear-thinning the grease is. Despite certain parameters represent the same property/behaviour in several models, their values should not be compared quantitatively, since the flow curves are treated very differently in each of them.

The different models can be compared in Figure 3.12, for the flow curves of grease M2 at 60 °C. The high shear viscosity was considered to be equal to the viscosity of the base oil for the three cases. Analysing this figure, it is possible to see that the wall slip region was excluded from the data of interest and not considered for any of the models. In the case of the Carreau and Cross models, this region is replaced entirely by the low shear viscosity curve measured in the oscillatory tests.

Table 3.7 shows the optimized parameters of each model for the flow curves shown in Figure 3.12. For any model, the optimization error increases for higher temperatures. The flow curves at 110 °C are more irregular and therefore, it is harder for the model to approximate these curves with accuracy. It is also clear that the Cross model is the one which shows the worst approximation to the experimental points, at any temperature.

Observing the results of the optimized parameters obtained from all the models, it is possible to see that they actually point to different directions. As the temperature

Table 3.7: Optimization parameters of Palacios & Palacios, Carreau and Cross models obtained for the flow curves of grease M2 at different temperatures.

	Temp.	k [Pa.s^n]	n	τ_y [Pa]	Error [%]
Palacios & Palacios	60 °C	131.3	0.34	342	0.6
$\eta = \eta_\infty + \frac{\tau_y}{\dot{\gamma}} + k \cdot \dot{\gamma}^{(n-1)}$	80 °C	22.7	0.47	696	0.6
	110 °C	1.0	0.66	472	1.7
	Temp.		n	G_{cr} [Pa]	Error [%]
Carreau	60 °C		0.19	186	0.9
$\eta = \eta_\infty + (\eta_0 - \eta_\infty) \cdot \left[1 + \left(\frac{\eta_0 \dot{\gamma}}{G_{cr}}\right)^2\right]^{(n-1)/2}$	80 °C		0.18	165	2.9
	110 °C		0.11	150	3.3
	Temp.	k [Pa.s^n]	m		Error [%]
Cross	60 °C	55.8	0.84		5.0
$\eta = \eta_\infty + (\eta_0 - \eta_\infty) \cdot \left[1 + (k \cdot \dot{\gamma})^m\right]^{-1}$	80 °C	49.4	0.85		6.5
	110 °C	84.5	0.90		8.0

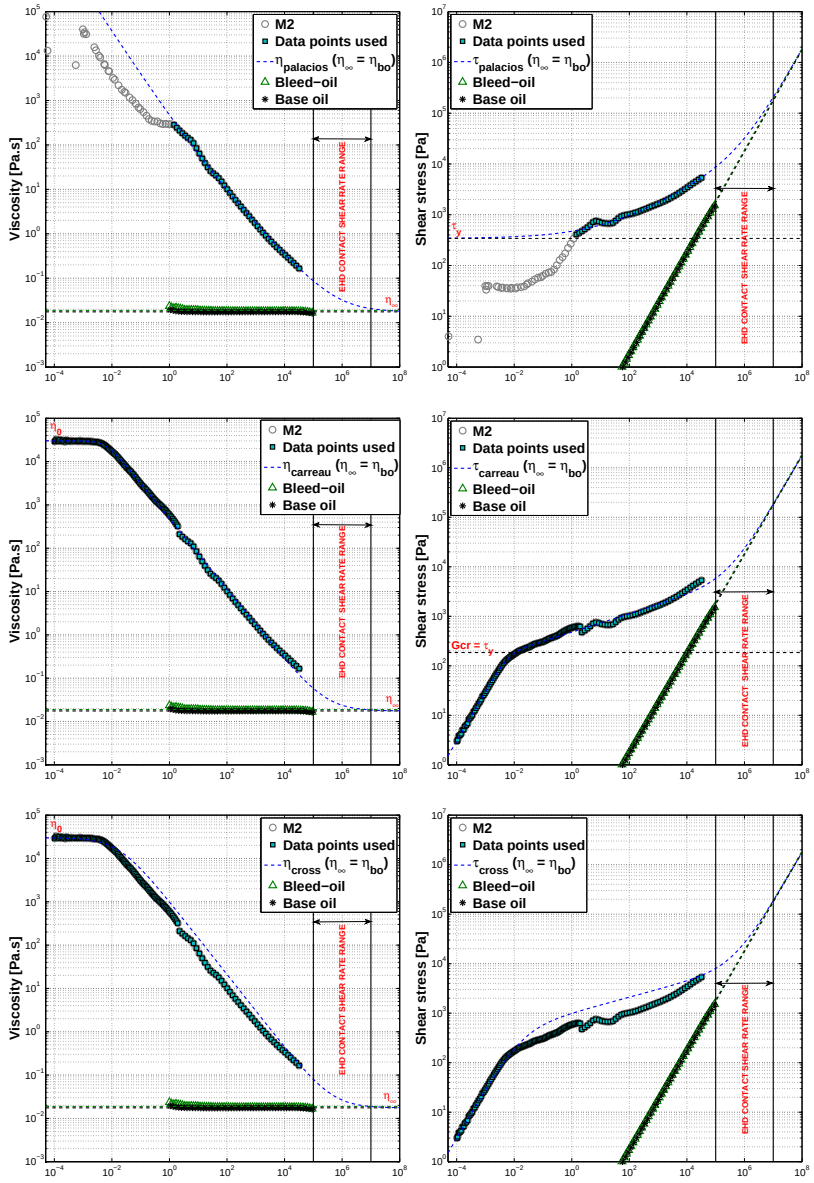

Figure 3.12: Palacios & Palacios, Carreau and Cross rheological models applied to the flow curves of grease M2, measured at 60 °C.

increases, the value of the shear-thinning index of the Palacios & Palacios model increases, while for Carreau model it decreases, albeit slightly. This means that for the first case, the shear dependence is decreasing, while for the second is increasing. In the case of the Cross model, the shear-thinning index also increases with temperature very slightly, supporting the idea that the viscosity dependence on shear rate is higher at higher temperatures.

On the other hand, as the temperature increases, the value of G_{cr} decreases, while the value of τ_y is generally increasing. From the literature, the yield stress should decrease with temperature, as the lubricant becomes more fluid and therefore

the stress required to make it flow should be smaller. The same would be expected from the consistency index: as the temperature increases the value of k should decrease reflecting the decreasing consistency of the grease. This behaviour was observed for both Palacios & Palacios and Cross models, apart from the exception of the Cross model at 110 °C.

Analysing the results under the typical film thickness shear rate range (10^5 - 10^7 s^{-1}), the extrapolated viscosity of the grease might be considerably different from the viscosity of the base oil, whatever the model considered. None of the models showed a clear trend regarding the grease behaviour with temperature, but they all gave good approximations to the experimental data. However, given that the Carreau model requires the optimization of only two parameters while using a larger number of experimental points and the average error was also small, this model was preferred to represent the flow curves of each grease.

Figures 3.13 shows the measured flow curves at 80 °C and the optimized model of Carreau for greases M1, M2 and M3, formulated with the same base oil but different PP content. The optimized parameters are shown in Table 3.8 not only for 80 but also for the curves measured at 60 and 110 °C (which are not graphically represented here). The average error (E) between the optimized curve and the experimental results is also shown. According to both the figure and the table, the value of G_{cr} generally increases with the thickener content from M1 to M3, apart for a few exceptions. On the other hand, the shear-thinning index is more or less constant not only between temperatures but also between greases with different thickener content.

It is interesting to notice that the value of G_{cr}, at any temperature, is between the values of τ_{co} and τ_y, previously calculated in section 3.10.1 (see Table 3.5). This makes this procedure an important technique to determine the critical stress at which flow begins, specially because it combines data from two different measurements.

Table 3.8: Optimized parameters of the model of Carreau, applied to the flow curves grease M1, M2 and M3 at different test temperatures.

	60 °C			80 °C			110 °C		
	G_{cr}[Pa]	n	E [%]	G_{cr} [Pa]	n	E [%]	G_{cr} [Pa]	n	E [%]
M1	154	0.21	1.20	86	0.20	2.88	26	0.22	8.5
M2	187	0.19	1.27	**161**	0.18	1.73	**152**	**0.11**	5.3
M3	233	0.20	0.71	147	0.19	1.34	71	0.19	8.17

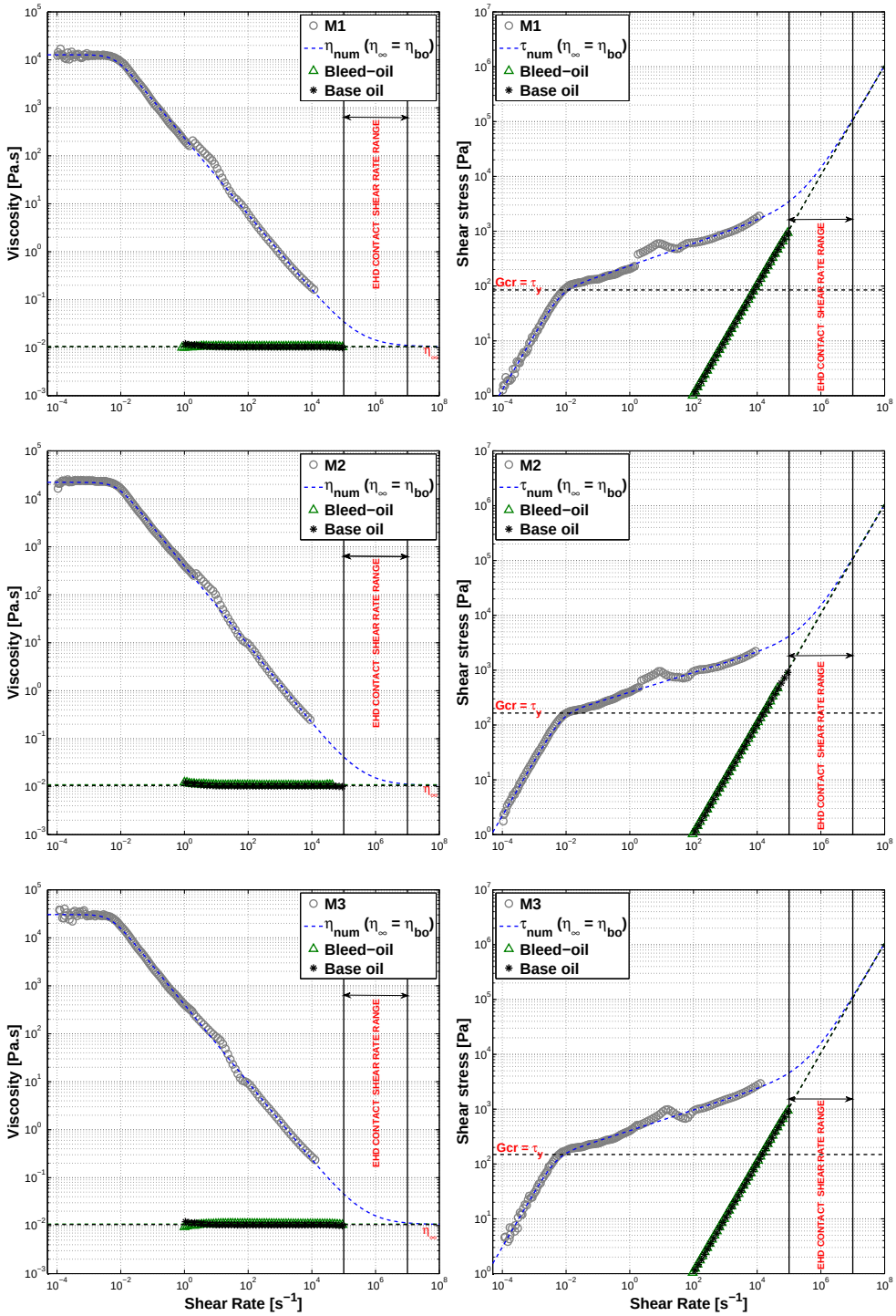

Figure 3.13: Flow curves and optimized Carreau's model of greases M1, M2 and M3, measured at 80 °C.

Figures 3.14 compares the measured flow curves and the optimized model for greases M5, MLi and MLiM. The optimized parameters are shown in Table 3.9 not only for 80 but also for the curves measured at 60 and 110 °C (which are not graphically represented here). The average error (E) between the optimized curve and the

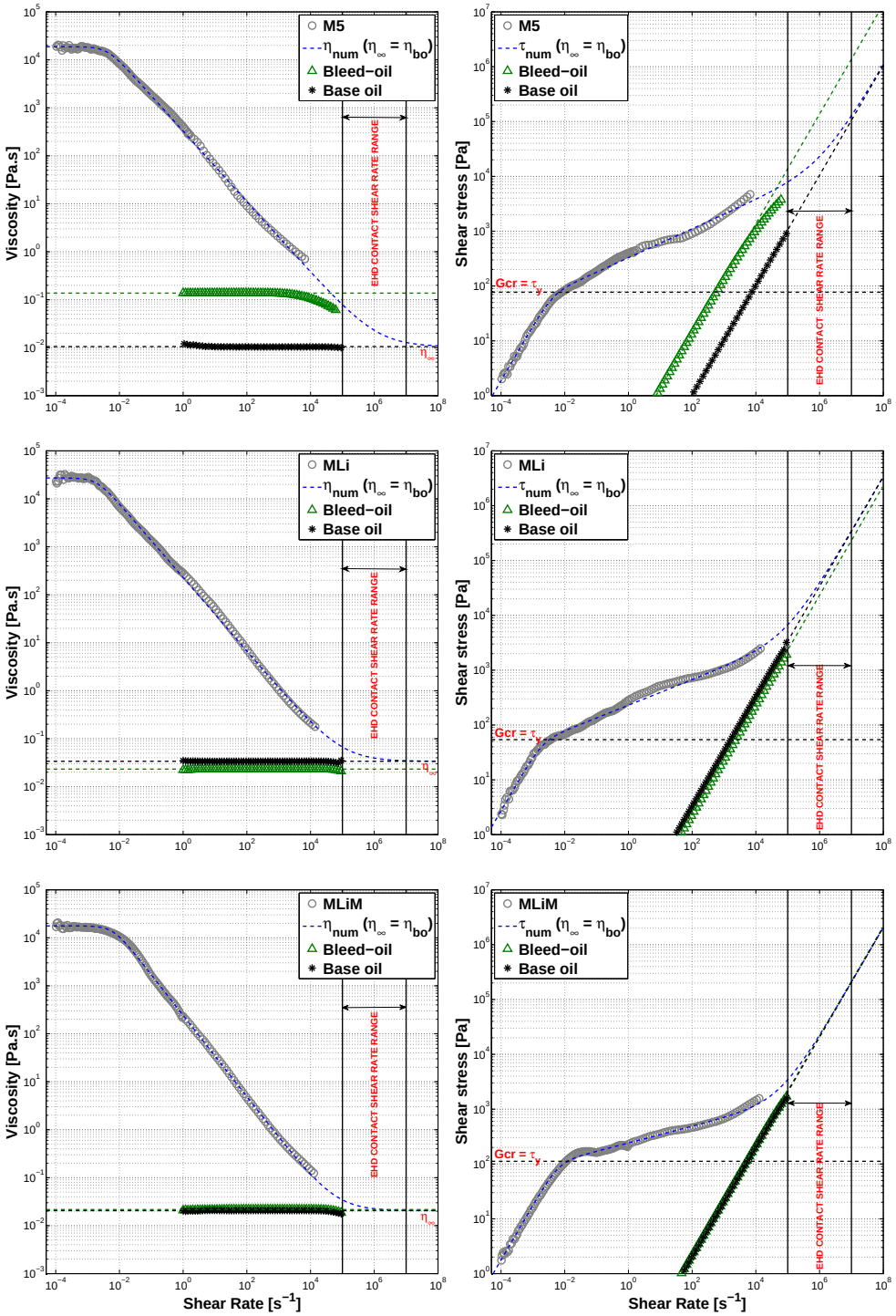

Figure 3.14: Flow curves and optimized model of Carreau, of greases M2, M5 and MLi, measured at 80 °C.

experimental results is also shown.

A few things are worth noticing. The first is related to the value of G_{cr} of grease MLi which is smaller than for any other of the greases whatever the temperature considered. Besides that, the shear-thinning index seems higher for grease MLi and

Table 3.9: Optimized parameters of the model of Carreau, applied the flow curves grease M5, MLi and MLiM at different test temperatures.

	60 °C			80 °C			110 °C		
	G_{cr}[Pa]	n	E [%]	G_{cr} [Pa]	n	E [%]	G_{cr} [Pa]	n	E [%]
M5	134.3	0.24	1.77	79.8	0.26	1.03	53.4	0.25	2.66
MLi	99.2	0.21	0.80	53.7	0.23	1.63	30.4	0.24	1.71
MLiM	111.9	0.19	0.42	111.9	0.15	0.90	63.5	0.14	1.87

specially higher for grease M5. Finally, and most importantly, the flow curve of grease M5 is even farther from the base oil's curve, under the typical shear rate range of the EHD contacts, than any other grease. This indicates that, for this grease, to consider the base oil as representative of the grease behaviour might be a very rough estimation. Observing the viscosity curve of the bleed-oil, it is clearly closer to the numeric flow curve of the grease in this region but given that the bleed-oil itself is shear-thinning it is hard to predict its viscosity.

3.11 Closure

An extensive characterization of each grease and its corresponding base oil and bleed-oil, was performed. The different formulations were discussed regarding the base oil nature/viscosity, the thickener content/type and also the elastomer content.

Samples were characterized chemically through FTIR and the different thickener types and base oil natures were clearly identified. The thickener morphology was studied with SEM and AFM techniques and the differences between different thickener types were addressed.

The physical characterization of the greases was performed through rheological measurements and oil bleeding tests. The influence of the thickener content was observed in both tests. Different rheological models for the grease's shear-thinning behaviour were discussed in relationship to the experimental data available. The optimization of the models to the experimental flow curves of each grease allowed to compare different grease formulations.

The properties of the base oil were compared to the bleed-oil's and discussed with respect to which of them is more representative of the grease behaviour. The elastomer's influence as viscosity improver was also observed.

The observations performed in this chapter will be the cornerstone of the analysis of the tribological behaviour of each grease reported in the following chapters.

4 Film Thickness of fully flooded grease and oil lubricated contacts

4.1 Introduction

The mechanisms which rule the grease lubrication of rolling contacts are still not completely established. While in the case of fully flooded oil-lubricated contacts the EHD theory is well defined, in the case of grease lubrication this theory is more complex.

Still, there has been a growing interest in the topic over the last decades and many studies from different authors have reached a few generalized conclusions. It was already observed that both the oil released from the grease and the thickener lumps cross the EHD contact, contributing to the film formation at low speeds [30, 31, 96]. Other studies also suggest that lubricating greases, with similar formulations, generate higher film thickness for higher base oil viscosities and thickener content [6]. Furthermore, a few authors also found that the grease builds-up a higher film thickness than its base oil, under fully flooded lubrication [28, 30, 31, 97]. This difference was reported to be mainly dependent on the base oil viscosity, thickener type and its content [6].

Cann *et al.*, measured the grease film thickness in a ball-on-disc device and clearly showed that the film thickness h_G was composed by the sum of a static and dynamic film components: $h_G = h_R + h_{bo}$. The static film is a layer adsorbed on the surfaces whether or not in movement (residual layer - h_R), while the dynamic part is due to the elasto-hydrodynamic effect, like predicted by the EHD equations (typical oil film - h_{bo}). Cann [36] also wrote that the thickener will not enter the contact at higher speeds but will be pushed to the side, which means that at moderate to high speeds, the film thickness can be calculated using the standard EHD film thickness equations, using the base oil viscosity as the viscosity of the active lubricant in the contact. Residual films of thickness around 6 nm to 80 nm were found, consisting of significant amounts of thickener [34].

Other authors found that the oil released from the grease under static or dy-

namic conditions ("bleed-oil") can show, for certain grease formulations, very different properties than the base oil [37, 98, 99] and evidence was found that the film thickness and traction coefficient produced by this bleed-oil is much closer to the greases' [39, 40, 99].

More recently, the film thickness behaviour at ultra-low speeds was investigated [100,101] and the thickener contribution to the film thickness formation at low speeds was addressed again. Moreover, the film thickness in rolling bearings lubricated with grease was also measured and a parallelism between full rolling bearing tests and single contact test results was achieved [100, 101].

4.2 Background on the analytical models for film thickness calculation

The film thickness behaviour of base oils with Newtonian behaviour is well understood for a long time. Since these oils do not show significant shear thinning, shear degradation or thixotropic behaviour under typical EHD conditions, there are a few equations which can predict the film thickness very accurately [102–106]. The main differences between these models is the way the viscosity and density were treated regarding pressure and temperature. One of the most accepted models to describe the viscosity dependence on pressure and temperature is the Roelands equation. However, this equation has already been criticised by other authors [107] who have performed very high pressure viscosity measurements for many liquids, claiming that the viscosity does not follow the Roelands law.

Still, the film thickness equation proposed by Hamrock *et al.*, here given by Equation 4.1, was obtained using the Roelands equation to describe the viscosity dependence on pressure and temperature while also considering the fluid to be compressible (Dowson and Higginson [108]). In Equation 4.1, the thermal correction ϕ_T was also included, which contemplates a correction to the film thickness due to lubricant shear heating at the contact inlet [109].

$$h_{0c} = \phi_T \cdot 1.345 \cdot R_x \cdot \bar{U}^{0.670} \cdot G^{0.530} \cdot W^{-0.067} \cdot C_0 \tag{4.1}$$

This Equation 4.1, although very accurate for Newtonian fluids, largely overestimates the film thickness for shear-thinning lubricants [73]. The film thickness of non-Newtonian fluids, which have been the scope of a few authors for the latest years, must consider not only the viscosity dependence on pressure and temperature, but also the dependence on the shear deformation.

Derived by Katyal and Kumar [73] and following a similar approach as Hamrock and Dowson [110], the Equation 4.2 predicts the central film thickness for shear-thinning lubricants in EHD point contacts under pure rolling. The model is a numerical regression based on a full numerical simulation where the Reynolds equation is solved using the Carreau viscosity model and the pressure-viscosity relation of Barus [75].

$$h_0^k = 1.099 \cdot R_{xk} \cdot U_k^{0.652} \cdot G_k^{0.570} \cdot W_k^{-0.042} \cdot \bar{R} \tag{4.2}$$

In this equation, U_k, G_k and W_k are dimensionless parameters very similar to Hamrock and Dowson's parameters. The $\bar{R}$ factor is the shear-thinning correction factor and it also depends on the dimensionless parameters U_k, G_k and W_k. If the lubricant oil presents a non-Newtonian shear-thinning behaviour, $\bar{R}$ will be less than 1, indicating the film thinning. Otherwise, $\bar{R}$ should be equal to the unity allowing to use Equation 4.2, for Newtonian lubricating oils. This $\bar{R}$ factor follows the Carreau viscosity model previously discussed in Chapter 3. According to Equation 3.1, the viscosity curve of a the shear-thinning lubricant should show the behaviour illustrated in Figure 4.1.

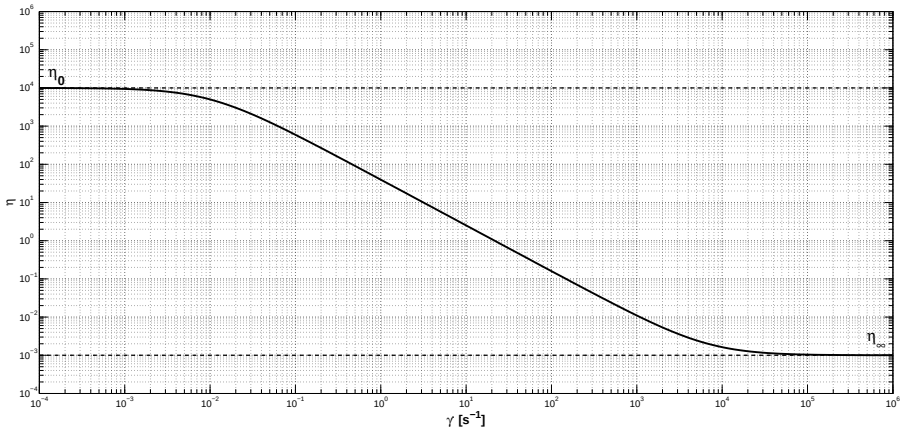

Figure 4.1: Carreau viscosity model representation.

The theoretical film thickness h_{0c}^k can still be corrected to include the inlet shear heating effect, using the thermal reduction factor ϕ_T, as shown in Equation 4.3 [109].

$$h_{0c}^k = \phi_T \cdot h_0^k \tag{4.3}$$

Regarding the film thickness of lubricating greases, the EHD theory for rolling contacts under fully flooded conditions is not fully established yet. The initial film thickness is known to be higher than the film thickness of the base oil in fully flooded

conditions, up to the point where starvation occurs and the film is largely reduced.

The initial fully flooded film thickness has been modelled by some authors assuming the initial thickness to be proportional to the thickener concentration. Hurley even developed an empirical formula for this [46]. Other authors however, chose to use the grease rheology as an input, developing a model for fully flooded grease lubricated contacts [5, 45, 97, 111]. The Herschel-Bulkley and Bingham rheological models are the most commonly used non-Newtonian models. Using these models the authors found slightly higher values of film thickness compared to those calculated with the base oil viscosity only.

Yang and Qian [4], using the Bingham rheology model, showed that the conventional EHD formula could be used for film thickness calculation if the grease's viscosity at high shear rates was used instead of the base oil's. Other researchers developed simple models for film predictions of grease under fully flooded conditions. Examples of these models are shown in Equations 4.4 [6] , 4.5 [4] and the previously referred to Equation 4.6 [112]. The equations were re-arranged to make it easier to calculate the ratio between the film thickness of the grease (h_G) and the film thickness of its base oil (h_{bo}).

$$\frac{h_G}{h_{bo}} = \frac{(1 + B \cdot \Phi)^{0.67}}{100} + 1 \tag{4.4}$$

$$\frac{h_G}{h_{bo}} = \left(\frac{k}{\eta_{bo}}\right)^{0.74} \tag{4.5}$$

$$\frac{h_G}{h_{bo}} = \frac{h_R}{h_{bo}} + 1 \tag{4.6}$$

In Equation 4.4, B is a constant taken as 2.5, according to [6] and Φ is the volume fraction of soap. In Equation 4.5, η_{bo} is the base oil viscosity and k is the consistency index calculated according to Bingham plastic rheological model.

More recently, and already considering the film thickness increase in the very slow speed range observed by several authors [100,101,113,114], Morales-Espejel *et al.* developed a model to reflect this behaviour. The model is capable of characterizing a grease at any operating temperature using only a single film thickness measurement to estimate the effective grease viscosity [115]. The knowledge of this effective grease viscosity is very important to determine the adequate lubrication conditions for a rolling bearing operating at a given speed.

4.2.1 Specific Film Thickness

The concept of specific film thickness (Λ), introduced by Tallian [116] in 1967, is important to identify which lubrication regime the mechanism is running into. Being a single ball-on-disc contact, the contact between a rolling element and the raceway of a rolling bearing or the contact between gear teeth, it is always important to know the specific film thickness for each operating condition in order to understand the relationship between the lubricant's film thickness (h_{0c}) and the roughness of the intervening surfaces (σ_1, σ_2) as shown in Figure 4.2. The specific film thickness can be calculated with Equation 4.7:

$$\Lambda = \frac{h_{0c}}{\sigma} \tag{4.7}$$

where σ is calculated with Equation 4.8.

$$\sigma = \sqrt{{\sigma_1}^2 + {\sigma_2}^2} \tag{4.8}$$

According to Spikes [117] and following the scheme of Figure 4.2, the full film condition is reached when Λ is higher than 3, which means that the lubricant film completely separates the surfaces and its thickness is much higher than the composite

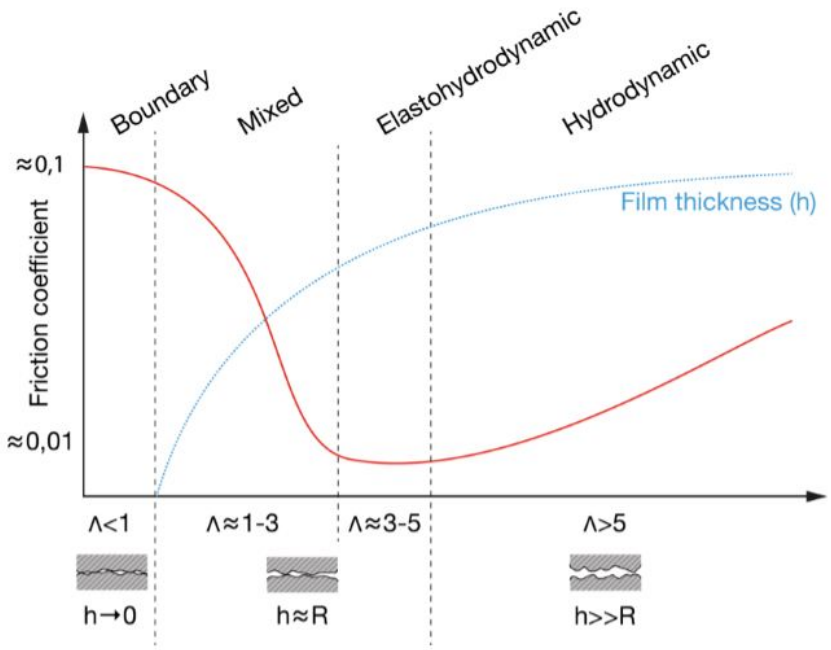

Figure 4.2: Typical Stribeck curve of a lubricant under constant load, temperature and slide-to-roll ratio and its correlation to the film thickness curve under the same operating conditions.

roughness of the surfaces. If Λ is less than 3, the mechanism is running under mixed lubrication which means that the lubricant film is still able to separate the rolling surfaces, despite it is already frequent for metal-to-metal contacts to occur. The lubricant film thickness is now around the same order of magnitude than the surfaces' roughness. When the specific film thickness goes under 1 (and particularly below 0.5, according to [117]) the boundary lubrication regime is reached. The lubricant film can no longer separate the surfaces and the load is now supported by the surface's asperities which means that the lubricant's film thickness is now smaller than the composite roughness of the surfaces. Although it is common to calculate the specific film thickness using the central film thickness (h_{0c}), it might be important to calculate it using the minimum film thickness (h_m), specially when the operating conditions are such that the lubrication regime approaches boundary film lubrication.

4.3 Film thickness measurement procedure

The EHD2 is an equipment produced by PCS Instruments which allows the measurement of the lubricant film thickness in ball-on-disc or roller-on-disc configuration, over different ranges of temperature, speed, load and slide-to-roll ratio. The device uses the space layer interferometry method which allows the measurement of thin-films using the setup shown in Figure 4.3. Light is shone into the contact between the ball and the disc. Part of this light is reflected from the underside of the glass disc and some passes through any lubricant film and is then reflected back from the steel ball. Since the two beams of light have travelled different distances they interfere, resulting in an interference image from which the film thickness can be computed.

The test conditions are shown in Table 4.1. Before each test a heat period of 30 minutes was applied to ensure the temperature stabilization. After this period, the space layer thickness was measured at the disc track radius, without any lubricant between the ball and the disc to set the zero and trigger point. The entrainment speed was then ramped up 3 times ranging from ≈0.01 to 2 m/s at constant slide-to-roll ratio, and a combined curve of the three measurements was created. The entrainment speed and SRR are defined according to Equations 4.9 and 4.10, respectively.

$$U = \frac{u_{disc} + u_{ball}}{2} \tag{4.9}$$

$$SRR = 2 \cdot \frac{|u_{disc} - u_{ball}|}{u_{disc} + u_{ball}} \tag{4.10}$$

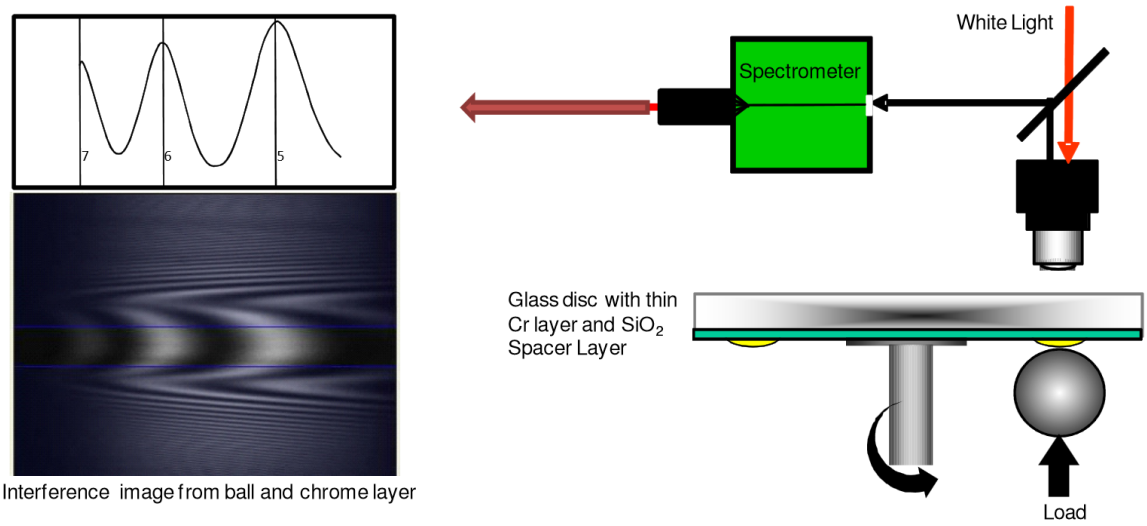

Figure 4.3: Diagram of the optical interference technique used in the EHD2 equipment.

Table 4.1: Ball-on-disc test conditions for film thickness measurement.

	Ball	Disc	Units
Radius - $R_{x,y}$	9.525	∞	mm
Average roughness - Ra	$\leq$ 20	$\approx$ 5	nm
Material	AISI 52100	Glass	—
Elastic modulus - E	207	64	GPa
Poisson coefficient - ν	0.29	0.20	GPa
Load - F	50		N
Entrainment speed - U	0.01-2		m/s
Slide-to-roll ratio - SRR	3		%
Temperature - T	20, 40, 60, 80, 110		°C
Equivalent modulus - E*	$\approx$ 51.8		GPa
Maximum Hertzian pressure - p_0	$\approx$ 0.66		GPa
Hertzian half-width - a	$\approx$ 190.7		μm

The fully flooded condition was ensured using a grease scoop which forced the grease back into track. The temperature deviation at each ramp up was inferior to ±2 °C from the average.

At the end of each ramp up, a zero speed film thickness was also measured, allowing to identify if the disc track has been damaged in the process (measuring a negative film thickness) and at the same time, measuring the residual film thickness between ball and disc. The zero speed film thickness is measured after unloading the

ball and without entrainment speed. The full load (50 N) is then re-applied and the static film thickness is measured only after 5 seconds, allowing the squeezed film to spread. An average of the three measurements for each grease was calculated.

4.3.1 Space Layer Imaging Method (SLIM)

The EHD2 equipment can also be adapted to measure the film thickness profile across the full contact area, using the SLIM method [118]. Instead of using a spectrometer to determine the wavelength of the light returned from the image of the EHL contact, this method uses a high resolution sensitive RGB (red, green, blue) colour camera to capture an interference image of the whole contact area. The colours of the pixels can be used to calculate the film thickness based on a previously determined colour-space calibration to match the colours in the image to effective film thickness values. This method allows to produce 3D maps of the film thickness across the contact area very quickly.

Although it is possible to grab images of any film thickness profile, the colour-space calibration only allows to determine the thickness of very thin lubricant films (0-250 nm) with a resolution of ±5 nm. The film thickness of grease lubricated contacts under fully flooded conditions is quite frequently above the maximum value and therefore, this technique was used to analyse the film thickness evolution despite not being used to calculate the central or minimum film thicknesses.

4.4 Oil lubricated contacts - results

4.4.1 Base oil film thickness

In order to correctly understand grease lubrication, it is also necessary to investigate the behaviour of its base oil. Three different base oils were used in the formulation of the greases tested in this work. Two of them are synthetic and the other is a blend of mineral nature. The nature of the synthetic oils is poly-alpha-olefin (PAO) but they have different viscosity grades. Moreover, one of them was also blended with 5 % of an ester based oil. Hence, the characteristics of these three base oils are quite different (please refer to Table 3.1 of Chapter 3).

In Figure 4.4, the measured film thickness of the base oils is shown at different operating temperatures. The tests were all performed using the same procedure shown in the previous section and Table 4.1, but the entrainment speed range was not always the same depending on the test's operating temperature. With increasing temperature the film thickness would reduce and the glass disc might be ruined if the

film thickness dropped to a very low value. With this in mind, the tests performed at higher temperature generally started at higher entrainment speeds.

According to Figure 4.4, it is possible to observe the film thickness decrease with temperature for all base oils. As the viscosity drops, the lubricant film is also reduced. As expected, the film thickness (h_{bo}) at any temperature is higher for the base oils of also higher viscosity, following this order:

$$h_{bo}{}^{MIN\ blend} \geq h_{bo}{}^{PAO\ blend} > h_{bo}{}^{PAO\ base} \tag{4.11}$$

It is also interesting to notice the decrease of the film thickness due to thermal effects at high entrainment speeds and low operating temperature (20 and 40 °C) for the Mineral and PAO blend oils. The high viscosity of these oils at these temperatures

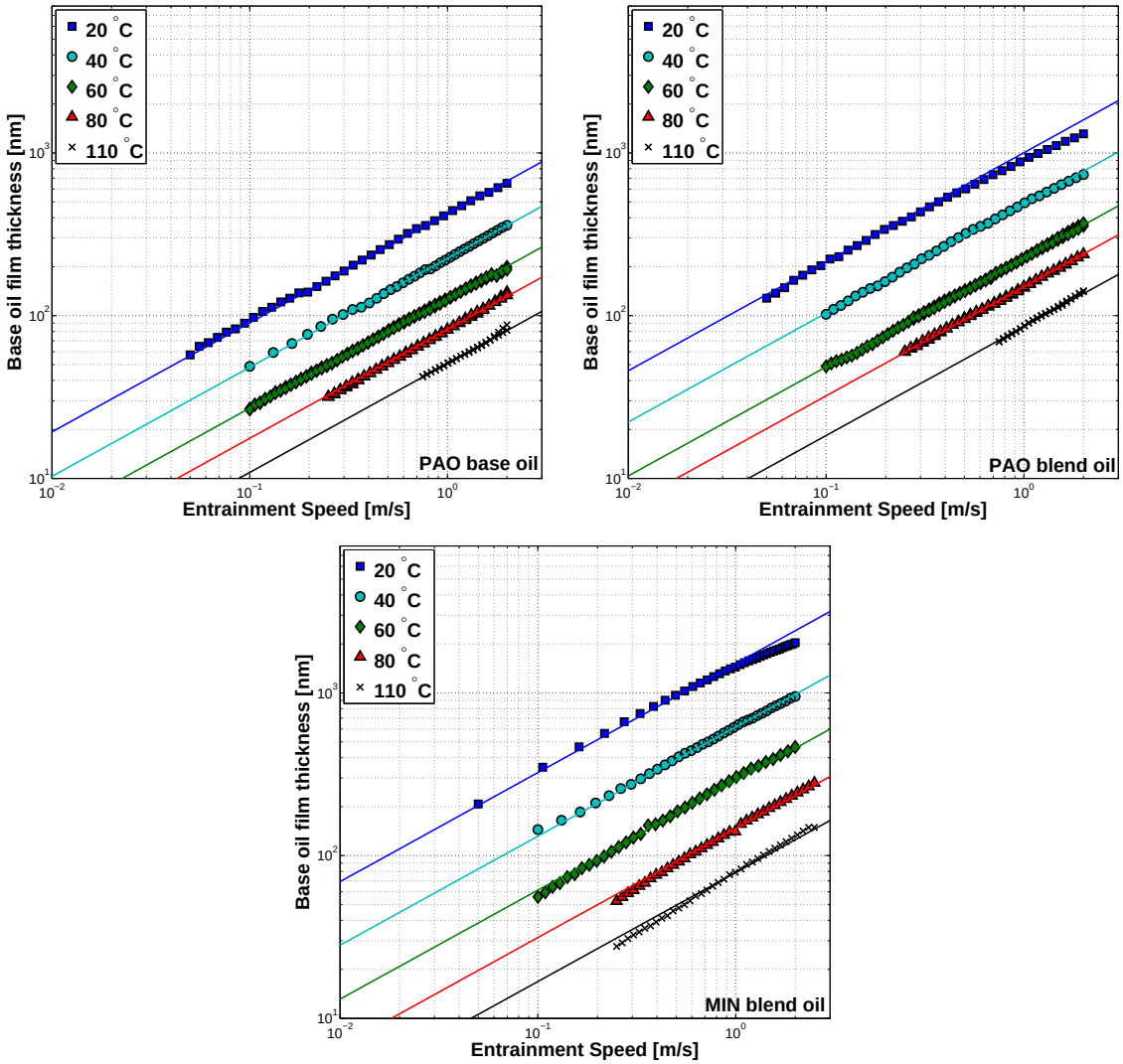

Figure 4.4: Film thickness of the PAO base oil, PAO blend oil and MIN blend oil, measured at different operating temperatures.

generates an overheating at the contact meniscus and consequently, the viscosity drops decreasing the film thickness in the process.

In the end of the test at each temperature, the zero speed film thickness was measured. The measured values were always below 10 nm and no correlation between different formulations was found.

4.4.2 Bleed-oil film thickness

The film thickness of the oil bled by the grease, here called bleed-oil, was also measured. The results at 60, 80 and 110 °C are shown in Figure 4.5. Some of the previously shown results obtained with the base oil are also shown for easier comparison.

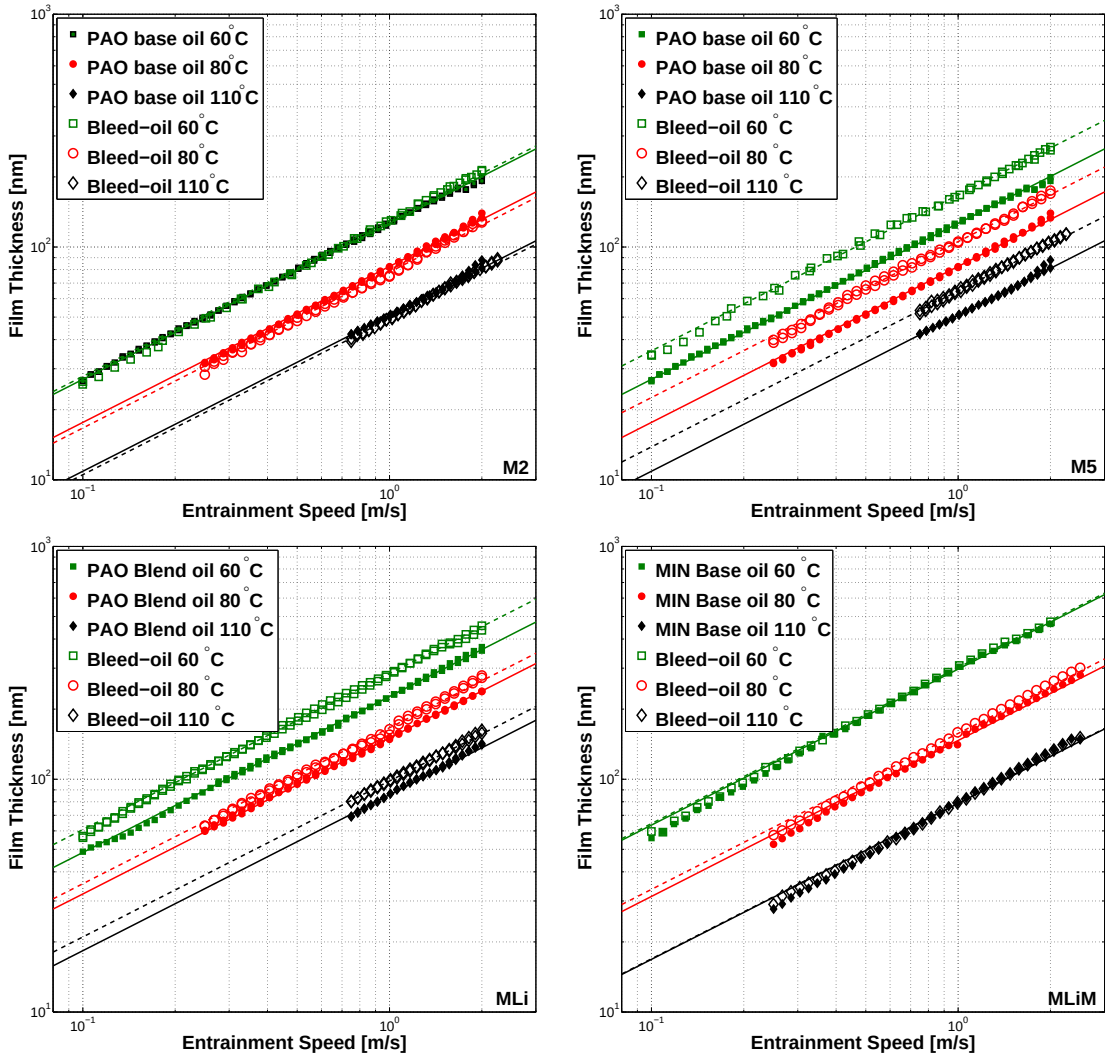

Figure 4.5: Film thickness of the bleed-oils of greases M2, M5, MLi and MLiM measured at different operating conditions. The base oil's film thickness measured under the same operating conditions temperatures is also shown.

According to Figure 4.5, the same behaviour observed for the base oils is also observed here. The film thickness increases linearly with the entrainment speed in logarithmic scale and decreases with increasing temperature, following the decrease of the lubricant's viscosity. The thermal effects at high speeds found at 20 and 40 °C for the base oil of greases MLi and MLiM, were not observed since these tests were only performed at temperatures higher than 60 °C.

Whenever the base oil shows the same viscosity as the bleed-oil, their film thickness is also very close, which is the case of grease M2 and MLiM. However, for grease M5 and MLi, given that their bleed-oils show different properties than the base oils, the film thickness is also different. The bleed-oil of grease M5 shows a higher viscosity that the base oil used in its formulation and despite being highly shear-thinning even at low shear rates, its film thickness is still higher.

A different behaviour was found for the bleed-oil of grease MLi. Despite its viscosity being smaller than the viscosity of the base oil, the film thickness is still higher for the bleed-oil. Since the tests were performed exactly under the same conditions and hence the replenishment should also be the similar, the other relevant parameter which could explain the difference is the pressure-viscosity coefficient. Therefore, the film thickness of the bleed-oils (h_{bl}) follows a different order from their viscosity:

$$h_{bl}{}^{MLi} \geq h_{bl}{}^{MLiM} > h_{bl}{}^{M5} > h_{bl}{}^{M2} \tag{4.12}$$

The zero speed film thickness was measured, the same way as with the base oils. The measured values were always below 10 nm and once again, no correlation between different formulations was found.

4.4.3 Film thickness prediction of base and bleed-oils

There are several equations commonly used to predict film thickness of lubricating oils. The main differences between these models are related to the way the viscosity and density behaviour is modelled regarding pressure and temperature. The pressure-viscosity coefficient (α) is one of the most important parameters to calculate the film thickness, since it defines the way the viscosity changes with the high pressures involved in the EHD contact. This parameter however, is very hard to measure and it requires the use of very specific and complex equipment.

For a certain range of contact pressures, the α-value can be predicted using Gold's equation [77], using specific parameters for each oil nature. Still, quite frequently, the film thickness calculated using this α-value is very far from the experimental measurements.

The Hamrock and Dowson's (H&D) equation was used to predict the film thick-

ness for the base oils and for the non-shear-thinning bleed-oils, using the Gold's equation for the calculation of the pressure-viscosity α-value. However, the bleed-oil of grease M5 shows shear-thinning behaviour and therefore, for this bleed-oil only, the Katyal and Kumar's model for shear-thinning fluids was used. The results are shown in Figure 4.6.

Despite being close for certain operating conditions, the predictions do not match the measured film thickness. The predictions for the PAO and the MIN base oils are very close, especially at high temperatures, but generally they underestimate the measured film thickness. The predictions for the bleed-oils of greases M2 and MLiM follow the same behaviour. In the case of the PAO blend oil, the predictions

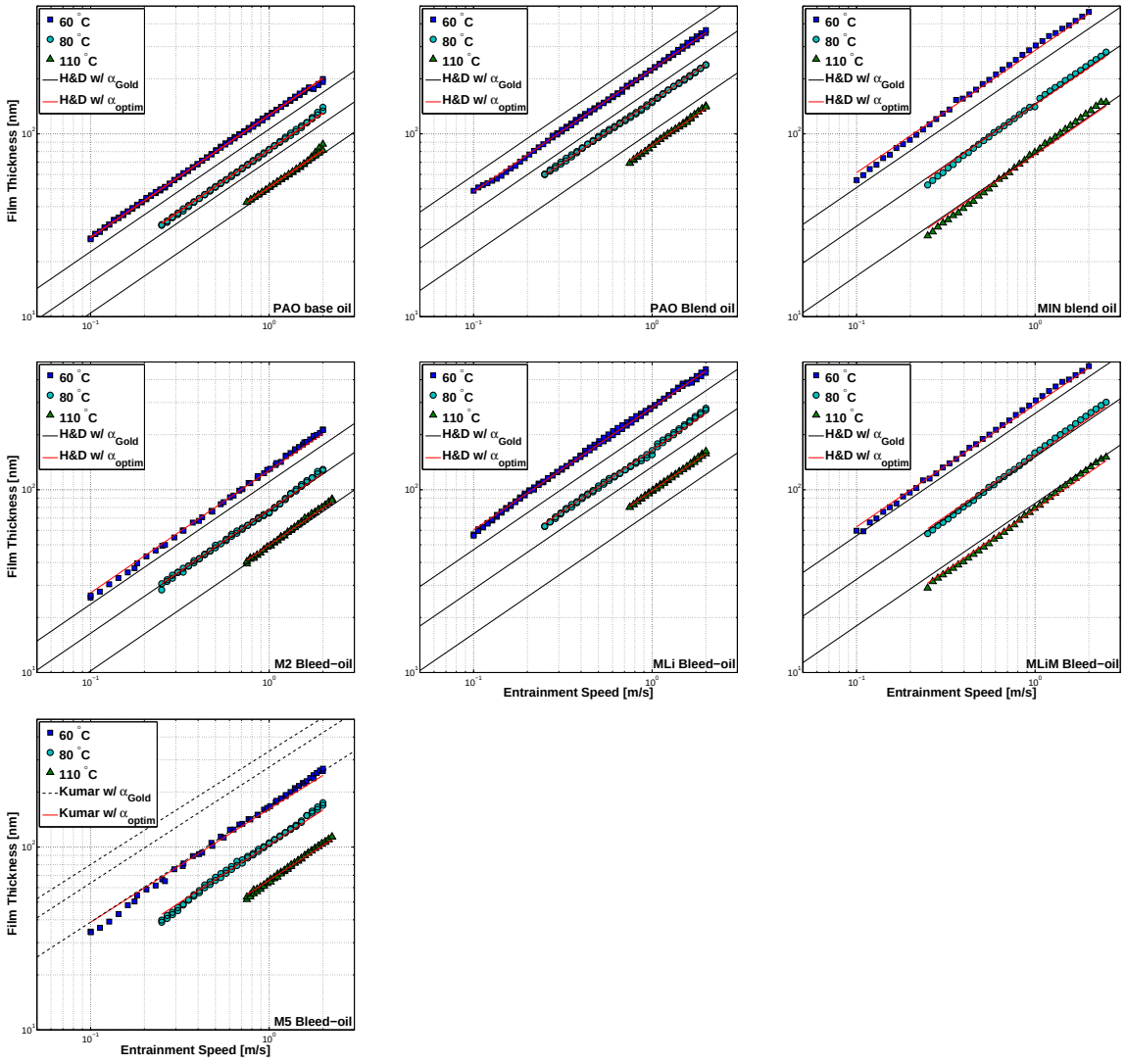

Figure 4.6: Film Thickness measurements of base and bleed-oils at different temperatures. The film thickness predictions according to Hamrock and Dowson (H&D) or Kumar *et al.* are also shown, calculated using the pressure-viscosity value obtained through Gold's Equation (α_{Gold}) and also its optimized value (α_{optim}).

are far higher than the measured values even for the tests at higher temperature. However, in the case of the bleed-oil of grease MLi, the opposite behaviour is observed and the predictions are smaller than the measured values. The differences observed should certainly be related to the way the pressure-viscosity coefficient is calculated.

The film thickness measured with the bleed-oil of grease M5, shows a much smaller value than its prediction calculated with the Katyal and Kumar's model. The difference should be related not only to the way the pressure-viscosity coefficient is calculated using Gold's equation (the kinematic viscosity used was calculated from the first Newtonian plateau, even though the oil is shear-thinning) but might also be due to the inaccurate calculation of the G_{cr} and n parameters or even due to the way the shear-thinning behaviour is being taken into account in Katyal and Kumar's model.

Recently, Van Leeuwen [119, 120] have used film thickness measurements to inversely calculate the pressure viscosity coefficient, which seems to be the suitable way to determine the α-value when high pressure viscosity measurements are not available. However, Bair *et al.* [121,122] contested these measurements, showing that the α-value obtained with this process could be much different values depending on the geometry (and consequent scale effect) used for the film thickness measurements. Nevertheless, in this work, a similar approach to Van Leeuwen's was used, and the α-value was optimized to match the experimentally measured film thickness of each base and bleed-oils.

Table 4.2: Optimized pressure-viscosity coefficient α [GPa^{-1}], calculated from the film thickness curves measured at different operating temperatures.

Temperature [°C]		60	80	110
PAO base oil	α_{Gold}	11.1	10.4	9.7
	α_{optim}	14.1	12.9	11.6
M2 bleed-oil	α_{Gold}	11.2	10.5	9.7
	α_{optim}	12.8	11.8	10.8
M5 bleed-oil	α_{Gold}	16.0	14.7	13.4
	α_{optim}	**3.4**	**3.3**	**3.2**
PAO blend oil	α_{Gold}	13.1	12.1	11.1
	α_{optim}	9.2	8.7	8.1
MLi bleed-oil	α_{Gold}	12.6	11.5	10.5
	α_{optim}	21.2	18.3	15.6
MIN blend oil	α_{Gold}	17.3	15.6	14.0
	α_{optim}	19.2	16.5	14.0
MLiM bleed-oil	α_{Gold}	17.4	15.7	14.1
	α_{optim}	18.7	16.1	13.8

After the optimization of the pressure-viscosity coefficient, the predictions show a very good agreement with the experimental results, as shown in Figure 4.6. The optimized pressure-viscosity coefficient values are shown in Table 4.2. As expected, the pressure-viscosity coefficient decreases with temperature, following the decrease of viscosity. The optimized coefficients are of the same order of magnitude but their value is higher than those predicted using Gold's equation, with the exception of the PAO blend oil and the bleed-oil of grease M5 whose optimized coefficients are smaller.

The optimized s and t parameters for Gold's pressure-viscosity coefficient equation, are shown in Table 4.3.

Table 4.3: Optimized s and t parameters.

	s	t
PAO base oil	8.084	0.1818
M2 bleed-oil	7.762	0.1594
M5 bleed-oil	2.569	0.0466
PAO blend oil	5.831	0.1055
MLi bleed-oil	9.813	0.3012
MIN blend	8.429	0.2054
MLiM bleed-oil	9.479	0.2783

4.5 Grease lubricated contacts - results

In Figure 4.7, the film thickness results of grease M2, M5, MLi and MLiM are shown, measured at different operating temperatures. As observed by several other authors, under moderate to high speeds the film thickness of all greases increases with the entrainment speed at rate of $\approx U^{0.67}$. This factor of 0.67, predicted by Hamrock and Dowson's equation, was found to be slightly different for each grease, despite it did not change much with temperature. This behaviour is illustrated by the dotted straight lines shown in Figure 4.7, which represent the slope of the film thickness, increasing linearly with the entrainment speed in a log-log scale. It is also possible to verify that the film thickness in this region decreases with the increase of the operating temperature. As the viscosity decreases, the lubricant film will also become smaller.

According to these results, it is interesting to notice that the film thickness behaviour under moderate to high speeds is independent of the thickener type or the base oil nature/viscosity. However, it is also clear that the base oil viscosity has a great influence on the film thickness value at this speed range: the higher is the base oil viscosity, the higher will be the film thickness in this region.

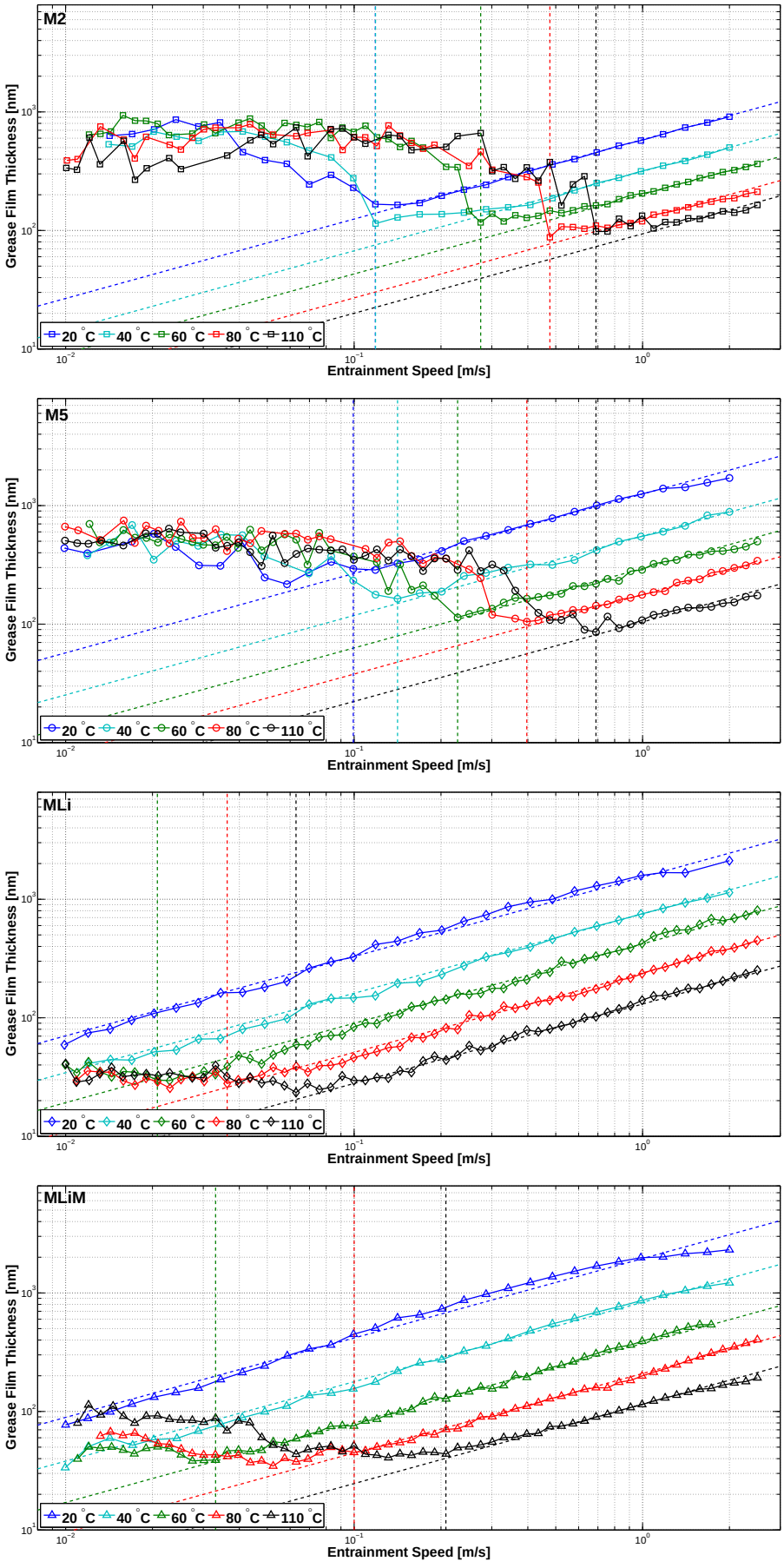

Figure 4.7: Film thickness of greases M2, M5, MLi and MLiM, measured under different operating temperatures.

As a general rule, the following relationship can be established regarding the film thickness under moderate to high speeds, at any operating temperature:

$$h_G{}^{MLiM} \geq h_G{}^{MLi} > h_G{}^{M5} > h_G{}^{M2} \tag{4.13}$$

The LiX thickened greases, formulated with base oils of higher viscosity than the PP thickened greases, also show higher film thickness in this region, as expected.

At low entrainment speeds, the behaviour between greases formulated with different thickener types becomes more relevant. Below a certain transition speed (u_{tr}), the film thickness increases with the decrease of the entrainment speed at a very high rate until it reaches a plateau. In this region, the measurements fluctuate widely and lead to a very high standard deviation which presumably should be related to more frequent thickener lumps entering and leaving the contact [92].

In this particular zone, the polymer thickened greases show much higher film thickness than the lithium thickened greases. Since this is the opposite behaviour observed in the moderate to high speeds range where the base oil viscosity has the greater influence, the differences verified in the low speed region should be related to the thickener type or even its morphology/size. In fact, in this region, the order of magnitude of the film thickness and that of the thickener's diameter (PP elements or Li fibres), is very similar.

To address this difference in behaviour, contact area pictures of the film thickness profile were also obtained for the same entrainment speed range, using the SLIM method which allows to obtain the complete film thickness profile over the contact area. The resulting images are shown in Figure 4.8. The central film thickness curves at 60 °C of greases M1 and MLi are also shown, for easier comparison.

Analysing the film thickness profiles at low entrainment speeds (for instance, picture A), it is possible to observe thickener lumps entering the contact for both types of greases (M1 and MLi). However, with the increasing entrainment speed, the film thickness behaviour starts to change and after reaching a certain transition speed, the film thickness profile resembles an oil-like contact, showing the typical horse-shoe profile (picture B).

The transition speed showed poor repeatability and was often found at slightly different values which could be related to the initial amount of grease available or its distribution. Still, it is interesting to notice that the transition speed happens at much higher speeds for the polymer greases than for the lithium greases. This fact should be related to the thickener size and to how easy it should be for the thickener lumps to be pushed off to the sideways of the contact area. Not only the transition speed is much smaller for the lithium greases, but also the plateau is

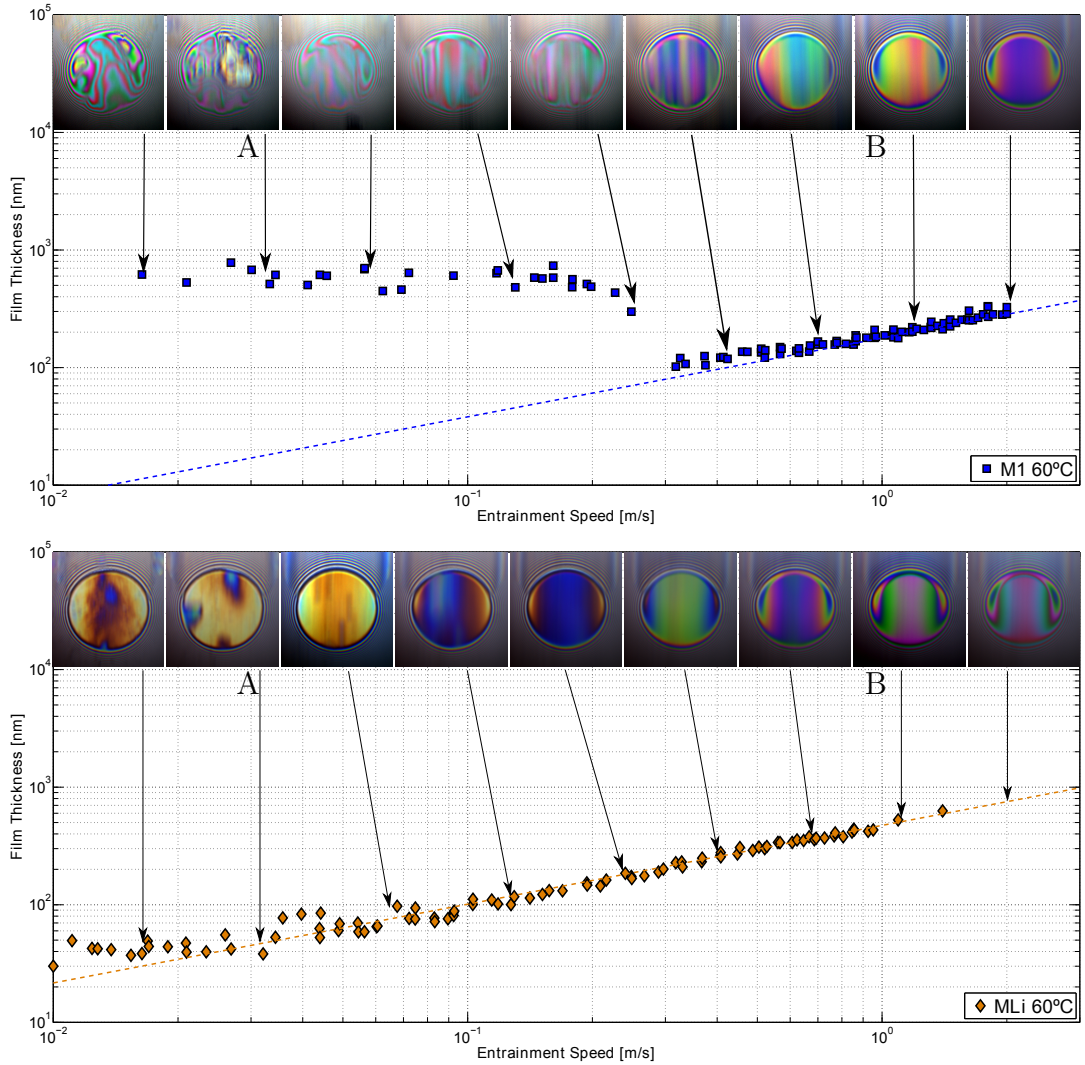

Figure 4.8: Film thickness measurements of grease M1 and MLi at 60 °C. Pictures of the film thickness profile over the contact area are also shown.

reached at a much lower entrainment speed, resulting into a lower film thickness in this region. Other authors have tested similar greases also formulated with lithium complex and found values of the film thickness plateau higher than those reported in this work [100, 101]. Furthermore, the transition speed increases with increasing temperature, as the curves move down and to the right, reflecting the decrease of the lubricant's viscosity [100, 101, 115].

Table 4.4 shows the average value of film thickness in the plateau region h_{pl} and its standard deviation σ, for each grease at different operating temperatures. The transition speed value u_{tr} is also shown, as well as, the average zero speed film thickness of the three measurements at each temperature. This transition speed was defined as the first speed value at which the film thickness is in the linear region under moderate to high speeds. According to Table 4.4, the standard deviation

Table 4.4: Transition speed and film thickness at the plateau region of greases M2, M5, MLi and MLiM at different operating temperatures. The zero speed film thickness (h_R) is also shown.

Grease		20 °C	40 °C	60 °C	80 °C	110 °C	Avg.
M2	u_{tr} [mm/s]	119	119	275	477	689	—
	h_{pl} avg. [nm]	629	605	748	607	511	620
	h_{pl} σ [nm]	172	62	91	117	146	—
	h_R avg. [nm]	384	434	281	464	707	454
M5	u_{tr}[mm/s]	99	141	228	397	689	—
	h_{pl} avg. [nm]	412	460	525	579	504	496
	h_{pl} σ [nm]	100	101	72	95	81	—
	h_R avg. [nm]	10	147	300	393	369	244
MLi	u_{tr} [mm/s]	—	—	21	36	63	—
	h_{pl} avg. [nm]	—	—	36	30	33	33
	h_{pl} σ [nm]	—	—	3	3	4	—
	h_R avg. [nm]	18	23	59	61	66	45
MLiM	u_{tr} [mm/s]	—	—	33	100	208	—
	h_{pl} avg. [nm]	—	—	47	61	91	66
	h_{pl} σ [nm]	—	—	3	5	11	—
	h_R avg. [nm]	17	9	17	277	155	95

of the film thickness under the plateau region can be substantially high. The fact that thickener lumps are frequently crossing the contact area under low entrainment speeds is responsible for the high standard deviation. However, the average value of the film thickness in the plateau region is very similar and of the same order of magnitude between measurements performed at different operating temperatures, which shows that the operating temperature does not have a significantly influence on the film thickness in this region. The plateau observed at low speeds seems almost independent of the operating temperature.

4.5.1 Influence of the thickener content

The central film thickness of greases M1, M2 and M3 at 60, 80 and 110 °C are shown in Figure 4.9, in a log-log scale.

Under moderate to high entrainment speeds, the thickener content difference between the polymer greases does not seem to significantly influence their film thickness, all curves looking very close. However, under low entrainment speeds, a higher thickener content leads to higher film thickness or at least to more frequent thickener lumps entering the contact. The average film thickness of the plateau at 60, 80 and

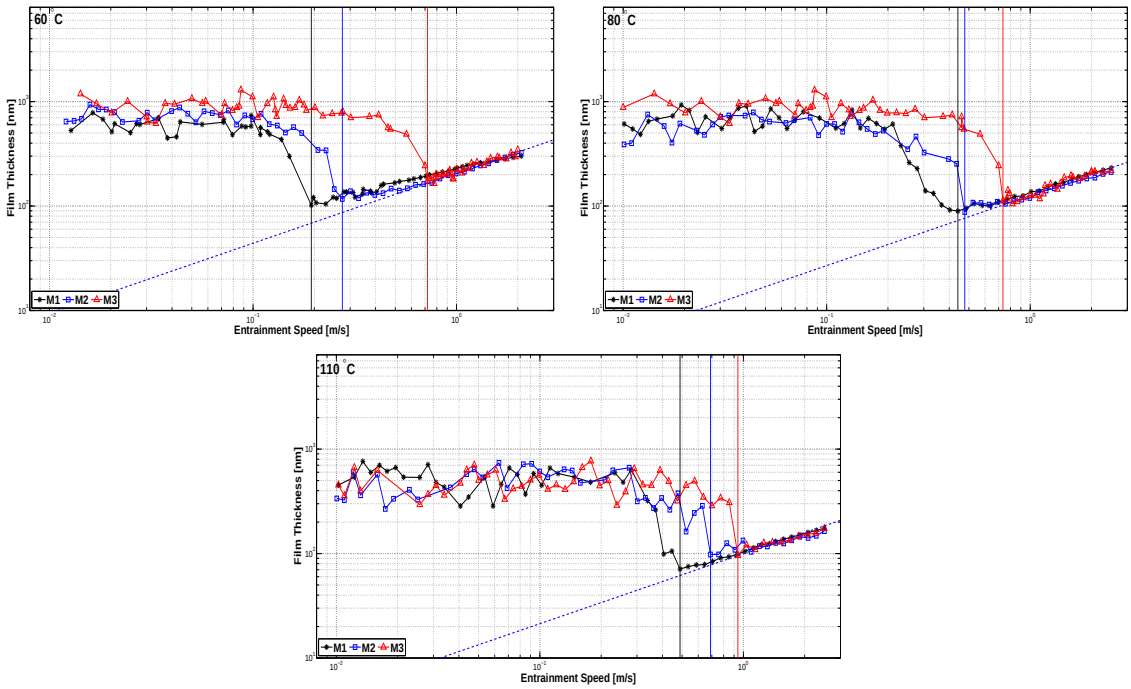

Figure 4.9: Film thickness measurements of greases M1, M2 and M3, formulated with different thickener content, at 60, 80 and 110 °C.

110 °C, is shown in Table 4.5.

From these average values, it seems that the thickener content influences the film thickness at low speeds, following the order:

$$h_{pl}^{M3} > h_{pl}^{M2} > h_{pl}^{M1} \tag{4.14}$$

Furthermore, according to this Figure 4.9, it seems that the transition speed increases with the thickener content and therefore, it also depends on the grease formulation, following this relationship:

$$u_{tr}^{M3} > u_{tr}^{M2} > u_{tr}^{M1} \tag{4.15}$$

While for the polymer greases the increasing thickener content leads to higher film thickness in the plateau region and the transition happens at also higher entrainment speed values, no tests where performed on greases with different thickener types or contents. Therefore, this behaviour might be a characteristic only of this type of grease.

In Table 4.5, the average zero speed film thickness (h_R) results are also shown. It is possible to see that the values found are very close to the values of the film thickness plateau at very low speeds shown in Figure 4.9. It was not possible to identify any relationship between the zero speed film thickness and temperature. In

Table 4.5: Transition speed and film thickness at the plateau region of greases M1, M2, M3 at different operating temperatures. The zero speed film thickness (h_R) is also shown.

Grease		60 °C	80 °C	110 °C	Avg.
M1	u_{tr}[mm/s]	193	441	488	—
	h_{pl} avg. [nm]	595	679	528	601
	h_{pl} σ [nm]	87	138	139	—
	h_R avg. [nm]	321	318	239	292
M2	u_{tr} [mm/s]	275	477	689	—
	h_{pl} avg. [nm]	748	607	511	622
	h_{pl} σ [nm]	91	117	146	—
	h_R avg. [nm]	281	464	707	484
M3	u_{tr}[mm/s]	720	735	940	—
	h_{pl} avg. [nm]	912	924	489	774
	h_{pl} σ [nm]	179	167	121	—
	h_R avg. [nm]	678	499	570	582

fact, it seems that h_R is not greatly affected by it, since the value is very similar between temperatures for some greases.

4.5.2 Base oil versus bleed-oil

Several authors point out that at high shear rates, the grease rheology gets close to the base oil's and therefore, also the film thickness of the grease approaches the base oil's one at high speeds [28, 30, 31, 97]. Yet, a few authors also found some correlation between the grease's film thickness and the film thickness produced by the bleed-oil under fully flooded condition [39].

In order to investigate this relationship, the measured film thickness of greases M2, M5, MLi and MLiM, as well as their corresponding base and bleed-oils, were compared at different operating temperatures. Figures 4.10 and 4.11 show this comparison. According to these figures, it is possible to observe that each grease produces a higher film thickness than the base oil's for both the polymer and the lithium complex thickened greases in fully flooded conditions. The same behaviour can be observed regarding the bleed-oil, although in the case of grease M5 and MLi, the film thickness of the bleed-oil is much closer to the grease's than the base oils. This behaviour was also observed before by other authors [6, 103, 123].

The ratio between the film thickness of each grease and its base oil (h_G/h_{bo}) or its bleed-oil (h_G/h_{bl}), can be seen in Table 4.6, calculated only for the moderate to high entrainment speed region. According to this table, the film thickness of the

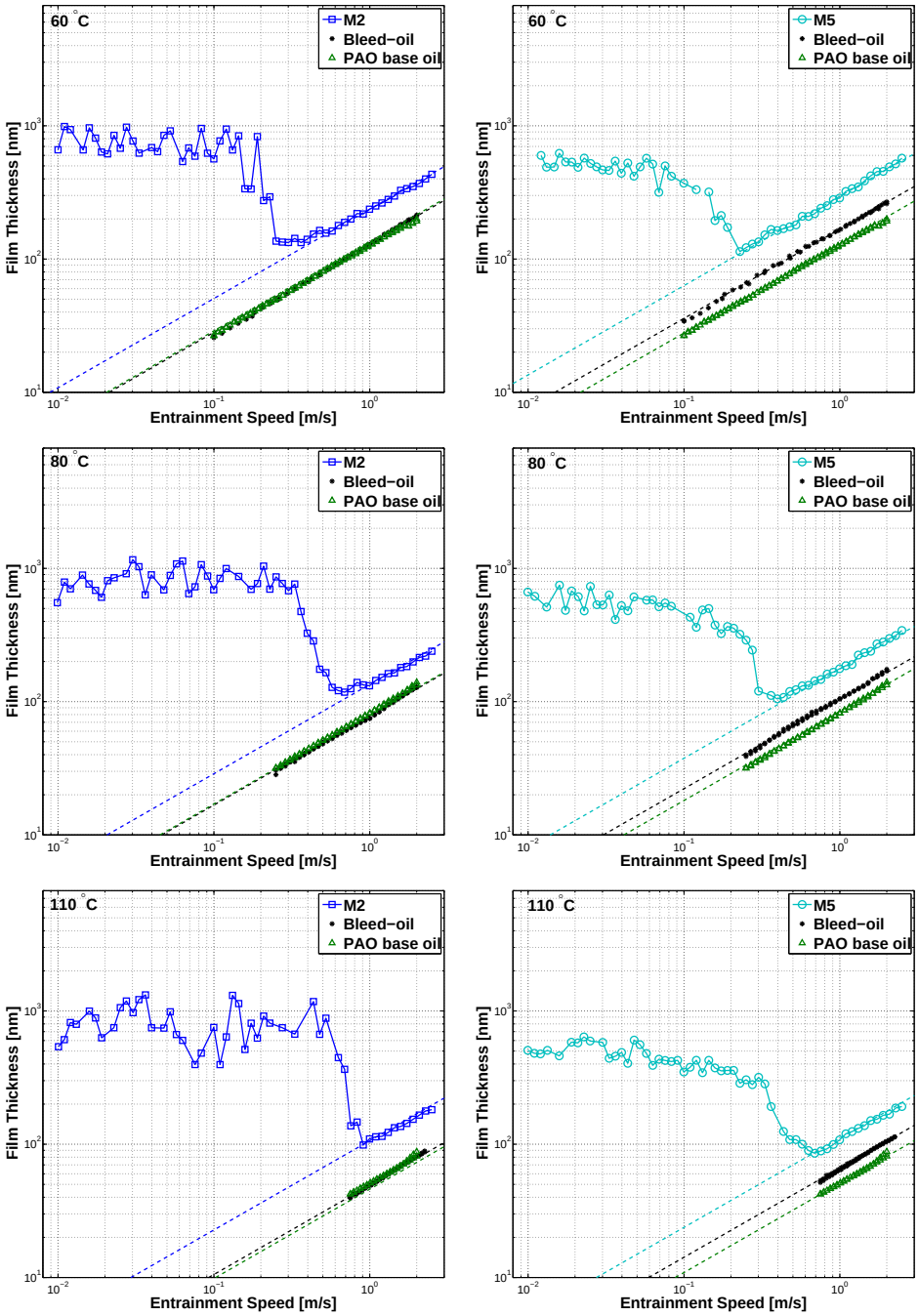

Figure 4.10: Measured film thickness of greases M2 and M5 and their respective base and bleed-oils, over different operating temperatures.

greases is, at least, 30 % higher than the base oil's, for the better case. However, this value can be much higher and for some greases at certain operating temperatures, the ratio was even higher than 2.

Apart from a few exceptions, the ratio does not seem to be largely affected by temperature, which means that the relationship between the film thickness of grease and base/bleed-oil is fairly the same at any operating temperature.

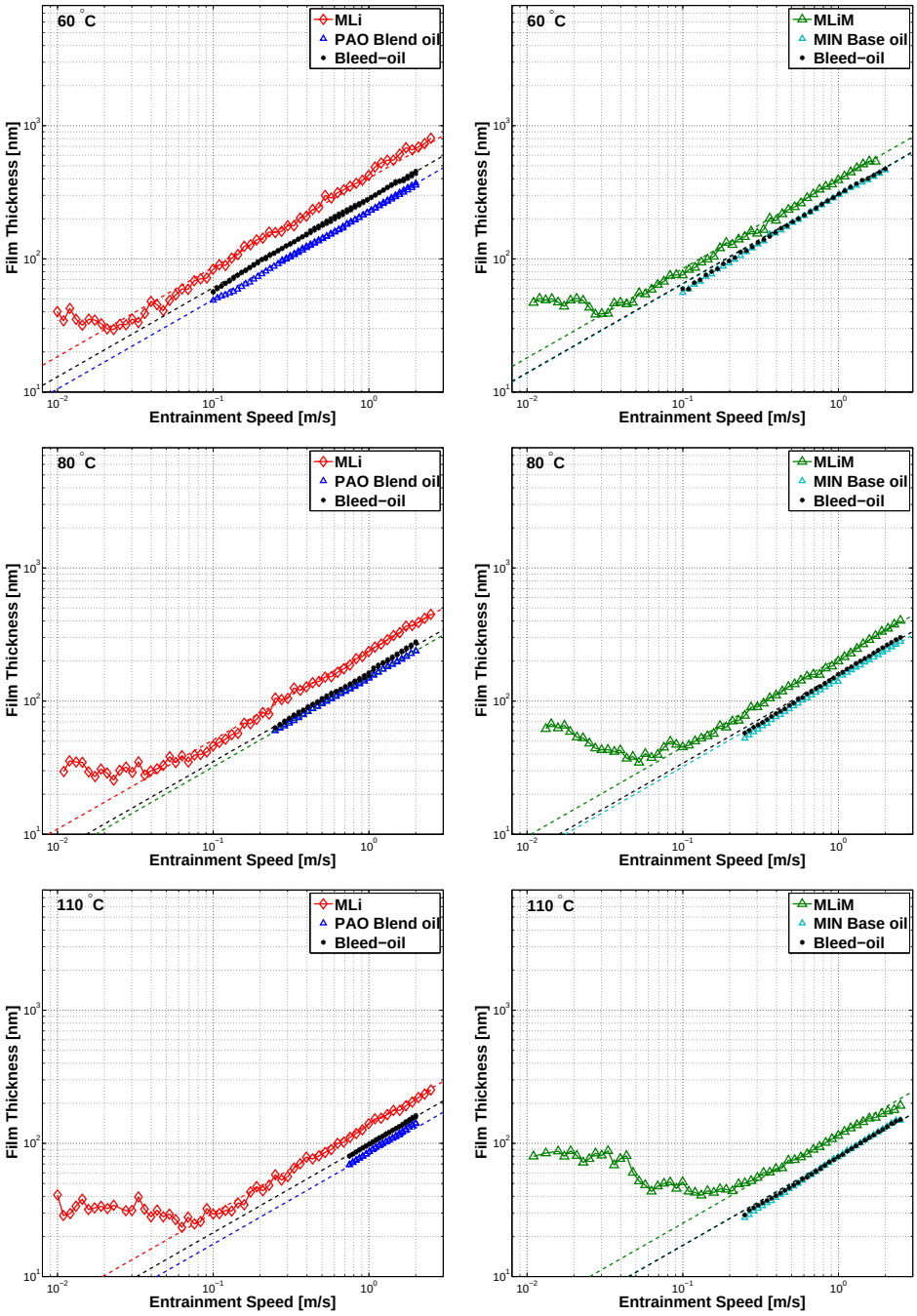

Figure 4.11: Measured film thickness of greases MLi and MLiM and their respective base and bleed-oils, over different operating temperatures.

As expected, the greases whose bleed-oil shows similar viscosity to the base oil also show similar film thickness ratio between both oils. This behaviour was found for greases M2 and MLiM. For the other two greases, M5 and MLi, the bleed-oil shows different properties than the base oil and thus, the film thickness ratios ($\frac{h_G}{h_{bo}}$ and $\frac{h_G}{h_{bl}}$) are quite different. In this situation, the film thickness of the bleed-oil is much closer to the grease's. This is specially important in the case of grease M5, even taking into

Table 4.6: Ratio between the film thickness of each grease and its base oil (h_G/h_{bo}) or its bleed-oil (h_G/h_{bl}), calculated only for the moderate to high entrainment speed ($U > u_{tr}$) region.

Temperature	60 °C		80 °C		110 °C	
Grease	h_G/h_{bo}	h_G/h_{bl}	h_G/h_{bo}	h_G/h_{bl}	h_G/h_{bo}	h_G/h_{bl}
M2	1.9	1.8	1.7	1.7	2.0	2.1
M5	2.4	1.8	2.2	1.7	2.1	1.6
MLi	1.8	1.6	1.6	1.5	1.7	1.4
MLiM	1.3	1.3	1.3	1.3	1.5	1.5

account the shear-thinning behaviour of its bleed-oil under low shear rates.

From the analysis of Figure 4.10 and Table 4.6, it is possible to observe that the presence of the elastomer greatly contributes to the increase of the film thickness under moderate to high speeds, especially when compared to the base oil alone. Not only the viscosity and film thickness of the bleed-oil are higher, but also the film thickness of grease M5 is higher than grease M2.

In the case of the grease MLi (see Figure 4.11), the film thickness of the bleed-oil is higher than the base oil, despite the viscosity of the bleed-oil being smaller. An explanation to this behaviour could not be found but it might be related to the different pressure-viscosity behaviour of the bleed-oil. Similar results were found by other authors [39, 99].

Although the film thickness of the bleed-oil is closer to the grease's, it is still much smaller, which shows that even if we consider the bleed-oil properties for the film thickness calculation, the value obtained would still be smaller than the film thickness of the greases under fully flooded condition.

4.5.3 Film thickness prediction of greases under fully flooded conditions

Following the background on the film thickness calculation reported earlier, a comparison between the measured values of the greases' film thickness and its prediction using Equations 4.4, 4.5 and 4.6 was performed. All these equations try to estimate the film thickness of lubricating greases under fully flooded conditions based on the film thickness of their base oils under moderate to high entrainment speeds ($U > u_{tr}$). Therefore, these equations are not prepared to represent the film thickness behaviour under low entrainment speeds where the thickener influence is observable.

Table 4.7: Comparison between the original and the optimized parameters used in Equations 4.4, 4.5 and 4.6, to predict the film thickness of the greases M2, M5, MLi and MLiM under moderate to high entrainment speeds (U > u_{tr}), at 80°C.

		M2	M5	MLi	MLiM
Measured h_G/h_{bo}, (U > u_{tr})		1.7	2.2	1.6	1.3
$h_G = \left(\frac{(1+B\cdot\Phi)^{0.67}}{100} + 1\right) \cdot h_{bo}$	Φ [%]	13.0	13.0	17.5	10.5
	B	2.5	2.5	2.5	2.5
	B_{optim}	23.3	95.3	26.0	26.0
$h_G = \left(\frac{k}{\eta_{bo}}\right)^{0.74} \cdot h_{bo}$	η_{bo} [Pa.s]	0.010	0.010	0.034	0.021
	$k_{palacios}$ [Pa.s^n]	23	62	107	87
	k_{cross} [Pa.s^n]	50	49	106	67
	k_{optim} [Pa.s^n]	0.017	0.029	0.064	0.034
$h_G = h_R + h_{bo}$	h_{bo} [nm]	82	82	151	141
	h_R [nm]	464	393	61	277
	h_R^{optim} [nm]	423	101	86	59

Figure 4.12 shows the measured film thickness of greases M2 and MLi and their base oils, at 80 °C. These two greases were selected because they show very different film thickness curves. This figure also shows the film thickness prediction of each grease using Equations 4.4, 4.5 and 4.6, using the original parameters (B, k and h_R) and their optimized values, in order to minimize the average error between the experimental and the numerical results, under moderate to high entrainment speeds (U > u_{tr}). A comparison between the original and optimized parameters is shown in Table 4.7.

These equations are unable to describe the film thickness behaviour at low speeds, but they also fail to provide a fair approximation to the greases' film thickness at high entrainment speeds and under fully flooded conditions, at least using the original parameters (B, k and h_R).

After the optimization, the prediction of the film thickness in this region is much better, specially for Equations 4.4 and 4.5. However, the order of magnitude of the optimized parameters is much different from the original one.

Regarding Equation 4.4, the value of B_{optim} is around 10 times greater than the original value, since the film thickness of the greases is at least 30% higher than the base oils, for the better case. In the case of grease M5, the difference is even larger due to the elastomer content.

Equation 4.4: $h_G = \left(\frac{(1+B\cdot\Phi)^{0.67}}{100} + 1\right) \cdot h_{bo}$

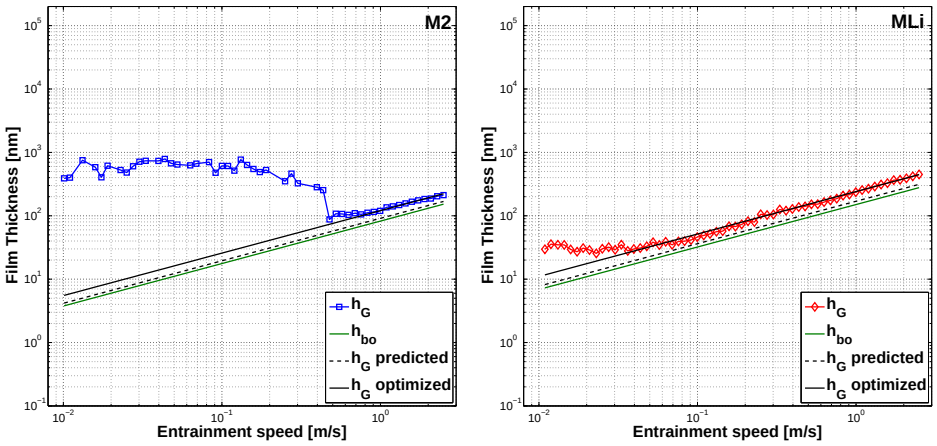

Equation 4.5: $h_G = \left(\frac{k}{\eta_{bo}}\right)^{0.74} \cdot h_{bo}$

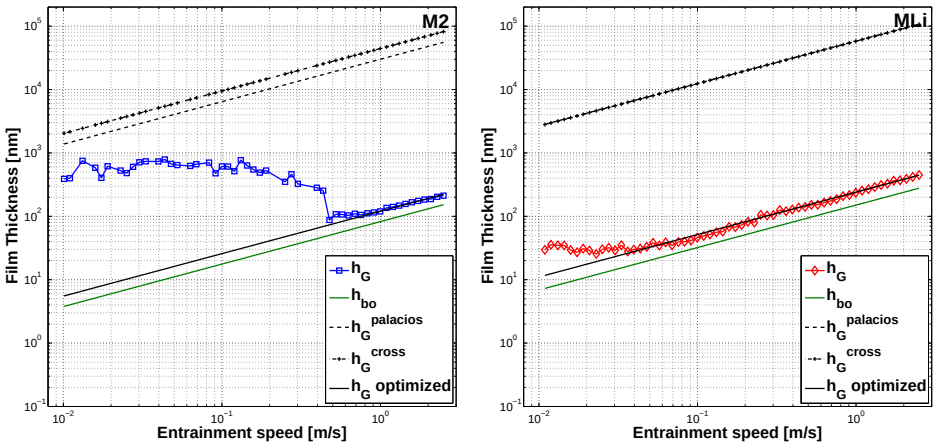

Equation 4.6: $h_G = h_R + h_{bo}$

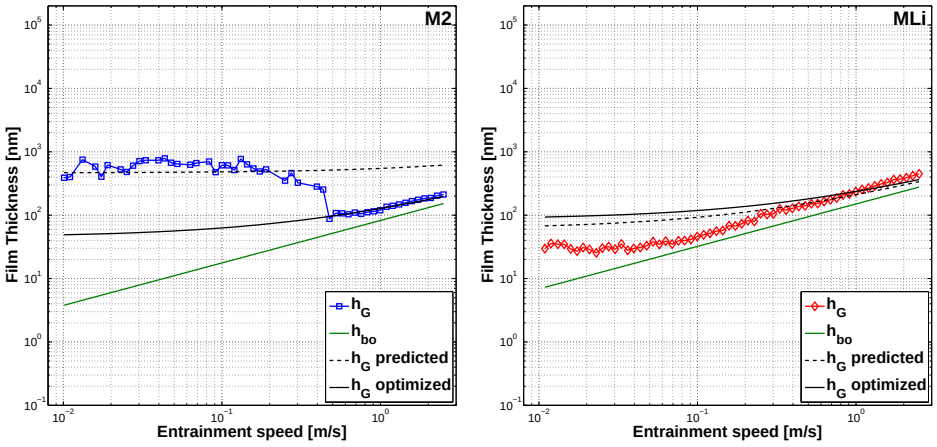

Figure 4.12: Comparison between different equations for predicting the film thickness of lubricating greases. The results are shown for the film thickness of greases M2 and MLi at 80 °C.

There are several things which my explain these differences, related to the simplifications performed when developing this Equation 4.5 [6]:

- the volume fraction might not be equivalent to soap concentration, for soap concentrations higher than 10 %;
- the differences in atomic weight of the thickener elements were not taken into account, which might be particularly important for the PP thickener;
- the pressure-viscosity coefficient of the grease is assumed to be equal to the base oil's.

Therefore, since all tested greases show thickener concentrations above 10 % and also very large h_G/h_{bo} ratios, a much larger vale of B is necessary.

The case of Equation 4.5 is even worse: the original value of k, obtained from two different rheological models applied to the measured flow curves of each grease, is many orders of magnitude higher than the optimized value. Since this parameter is very dependent on the method used to obtain the flow curves (rheometer geometry, gap size, pre-shear procedure, etc), such differences were to be expected. Furthermore, the rheological model used to calculate the consistency index k is also very important and might lead to very different results, even if the same phenomena are being taken into consideration (e.g. the yield stress). Finally, and probably the most important, is the fact that k should have been determined for sheared or worked greases since it should be more representative of the grease at the contact inlet [124].

Finally, Equation 4.6 was not able to reproduce the film thickness behaviour of the greases based on the film thickness of the base oil plus the zero speed film thickness (h_R), specially because its value is very high for the polymer greases. In the case of the lithium thickened greases, the approximation using this equation was closer. After the optimization however, the film thickness under moderate to high speeds shows a much interesting result for the polymer greases while it is practically unchanged for the lithium greases.

Still, this Equation 4.6 is the most interesting because it suggest that it would be possible to obtain a distribution function between the film thickness of the base oil (h_{bo}) and a residual or low speed film thickness (e.g. h_R or h_{pl}), in order to predict the complete film thickness curve for the whole entrainment speed range.

4.5.3.1 On the estimation of the grease properties (η, α) from film thickness measurements

One of the things which makes it difficult to predict film thickness of lubricating greases is the fact that the grease properties at the inlet are unknown. Using a similar procedure to the one applied in the determination of the pressure-viscosity coefficient of the base and bleed-oils (see section 4.4.3), the viscosity and pressure-viscosity coefficient of each grease were calculated.

The Hamrock and Dowson's equation for the film thickness of an elliptical contact, shown before in Equation 4.1, was used to predict the film thickness of the greases. Assuming this equation correctly represents the grease behaviour under moderate to high entrainment speeds, and assuming that Gold Equation's for calculating the pressure-viscosity coefficient is also valid for greases, it is possible to roughly estimate the grease properties using the film thickness curves shown in Figure 4.7.

Equation 4.1 can be re-arranged for all the curves measured at the same operating conditions (surfaces' material, load and SRR) in the following form:

$$h_{0c} = K \cdot U^{0.67} \cdot \eta^{0.67} \cdot \alpha^{0.53} \tag{4.16}$$

where K is a constant.

Under moderate to high speeds (U > u_{tr}), the film thickness of the grease follows the tendency given by Equation 4.16, increasing linearly with the entrainment speed in logarithmic scale, as shown in Figure 4.7. Therefore, a single value of the $\eta^{0.67} \cdot \alpha^{0.53}$ product can be calculated for each operating temperature in order that h_{oc} matches h_{exp}, according to Equation 4.17:

$$h_{exp} = h_{0c} \Longrightarrow {\eta_i}^{0.67} \cdot {\alpha_i}^{0.53} = K_i \tag{4.17}$$

where i is referred to the different operating temperatures. This procedure assumes that η and α are independent of the shear rate for U > u_{tr} and therefore a single value of η and α can be used to predict the film thickness of the grease for this whole region. Combining Equation 4.17 with Gold's equation describing the relationship between the viscosity and the pressure-viscosity coefficient, it is possible to calculate the pair (η_i, α_i) for each operating temperature, according to Equation 4.18.

$$\begin{cases} {\eta_i}^{0.67} \cdot {\alpha_i}^{0.53} = K_i \\ \\ \alpha_i = s \cdot \left(\frac{\eta_i}{\rho_i}\right)^t \cdot 10^{-9} \end{cases} \tag{4.18}$$

Table 4.8: Calculated values of viscosity η and pressure-viscosity coefficient α of greases M2, M5, MLi and MLiM.

	M2		M5		MLi		MLiM	
T [°C]	η	α	η	α	η	α	η	α
20	0.330	6.5	0.925	7.5	1.227	7.7	1.360	10.6
40	0.143	5.9	0.307	6.5	0.468	6.8	0.433	9.1
60	0.078	5.4	0.131	5.8	0.212	6.1	0.147	7.8
80	0.042	5.0	0.066	5.3	0.099	5.6	0.067	7.0
110	0.028	4.7	0.032	4.8	0.044	5.0	0.030	6.3

Units: η in Pa.s and α in GPa^{-1}

The values of s and t were attributed to the nature of the base oil of each grease, according to Table 3.3.

The calculated (η_i, α_i) properties are shown in Table 4.8. Analysing this table, it is possible to see that both η and α decrease with the operating temperature, as it should be expected. According to Hamrock and Dowson's equation, the higher is the product of $\eta^{0.67} \cdot \alpha^{0.53}$, the higher should be the film thickness. Since greases M2, M5 and MLi were formulated with base oils of the same nature, their pressure-viscosity coefficients are also similar, although their viscosities are not.

The calculated viscosities show values much higher than those generally found for oils in EHD contacts. On the other hand, the calculated values of α are smaller than what is generally expected for lubricants (above 10 GPa^{-1}). The calculated values are in fact, even smaller than those previously calculated for the base oils of the same greases (see Table 4.2). Which means that the relationship between the viscosity and the pressure-viscosity, as predicted by Gold *et al.*, might not be valid for greases or at least different s and t parameters might be necessary.

The viscosity and pressure-viscosity coefficient were only calculated in order to obtain a rough estimation of the greases properties. Although they were not used in any other calculation along this work, these properties will be important to plot the coefficient of friction of each lubricant in relation with each other, based on their different film thicknesses. This subject will be further analysed in Chapter 5.

It should also be taken into account that the values of η and α derived from Hamrock and Dowson's equation, are relative to atmospheric pressure at the contact inlet where the generality of the oils show Newtonian behaviour. However, this is not the case of lubricating greases, given their shear-thinning behaviour. With that in mind, the shear rate of the film thickness curves shown in Figure 4.7 was calculated,

according to Equation 4.19

$$\dot{\gamma} = \frac{\Delta U}{h_G} \tag{4.19}$$

where ΔU is the difference between the speeds of the ball and of the disc - sliding speed. The calculated shear-rate of the film thickness curves at 80 °C is shown in Figure 4.13. It is possible to observe that the shear-rate increases with the increase of the entrainment speed since the sliding speed is also increasing (even if the SRR is constant). The transition speed (u_{tr}, Table 4.4), is also shown in Figure 4.13.

The maximum and minimum shear-rates occur under the minimum (0.01 m/s) and maximum (2.5 m/s) entrainment speeds, for all curves. These limits can now be plotted over the flow curves discussed in Chapter 3 (see Figures 3.13 and 3.14). The results at 80 °C are shown in Figure 4.14.

At this temperature and under an entrainment speed of 0.01 m/s, all greases are in the low speed region where thickener material contributes to increase the film thickness. The corresponding shear rate is low because the films are thick and the speed is low, and consequently the grease's viscosity at that shear rate should be much higher than the base oil's. This seems particularly important in the case of the polymer greases.

The opposite behaviour is observed at 2.5 m/s. At this entrainment speed, all greases are in the high speed region where the film thickness is so large that the sheared thickener material should not influence it or, given that the shear rate is so high, the thickener material can no longer enter the contact, being pushed aside. At these shear rate values, the viscosity of the grease should now be much closer to the

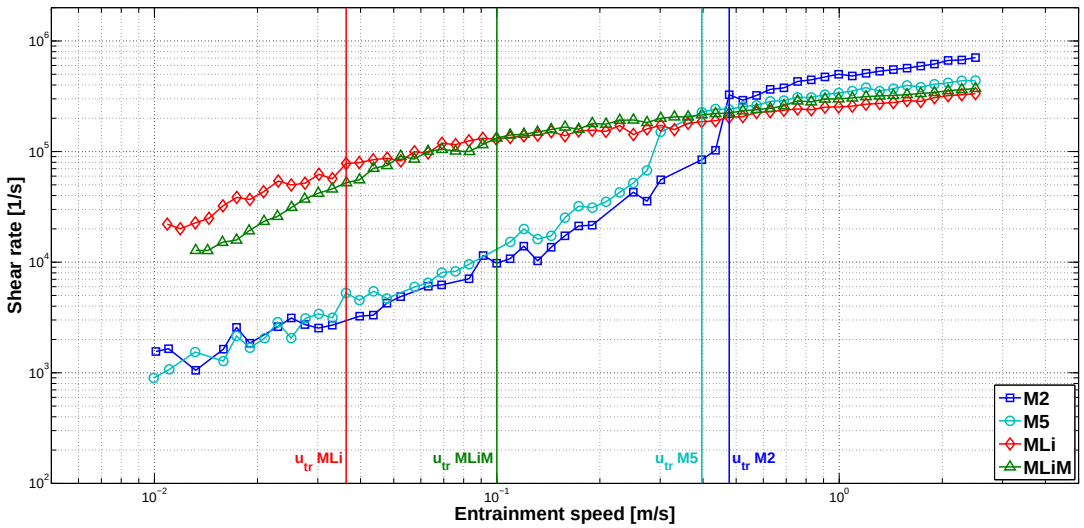

Figure 4.13: Shear rate calculated from the film thickness curves of greases M2, M5, MLi and MLiM at 80 °C.

base oil's, as shown in Figure 4.14.

The viscosity values shown in Table 4.8, calculated according to Hamrock and Dowson's equation for the moderate to high speed region, are also plotted in Figure 4.14, as orange circles. These values should be representative of the viscosity of the grease at atmospheric pressure in the vicinity of the contact inlet. Which means that, despite the grease's shear-thinning behaviour, there should be a single combination of viscosity and pressure-viscosity coefficient, at a certain shear-rate, that defines the film thickness onwards.

In the case of the flow curves of greases MLi and MLiM, this viscosity value corresponds to a shear rate value which is very close, although higher, to the shear rate at 0.01 m/s. However, in the case of the polymer greases, the viscosity value corresponds to a shear rate value which is much higher than the shear rate at 0.01

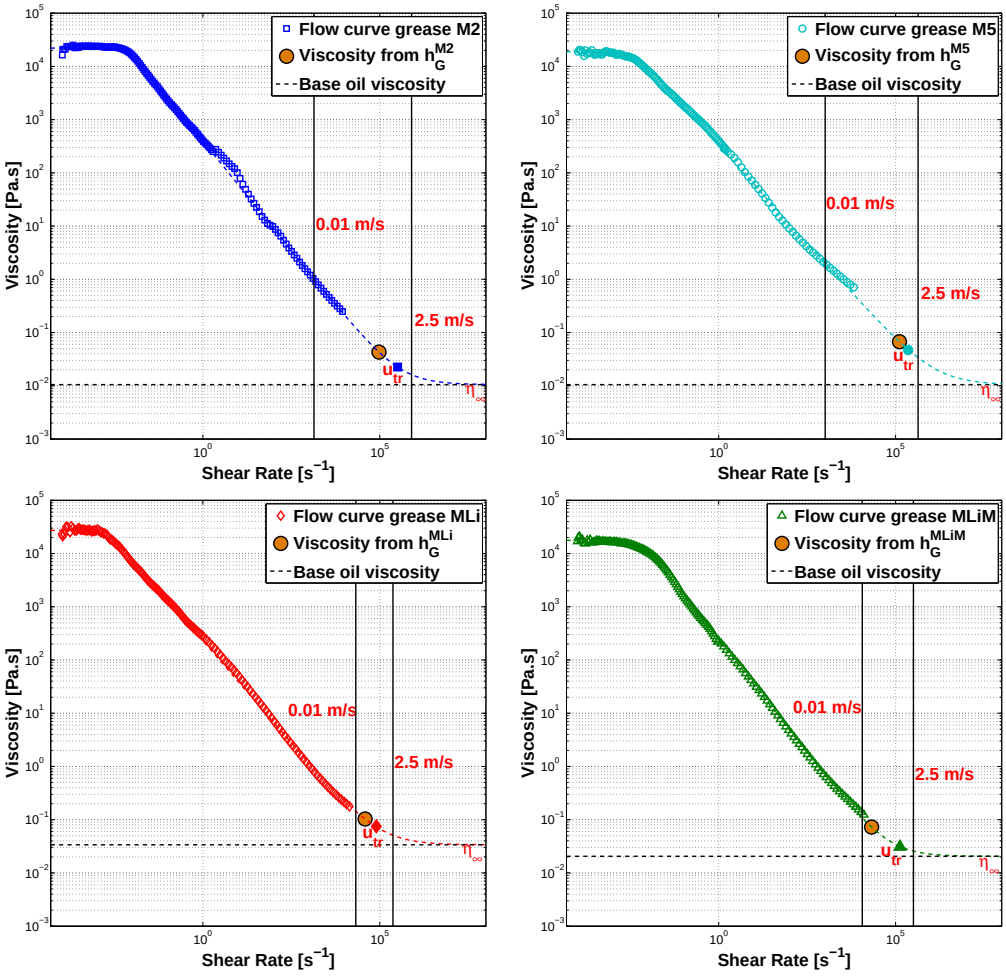

Figure 4.14: Flow curves of greases M2, M5, MLi and MLiM at 80 °C. The minimum and maximum shear rate values calculated from the film thickness curves are represented by vertical black lines. The viscosity values corresponding to the shear-rate value of the transition speed ($u_{tr} \rightarrow \dot{\gamma}_{tr}$) are also identified.

m/s. However, in both cases, this value viscosity corresponds to a lower shear-rate value than $u_{tr} \rightarrow \dot{\gamma}_{tr}$.

To conclude, the properties of the grease at the inlet and also inside the EHD contact are very important but also extremely hard to evaluate. Associated with the fact that the thickener can also contribute to the film thickness, it is difficult to predict the film thickness under a wide range of operating conditions with the current models available, specially if only the base oil viscosity is used as input.

4.6 Closure

The film thickness under fully flooded conditions was measured for differently formulated greases, on a ball-on-disc apparatus, under different operating conditions. The thickener and base oil roles in the lubrication process were addressed, specially in what concerns the grease lubrication mechanisms.

It was found that under fully flooded conditions, the thickener is also part of the active lubricant inside the contact. Under low entrainment speeds, the lubricating greases produce a very high film thickness plateau. Thickener lumps were observed crossing the contact very frequently under this plateau region, locally increasing the film thickness to values which are much higher than those expected from the base oil. In this region at low entrainment speeds, the film thickness shows a very high standard deviation and it seems to be fairly independent of the operating temperature. The plateau was found to be extremely dependent on the grease formulation, specially regarding the thickener type but also its content:

- the lithium complex thickened greases show much smaller film thickness plateau than the polymer greases, which should be related to the thickener element's size (same order of magnitude);

- the higher is the thickener content, the higher is the film thickness in the plateau region at low entrainment speeds, for the tested polymer greases.

As the entrainment speed increases, the plateau region ends and the film thickness of the grease increases linearly with the entrainment speed at a rate of $\approx U^{0.67}$, as predicted by Hamrock and Dowson's equation for fully flooded oil lubricated contacts. The film thickness of the tested lithium complex thickened greases is higher than the polymer greases under moderate to high speeds, given the higher viscosity of their base oils. However, under low to moderate speeds, the opposite was observed which was attributed to the thickener type. The transition speed at which the film thickness behaviour changes from the typical linear slope to the plateau, increases with

increasing thickener content, for the polymer greases tested. This transition speed is also influenced by the temperature, increasing with it for all the tested greases.

The film thickness of the grease at high speeds follows a parallel slope to the film thickness of its corresponding base oil and bleed-oil. The film thickness of the bleed-oil is equal or higher than the base oil, but still much smaller than the grease's. This happened for all tested greases despite thickener type, content or elastomer content.

The current literature regarding the prediction of the film thickness for grease and oil lubrication was analysed and discussed regarding the experimental measurements. The film thickness of the lubricating fresh greases under fully flooded conditions could not be accurately predicted using any of the models researched in the bibliography.

5 Friction coefficient in fully flooded grease and oil lubricated contacts

5.1 Introduction

The traction behaviour of lubricating oils is well documented [125–128]. It is known that the traction coefficient depends on the low shear viscosity, the limiting shear modulus and the limiting shear stress the lubricant can withstand [125, 127]. However, even for oil lubrication, two different approaches to predict the oil traction behaviour have been extensively discussed and no consensus was found yet [129–131]. One of the approaches defines the traction parameters by adjusting them in order to obtain the best numerical fitting with traction measurements [132, 133], while the other focuses on laboratory data and high pressure rheology measurements [134–136]. The end results are often very different.

If there are still doubts about the traction behaviour of lubricating oils, the case of grease lubrication is even worse. The reason is that only few researchers are studying the subject, and that the properties of the active lubricant inside the contact are still unknown and therefore, it is still hard to predict the correct lubrication regime. Recently, with the investigation of the film thickness formation in fully flooded grease lubricated single-contacts [2, 100, 101], the thickener role and its influence on the film formation under low to moderate rolling speeds allowed for a better understanding of grease lubrication phases, as it was also discussed in the previous Chapter 4. However, there is still little published research related to friction on grease lubrication. It is frequent to describe the grease behaviour based on the properties of the base oil not only for predicting the COF but also for the film thickness. Such assumptions often lead to wrong predictions [37, 39, 71, 98, 137], since the properties of the active lubricant at the contact inlet might be considerable different from those of the original base oil that the grease was formulated with (thickener, additives, etc.).

Although it was not the main objective of this work, the knowledge of the traction properties of the lubricating greases is very important for their development and for the correct selection of a lubricant to a given application. Moreover, the

measurement of the coefficient of friction for different operating conditions might allow to better understand how certain aspects of the grease formulation can affect its performance, further investigating the grease lubrication mechanisms in simple but useful single contact ball-on-disc tests.

5.2 Traction curves

5.2.1 Measurement procedure

The EHD2 equipment also allows the measurement of a lubricant's traction coefficient in ball-on-disc or roller-on-disc configuration, over different ranges of temperature, speed, load and slide-to-roll (SRR) ratio.

The traction coefficient was measured in a ball-on-disc configuration measured under controlled temperature, constant load and constant entrainment speed, while the SRR changes over a pre-defined range. The procedure is then repeated under the same conditions but for different entrainment speeds allowing to build a traction coefficient map over speed and slide-to-roll ratios.

The traction coefficients are strongly dependent on the Hertzian pressure. Since both the disc and the ball are made of steel and the maximum available load of the EHD2 machine is 50 N, the Hertzian contact pressure is close to ≈1.09 GPa. The geometry, the surface roughness and the load involved in these tests are shown in Table 5.1. The traction curves were measured with the smooth disc for all greases and all operating conditions, but also with the rough disc for selected operating conditions, in order to understand the influence of surface roughness.

A slide-to-roll ratio (SRR) in the range between 1 to 15 % was imposed, which covers the typical SRR range found in rolling bearings, typically around 3 to 5 %. The traction coefficient is measured for positive and negative SRR, i.e., it is measured with the ball rotating faster than the disc and vice-versa, starting from 1% to 15% and then coming back to 1%. The full procedure is shown in Table 5.2.

The measurements were obtained using a scoop to ensure fully flooded conditions in grease lubricated contacts. The operating temperatures of 60, 80 and 110 °C were selected not only because the rolling bearing tests would be performed at these temperatures, but also because lower film thicknesses were desirable.

Table 5.1: Ball-on-disc tests: material, surface roughness and load, for traction and Stribeck curves measurements.

Parameter	Ball	Smooth disc	Rough disc
$R_{x,y}$ [mm]	9.525	—	
Ra [nm]	≤ 20	≈ 2	≈ 300
Material	AISI 52100		
E [GPa]	207		
ν [-]	0.29		

Table 5.2: Ball-on-disc tests: operating conditions for measuring the traction curves.

Temperature - T [°C]	60, 80, 110
Entrainment speed - U [m/s]	0.05 → 0.2 → 0.9 → 1.6
Slide-to-roll ratio - SRR [%]	stepwise from 1 → 15 → 1
Load - F [N]	50
Equivalent modulus - E* [GPa]	≈ 113
Maximum Hertzian pressure - p_0 [GPa]	≈ 1.09
Hertzian semi-width - a [μm]	≈ 146.8

5.2.2 Traction coefficient results

In order to better understand the traction coefficient results it is necessary to know the lubrication regime along the test. The traction coefficient was measured under low slide-to-roll ratios (1 to 15 %) and since this level of sliding adds only little to the extent of film-thinning observed under pure rolling [73], it is possible to use the measured film thickness curves shown in Chapter 4 to predict the specific film thickness of the traction coefficient tests.

The film thickness curves shown in Chapter 4 were measured under the same operating conditions (load, temperature, contact geometry, scoop), but for a steel ball on glass disc contact instead of the steel ball on a steel disc used for the traction measurements. Therefore, it is necessary to correct the film thickness curves of the steel-glass contact (${h_{0c}}^{sg}$) to the steel-steel contact (${h_{0c}}^{ss}$). This procedure was performed using Hamrock and Dowson's Equation [110] (see Equation 4.1). Calculating the ratio between the two film thickness equations for the same lubricant and same

contact geometry, the following expression is reached:

$$\frac{{h_{0c}}^{ss}}{{h_{0c}}^{sg}} = \frac{(U_1+U_2)_{ss}^{0.670} \cdot {E^*_{ss}}^{-0.073} \cdot F_{ss}^{-0.067}}{(U_1+U_2)_{sg}^{0.670} \cdot {E^*_{sg}}^{-0.073} \cdot F_{sg}^{-0.067}} \tag{5.1}$$

If the operating conditions of both tests are the same such that $(U_1+U_2)_{ss} = (U_1+U_2)_{sg}$ and $F_{ss} = F_{sg}$, the difference between the tests is related to the surfaces' materials only. Therefore, the previous expression results in Equation 5.2:

$$\frac{{h_{0c}}^{ss}}{{h_{0c}}^{sg}} = \left(\frac{E^{*sg}}{E^{*ss}}\right)^{0.073} \approx 0.946 \tag{5.2}$$

Which means that the film thickness of the traction tests (${h_{0c}}^{ss}$) should be around 5% smaller than the film thickness measured with a steel ball on glass disc contact (${h_{0c}}^{sg}$). A similar procedure has been reported earlier by De Laurentis *et al.* [138].

After applying the correction, the specific film thickness can now be calculated taking into account the composite roughness of the surfaces of the steel ball and steel smooth disc (Table 5.1 - $\sigma_c \approx 20.1$nm). The resulting curves are shown in Figure 5.1. The Λ limits shown as black horizontal lines in this figure, were established according to the literature, as reported in section 4.2.1 of Chapter 4.

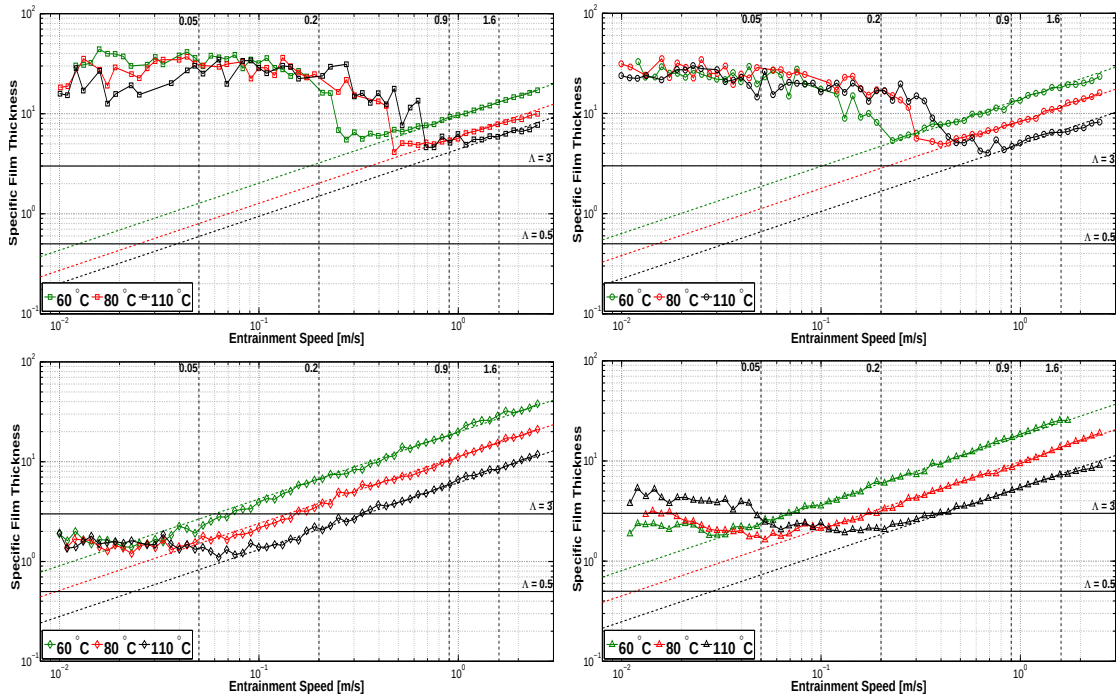

Figure 5.1: Specific film thickness of greases M2, M5, MLi and MLiM in a ball-on-smooth disc contact. The black dashed vertical lines, represent the entrainment speeds at which the traction coefficient measurements were performed.

Analysing Figure 5.1, it is possible to observe that under any of the tested speeds (0.05, 0.2, 0.9 and 1.6 m/s), the polymer thickened greases should all be operating in the full film lubrication regime ($\Lambda > 3$). At low speeds (U = 0.05 and 0.2 m/s) these greases are in the plateau region where the film thickness is very high and almost independent of the entrainment speed ($U < u_{tr}$). At higher speeds (U = 0.9 and 1.6 m/s), these greases are operating in the region where the film thickness increases linearly with the entrainment speed, in logarithmic scale ($U > u_{tr}$).

At low entrainment speeds (0.05 m/s), the lithium thickened greases MLi and MLiM should be running in mixed film lubrication conditions ($\Lambda < 3$), and also in the plateau region. Above that speed (0.2, 0.9 and 1.6 m/s), both greases are operating in the linear region and full film lubrication conditions ($\Lambda > 3$), with the exception of the curves at 110 °C and 0.2 m/s where both greases are still in the mixed lubrication regime.

Figure 5.2 shows the traction curves measured for grease M1, M2 and M3, using the smooth disc and for the operating conditions of Table 5.2. The traction coefficient tests were performed under full film lubrication regime for almost all the entrainment speeds tested, at any operating temperature. Under this regime, the traction coefficient decreases with the increase of the operating temperature due to the decrease of the viscous friction, as the viscosity of the active lubricant decreases. This effect is less pronounced under low entrainment speeds (0.05 and 0.2 m/s) where the film thickness of all greases is almost independent of the operating temperature, since thickener material enters the contact - plateau region ($U < u_{tr}$).

At high entrainment speeds (1.6 m/s), the contact operates under full film conditions (see Figure 5.1), whatever the temperature considered. No significant differences were observed between the greases with different thickener content and, as expected, the traction coefficient decreases when the temperature increases from 60 to 110 °C. For a constant temperature, e.g. 80 °C, it is clear that the traction coefficient increases when the entrainment speed decreases, again without significant differences between the greases. For lower entrainment speeds, the traction coefficients become almost constant (e.g. 0.05 m/s and 0.2 m/s, at 80 °C), since there should be thickener material entering the contact and the film thickness should now be less dependent on the entrainment speed (as shown in the specific film thickness curves of Figure 5.1). At the lowest entrainment speed, 0.05 m/s, a larger scatter is observed on the traction coefficient measurements not only because thickener lumps should be crossing the contact ever so often but also because it is hard for the system to keep the entrainment speed constant while changing the SRR for such low speeds.

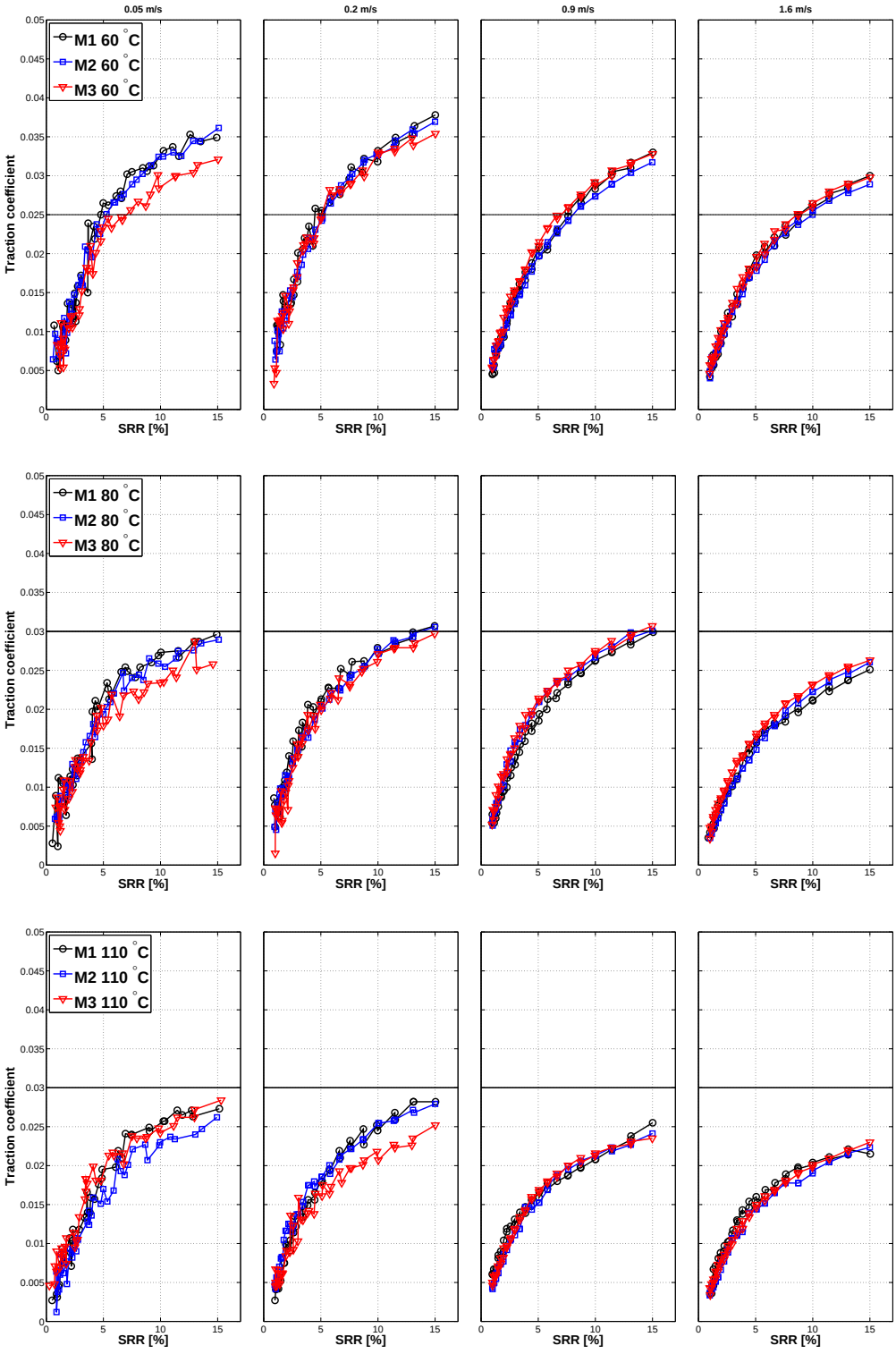

Figure 5.2: Traction curves of grease M1, M2 and M3 at different operating temperatures and entrainment speeds (over the columns).

Figure 5.3 shows the traction curves measured for greases M2, M5, MLi and MLiM, using the smooth disc and for the operating conditions of Table 5.2. Grease M2 is repeated here for easier comparison. All the observations previously made for grease M1, M2 and M3 are valid for greases M5, MLi and MLiM. According to the results

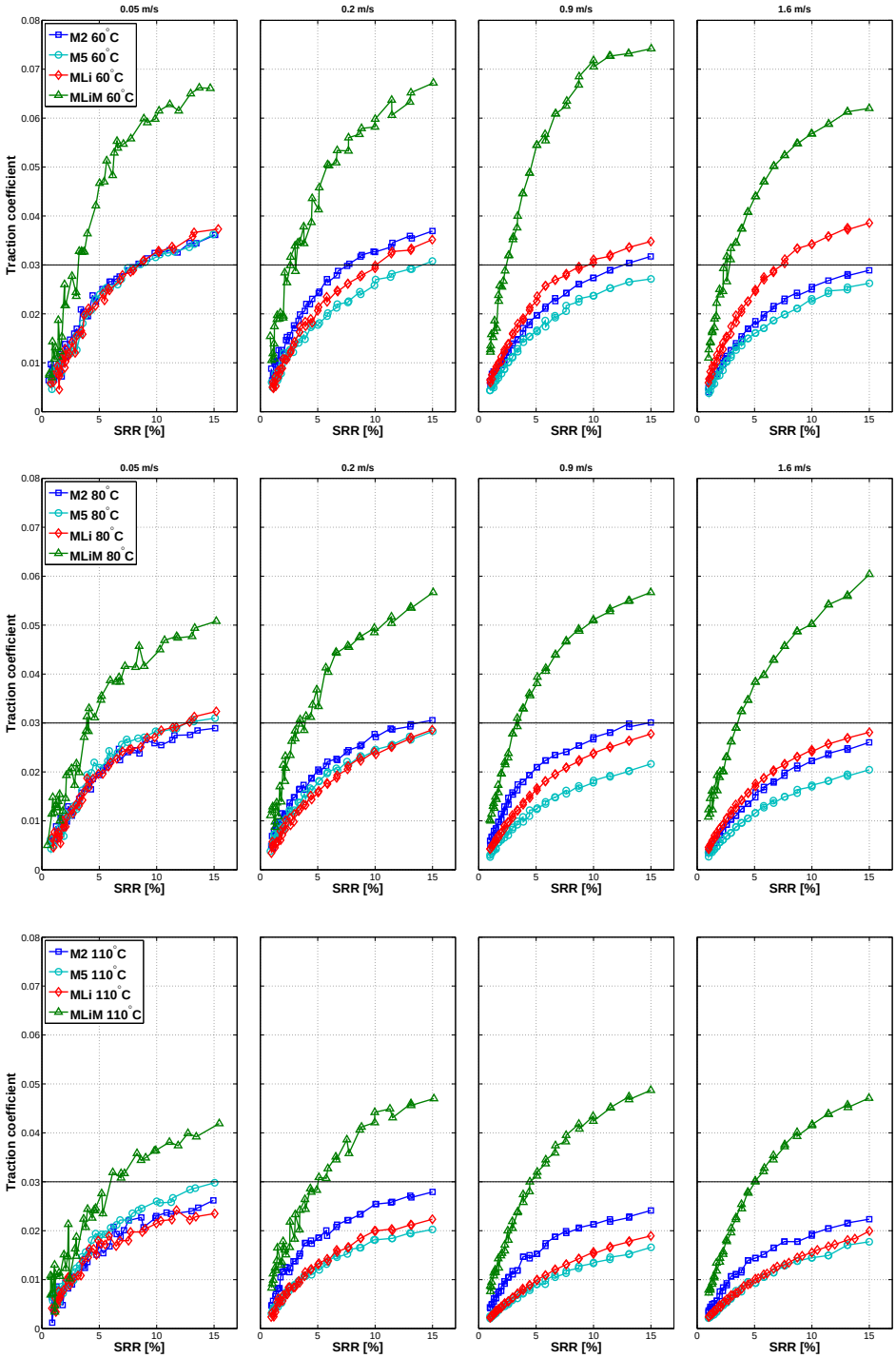

Figure 5.3: Traction curves of grease M2, M5, MLi and MLiM at different entrainment speeds and operating temperatures (over the lines).

shown in Figures 5.2 and 5.3, the traction coefficient increases linearly for low values of SRR. Above ≈5 %, the traction coefficient behaviour becomes highly non-linear. This is valid for all greases under any operating condition (speed and/or temperature). No traction coefficient plateau or thermo-viscous behaviour was observed under the SRR range tested.

When comparing the results of greases M2, M5, MLi and MLiM, it is clear that grease MLiM is the one always showing the highest traction coefficient for all operating conditions. Since its film thickness in not very different from the one of grease MLi, the differences should probably be related to the mineral nature of its base oil.

It is also interesting to notice that at 60 °C, the traction coefficient of grease MLi is higher than the traction coefficient of grease M2 for U > u_{tr}. However, this relationship starts to reverse as the temperature increases. At 110 °C the traction coefficient of grease M2 is already higher than the one of grease MLi.

Another interesting remark is related to grease M5, which has a formulation very similar to grease M2, but contains an elastomer as co-thickener. This elastomer is known to bleed out of the grease under operation, contributing to the increase of the bleed-oil viscosity, as shown in Chapter 3. It was also clear in Chapter 4 that grease M5 produces a higher film thickness than grease M2 for U > u_{tr}, which might explain why the traction coefficient is lower for almost all the operating conditions, but specially under high entrainment speeds.

Once again, at the lowest operating speed (0.05 m/s), a larger scatter of the traction coefficient measurements is observed for all greases and no significant differences are observed between greases M2, M5 and MLi. From the results shown in Figure 5.3, a general order might be established regarding the value of the traction coefficient, μ:

$$\mu^{MLiM} >> \mu^{M2} \geq \mu^{MLi} > \mu^{M5}$$

5.2.2.1 Grease scoop and surface roughness influence on the traction coefficient measurement

The traction coefficient tests were performed using a scoop, which ensures that the grease is lead back to the contact track, ensuring that the contact is replenished and generating fully flooded conditions. This effect of the scoop in the replenishment of the contact and consequently on the traction coefficient can be seen in Figure 5.4a. At this entrainment speed (U = 0.9 m/s), the tests performed without scoop showed a much higher traction coefficient. The lack of scoop should be responsible for a defective replenishment which might lead to starvation, specially at high entrainment

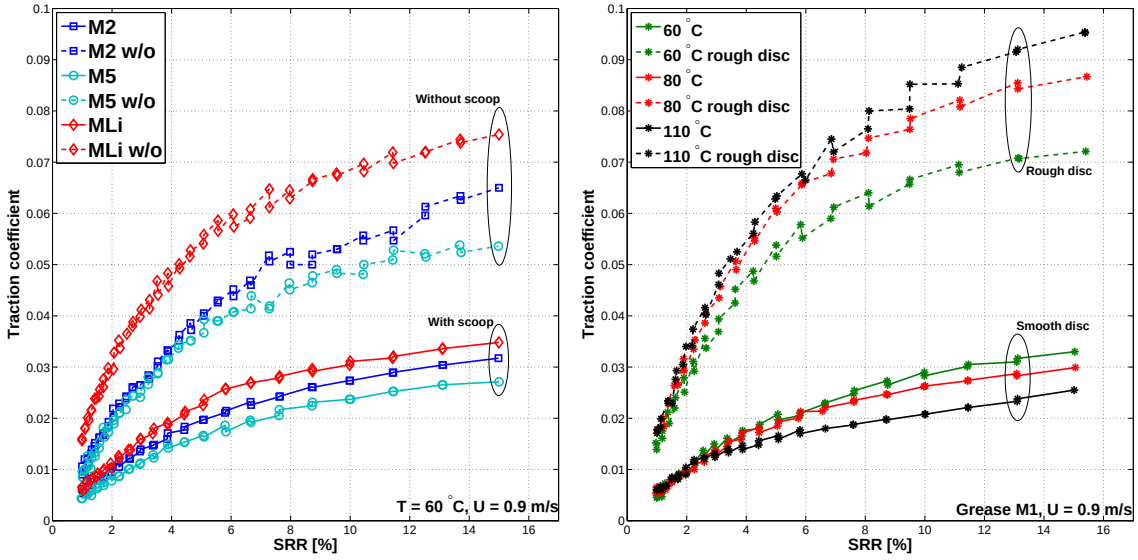

Figure 5.4: (a) Traction curves of greases M2, M5 and MLi at 60 °C measured with and without (w/o) scoop to ensure fully flooded conditions.
(b) Traction curves of grease M1, measured with discs of different roughness and with scoop.

speeds (U > u_{tr}). A starved contact shows smaller film thickness and therefore, more frequent asperities interactions and increased traction/friction coefficient.

Although all traction curves have been performed with a smooth disc (see Table 5.1), the influence of the roughness of the disc was also investigated. The results presented in Figure 5.4b show that the traction coefficient increases very significantly with the increase of the average roughness of the disc's surface for the same operating conditions. Increasing the surface roughness leads to a lower specific film thickness and changes the lubrication regime from full film to mixed/boundary film lubrication, generating higher traction coefficients.

In the tests performed with the smooth disc, the lubrication regime at this entrainment speed (U = 0.9 m/s) was full film. Therefore, the higher the temperature the lower was the traction coefficient, since the viscous friction decreases with increasing temperature. However, this tendency is inverted when the rough disc is used. In this situation, the increasing temperature leads to mixed or even boundary lubrication and consequently, more frequent interactions between the asperities of the intervening surfaces'.

5.3 Stribeck curves

5.3.1 Measurement procedure

The Stribeck curves curves are generally measured under controlled temperature, constant load and constant SRR, while varying the entrainment speed.

The specific film thickness curves from the traction coefficient measurements presented in Figure 5.1, indicate that it is very hard to reach Λ values below 0.5 using a smooth disc: one must be prepared to increase the temperature above 110 °C or to decrease the entrainment speed below 0.05 m/s, both unadvisable courses of action for the EHD2 measuring device. Furthermore, the traction measurements performed with a rough disc (see Figure 5.4b) revealed a very significant increase of the traction coefficient for the same operating conditions, suggesting that a mixed/boundary film could be achieved by increasing the roughness of the disc.

Therefore, in order to reach lower specific film thickness and get closer to boundary lubrication, a smooth disc was ground so that its surface became rougher. The properties of this rougher disc are shown in Table 5.1.

Three Stribeck curves were measured under constant SRR (5 and 50 %), at different operating temperatures, according to the procedure shown in Table 5.3. An average curve was then calculated from the three measurements. The test temperatures were chosen in order to measure the COF under different lubrication regimes. A SRR of 5 % was selected because it is a reference value for rolling bearings. However, in order to study the effect of increasing the SRR in the value of the COF, a single measurement with a SRR of 50 % was also performed for each grease, at 40 °C.

Once again, fully flooded conditions were ensured by using a grease scoop.

Table 5.3: Ball-on-disc tests: operating conditions for measuring the Stribeck curves.

Temperature - T [°C]	20, 40, 60, 80, 110
Entrainment speed - U [m/s]	0.04 → 2 (logarithmic ramp)
Slide-to-roll ratio - SRR [%]	5, 50
Load - F [N]	50
Equivalent modulus - E* [GPa]	≈ 113
Maximum Hertzian pressure - p_0 [GPa]	≈ 1.09
Hertzian half-width - a [μm]	≈ 146.8

5.3.2 Stribeck curves results

In order to determine the lubrication regimes of the Stribeck curves measurements at different operating conditions, the same procedure reported in the previous section was used.

The film thickness measurements of each grease at different operating temperatures were corrected to represent the film thickness in a steel ball on steel disc contact, according to Equation 5.2. The specific film thickness was then calculated but now considering the composite roughness of the surfaces of the steel ball and the rough disc (Table 5.1 - $\sigma_c \approx 300$ nm). The calculated specific film thickness is shown in Figure 5.5. Comparing this figure with Figure 5.1, it is clear that a higher composite roughness greatly reduces the specific film thickness and therefore the lubrication regime is now very different.

According to Figure 5.5, the polymer greases operate mainly in mixed film ($\Lambda < 3$) lubrication only reaching boundary film ($\Lambda < 0.5$) for temperatures higher than 40 °C. On the other hand, the lithium thickened greases cross all lubrication regimes, reaching boundary film lubrication under low entrainment speeds and/or high temperature, and full film for low temperature (20 and 40 °C) and high speeds.

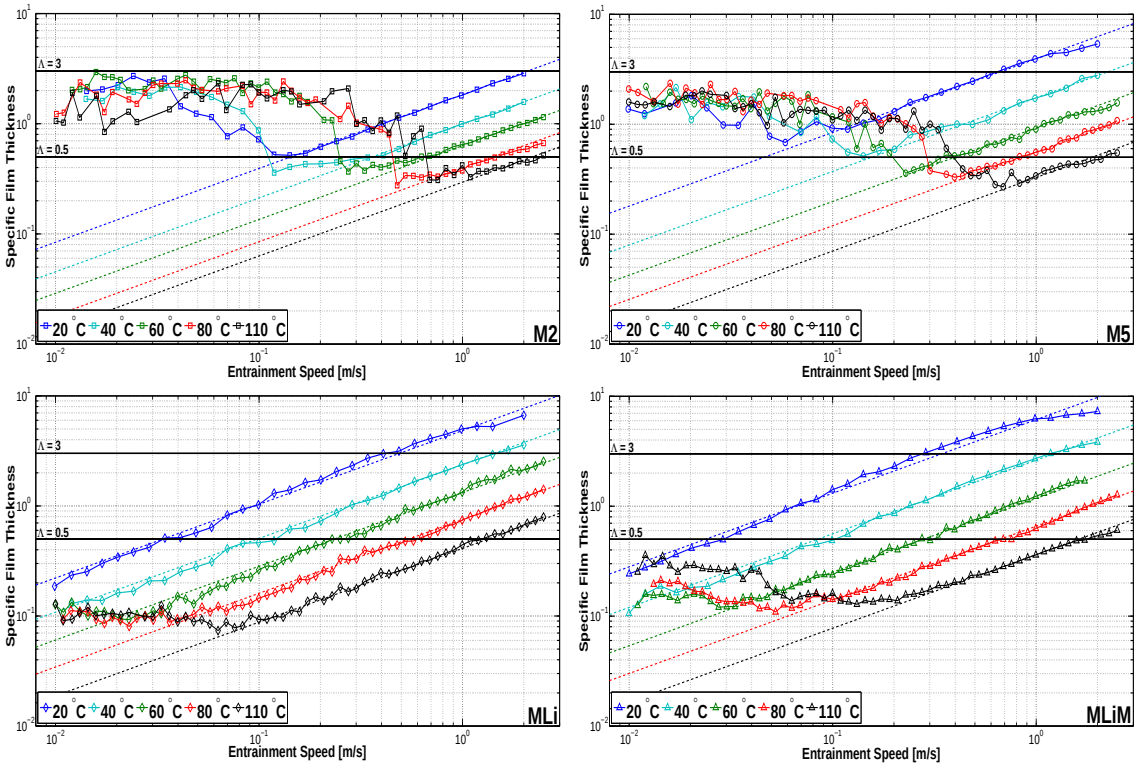

Figure 5.5: Specific film thickness of greases M2, M5, MLi and MLiM in a ball-on-rough disc contact.

Figure 5.6 shows a typical Stribeck curve. The coefficient of friction (COF) is plotted against the Hersey parameter [20], as shown in Equation 5.3.

$$S = U \cdot \eta \cdot F^{-1} \tag{5.3}$$

where U represents the entrainment speed, η is the lubricant's viscosity at the operating temperature and F is the normal load applied to the ball. Three lubrication regimes are clearly identified: boundary film, mixed film and full film (elasto-hydrodynamic).

The COF is frequently plotted versus this S parameter or only versus the entrainment speed, U. However, Brandão *et al.* [127] proposed a modified parameter S_p, to better represent the COF over different operating conditions [127]. This dimensionless parameter, represented by Equation 5.4, "normalizes" the abscissa of the curves, allowing to directly compare the coefficients of friction of different lubricants, when tested with the same surface's geometry, roughness and material, while taking into account the operating conditions (U, F) and the lubricant properties (η, α) at the average operating temperature of the test.

$$S_p = \frac{\eta \cdot U \cdot \alpha^{1/2}}{F^{1/2}} \tag{5.4}$$

In grease lubrication, the lubricant properties are generally attributed to the base oil's. If that is the case, the pressure-viscosity coefficient can be calculated using

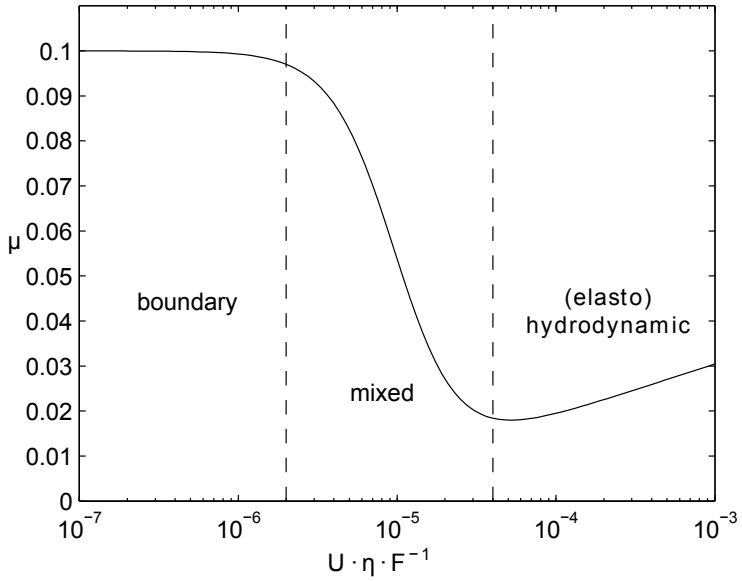

Figure 5.6: Typical behaviour of the coefficient of friction μ according to the Stribeck curve, showing the progress of the lubrication regimes as a function of the rolling speed. Courtesy of Brandão *et al.* [127].

Gold's Equation [77] (see Equation 3.7), taking into account the viscosity of the base oil at each operating temperature, T. The s and t values, taken from [77], are also attributed to the base oil's nature.

The inclusion of the α value is a way to account for the different natures of the lubricants (mineral, poly-alpha-olefin, ester...), if their viscosity at the operating temperature is the same. Furthermore, the combination of the viscosity and pressure-viscosity ensures that the film thickness influence is contemplated [127], which was not the case of the original Hersey parameter [20].

In this chapter however, the Hersey parameter was calculated from the values shown in Table 4.8. The reason for this is that the base oil is not representative of the grease's film thickness in fully flooded conditions. And since the actual measurements of the grease's film thickness are available and were used to determine the properties shown in Table 4.8, then these properties should be representative of the properties of the grease, if the geometry and operating conditions of the Stribeck curves are the same.

The Stribeck curves of grease M2 at different operating conditions are plotted in Figure 5.7a, as function of the entrainment speed. From the analysis of this figure, it is possible to observe that the coefficient of friction of grease M2 shows a very different behaviour from the typical Stribeck curve. The COF rises with the increase of the entrainment speed and reaches a maximum value after which it decreases again. This maximum is reached at different entrainment speeds, but its value is similar for curves

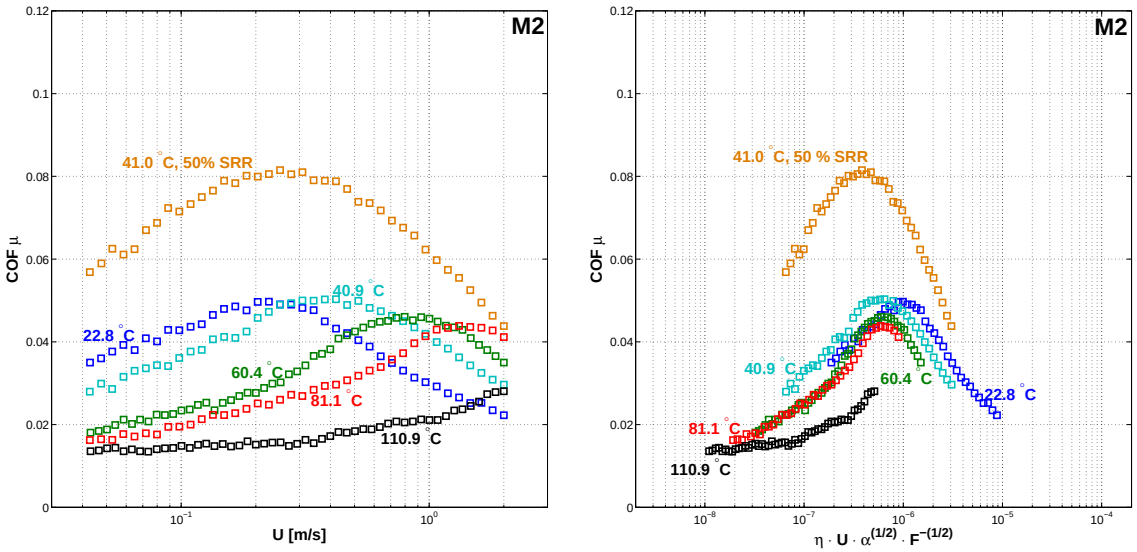

(a) Entrainment speed **(b)** Hersey modified parameter

Figure 5.7: Stribeck curves of grease M2. All curves were obtained with a SRR of 5 %, except the one labelled with 50 %. The average operating temperature of each curve is also stated.

measured at different temperatures. The transition speed, at which the maximum COF is reached, generally increases with the increase of the operating temperature. This was observed for all tested greases and shows a similar behaviour to the film thickness curves shown in Chapter 4.

On the other hand, Figure 5.7b shows the same Stribeck curves but now plotted versus S_p. In this figure, the maximum value of the COF between curves measured at different temperatures is reached at quite close S_p numbers (around 7×10^{-7} for a SRR of 5 %). This result seems to indicate that even if the entrainment speed is different, the lubrication regime at that abscissa is the same between temperatures. As the operating temperature increases, the curves move slightly to the left, towards boundary lubrication.

Calculating the S_P parameter which corresponds to the transitions between lubrication regimes shown in Figure 5.5, the following relationships can be established:

- Full film: $\Lambda \geq 3 \rightarrow S_p \geq 7\times10^{-6}$;
- Mixed film: $0.5 \leq \Lambda \leq 3 \rightarrow 5.5\times10^{-7} \leq S_p \leq 7\times10^{-6}$;
- Boundary film: $\Lambda \leq 0.5 \rightarrow S_p \leq 5.5\times10^{-7}$.

Figure 5.8 shows the Stribeck curves of greases M2, M5, MLi and MLiM measured under different operating conditions. The lubrication regime limits are also represented. According to these limits, the Stribeck curves of greases M2 and M5 suggest that the COF increases with the decrease of entrainment speed, reaches a maximum at the end of the mixed film ($\Lambda = 0.5$) lubrication zone and then decreases again already in boundary film lubrication. This behaviour can only be explained by comparison with the film thickness results of the previous section. Under low entrainment speeds ($U < u_{tr}$) and fully flooded conditions, the thickener is responsible for increasing the film thickness [100, 101, 115] which reflects in a decrease of the friction coefficient in this zone.

However, in the case of grease MLi and MLiM, the results obtained are different. The curves seem to start from a plateau and then to decrease with the increase of S_p (and entrainment speed). This behaviour is similar to the typical Stribeck curve where the COF starts from a plateau in boundary lubrication and then starts to decrease as it reaches mixed film lubrication.

The effect of increasing the SRR can also be seen in Figure 5.8 and is very similar between greases: the COF increases in the tests performed with higher SRR values, as the lubricant is more severely sheared. This phenomenon was observed for all greases, independently of the thickener type. The maximum value of the COF

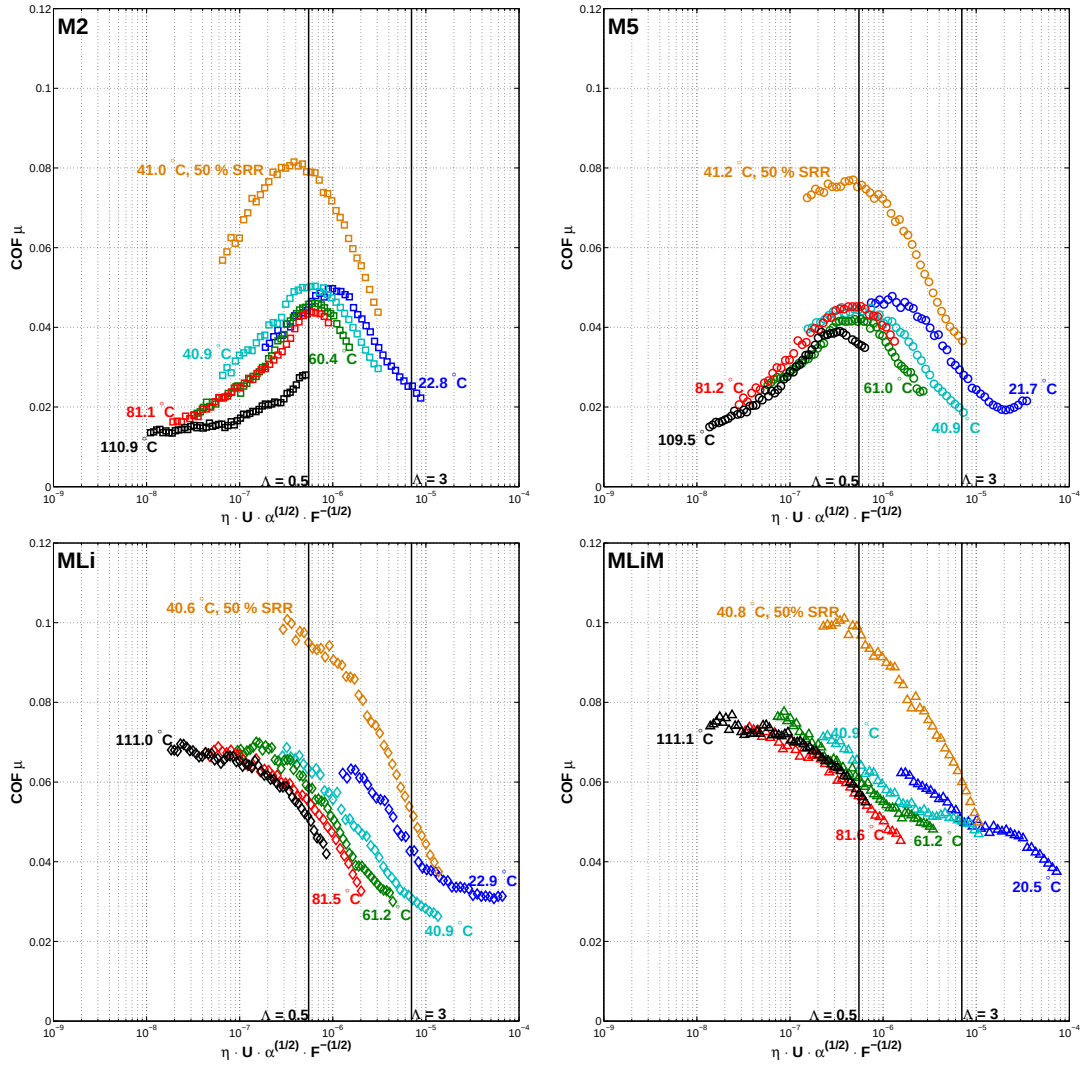

Figure 5.8: Stribeck curves of greases M2, M5, MLi and MLiM plotted against the modified Hersey parameter S_p. All curves were obtained with a SRR of 5 %, except the one labelled with 50 %. The average operating temperature of each curve is also stated.

increases and its dependence on the rolling speed is also higher. The overall behaviour of the curves is the same for both the PP and LiX thickened greases.

In Figure 5.9, the Stribeck curves of greases M2, M5, MLi and MLiM are compared under the same operating conditions. The COF of the lithium thickened greases MLi and MLiM is always higher than the polymer greases M2 and M5 when compared under the same S_P numbers (and therefore, same lubrication regime). Their COF always decreases with the increase of the S_P number for any operating condition and its behaviour is much different from the polymer greases under low entrainment speeds. Once again, this difference is surely related with the thickener type/dimensions/morphology, because a similar behaviour was also observed in the film thickness tests.

The COF's of greases MLi and MLiM are very similar under low speeds and/or high operating temperatures which was expected since they are formulated with the same thickener type. Under mixed and full film lubrication regimes, the COF of grease MLiM is higher than grease MLi which should be due to the different natures of the base oils, given that their viscosities are similar.

Grease MLiM shows higher coefficient of friction than grease MLi and even higher than the polymeric greases M2 and M5 at any operating temperature. This difference gets more important as the operating temperature increases and the curves move to the left towards boundary lubrication.

The friction behaviour of greases M2 and M5 is very similar, specially in the mixed film regime ($0.5 < \Lambda < 3$). Although grease M5 shows higher film thickness than grease M2 under high entrainment speeds, their COF is very similar at temperatures below 80 °C. Above this value, the COF of grease M5 is always higher than the COF of grease M2 which is also in agreement with the film thickness measurements shown in Figure 5.5, since the film thickness of grease M2 in the plateau region ($U < u_{tr}$) was higher than grease M5.

Table 5.4 shows the maximum and minimum values of the COF of each grease for the tests performed under a SRR of 5%. The differences between the polymer and lithium thickened greases are obvious. However, the fact that a decrease of the COF was not observed under low entrainment speeds for greases MLi and MLiM, it does not necessarily mean that their behaviour is different, but only that an even smaller entrainment speed might be needed for the same behaviour to be observed [100, 101].

Table 5.4: Maximum and minimum COF of grease M2, M5, MLi and MLiM, measured in the tests performed at different operating temperatures and a SRR of 5%.

	COF_{min}	@ operating conditions	COF_{max}	@ operating conditions
M2	0.014	110 °C, 0.04 m/s	0.050	40 °C, u_{tr}
M5	0.015	110 °C, 0.04 m/s	0.048	20/40 °C, u_{tr}
MLi	0.026	40 °C, 2 m/s	0.070	110 °C, 0.04 m/s
MLiM	0.038	20 °C, 2 m/s	0.078	110 °C, 0.04 m/s

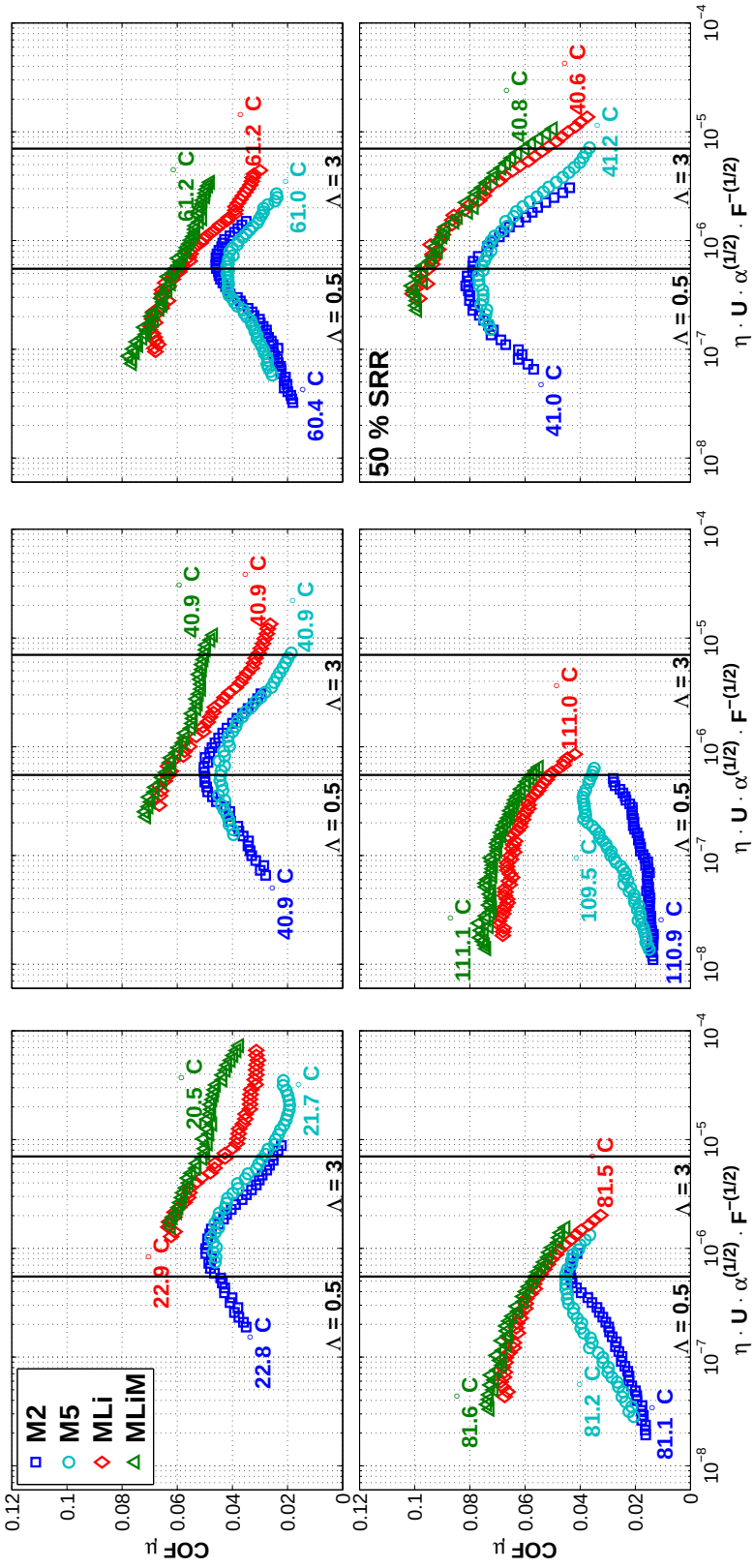

Figure 5.9: Stribeck curves of grease M2, M5, MLi and MLiM at different operating conditions.

5.3.2.1 Thickener content

In Figure 5.10, the Stribeck curves of the polymer greases M1, M2 and M3 are shown, for different testing conditions. These greases show very similar COF for higher S_p numbers in the mixed lubrication zone, independently of the operating temperature or SRR. As the entrainment speed increases and the lubricant film thickness becomes more relevant, the COF of the greases overlap as expected from greases formulated with the same base oil.

However, the differences in the thickener content can be seen for lower S_p numbers. Based on these results, the maximum value of COF decreases with increasing thickener content. Below the transition speed where the maximum value occurs, the COF is higher for grease M1 (11 % PP) and smaller for grease M3 (15 % PP). The transition speed also increases with increasing thickener content.

The reason behind this is unclear but it might be related to more frequent

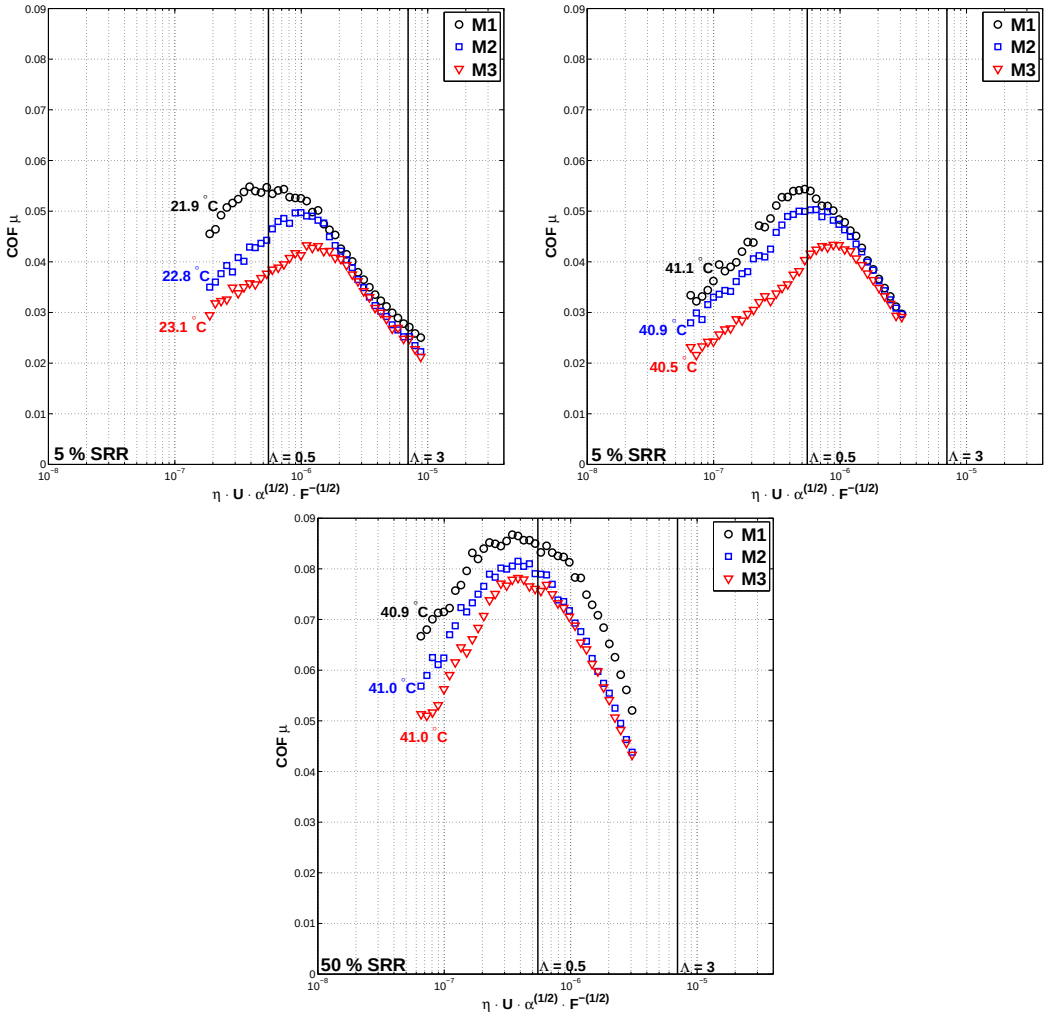

Figure 5.10: Stribeck curves of grease M1, M2 and M3 at different operating conditions.

thickener lumps entering the contact due to the higher thickener content or eventually related to the consistency of the grease (which increases with the thickener content) and its effect on the contact replenishment under fully flooded conditions.

5.3.2.2 Grease vs base oil

In order to better understand the coefficient of friction behaviour of the tested greases, Stribeck curves of their base oils were also measured. The curves, measured at different operating conditions, are shown in Figures 5.11 and 5.12, comparing each grease with its base oil. The S_P numbers were calculated using the properties of the grease from Table 4.8 and those of the base oils, from Table 4.2.

Analysing Figures 5.11 and 5.12, it is possible to observe that the COF of the

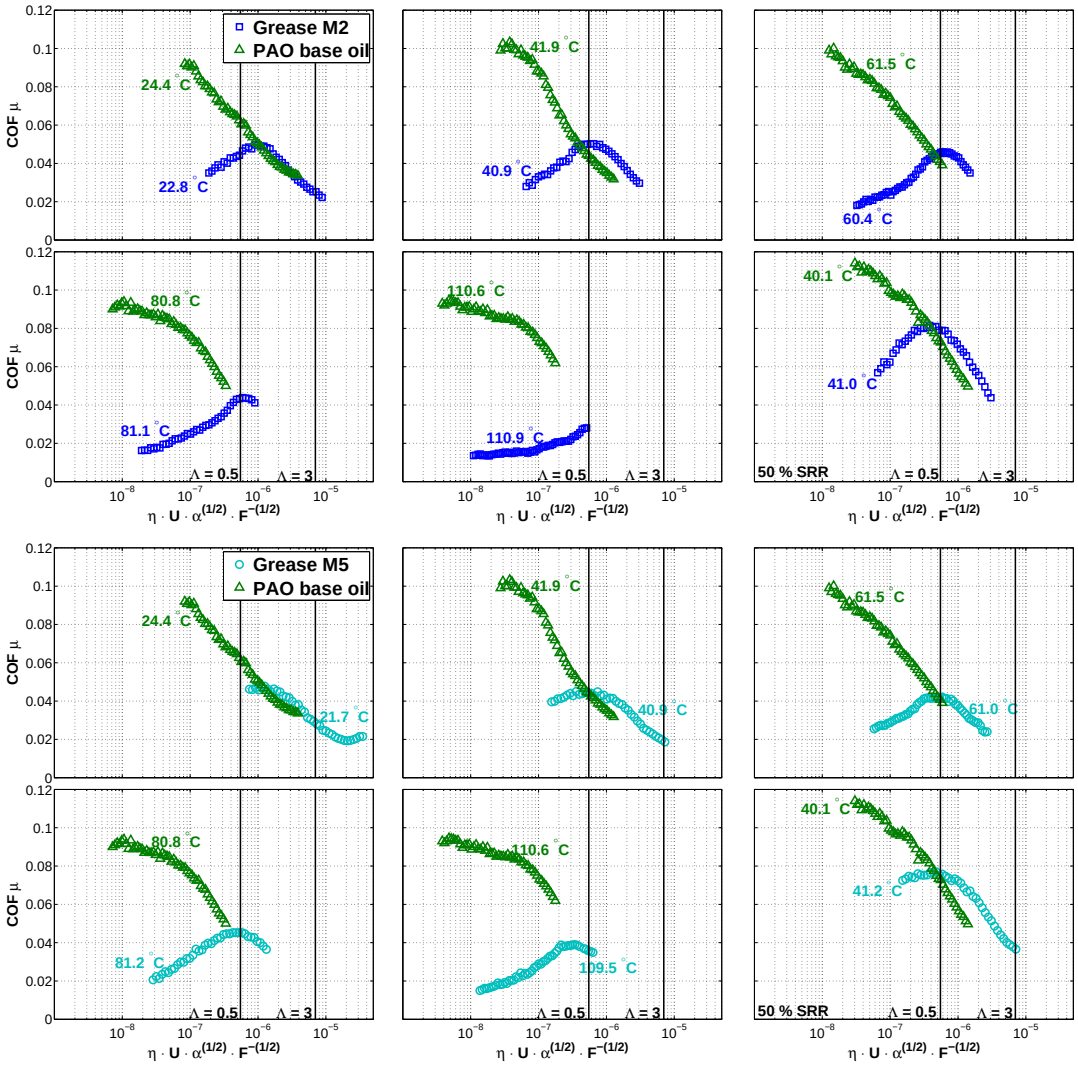

Figure 5.11: Stribeck curves of greases M2 and M5 and their corresponding base oils, at different operating conditions.

greases in the mixed film lubrication zone ($0.5 < \Lambda < 3$) shows a similar behaviour to the base oil. In this region, the COF decreases with the increase of the S_p because the film thickness is increasing with speed. Since the greases generates a thicker film than its base oils in fully flooded conditions (see Figures 4.10 and 4.11), the COF of the grease in this zone is also generally higher than the base oil, due to higher viscous friction, promoted by a stronger hydrodynamic effect.

On the other hand, under the operation conditions which promote boundary film ($\Lambda < 0.5$) lubrication - i.e. low speeds and high operating temperatures - the base oil generally shows a higher COF than the grease. In this region, the COF of the base oil keeps rising as the speed decreases, until it reaches a plateau (COF $\approx$ 0.1) at very low speeds. The plateau is reached at much higher COF values than the greases' under the same S_p numbers. The fact that, in fully flooded conditions and

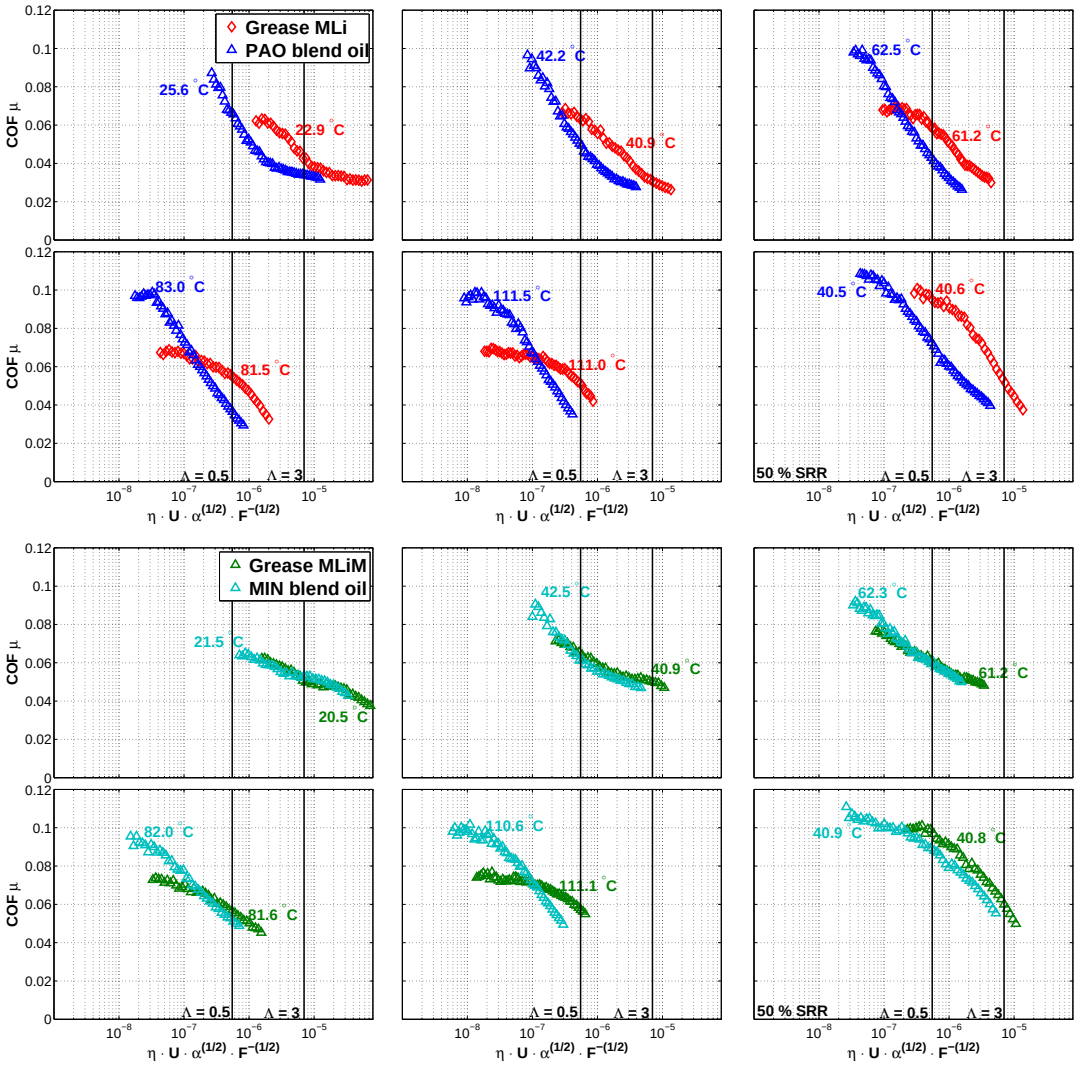

Figure 5.12: Stribeck curves of greases MLi and MLiM and their corresponding base oils, at different operating conditions.

low speeds, there is thickener material entering the contact, contributes to increase the film thickness and to decrease the COF. Otherwise, the COF would also continue to increase, similarly to the base oils, as the lubrication regime gets closer to boundary film or even dry lubrication conditions.

Although this was observed for all greases independently of their formulation, this phenomenon is much more relevant in the case of the polymer greases. In fact, analysing Figure 5.5, the film thickness of the polymer greases at low entrainment speeds (mixed film) is much higher than the film thickness of the lithium thickened greases (boundary film), explaining why the COF of these greases is also so different under low S_P numbers.

It is useful to plot Stribeck curves of COF against the S_p parameter, because, by doing so, the curves position themselves in the horizontal axis according to lubrication regime. However, when comparing each grease with its base oil, it is also interesting to plot them over a common abscissa, such as the entrainment speed. Figure 5.13 shows the measured Stribeck curves plotted versus speed, for a few selected operating conditions.

Although all the observations previously made regarding Figures 5.11 and 5.12 are still valid for Figure 5.13, the interpretation of a few behaviours is easier. It is now clear that the COF of each grease and its base oil are equal or very close under high speeds, even if the film thickness of the grease is higher for those conditions. It is also clear that at low entrainment speeds, the COF of the greases is much smaller than the COF of the corresponding base oils, difference which was already attributed to thickener material entering the contact. This phenomenon is intensified as the temperature increases and the lubrication regime approaches boundary film.

The differences between greases M2 and M5 are also more clear. Despite being formulated with the same base oil and the same thickener content, the fact that grease M2 and M5 show different behaviours is related to the elastomer (co-thickener) content. As observed in other works [39], the oil which effectively is released from the grease under static or dynamic conditions - here called “bleed-oil” - might have physical properties significantly different from the base oil. These different properties depend on the thickener type, elastomer content and/or the additive package. In the case of grease M5, the elastomer originates a bleed-oil of much higher viscosity than the original base oil, despite showing shear-thinning behaviour. The consequence of having an active lubricant of higher viscosity reflects in higher film thickness, which by turn might lead to lower friction depending on the lubrication regime. This is also why the COF of grease M5 is much smaller than the COF of the PAO base oil for the complete speed range. For these formulations whose base oil shows different properties from the bleed-oil, then the base oil might not be representative of the

grease behaviour.

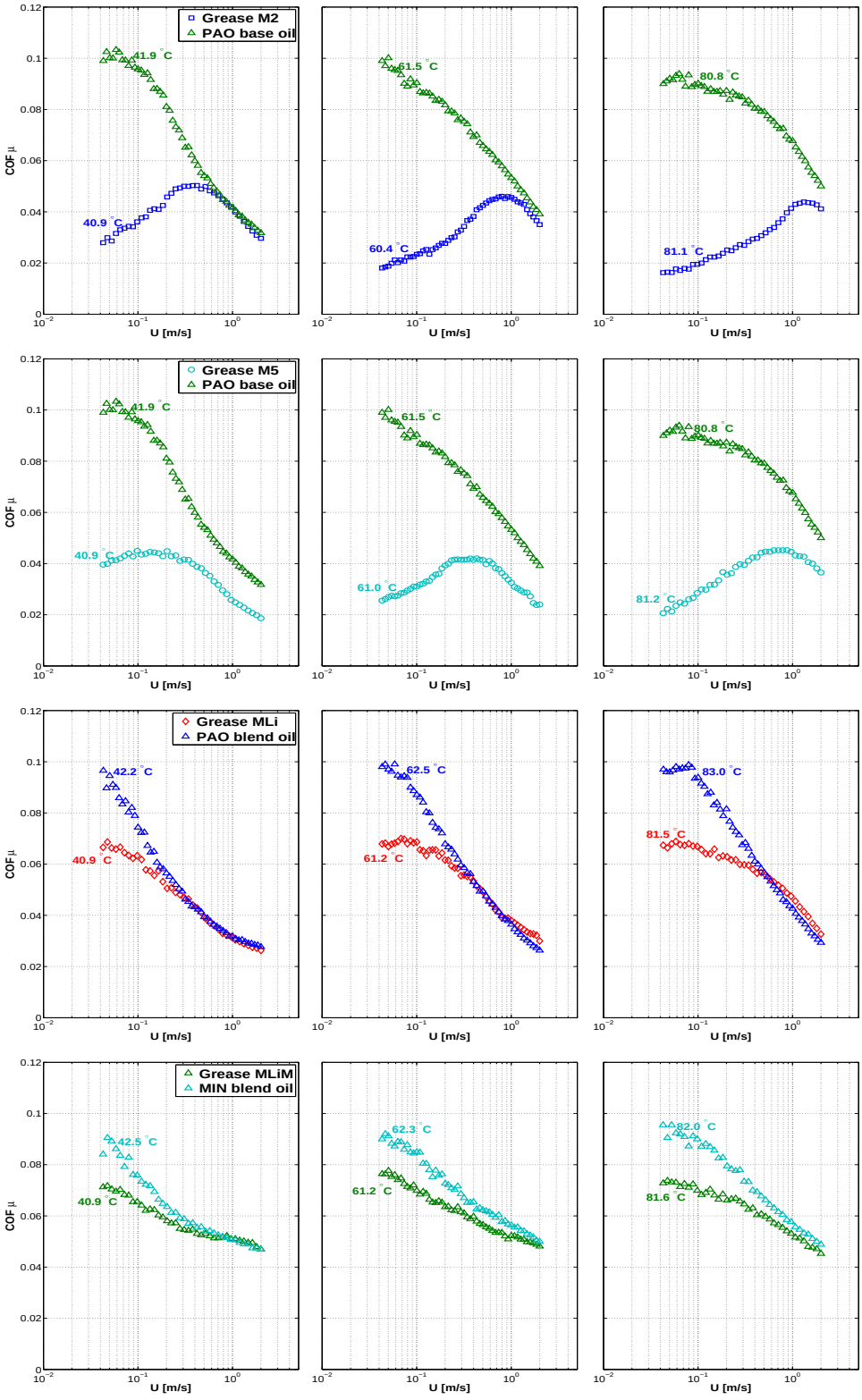

Figure 5.13: COF of friction of greases M2, M5, MLi, MLiM and their base oils, plotted versus the entrainment speed. Test conditions: 40, 60 and 80 °C, 5 % SRR.

5.4 Closure

Traction and Stribeck curves were performed with four differently formulated polymer thickened greases and two lithium thickened greases, under fully flooded conditions.

The traction measurements were performed with a smooth disc and high specific film thickness, mainly operating under mixed and full film lubrication. In these conditions it was not possible to observe significant differences between greases formulated with different thickener content given that the friction behaviour is mainly ruled by the base oil viscosity. However, it was possible to differentiate the greases formulated with different thickener types and/or different base oil viscosity/nature. Grease MLiM always showed the highest traction coefficient and on the other hand, grease M5 always showed the smallest.

As expected from the film thickness results shown in Figure 4.8 of the previous chapter, the thickener contributes to the increase of the film thickness at low entrainment speeds. This increase also affects the friction behaviour, as shown by the Stribeck curves reported here. These curves were measured with a rough disc, to promote smaller specific film thickness values.

Particularly for the polymer greases, the coefficient of friction increases with the decrease of the entrainment speed (typical from mixed lubrication regime) and after reaching a maximum value it starts to decrease again. This maximum should occur when the boundary lubrication regime is reached. However, the fact that thickener material enters the contact under low speeds should be responsible for the consequent decrease in the coefficient of friction.

In the case of the lithium thickened greases MLi and MLiM the previously described behaviour could not be observed. These greases show the typical behaviour of a Stribeck curve where the coefficient of friction increases almost linearly with the decrease of the entrainment speed at constant operating temperature, as expected from mixed film lubrication. The maximum value of COF is reached and then a plateau is formed, typical from boundary film lubrication. The reason for this difference should lie in the fact that the film thickness plateau at low speeds for this grease is reached at much lower entrainment speeds and at very low film thickness values.

Comparing the results of the differently formulated greases M2, M5, MLi and MLiM it should be noticed that the LiX thickened greases always show higher coefficient of friction, particularly grease MLiM, formulated with a mineral based oil. While this should be already expected due to being formulated with a base oil of higher viscosity, the fact that this happens when operating under the same S_p numbers and therefore similar lubrication regime (despite different combinations of viscosity and

entrainment speed), indicates that these greases show higher coefficient of friction even when the film thickness should be very similar to the polymer greases'.

Finally, it was found that the friction behaviour of the greases is very similar to their base oils in the mixed film lubrication regime. However, under boundary film lubrication the COF of the base oils is always higher than the greases.

6 Starved grease lubricated contacts

6.1 Introduction

Starvation was first visually observed using optical interferometry in oil lubricated contacts by Wedeven *et al.* [103] in 1971, followed by Chiu *et al.* [139] and later by Pemberton and Cameron [140]. Wedeven *et al.* [103] observed that if the inlet region is properly flooded with lubricant, the inlet pressure build-up will generate a film thickness which is insensible to further increase in the lubricant supply - fully flooded condition [103]. However, if there is no replenishment or if the inlet region is insufficiently filled, a lubricant-air meniscus is formed at the contact inlet when the lubricant layers from the rolling element and raceway merge [2, 99]. The pressure build-up is delayed and the film will be restricted and dependent on the lubricant supply available at the inlet. This phenomenon will not only severely reduce the film thickness, but as the contact gets further starved, the pressure spike close to the outlet will get smaller, up to the point where the pressure build-up resembles an Hertzian dry-contact [2]. As the contact starves, the central film thickness approaches the minimum film thickness and the load caring capacity is decreased. This condition where an increase in the lubricant supply results in increased film thickness, is called starvation.

The film thickness and friction tests reported in the previous chapters were performed assuming the contact is fully flooded. This condition was ensured using a scoop which continuously feeds the contact with grease. However, if no scoop is used, the lubricant supply continually decreases with successive over-rollings because the grease is pushed to the sides [2, 141]. Even though starvation can also happen in oil lubricated contacts, it is much more frequent in grease lubrication mainly because of the very high viscosity of the grease at low temperatures and low shear and consequently, its low mobility [2, 92, 141].

Aihara and Dowson [142] performed an experimental study in a two-disc machine, suggesting that the grease's film thickness under starvation was about 70% of the fully flooded film thickness of the base oil. Kauzlarich and Greenwood pointed that shear degradation of the grease leads to a reduction of the film thickness with

time [97]. Later, Aström *et al.* [143] found that the grease's yield stress (τ_y) and/or high viscosity at low shear rates is responsible for slower contact replenishment. The authors also claimed that spin helps to transport the grease from the side bands to the inlet, contributing to a better replenishment.

Cann *et al.* [92] performed film thickness measurements over time at constant operating conditions and observed that the degree of starvation (ratio between the starved and the fully flooded film thickness) increases with rolling speed, base oil viscosity and thickener content, but it decreases with temperature. The thickener content affects the grease consistency and a starved film thickness plateau is reached sooner for greases with higher thickener content. Furthermore, they also found that higher thickener content also slows the oil bleeding, restricting the film build-up. Increasing base oil viscosity also increases the degree of starvation which might also be related to the smaller oil bleeding it promotes. On the other hand, the temperature increase and the consequent decrease in consistency improves the replenishment and the degree of starvation is reduced.

Also using optical interferometry to visually determine when starvation occurs in a ball-on-disc contact, Kaneta *et al.* [31] found that starvation takes place quicker with greases formulated with high viscosity oils. They also found that starvation occurs easily with higher speeds because the time for replenishment between over-rollings is shorter, hindering replenishment. More recently, Chen *et al.* [141] performed film thickness measurements over increasing speed in a ball-on-disc device and found that starvation occurs at smaller speeds with greases formulated with base oils of smaller viscosity, contradicting what was expected for oil lubrication where smaller viscosity oils show better replenishment.

Mérieux *et al.* defined the most common behaviours in starved grease lubrication [144], according to Figure 6.1. In this figure, the film thickness decreases with time as the contact gets depleted from lubricant, quickly dropping from the fully flooded value (a). From here, the film thickness may continually drop (b) or eventually stabilize (c). Quite often, it is also possible that replenishment is recovered and the film thickness may rise again (d).

According to Cann [112], the level in which film thickness stabilizes (residual layer) is composed by a liquid layer of base oil on top of a solid-like, thickener-rich layer, with thickness values between 6 nm and 80 nm [34]. That layer, measured at the end of the test at zero speed (h_R), is a portion (or all) of the static layer. Such behaviour was well predicted by the thin layer flow model developed by Venner, *et al.* [41] using the base oil viscosity as input and the thickener layer thickness as zero level. Such comparisons can be found in [145]. This is a remarkable result and points to new lines of research aiming at studying thickener-additives-surface interaction

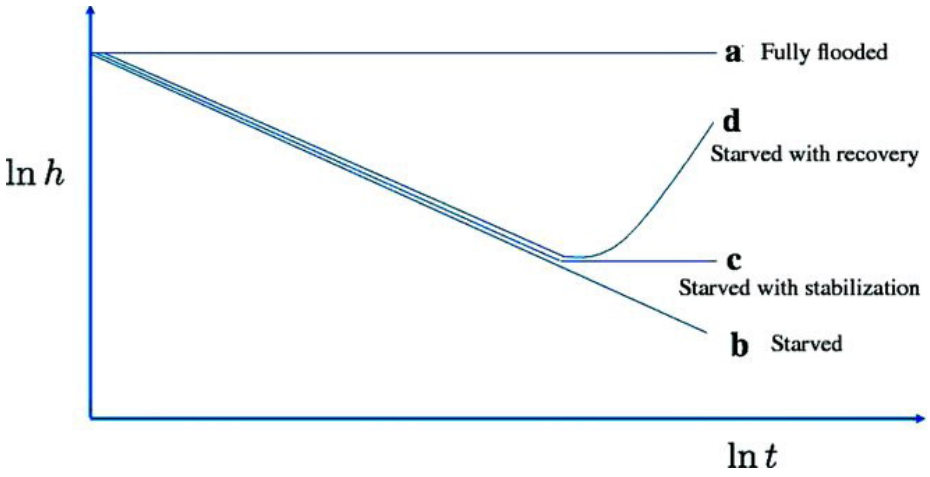

Figure 6.1: Characteristic starvation behaviour for grease lubrication [144].

and their characteristics when thick boundary layers are formed.

In spite of the fact that some grease lubricated rolling bearings operate under fully flooded conditions, the large majority operates under starvation. To achieve the fully flooded condition, it would be necessary to continuously supply a flow of grease to the rolling bearing which is generally undesirable since it promotes high torque and excessive churning, resulting in high operating temperatures and ultimately, failure [92]. Therefore, in normal operating conditions and depending on the initial grease volume and distribution, the contacts will eventually starve due to side flow, centrifugal effects and/or gravity, cage scraping, surface tension, air flow or oil bleeding from grease and evaporation [2].

6.2 Measurement procedure

6.2.1 Film thickness

Three different tests were performed to evaluate the film thickness evolution with time:

1. central film thickness, measured over entrainment speed;
2. central film thickness, measured over time;
3. film thickness profile pictures across the contact area, measured over time.

The same materials reported in Chapter 4 were used here. In any of the three different tests, all operating conditions were set constant except for time or entrainment speed. In the first test type, three speed ramps were performed at constant load, temperature and SRR as reported in Table 4.1 of Chapter 4.

The ball-on-disc device used in this work does not allow for the scoop to be removed during the actual test and therefore, no scoop was used right from the beginning. Since the lubricant supply should be changing with each ramp, no average of three measurements was calculated. However, given that the ramps were performed from low to high speeds, the first ramp should be representative of the fully flooded result. The speed ramps were performed controlling the temperature at 20, 40 and 80 °C.

In the second test type, the central film thickness was measured for each grease at the conditions stated in Table 6.1. Test number 1 was used as reference while the other tests were performed only changing one of the conditions at each time. At the end of each test a zero speed thickness was also measured. The test duration was 1800 s, although the results will only be shown for the first 1200 s since it was frequent for the disc track to show some damage after this time for some of the tests.

Finally, in the third test type, the same operating conditions shown in Table 6.1 were used but instead of using a spectrometer to obtain the monochromatic interference fringes which allow to calculate the central film thickness, the Space Layer Imaging Method (SLIM) [118] was used. This method uses a sensitive RGB (red, green, blue) colour camera to capture an image of the contact area. The colours of the pixels can be used to calculate the film thickness, producing 3D maps of the film thickness profile across the contact area. These testes were only performed to better understand how the film thickness profile would change along the test duration, but the central film thickness was not computed from them.

6.2.2 Coefficient of friction

The coefficient of friction was also measured to investigate starvation. Using the same ball-on-disc device and the same specimens (ball-on-smooth steel disc) reported in Table 5.1 of Chapter 5, the coefficient of friction was measured over time at constant operating conditions. Once again, four different tests were explored, according to the conditions reported in Table 6.1.

Table 6.1: Operating conditions of the central film thickness measurements and coefficient of friction measurements.

Test number	Ref. - 1	2	3	4
Entrainment speed - U [m/s]	0.5	1	-	-
Temperature - T [°C]	40	-	80	-
Slide-to-roll ratio - SRR [%]	5	-	-	50
Load - F [N]	50	-	-	-

6.3 Film thickness results

6.3.1 Central film thickness measured over entrainment speed

The central film thickness of the ball-on-disc contact, measured over increasing entrainment speeds at 20 °C is shown in Figure 6.2, for greases M5 and MLi. The fully flooded result at each temperature, shown before in Figure 4.7 of Chapter 4, is also shown here for easier comparison.

According to Figure 6.2, the differences between the first and third speed ramps are very clear, showing that the longer the test duration, the higher is the deviation from the fully flooded result. The lack of scoop causes the contact to gradually starve as the time of the test increases, associated of course with the increasing speed (and centrifugal forces) which pushes the grease away from the contact.

It is also evident how the lack of scoop greatly increases the scatter of the results not only in low speed region, but also in high speed region. It was also common to measure film thickness values above the fully flooded result for certain speeds. The grease's chaotic and random behaviour [146] makes it hard to measure a representative film thickness for a certain operating condition. It was also difficult to obtain repeatable curves, without the scoop to "control" the replenishment. In the case of the polymer greases, probably due to the increased thickener size, it was even harder.

In Figure 6.3, the central film thickness results are shown for different operating temperatures. In this figure, only the 3^{rd} speed ramp is shown, compared to the fully flooded result.

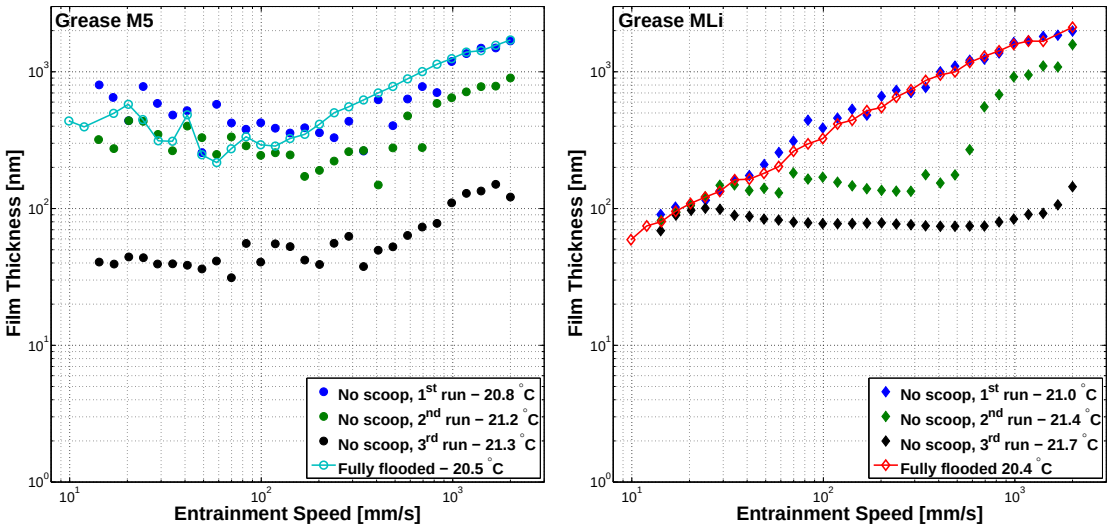

Figure 6.2: Central film thickness of a ball-on-disc contact, measure over increasing entrainment speed for greases M5 and MLi at T=20 °C and SRR = 5 %.

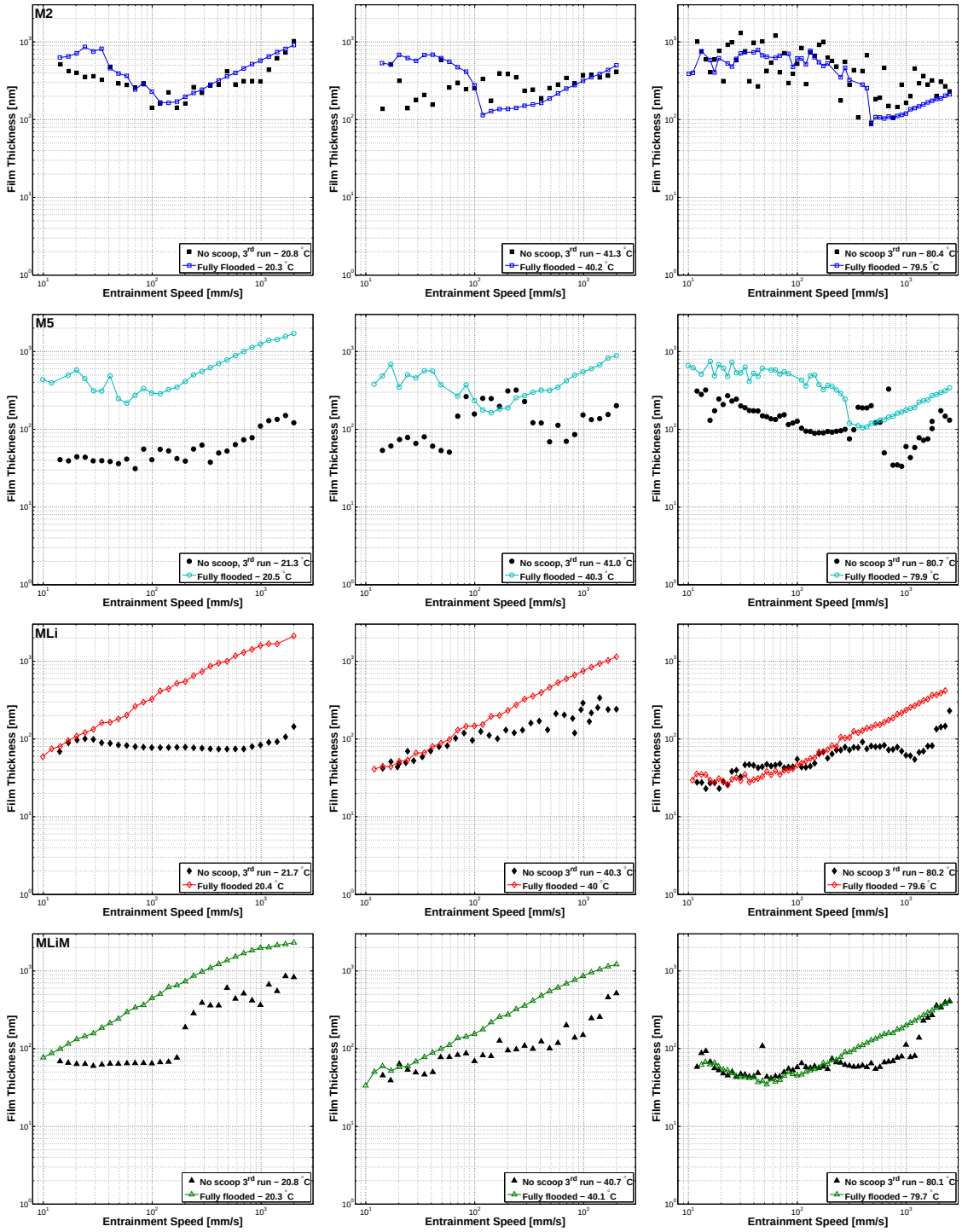

Figure 6.3: Film Thickness curves of greases M2, M5, MLi and MLiM, measured over increasing entrainment speed at 20, 40 and 80 °C.

Regarding the effect of increasing speed, it was observed that generally, there is a speed value at which the film thickness drops from the typical slope of $U^{0.67}$. That speed seems to increase with increasing temperature, showing that the higher the operating temperature, the contact replenishment is easier and therefore, the

starvation phenomenon happens later.

For the LiX thickened greases, as soon as starvation occurs, the film thickness becomes almost independent of speed, even in the low speed region were the thickener should contribute for the film thickness. However, it was frequent for the replenishment to recover as the speed increased. In this situation, the film thickness increased again, approaching the fully flooded result. This recovery was also observed for the polymer greases, under certain operating conditions.

At 80 °C, the film thickness curves of all greases besides M5, are closer to the fully flooded result. In this situation, the grease consistency is lower which should facilitate the replenishment. However, the film thickness decay at high speeds is still observed. In the case of grease M2 at 80 °C, it is not possible to define a clear behaviour since the three curves are a cloud of points at different film thickness values which do not follow any trend.

6.3.2 Central film thickness measured over time

The central film thickness of grease MLi, measured over time in the ball-on-disc contact at a temperature of 40 °C, 5 % of SRR and under an entrainment speed of 0.5 m/s, is shown in Figure 6.4.

The fully flooded result measured under the same operating conditions is shown as a black horizontal line and a red dash-dotted line, respectively for the grease and base oil. The film thickness value corresponding to the plateau found at low speeds (see section 4.5 of Chapter 4) on the film thickness curves of the each grease under fully flooded conditions is also represented, as a green dashed line. In the same figure, pictures of the film thickness profile over the contact area are also shown, obtained using the SLIM method. Although these pictures do not correspond directly to the central film thickness curves, they should be illustrative of the film thickness evolution over time under these operating conditions.

It is generally observed that the initial film thickness value is similar, but frequently higher than the fully flooded film thickness of each grease under the same operating conditions. In the case of the polymer greases it is common to find even higher values, closer to the film thickness plateau under low speeds. Just a few seconds into the test, the film thickness of all greases drops quickly. After some time, the film thickness decay rate slows considerably, reaching the stabilization stage (see Figure 6.1), as expected from the literature [144].

In the stabilization zone, the film thickness decreases very slowly but it is frequent to observe considerable scatter as the thickener lumps cross the contact. Although this was observed for all greases, it is specially relevant in the case of

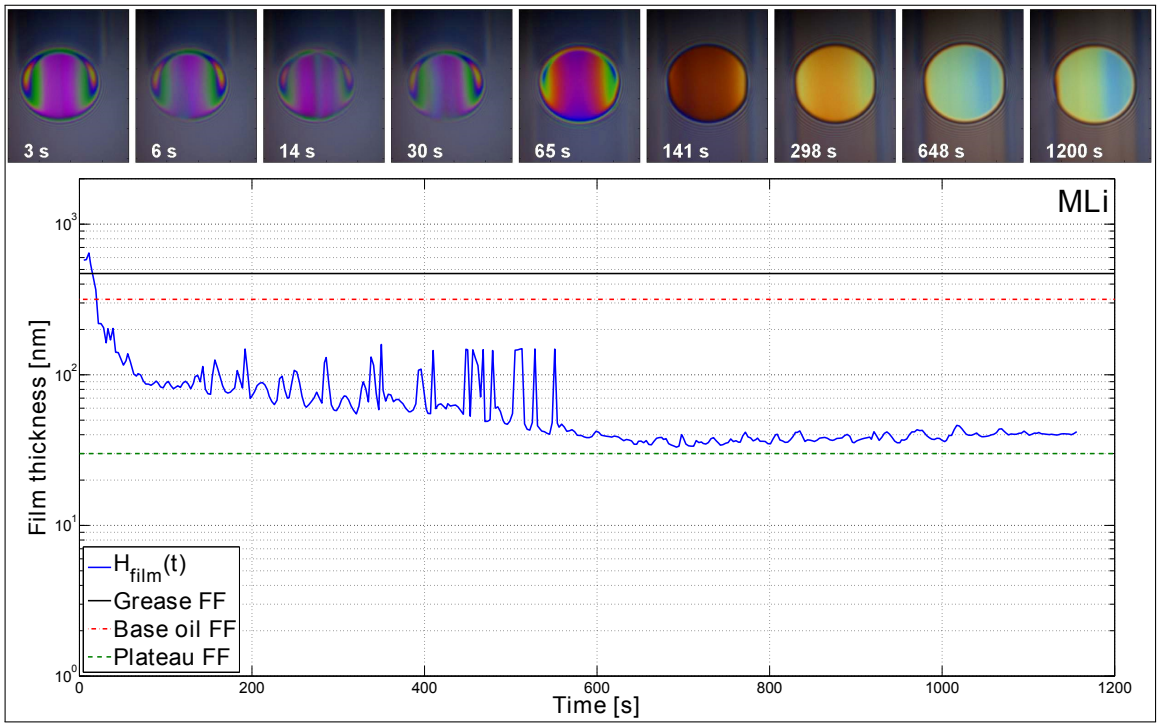

Figure 6.4: Central film thickness of a ball-on-disc contact, lubricated with grease MLi under U=0.5 m/s, P=50 N, SRR=5 % and T=40 °C.

the polymer greases where larger and more frequent lumps cross the contact very frequently, reflecting in high film thickness peaks. Sometimes the opposite is observed and the replenishment suddenly fails and a very sharp valley is formed. It was also common for the replenishment to improve for a while and consequently, the film thickness also increased. However, this loss and recovery balance seems completely random and independent of grease formulation.

Analysing the film thickness pictures it is also possible to see that generally, in the first 100 seconds of operation, the film thickness profile resembles a "horse-shoe" which is typical of a fully flooded contact. As the time increases, this profile will continuously change until starvation is reached. As an example, Figure 6.5 shows the top view of the film thickness profile of grease MLi in the operating conditions of Test 3 (see Table 6.1), after 5, 29 and 140 seconds of test time. In the same figure, cross-section film thickness curves are shown, taken over a central line parallel to the rolling direction and over a line transverse to the rolling direction. From these curves it is possible to observe the evolution of the central and minimum film thicknesses during the test. As the time increases and the contact gets further starved, the ratio $h_m/h_{0c} \longrightarrow 1$ and starved conditions are reached.

Figures 6.6 and 6.7, show the central film thickness curves of greases M2, M5, MLi and MLiM measured over time, under the operating conditions reported in Table

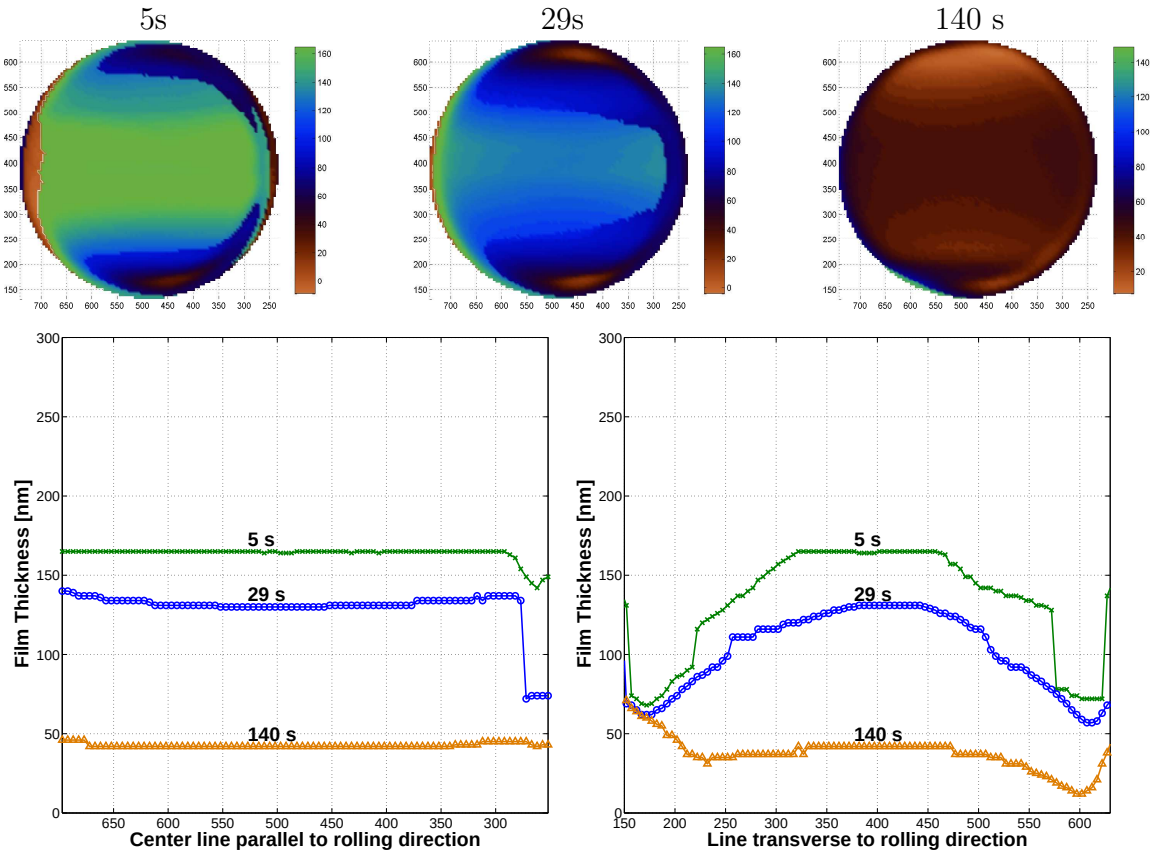

Figure 6.5: Film thickness profiles of grease MLi, taken during Test 3: top view (top) and cross sections parallel to the rolling direction (bottom left) and transverse to the rolling direction (bottom right).

6.1. All curves show a behaviour similar to the one reported for grease MLi in Figure 6.4. To analyse the influence of different operating conditions, each test was compared to the reference Test 1. The average and standard deviation of the film thickness in the stabilization zone is shown in Table 6.2 for all tests and greases. The zero speed film thickness measured at the end of the test is also shown, despite no relationship could be found regarding grease formulation or operating conditions.

In the beginning of reference **Test 1**, all greases show a film thickness value higher than the greases' fully flooded result, quickly decreasing to film thickness values below the fully flooded base oil result. In the case of the lithium thickened greases, the film thickness value in the stabilization zone is higher, although very close to the greases' film thickness plateau at low speeds.

Performing the tests under higher entrainment speed (**Test 2**), the film thickness decay rate increases for all greases. Once again, the polymer greases show initial values of film thickness near the low speed plateau and the lithium greases film thickness values above the greases' fully flooded result. However, the film thickness in the stabilization zone seems to have increased for greases M5 and MLi, but to decrease

Table 6.2: Average ($\overline{h}_{st}$) and standard deviation ($\sigma_{\%}$) of the central film thickness of greases M2, M5, MLi and MLiM from 1000 to 1200 s. The zero speed film thickness (h_R), measured at the end of the test, is also shown.

Test conditions		Test 1 40 °C 0.5 m/s 5 %	Test 2 40 °C **1 m/s** 5 %	Test 3 **80 °C** 0.5 m/s 5 %	Test 4 40 °C 0.5 m/s **50 %**	Trends in starvation tests
M2	h_G	192	318	98	192*	
	$\overline{h}_{st}$	123	80	321	30	$U \nearrow$ $h_{0c} \searrow$ $h_R \searrow$
	$\sigma_{\%}$	17	56	85	10	$T \nearrow$ $h_{0c} \nearrow$ $h_R \nearrow$
	h_R	14	8	266	28	$SRR \nearrow$ $h_{0c} \searrow$ $h_R \nearrow$
M5	h_G	320	551	121	320*	
	$\overline{h}_{st}$	112	121	66	50	$U \nearrow$ $h_{0c} \nearrow$ $h_R \nearrow$
	$\sigma_{\%}$	13	85	156	12	$T \nearrow$ $h_{0c} \searrow$ $h_R \nearrow$
	h_R	7	20	23	45	$SRR \nearrow$ $h_{0c} \searrow$ $h_R \nearrow$
MLi	h_G	470	756	146	470*	
	$\overline{h}_{st}$	41	79	76	7	$U \nearrow$ $h_{0c} \nearrow$ $h_R \nearrow$
	$\sigma_{\%}$	5	27	8	29	$T \nearrow$ $h_{0c} \nearrow$ $h_R \nearrow$
	h_R	11	51	68	15	$SRR \nearrow$ $h_{0c} \searrow$ $h_R \cong$
MLiM	h_G	558	867	131	558*	
	$\overline{h}_{st}$	123	59	24	9	$U \nearrow$ $h_{0c} \searrow$ $h_R \nearrow$
	$\sigma_{\%}$	34	54	13	11	$T \nearrow$ $h_{0c} \searrow$ $h_R \nearrow$
	h_R	7	29	15	17	$SRR \nearrow$ $h_{0c} \searrow$ $h_R \nearrow$

h_G - fully flooded film thickness of the grease under the same operating conditions.

h_G, $\overline{h}_{st}$ and h_R in nm. $\sigma_{\%}$ in %.

* - fully flooded values measured under the operating conditions of Test 1.

in the case of greases M2 and MLiM. According to Table 6.2, the film thickness' standard deviation in this zone increased for all greases apart from MLiM.

In the tests performed at higher temperature (**Test 3**), all greases show very high film thickness values in the first seconds, gradually decreasing to values near the film thickness of the base oil in fully flooded conditions. The only exception was grease MLiM whose film thickness dropped to very low values even lower than the base oil or the low speeds plateau. At this temperature (80 °C), the scatter was considerably higher than at 40 °C, specially for the polymer greases as it can be seen in Table 6.2.

Finally, the tests performed at higher SRR (**Test 4**) show that replenishment is considerable affected by increasing the sliding speed. Although the initial film thickness is smaller than both fully flooded results of grease and base oil, the film decay rate is slower than for the other tests. However, the film thickness in the

stabilization zone is reached at smaller film thickness values than for the reference test, as shown in Table 6.2.

The tests performed at a SRR of 50 % proved to be extremely harsh to the surface of the glass disc. It was very frequent for the track to get damaged and the film thickness could no longer be evaluated, phenomenon which speaks for itself regarding how SRR affects the replenishment. Furthermore, and according to the film thickness profile pictures, the system struggles to keep the ball in place (clearly observed in the case of greases M5 and MLi above 600 s) increasing the difficulty to obtain representative film thickness curves at these operating conditions. Once again, the time at which the tests failed or the surface got damaged was found to be random.

The relationship between the grease formulation (thickener type or base oil nature) and the film thickness under starved conditions is not clear. However, it seems that the polymer greases generally produce higher film thickness values, specially when there is thickener material crossing the contact, which happens much more often than for the lithium complex thickened greases.

Grease M2

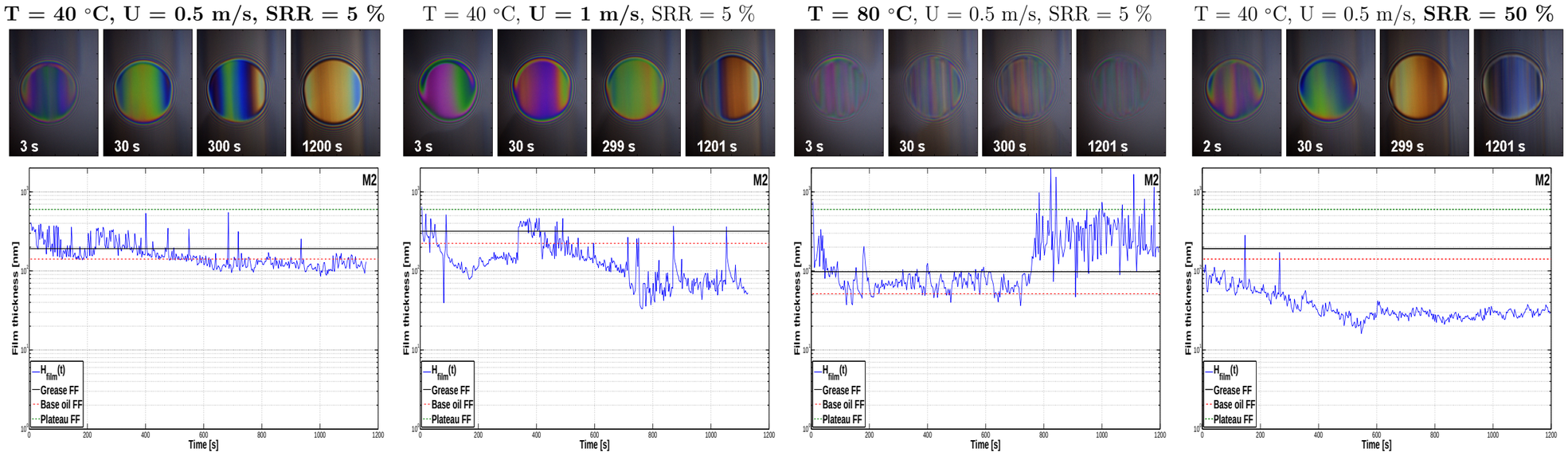

Grease M5

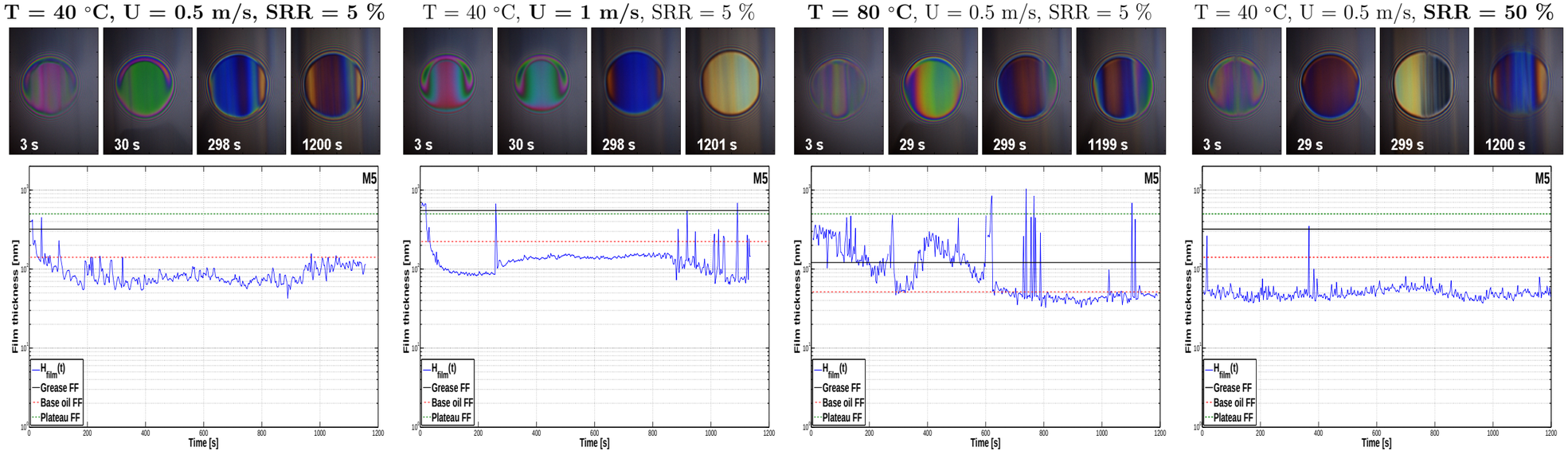

Figure 6.6: Film thickness of greases M2 and M5 measured over time, under constant operating conditions.

Grease MLi

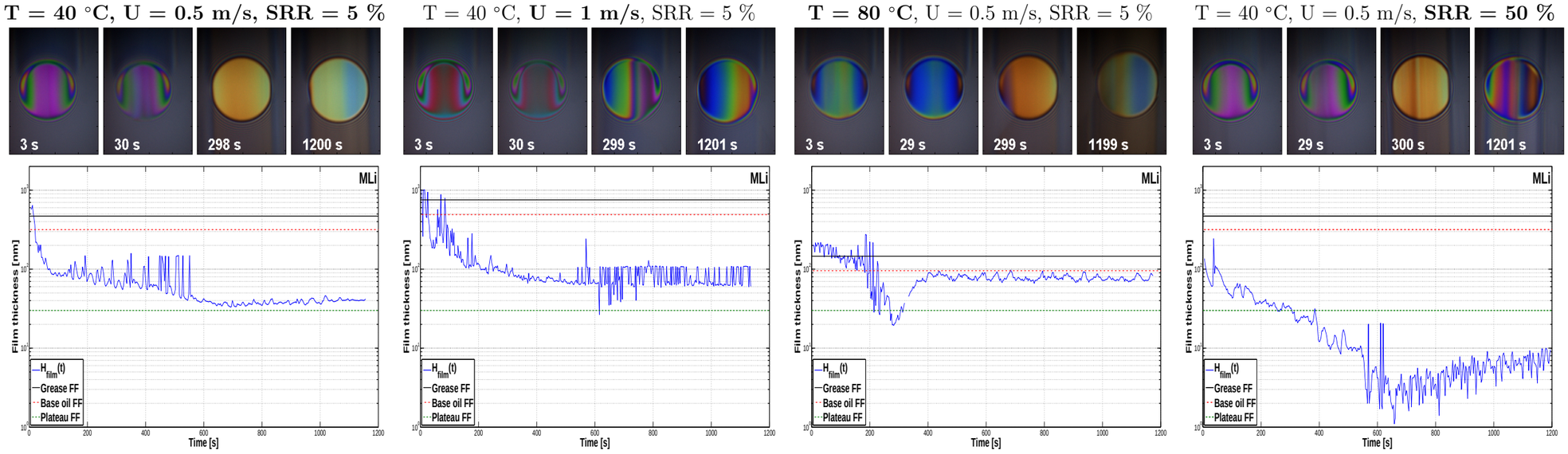

Grease MLiM

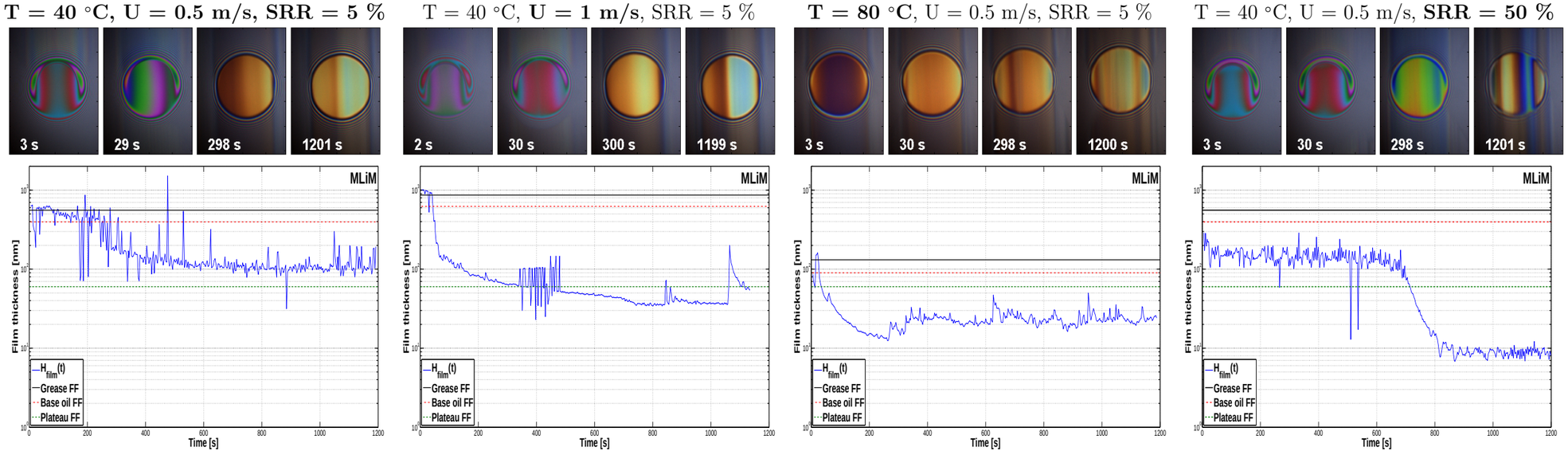

Figure 6.7: Film thickness of greases MLi and MLiM measured over time, under constant operating conditions.

6.4 Coefficient of friction results

The COF was measured over time under constant operating conditions in a ball-on-disc device, without using the scoop to force grease back into track. Each test was repeated four times and the result showing the highest deviation from the average was excluded. The average curves of the three measurements is shown in Figure 6.8 for greases M2, M5, MLi and MLiM. The results are plotted versus the number of ball revolutions.

Analysing Figure 6.8, it is possible to see that the coefficient of friction increases as the number of cycles increases. Since the operating conditions are kept constant along the test, this phenomenon is due to the film thickness decay, as the replenishment changes from fully flooded to starved conditions. For certain greases and certain operating conditions, the coefficient of friction increased continuously over the test duration while for others it reached a steady state, similar to what was observed for the film thickness results. However, in this case there is a clear trend regarding the coefficient of friction μ, of the different greases in last cycles of the test:

$$\mu^{MLiM} > \mu^{MLi} > \mu^{M5} > \mu^{M2}.$$

These results, associated with those reported in the previous section, show that even in starved conditions the polymer greases tend to provide thicker films and smaller coefficient of friction in the stabilization stage. The only test were this trend was not so clear was under a SRR of 50 %. In this situation, there is a large scatter on some of the measurements related to the same problems already reported for the film thickness results. At high load and high SRR, the system struggles to keep the ball in place due to high friction forces. Furthermore, the lubricant film breaks and builds up very fast as the replenishment changes and thickener lumps cross the contact, making it very difficult to obtain coherent measurements under this condition.

Analysing the results measured under different operating conditions, the trends are very similar between greases. Increasing the entrainment speed, the COF grows quicker and its value in the stabilization zone is higher than at lower entrainment speed, which should be due to quicker starvation. The same effect is observed for the tests performed at higher SRR, but the value of the COF in the stabilization zone is even higher. On the other hand, the tests performed at higher operating temperature originate lower COF values, due to the decrease of the viscous friction.

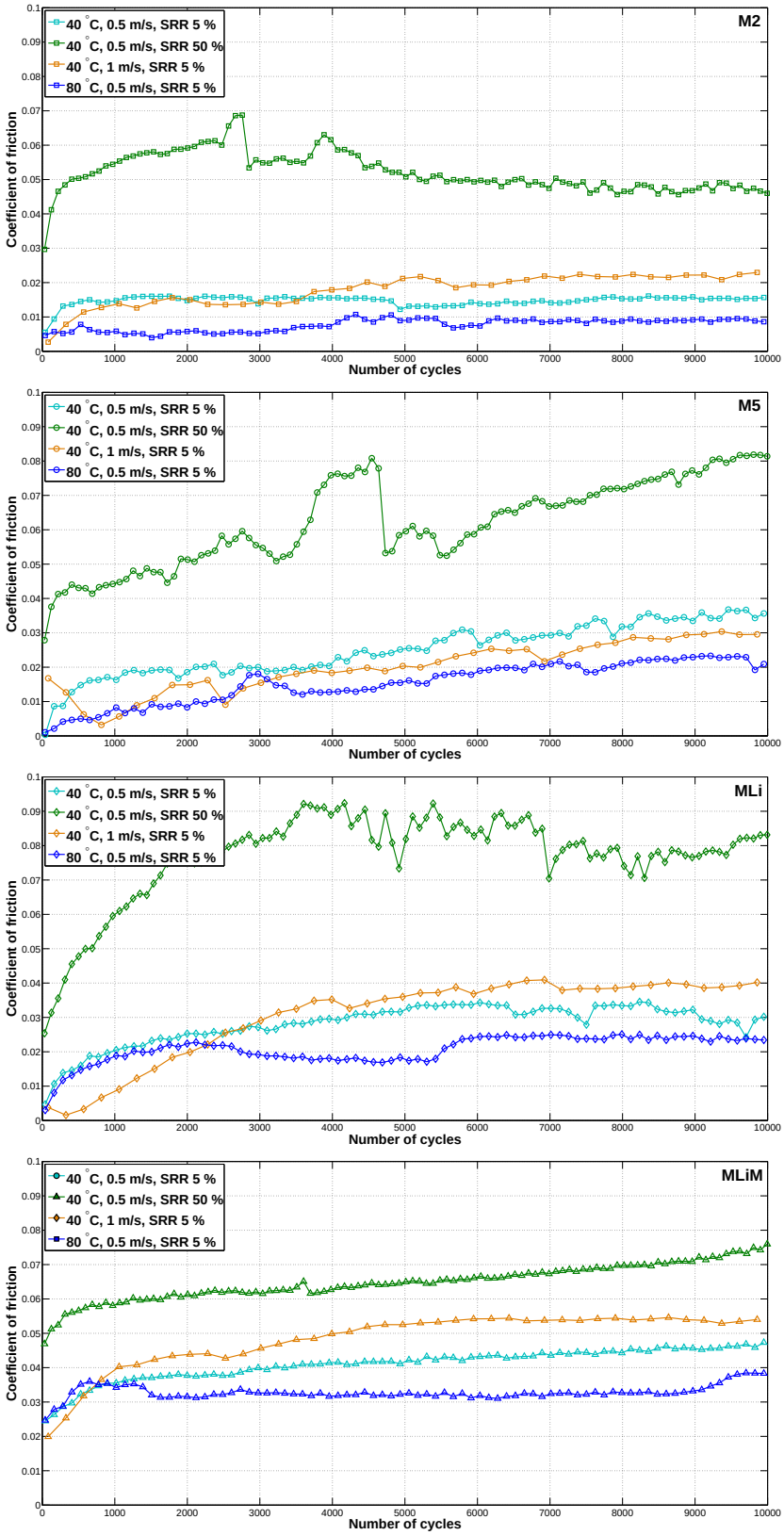

Figure 6.8: COF curves of greases M2, M5, MLi and MLiM, measured overtime, under different operating conditions.

Table 6.3: Average COF under starved conditions ($\overline{\mu}_{st}$) for the last 2000 cycles of greases M2, M5, MLi and MLiM.

Test conditions		40 °C 0.5 m/s 5 %	40 °C **1 m/s** 5 %	**80 °C** 0.5 m/s 5 %	40 °C 0.5 m/s **50 %**	Trends
M2	$\overline{\mu}_{st}$	0.016	0.022	0.009	0.047	$U \nearrow$ $\overline{\mu}_{st} \nearrow$ $T \nearrow$ $\overline{\mu}_{st} \searrow$ $SRR \nearrow$ $\overline{\mu}_{st} \nearrow$
M5	$\overline{\mu}_{st}$	0.035	0.027	0.022	0.079	$U \nearrow$ $\overline{\mu}_{st} \searrow$ $T \nearrow$ $\overline{\mu}_{st} \searrow$ $SRR \nearrow$ $\overline{\mu}_{st} \nearrow$
MLi	$\overline{\mu}_{st}$	0.031	0.039	0.024	0.079	$U \nearrow$ $\overline{\mu}_{st} \nearrow$ $T \nearrow$ $\overline{\mu}_{st} \searrow$ $SRR \nearrow$ $\overline{\mu}_{st} \nearrow$
MLiM	$\overline{\mu}_{st}$	0.046	0.054	0.035	0.073	$U \nearrow$ $\overline{\mu}_{st} \nearrow$ $T \nearrow$ $\overline{\mu}_{st} \searrow$ $SRR \nearrow$ $\overline{\mu}_{st} \nearrow$

6.5 Closure

Film thickness measurements were performed in a ball-on-disc device under different operating conditions. In order to promote starvation, the scoop which is generally used to ensure fully flooded conditions was removed. Two different tests were performed, measuring film thickness under increasing speed or over time. It was common to find a very high deviation of the results and the repeatability was often low, showing that the mechanisms of recovery and loss of lubricant at the inlet of the contact are extremely random and chaotic [146].

Regarding the tests performed with the lithium thickened greases under increasing entrainment speed, it was possible to identify the speed at which starvation occurs. This speed seems to increase with the operating temperature, suggesting that the replenishment is better at high temperature. In fact, the results of all greases are closer to the fully flooded result at higher temperature.

As soon as starvation occurs, the film thickness drops with increasing speed. However, it tends to stabilize, becoming independent of it, at least for the lithium greases. Still, recovery was sometimes observed as film thickness increased again.

In the case of the polymer greases, it was difficult to identify the speed at which starvation really occurs. However, it was possible to see a clear decrease in the film thickness values in the whole speed range tested.

Regarding the tests performed over time under constant operating conditions, it

was found that the film thickness generally starts at very high values decreasing very fast as the time progresses. The decay rate slows down after a while and a stabilization period is reached. Film recovery was often observed as the film thickness suddenly increased again. The effect of increasing the speed, slide-to-roll ratio and operating temperature on the starved film thickness were addressed.

A very high standard deviation was found for certain operating conditions and all greases. However, in the case of the polymer thickened greases the scatter was generally higher, suggesting that thickener lumps of larger size crossed the contact more often than for the lithium thickened greases. Furthermore, the average film thickness in the stabilization zone was also frequently higher.

Finally, the coefficient of friction was also measured over time. The COF quickly increases with time until it also reaches a stabilization stage. In this region, it was observed that the polymer greases show smaller friction than lithium thickened greases. The effect of changing the operating conditions on the coefficient of friction under starved conditions was also addressed but it was difficult to correlate with the film thickness tests since other important phenomena besides lack of replenishment (for instance, thermal effects) should be happening at the same time.

7 Rolling bearings friction torque

7.1 Introduction

Precision rolling bearings are a product of the advanced technology of the twentieth century [110] whose main function is to transmit load at very low friction. Still, the total power dissipated in rolling bearings can have a major contribution to the overall energy loss of a machine. For instance, the rolling bearings' power loss inside a planetary gearbox can reach up to 30 % of the total power loss [147].

The energy consumption in machine design has become more and more important, being a major concern for science and industry. The rolling bearing manufacturers are trying to improve rolling bearing designs in order to reduce the power loss generated, reduce the energy consumption, reduce the operating temperatures and improve the lubrication conditions while also reducing the environmental impact. The main focus of the lubricant manufacturers is to develop products which increase rolling bearing life, while reducing the energy dissipated [148–151].

According to Weigand [152] grease is the most common type of lubricant used in rolling bearings, in fact, about 90 % of all the rolling bearings are grease lubricated [2]. However, grease lubrication mechanisms which rule the film thickness formation and friction torque in rolling bearings, are still not fully understood.

According to Cann *et al.* [68, 70], the grease lubrication mechanisms after the churning phase depend mainly on bearing type, operating conditions and grease properties where base oil oxidation, thickener degradation, and anti-wear/boundary properties will all play a role. Very recently, in single ball-on-disc tests, the thickener influence on the film thickness and friction was addressed by several authors [100,101,153] and a correlation between rolling bearings and single ball-on-disc tests was found. Either by influencing the bleed-oil release, by changing the grease rheology/consistency or by directly contributing to the film thickness at low speeds, it has been observed experimentally that the thickener type and content are very important for the formation of the lubricant film. Nevertheless, only few works have been published on how friction is affected, especially in full bearing tests.

Most analytical tools to predict film thickness [5, 6, 41] and rolling bearing fric-

tion torque [42] in grease lubrication, only take into account the base oil properties disregarding other aspects of grease formulation (type of thickener, content, interaction with the base oil, additive package, etc). However, for many grease formulations the oil bled by the grease during work might have significantly different properties from the original base oil [39], making its study quite important.

If the study of a single EHD contact is very complex, the simulation of a full rolling bearing is even harder. There are several issues that are difficult to take into account in a friction torque model such as the evolution of micro-geometry during operation, the particularities of each oil or grease formulation or the evolution of their properties during operation (oil loss, thickener degradation, base oil oxidation). Current models have some limitations regarding the influence of the lubricant formulation in power loss predictions, specially for grease lubrication. Some of these limitations may only be overcome through extensive experimental testing.

The measurement of the rolling bearings friction torque has been done by several authors [154–164] other than rolling bearing manufacturers. In academic research, Blake and Truman [163] developed a new experimental arrangement to test tapper roller bearings. Takabi [158] developed a test rig to investigate the torque loss of different rolling bearing geometries but the system can only apply radial loads. Paleu *et al.* [165] developed a test rig to monitor the friction torque in high-speed rolling bearings (up to 120 000 rpm) under oil-mist conditions. Zhou and Hoeprich [166] developed a test rig for tapered roller bearings that allow to measure the torque of cup race, cone race, and rib separately. More recently, Cousseau *et al.* [156] developed a new rolling bearing assembly to measure friction torque in rolling bearings through the modification of a Four-Ball Machine. This rolling bearing assembly was also used in this work to measure the torque loss in thrust ball bearings (TBB) and thrust roller bearings (TRB).

7.2 Background on the numerical models for rolling bearings friction torque calculation

In this section three different friction torque (or power loss) models will be described: Coulomb, Palmgren and new SKF. The Palmgren model is currently known as 'old' SKF model. Other models like the one developed by Biboulet and Houpert [155] or Zhou and Hoeprich [166] showed good agreement with experimental data. However, these models are only valid for unique bearing geometries and therefore, will not be analysed here.

The most commonly used rolling bearings friction torque models developed by

the world leaders in bearings construction SKF® and FAG®, assume the grease's base oil viscosity and its nature as a calculation major input [8, 42]. So far as this is concerned, the total friction torque measured should be very similar, if not equal, for any greases formulated with the same base oil, which is the case for all the polymeric greases studied in this work. However, it should be expected that different formulations (thickener type, thickener and elastomer content, additives, etc.) should also lead to different friction torque behaviour and film thickness formation, not depending on base oil viscosity only.

7.2.1 Coulomb model

The friction torque function of Coulomb model [167] is independent of the rotational speed and only depends on the applied load (F, see Equation 7.2), bearing diameter (d_m) and the coefficient of friction (μ), as presented in Equation 7.1.

$$M_t = \mu \cdot F \cdot \frac{d_m}{2} \tag{7.1}$$

$$F = \sqrt{{F_r}^2 + {F_a}^2} \tag{7.2}$$

Eschmann performed a large number of rolling bearing tests and determined a reference coefficient of friction for the Coulomb model [167]. Manufacturers like NTN [168] and NSK [169] present in their catalogues a suggestion for the coefficient of friction μ for this model, depending on the bearing geometry.

7.2.2 Arvrid Palmgren model (1959)

The Palmgren model, also known as 'old' SKF friction torque model [170], divides the total friction torque in load dependent (M_1) and load independent (M_0) losses, as presented in Equation (7.3).

$$M_t = M_0 + M_1 \tag{7.3}$$

The load independent part is function of the kinematic viscosity of the lubricant (ν), on the rotational speed (n) and on the geometry of the rolling bearing (f_0), as shown in Equation (7.4).

$$M_0 = f_0 \cdot 10^{-7} \cdot (\nu \cdot n)^{2/3} \cdot d_m^3 \tag{7.4}$$

The load dependent friction torque is given by Equation (7.5) and depends on the applied load (F), on the rolling bearing geometry (f_1) and on the coefficient of

friction (μ_1).

$$M_1 = \mu_1 \cdot f_1 \cdot F \cdot \frac{d_m}{2} \tag{7.5}$$

Palmgren evaluated the rolling bearing friction torque through experimental tests of different bearing types and sizes. The results allowed him to determine the f_0, f_1 and μ_1 values. Different values from those found by Palmgren are also suggested by Eschmann [167], FAG [8] and some other rolling bearing manufacturers.

7.2.3 SKF rolling bearings friction torque model

The "new" SKF friction torque model [42] allows to quantify the different components of the rolling bearings friction torque. The model considers that the total friction torque is the sum of four different physical sources of torque loss, represented by Equation 7.6.

$$M_t = M_{rr}^{'} + M_{sl} + M_{drag} + M_{seal} \tag{7.6}$$

The total friction torque M_t is translated by the sum of the rolling friction torque M_{rr}', the sliding friction torque M_{sl}, the friction torque resulting from the lubricant churning M_{drag} and finally, the friction torque resulting from the interaction of the seals with the moving parts M_{seal}. The fact that this model takes into account all sources of power loss and is more efficient in detailing them as function of the operating conditions, makes it more suitable to apply to the rolling bearing tests performed for this work.

The thrust ball and thrust roller bearings (SKF 51107 and SKF 81107 TN) tested in this work do not have seals, so the M_{seal} torque loss term can be disregarded. The drag losses are also unaccounted for when discussing grease lubrication since generally, after the churning phase, these losses are very small. Furthermore, given the small size of the TBB/TRB used and the relatively low operating speeds tested, the M_{drag} component can also be disregarded. Therefore, the total internal friction torque of the tested thrust rolling bearings has only two terms: the rolling and sliding torques, respectively, $M_{rr}^{'}$ and M_{sl}, as represented in Equation 7.7.

$$M_t = M_{rr}^{'} + M_{sl} \tag{7.7}$$

The rolling friction torque can be calculated through Equations 7.8, corrected to include the "inlet shear heating" factor ϕ_{ish} (Equation 7.9), and the "kinematic

replenishment" factor ϕ_{rs} (Equation 7.10).

$$M_{rr}^{'} = \phi_{ish} \cdot \phi_{rs}[G_{rr} \cdot (n \cdot \nu)^{0.6}] \tag{7.8}$$

$$\phi_{ish} = \left[1 + 1.84 \times 10^{-9}(n \cdot d_m)^{1.28}\nu^{0.64}\right]^{-1} \tag{7.9}$$

$$\phi_{rs} = \left[e^{K_{rs} \cdot \nu \cdot n \cdot (d+D)\sqrt{\frac{K_z}{2(D-d)}}}\right]^{-1} \tag{7.10}$$

Depending on the rolling bearing geometry, the G_{rr} factor shown in Equation 7.8 is calculated using Equation 7.11 or 7.12, for thrust ball bearings (TBB) or thrust roller bearings (TRB), respectively.

$$TBB: \quad G_{rr} = R_1 \cdot {d_m}^{1.83} \cdot {F_a}^{0.54} \tag{7.11}$$

$$TRB: \quad G_{rr} = R_1 \cdot {d_m}^{2.38} \cdot {F_a}^{0.31} \tag{7.12}$$

The rolling torque $M_{rr}^{'}$ is mainly influenced by the viscosity of the lubricant at the operating temperature (in grease lubrication, the base oil or the bleed-oil viscosity should be considered) and also by the rotational speed. The product of the "kinematic replenishment" factor by the "inlet shear heating" factor decreases when the operating speed increases.

Since the total friction torque was measured experimentally $M_{exp} = M_t$, it is possible to calculate the sliding torque once the rolling torque is known, as shown in Equation 7.13.

$$M_{sl} = M_t - M_{rr}^{'} = M_{exp} - M_{rr}^{'} \tag{7.13}$$

However, the sliding torque can also be calculated using Equations 7.14, if the coefficients of friction μ_{bl} and μ_{ehd} are known or can be estimated, to calculate the the sliding coefficient of friction μ_{sl} (Equation 7.15).

$$M_{sl} = G_{sl} \cdot \mu_{sl} \tag{7.14}$$

$$\mu_{sl} = \phi_{bl} \cdot \mu_{bl} + (1 - \phi_{bl}) \cdot \mu_{ehd} \tag{7.15}$$

The G_{sl} parameter shown in Equation 7.14, is calculated differently depending on the rolling bearing geometry. For thrust ball bearings (TBB), Equation 7.16 should be used. In the case of thrust roller bearings (TRB), Equation 7.17 should be used instead.

$$TBB: \quad G_{sl} = S_1 \cdot {d_m}^{0.05} \cdot {F_a}^{4/3} \tag{7.16}$$

$$TRB: \quad G_{sl} = S_1 \cdot {d_m}^{0.62} \cdot F_a \tag{7.17}$$

The coefficient of friction μ_{bl} is dependent on the additive package of the lubricant and should reflect the coefficient of friction when the film thickness is very low - boundary film lubrication. Therefore, this μ_{bl} coefficient should be much higher than μ_{ehd} which represents the coefficient of friction under full film conditions. The coefficient of friction μ_{bl} should also depend on the grease formulation (thickener type and content).

The sliding torque is also highly dependent on the "load weighting" factor ϕ_{bl}. This factor increases when the specific film thickness decreases, affecting the sliding coefficient of friction μ_{sl}, and consequently, the sliding torque.

$$\phi_{bl} = \left[e^{2.6\times10^{-8}(n\cdot\upsilon)^{1.4}d_m}\right]^{-1} \tag{7.18}$$

The reference values of COF presented by the model to predict the sliding bearing friction torque are shown in Table 7.1.

As a general rule, the rolling friction torque M_{rr} follows the film thickness increase and hence, it increases with increasing speed at constant temperature, due to a more pronounced hydrodynamic effect. The sliding friction torque shows the opposite behaviour decreasing with the rotational speed since the lubrication regime is changing, which leads to less frequent interaction between surface's asperities. The balance between these two components will determine the total friction torque behaviour and in general, the overlapping of the two components defines a change in the friction generation mechanism and the rotational speed at which the lubrication regime changes. Depending on the active lubricant's viscosity, the main frictional

Table 7.1: Reference values of COF under boundary μ_{bl} and full film μ_{ehd} lubrication, proposed by SKF [42].

μ_{bl}		0.15
μ_{ehd}	mineral oils:	0.05
	synthetic oils:	0.04

Table 7.2: Reference values for the friction torque calculation of thrust ball bearings SKF 51107 and thrust roller bearings 81107 TN [42].

Rolling bearing		51107	81107 TN
Geometry Constants	R_1	1.03×10^{-6}	2.25×10^{-6}
	S_1	0.016	0.154
	K_z	3.8	4.4
Replenishment Constant	K_{rs}	6.00×10^{8}	

source may be sliding (boundary or mixed lubrication regime) or rolling friction torque (EHD lubrication).

The SKF friction torque model, explained above, features different kind of constants to predict the total friction torque of rolling bearings. Theses constants depend not only on the bearing type, geometry and number of rolling elements but also on the type of lubricant and lubrication regime (oil bath, oil jet, oil spot and grease lubrication). In the case of TBB and TRB lubricated with grease, the constants used are shown in Table 7.2. The geometry related constants S_1, R_1 and K_Z are independent of the rolling bearings' dimensions for these types of rolling bearings.

The K_{rs} constant is related to the degree of replenishment: the higher its value, the worst the contact feeding. For grease lubrication, this value is considered to be twice higher than for oil-bath lubrication. Although this value was left unchanged, it might be specially important in grease lubrication because there is a large range of grease consistency which clearly lead to very different contact replenishment. Furthermore, the rolling bearings tested in this work are open bearings which makes it harder for the grease to stay near the contact.

7.2.4 Rolling bearings friction torque models comparison

A comparison between the different models previously described is shown in Figure 7.1. In this figure, the three models to predict the friction of rolling bearings are applied to the operating conditions of a thrust ball bearing (TBB) SKF 51107 and thrust roller bearing (TRB) SKF 81107 TN, lubricated with 2 ml of grease M2, under a load of 6860 N for the TBB and a load of 5880 N for the TRB. The operating temperature was set constant at 60 °C and the rotational speed increased from from 100 to 1750 rpm (1000 rpm in the case of the TRB). The parameters used for the models of Coulomb and Palmgren are shown in Table 7.3 [167].

Table 7.3: Calculation parameters [167].

Coulomb		Palmgren	
TBB	TRB	TBB	TRB
$\mu = 0.0012$	$\mu = 0.004$	$f_0 = 1$ $f_1 = 1$ $\mu = 0.0015 \cdot (\frac{F}{C_0})^{\frac{1}{3}}$	$f_0 = 3$ $f_1 = 1$ $\mu = 0.0035$

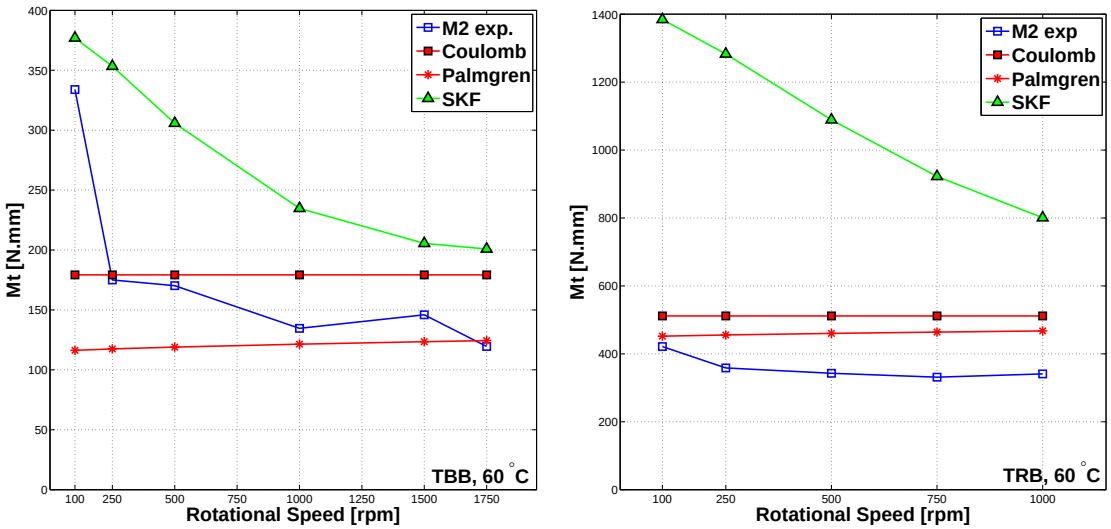

Figure 7.1: Comparison of three different friction torque models for rolling bearings.

The model of Coulomb does not depend on the operating speed and therefore, it fails to describe the measured friction torque behaviour for the whole speed range tested. According to Figure 7.1, for these operating conditions, Palmgren model predicts a friction torque which is only very slightly dependent on the rotational speed and hence, it also fails to describe the measured behaviour. Besides, it predicts a friction torque value very low for TBB and very high for TRB, when compared to the actual measurements.

Finally, and despite it predicts friction torque values much higher than those measured, the SKF model seems to predict the measured friction torque behaviour much better than the other models, at least its dependence on the rotational speed. For this reason and considering that it takes into account all the friction sources thoroughly, the SKF model was the one applied to the experimental tests performed for this work.

However, to apply this model and understand how the different grease formulations affect the different sources of friction, the following assumptions had to be made:

- All tests were performed after the churning phase - drag losses are minimal;
- The properties of the active lubricant at the contact inlet are those of the base oil;
- The SKF model correctly represents the rolling friction torque (M'_{rr}) behaviour, independently of the thickener content/type and base oil nature;
- The weight distribution function ϕ_{bl}, used to calculate the sliding coefficient of friction, correctly represents the lubrication regime;
- The coefficients of friction under boundary μ_{bl} and full film μ_{ehd} lubrication can be optimized to reflect the differences in grease formulation: thickener content/type, base oil nature and additive package;
- The coefficients of friction under boundary film μ_{bl} should be independent of the lubricant's viscosity and therefore, be constant for all the operating temperatures tested.

In the following sections, the model will be used and analysed based on these assumptions.

7.3 Rolling bearing assembly and test procedure

The friction torque tests were performed in a modified Four-Ball Machine, using a rolling bearing assembly in the place of the typical Four-Ball arrangement, shown in Figure 7.2. This procedure has been developed by Cousseau *et al.* [156] and also used by other authors [40, 171–174].

The rolling bearings were tested under an axial load of ≈7000 N (marked with P on Figure 7.2), which is the maximum load available. The friction torque was measured at different rotational speeds (n), increasing stepwise from 100 to 3250 rpm assuming that the operating temperature could be kept constant at a pre-defined value. Two different rolling bearings were used: SKF 51107 thrust ball bearing (TBB) and SKF 81107 TN thrust roller bearing (TRB). A representation of the SKF 51107 rolling bearing can be seen in Figure 7.2, marked with numbers 3 to 5. Figure 7.3 shows the cross section and dimensions of each bearing according to the manufacturer.

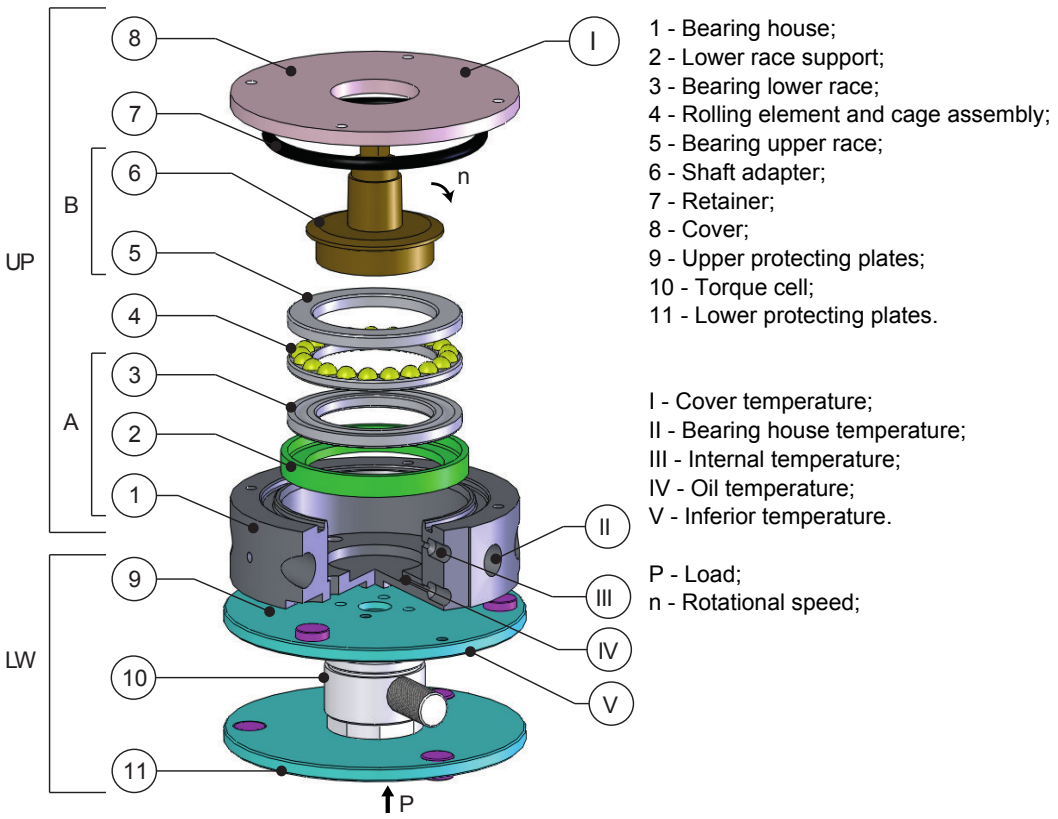

Figure 7.2: Rolling bearing assembly. Note: Numbers from 1 to 11 are related to the assembly components, while numbers from I to V are referred to the thermocouples locations.

Each new rolling bearing was lubricated with 2 ml of grease (about 30% of the rolling bearing's free volume) by the action of a syringe. Care was taken to assure that the initial grease distribution was as uniform as possible between tests.

Table 7.4 summarizes the operating conditions. The tests performed are well above the minimum required load ($0.01C$ for TBB and $0.02C$ for TRB) while also not exceeding the maximum static load rating. The limiting operating speeds are also met. The tests were performed under controlled operating temperature. This temperature is measured very close to the upper raceways using a thermocouple (number III) in Figure 7.2, which is associated with a digital PID controller, allowing to adjust and maintain the operating temperature steady through the activation of two electrical resistances, symmetrically applied to the bearing house. The assembly chamber is permanently submitted to air-forced convection, by action of two fans with 50 mm in diameter, which enables the evacuation of some generated heat. However, for certain operating speeds, the generated heat might be such that it is not possible to keep the temperature constant because the fans are not sufficient to cool the system.

Table 7.4: Operating conditions for the rolling bearings tests.

Parameter	TBB 51107	TRB 81107 TN
Mean diameter - d_m [mm]	43.5	43.5
Height - h [mm]	12	12
Number of rolling elements	21	20
Dynamic load rating - C [kN]	19.9	29
Static load rating - C_0 [kN]	51	93
Reference speed [rpm]	5600	2800
Limit speed [rpm]	7500	5600
Composite Roughness - σ_c [nm]	≈ 138	≈ 155
Temperature - T [°C]	60, 80 and 110	50, 60 and 80
Rotational speed - n [rpm]	100 to 3250	100 to 1250
Entrainment speed - U [m/s]	0.1 to 3.7	0.1 to 1.4
Axial load - P [N]	≈ 6860	≈ 5880
Maximum Hertzian pressure - p_0 [GPa]	≈ 2.33	≈0.93

Thrust ball bearing (TBB) 51107:

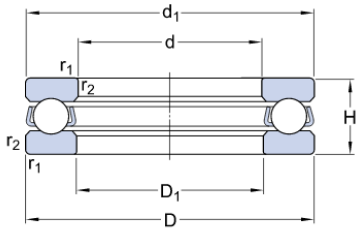

d		35	mm
D		52	mm
H		12	mm
d_1	≈	52	mm
D_1	≈	37	mm
$r_{1,2}$	min.	0.6	mm

Thrust roller bearing (TRB) 81107 TN:

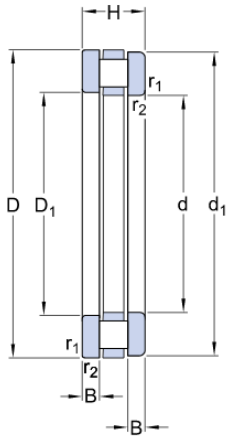

d		35	mm
D		52	mm
H		12	mm
d_1		52	mm
D_1		37	mm
B		3.5	mm
$r_{1,2}$	min.	0.6	mm

Figure 7.3: Cross section and dimensions of the TBB (top) and TRB (bottom) tested [42].

A run-in period of at least 15 hours at 500 rpm preceded each test, for roughness smoothing and grease distribution (churning phase). Following the run-in period, the electrical resistances were turned on and the temperature fixed. The friction torque was then measured for each speed step after the operating temperature was stabilized (smaller than 1 °C degree variation in a time window of 10 minutes). The procedure was then repeated at each different test temperature. If the operating temperature of the rolling bearing exceeded the imposed temperature no further speed steps were performed and the temperature was increased to the next step. The tests were always performed from the lowest to the highest temperature and from the lowest to the highest speed.

A piezoelectric torque cell KISTLER® 9339A (number 10 in Figure 7.2) was used to measure the friction torque. The device allows high accuracy measurements for short periods of time and constant temperature (±2 °C). For each speed step a total of 10 measurements were performed. Given the mean and standard deviation of the measurements, all the values which highly deviated from the mean were excluded. Still, given the chaotic behaviour which characterizes grease lubrication [146], a good repeatability of the measurements was sometimes hard to achieve and for certain operating conditions, high standard deviations were found.

7.4 Thrust ball bearings (TBB) friction torque

7.4.1 Specific film thickness inside the TBB

The friction torque and the lubrication regime inside a rolling bearing, are directly linked to each other. In fact, the rolling torque depends on operating speed, oil viscosity and applied load as does the film thickness. The sliding torque depends on the sliding coefficient of friction which is also influenced by the lubricant properties under the rolling bearing's operating conditions. Therefore, the knowledge of the lubrication regime is of extreme importance when analysing the friction torque.

The concept of specific film thickness (Λ) to define the lubrication regime is well known in machine design (see Chapter 4). However, the viscosity ratio κ is also widely used to define the lubrication regime, specially for rolling bearing technology [175]. A comparison of these two parameters Λ and κ has already been reported by Morales *et al.* [176] and Cann *et al.* [177].

This viscosity ratio, proposed by Heemskerk [178] and defined by Equation (7.19), is defined as the ratio between the operating viscosity and the viscosity re-

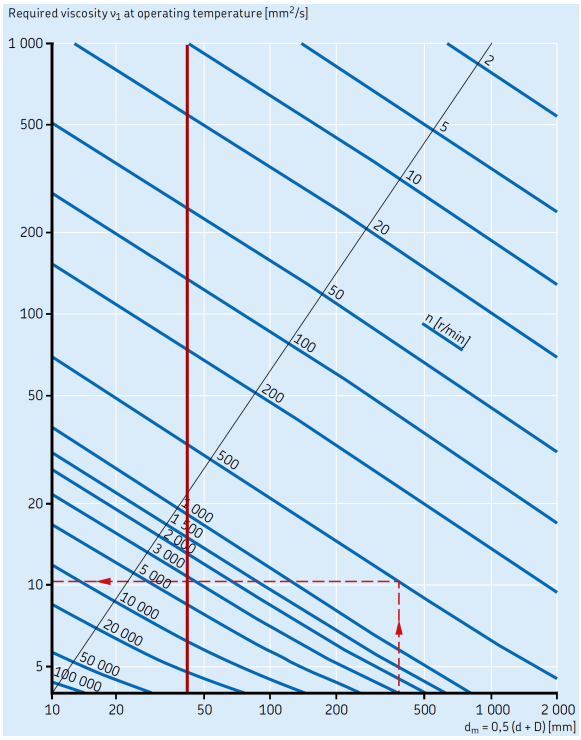

Figure 7.4: Viscosity ratio κ: ratio between the operating viscosity and the viscosity required to provide $\Lambda = 1$, according to SKF [42].

quired to provide $\Lambda = 1$.

$$\kappa = \frac{\nu}{\nu_1} \tag{7.19}$$

The viscosity required to provide $\Lambda = 1$, is given by the abacus proposed by SKF on the General Catalogue [42], shown here in Figure 7.4. The abacus does not allow to select a specific type of bearing since only the mean diameter (d_m) and the rotational speed are considered for the definition of ν_1. The vertical red line in Figure 7.4 represents the mean diameter of the TBB and TRB tested in this work. It allows, for any rotational speed, to determine ν_1, the viscosity required to provide $\Lambda = 1$ on a TBB or TRB with a mean diameter of 43.5 mm.

On the other hand, ISO 281 [175] defines the viscosity ratio κ_{ISO} as a function of the specific film thickness, according to Equation 7.20.

$$\kappa_{ISO} = \Lambda^{1.3} \tag{7.20}$$

Given the similarity with Λ, this κ_{ISO} ratio was not calculated for the tests performed in this work.

In Chapter 5, the specific film thickness of the Traction and Stribeck tests was calculated from actual film thickness measurements performed in the same ball-on-

disc device. In the case of the current rolling bearing tests, the operating conditions are quite different and therefore a different procedure must be followed. The reasons why the same procedure was not be employed for these tests are the following:

- The geometry of the ball-on-disc contact is very different from the geometry of the ball-raceway contact, although they are both elliptical contacts. The contact pressures are also very different since the load per rolling element is much higher and the ball radius much smaller. For the same reasons, the viscosity and pressure-viscosity of each grease, calculated from the measured film thickness curves should not be considered here for this geometry [121,122];

- The succession of over-rollings not only contributes to mechanically degrade the entrained grease but should also influence the replenishment of the next rolling element considerably. Phenomenon which does not happen in the single ball-on-disc contact [2];

- Grease lubrication phase: in the rolling bearing tests, it is not possible to know if the grease is in fully flooded conditions. It is assumed that the churning phase is over because of the large running in time and if so, the main grease lubrication mechanism is bleeding phase which generally translates into starved contacts [2];

- Replenishment: in the rolling bearings tests there is no scoop to control the grease flow and ensure the fully flooded conditions at which the film thickness measurements were performed;

Since no actual film thciknes measurements inside the bearings were possible, the central film thickness of the TBB ball-raceway contact was predicted using Hamrock and Dowson's [110] equation for elliptical contacts, as shown before in Equation 4.1. In the case of the TBB tested in this work, very little sliding is expected. Katyal and Kumar claim that sliding adds only little to the extent of film-thinning observed under pure rolling [73] and thus, the film thickness of a single ball-raceway contact of the TBB can be reasonably approximated by Equation 4.1. The geometry of a single ball-raceway contact was considered, as well as, the base oil properties (η, α_{Gold}) of each grease at the corresponding operating temperatures.

The specific film thickness was then calculated taking into account the composite roughness of the ball-raceway contact shown in Table 7.4. The results are shown in Figure 7.5, for the base oils of greases M2, M5 and MLi under the entrainments speeds at which the friction torque measurements were performed. Greases M1, M2 and M3 were formulated with the same base oil, and thus the film thickness was only

calculated for grease M2. Grease M5 was tested under a shorter entrainment speed range (100 rpm up to 2000 rpm) and only at 80 and 110 °C. Finally, grease MLiM was not tested with TBB.

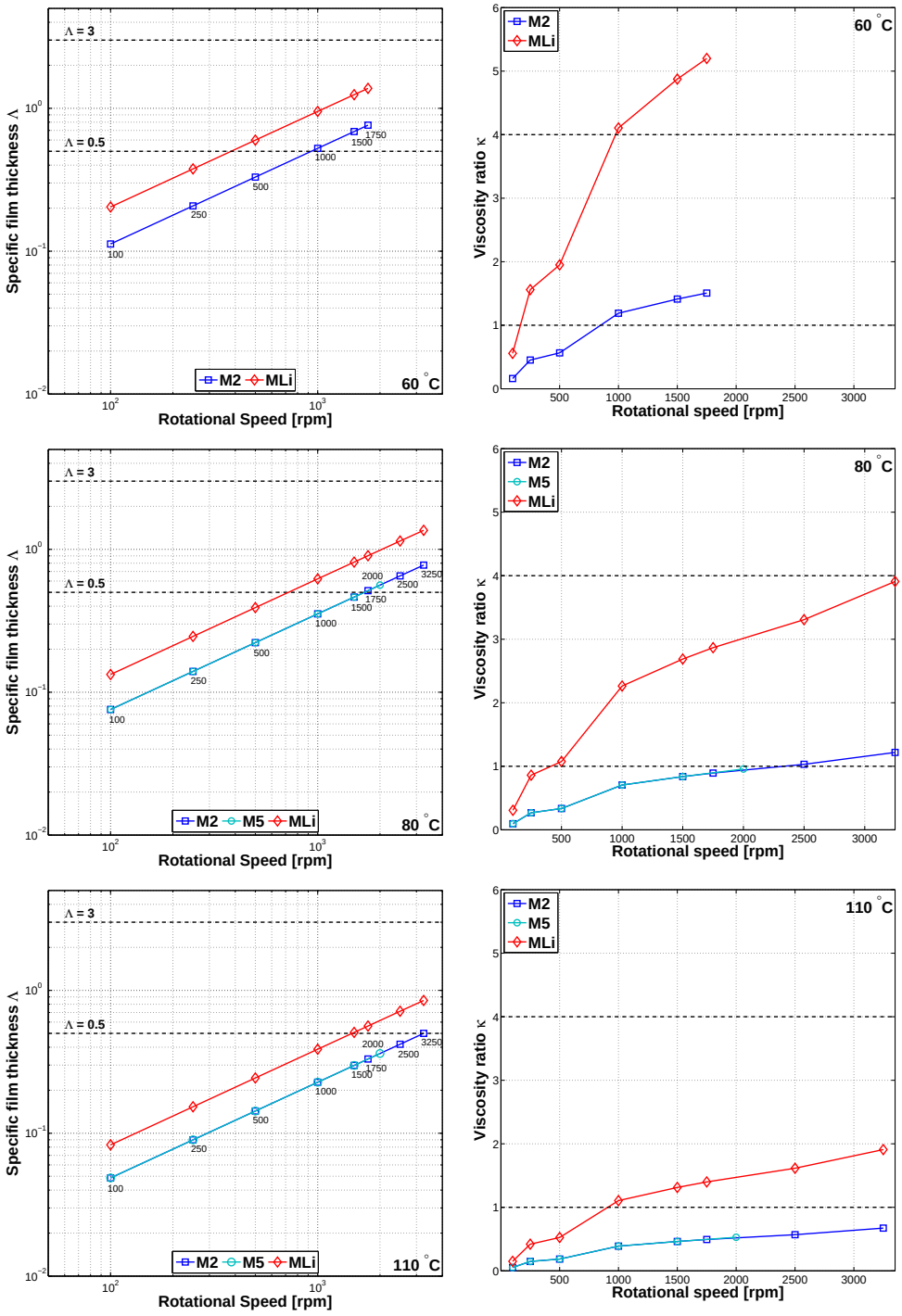

Figure 7.5: Figures to the left: Specific film thickness of a single ball-raceway contact of the TBB, considering the base oil as the active lubricant inside the contact. Figures to the right: SKF's viscosity ratio [42], considering the base oil as the active lubricant inside the contact.

Following Spikes' work on mixed film lubrication [117], the TBB is considered to operate in mixed-film lubrication for Λ higher than 0.5 and under full-film lubrication for Λ higher than 3. These transitions are represented by the horizontal dashed lines shown in Figure 7.5. According to this figure, the TBB should be operating mainly under mixed or boundary film lubrication depending on the operating speed and temperature. As the temperature increases, the specific film thickness decreases and even at high speeds the TBB operate close to boundary film lubrication. The TBB lubricated with grease MLi is expected to operate at higher specific film thickness given the higher viscosity of its base oil compared to the polymer greases.

Figure 7.5 also shows the viscosity ratio, according to the SKF abacus [42], for each test condition. A rolling bearing is considered to operate under mixed-film lubrication for κ higher than 1 and under full-film lubrication for κ higher than 4. According to the literature [1], the rolling bearing reaches the boundary film conditions for a viscosity ratio lower than 0.4. In the case of the tests performed with TBB, the oil temperature was kept constant and equal to 60, 80 and 110 °C, and consequently the viscosity ratio increases only with speed. TBB lubricated with grease MLi should be running under full film lubrication at 60 °C and rotational speeds above 1000 rpm. Other than that, it should run under mixed and boundary lubrication. TBB lubricated with greases M2 and M5 should operate under boundary lubrication at 110 °C, for any rotational speed.

7.4.2 Rolling bearings friction torque results

The TBB friction torques of greases M2, M5 and MLi, measured at the constant temperatures of 60, 80 and 110 °C, are shown in Figure 7.6. According to this figure, it is not possible to establish a clear relationship between different formulations and the measured friction torque. However, and despite the high standard deviation of a few measurements, the rolling bearings friction torque of all the tested greases shows a typical behaviour where the friction torque decreases with the rotational speed, following the increase of the film thickness. At 60 °C grease MLi generally produces higher friction torque than grease M2. As the temperature increases this behaviour starts to invert and, at 110 °C, it is grease M2 which clearly produces the highest friction torque. A very similar behaviour has been observed with these two greases when discussing the traction curves in a ball-on-disc contact (see Figure 5.3). This phenomenon should be related to the differences in grease formulation, specially the base oil viscosity.

[1] KLUBER Lubrication, *The element that rolls the bearing. Tips and advice for the lubrication of rolling bearings*, 2002

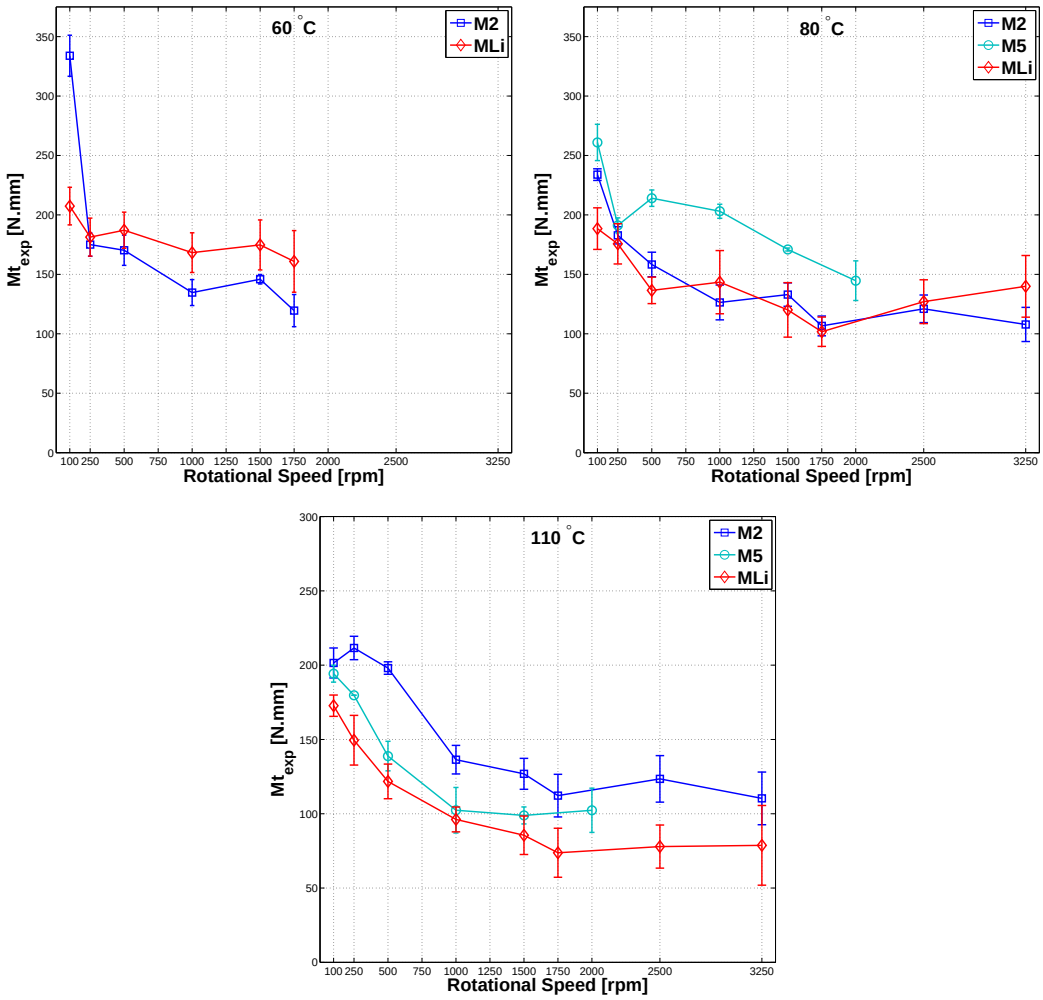

Figure 7.6: Friction torque of the TBB lubricated with grease M2, M5 and MLi, measured at constant temperature of 60, 80 and 110 °C and constant load of ≈ 7 kN.

The coefficients of friction μ_{bl} and μ_{ehd} from Equation 7.15, were then optimized in order to correctly describe the sliding friction torque behaviour as the lubrication regime changes with entrainment speed and temperature. The optimized values are shown in Table 7.5. These coefficients were optimized by minimizing the difference between the experimentally measured total friction torque and the predicted total friction torque, calculated with rolling bearing friction torque model (proposed by SKF). According to this table, the average error of the optimization is quite high for certain operating temperatures (higher than 10 %).

From these values, it is now possible to calculate the sliding coefficient of friction μ_{sl} through Equation 7.15. The optimized μ_{sl} is shown in Figure 7.7, plotted as function of the Hersey modified parameter S_P (see Equation 5.4, in Chapter 5) and compared to the value of μ_{sl} obtained from the experimental results through Equations 7.13 and 7.14. It it possible to observe that the optimized value of μ_{sl} deviates

quite a lot from the one expected from the experimental results, specially in the case of grease M5. The deviation gets worse when the operating conditions approach boundary film lubrication (low rotational speeds and high operating temperature).

Once again, it is very hard to establish any relationship between the different formulations and the coefficient of friction for these tests' results. Not only there was a high standard deviation of the measured friction torque, but also because the average error of the optimization is also quite high given the optimization constraints.

Table 7.5: Optimized coefficients of friction under boundary (μ_{bl}) and full film (μ_{ehd}) lubrication.

Tested greases		M2	M5	MLi	MLiM
	μ_{bl}	0.075	0.071	0.071	n.a.
60 °C	μ_{ehd}	0.024	n.a.	0.035	n.a.
Avg. error [%]		12.1	n.a.	9.3	n.a.
80 °C	μ_{ehd}	0.013	0.038	0.017	n.a.
Avg. error [%]		10.6	12.4	6.7	n.a.
110 °C	μ_{ehd}	0.001*	0.001*	0.001*	n.a.
Avg. error [%]		13.2	24.5	16.1	n.a.

*- lower limit imposed in the optimization of μ_{ehd}.

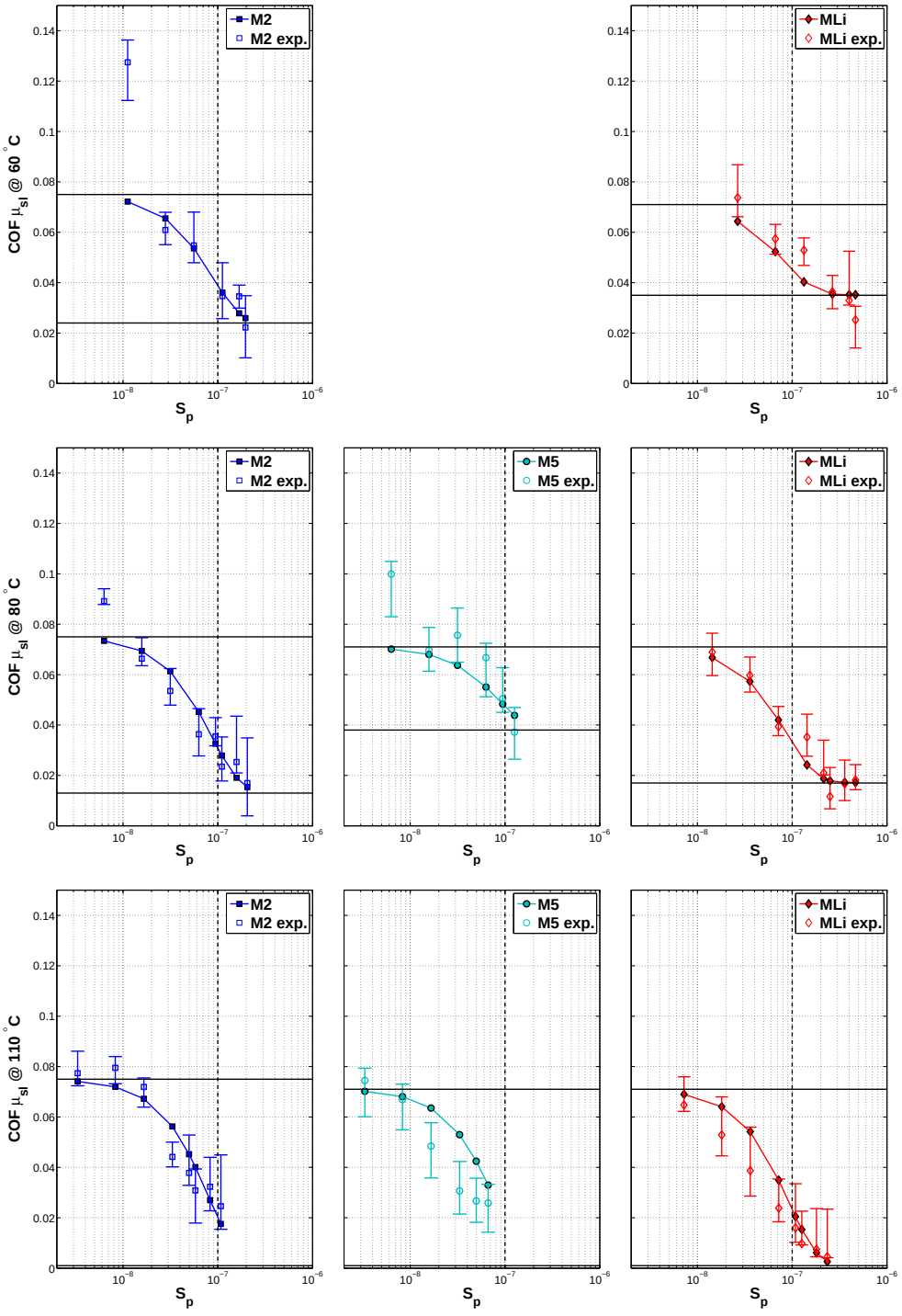

Figure 7.7: Comparison between the sliding coefficient of friction obtained from the experimental results (exp.) and the sliding coefficient of friction obtained from the optimization of μ_{bl} and μ_{ehd}, for greases M2, M5 and MLi at different operating temperatures.
The vertical dashed line is referred to the S_P value at which $\Lambda \approx 0.5$.

7.4.3 Influence of the thickener content

The thrust ball bearings friction torque was measured for greases M1, M2 and M3 over different rotational speeds and at constant operating temperatures, as shown in Figure 7.8. The standard deviation of the friction torque measurements at each speed step is also represented.

There is a clear relationship between the thickener content of the polymer greases and the rolling bearings friction torque. Grease M1, which was formulated with 11% of PP thickener, generally produced higher friction torque than grease M2 (13%) and M3 (15%), the latter showing the smaller overall friction torque. Since these polymer greases were formulated with the same base oil, it should be expected that the specific film thickness is the same for all the greases under the same operating conditions and therefore, the measured friction torque should also be very similar. However, the thickener content differences are relevant, especially as the rotational

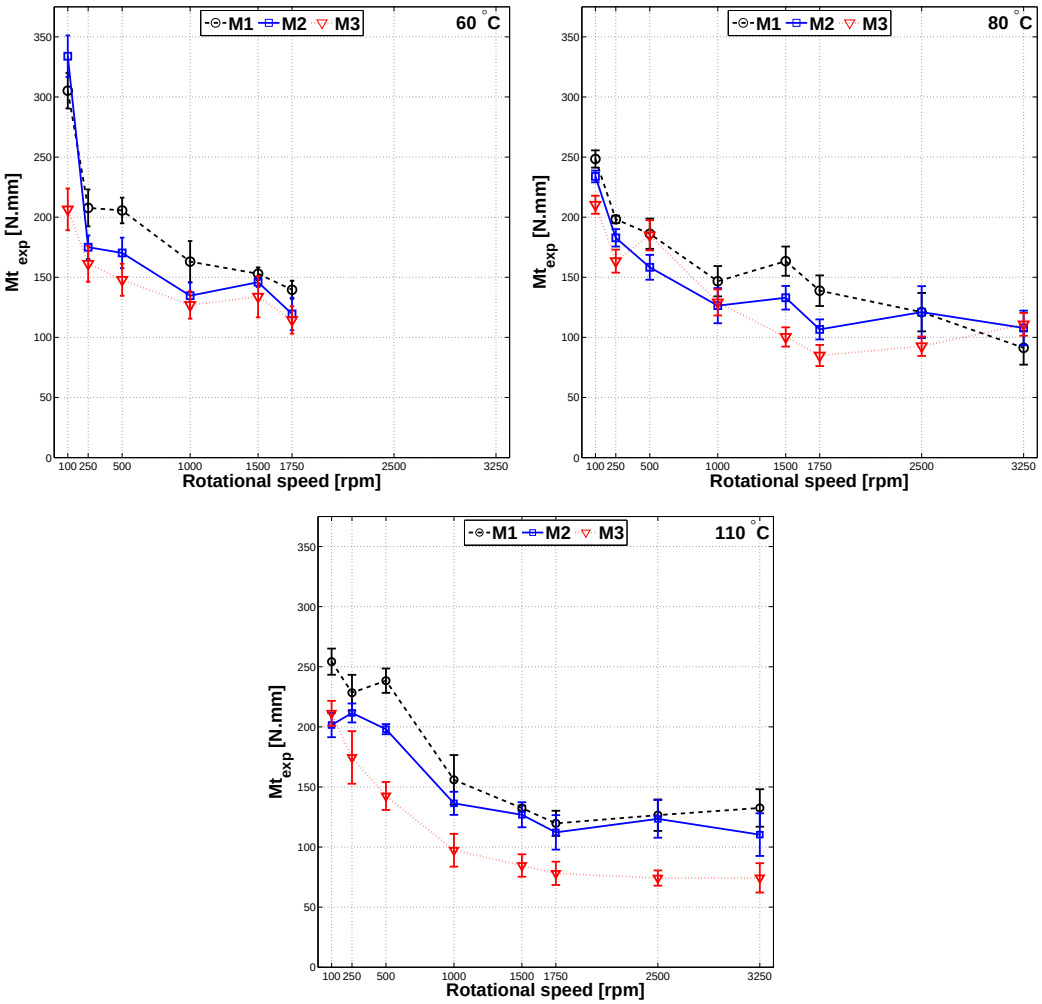

Figure 7.8: TBB friction torque measured at constant temperature of 60, 80 and 110 °C and constant load of ≈ 7 kN.

speed decreases and the specific film thickness is smaller.

The optimized coefficients of friction under boundary μ_{bl} and full film μ_{ehd} lubrication, are shown in Table 7.6. The average error of the optimization is also shown. According to this table, the optimized values of μ_{bl} decrease with increasing thickener content. Moreover, the values of μ_{ehd} decrease with the temperature increase since the value of ϕ_{bl} value gets closer to 1 (increase in the temperature leads to smaller film thickness and the lubrication regime approaches boundary lubrication) and therefore, the weight of the coefficient of friction under full film becomes less relevant in Equation 7.15. It is also possible to observe that the average error increases as the temperature increases, indicating that the model struggles to correctly represent the friction behaviour for rolling bearings running under very low specific film thickness when the value of ϕ_{bl} gets close to 1.

From the values presented in Table 7.6 and using the distribution function shown in Equation 7.15, it is possible to build Stribeck curves of the optimized μ_{sl} for each grease at different operating temperatures, as shown in Figure 7.9 plotted as function of the Hersey modified parameter S_P. The experimental values of the COF μ_{sl} (see Equation 7.14) obtained from the experimental results are also shown in Figure 7.9.

The horizontal lines represent the optimized values of μ_{bl} and μ_{ehd} (shown in Table 7.6), while the vertical dashed line represents the value of S_p which corresponds to a specific film thickness of Λ = 0.5. In the full film lubrication regime $\Lambda \geq 3$, the sliding coefficient of friction should decrease with the temperature increase. Since the viscosity of the active lubricant is decreasing, it is also expected that the viscous friction will decrease, down to the point where mixed film regime is reached.

Table 7.6: Optimized coefficients of friction under boundary film (μ_{bl}) and full film (μ_{ehd}) lubrication.

Tested greases	M1	M2	M3
Thickener [%]	11	13	15
μ_{bl}	0.087	0.075	0.062
60 °C μ_{ehd}	0.031	0.024	0.022
Avg. error [%]	7.9	12.1	6.8
80 °C μ_{ehd}	0.013	0.013	0.009
Avg. error [%]	11.6	10.6	11
110 °C μ_{ehd}	0.001*	0.001*	0.001*
Avg. error [%]	16.1	13.2	29.2

*- lower limit imposed in the optimization of μ_{ehd}.

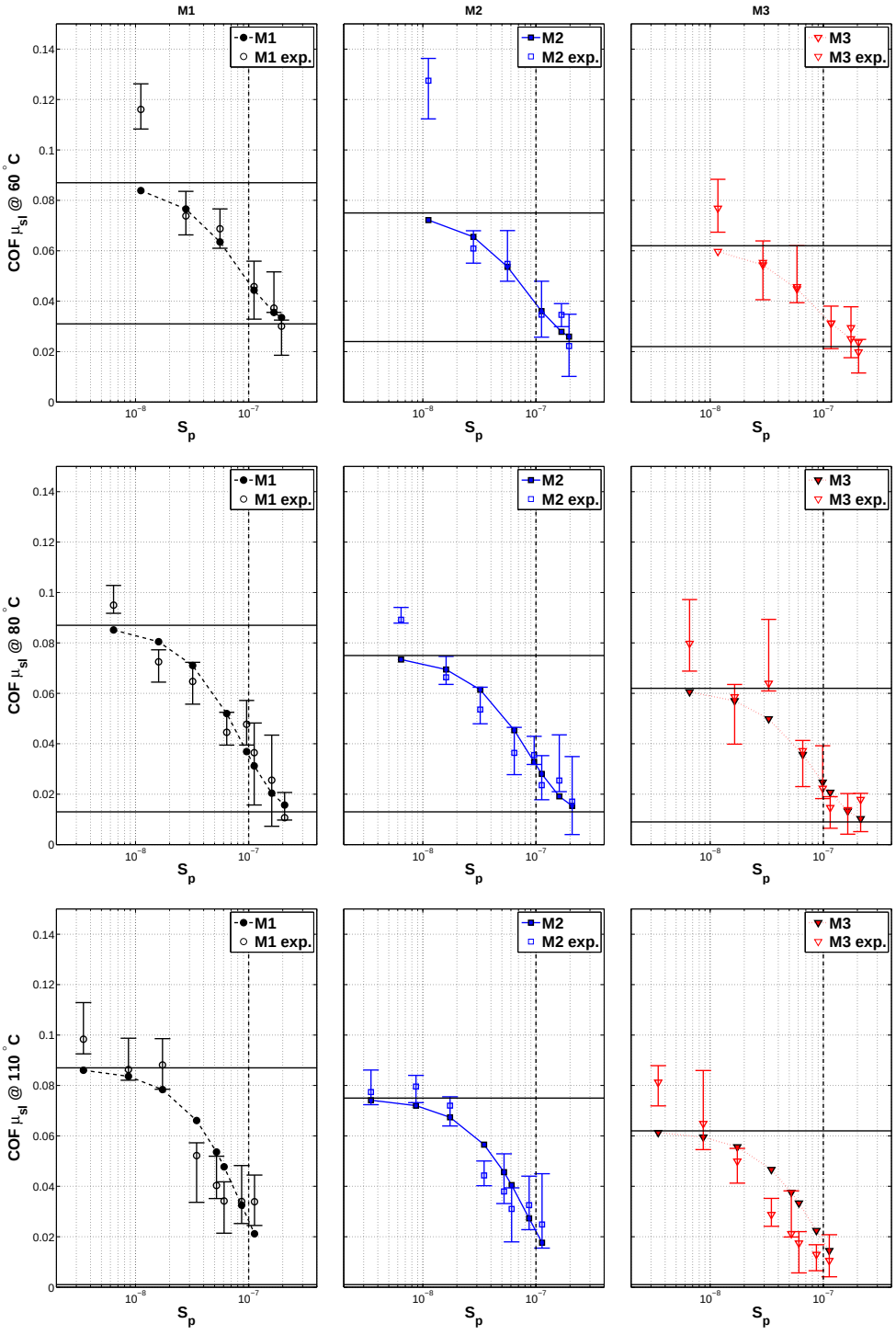

Figure 7.9: Comparison between the sliding coefficient of friction obtained from the experimental results (exp.) and the sliding coefficient of friction obtained from the optimization of μ_{bl} and μ_{ehd}, for greases M1, M2 and M3 at different operating temperatures.
The vertical dashed line is referred to the S_P value at which $\Lambda \approx 0.5$.

However, according to Figure 7.9, the lubrication regime of the rolling bearing tests performed, should be mixed film ($0.5 < \Lambda < 3$) or even boundary film lubrication ($\Lambda < 0.5$). Thus, for higher temperatures, the COF at the same rotational speed should also be higher. Therefore, with the increasing temperature, the calculated Stribeck curves move to the left (towards smaller S_p numbers). These curves allow to highlight the thickener content influence on the sliding coefficient of friction. Comparing each grease at the same operating temperature, it suggests that the higher the thickener content, the lower is the sliding coefficient of friction for low S_p numbers (close to or even under boundary lubrication). Furthermore, it is clear that for very low speeds the calculated μ_{sl} deviates from the experimental values, showing once again that the model works very well for the mixed lubrication region but not so likely for the operating conditions which lead to boundary lubrication.

For higher S_p numbers, the rolling bearing should be running under mixed film lubrication and in this region the thickener influence is smaller. Hence, the Stribeck curves of greases M1, M2 and M3 get closer in this region which was already expected since they are formulated with the same base oil. A similar relationship between the thickener content and friction had already been observed in ball-on-disc tests, shown in Figure 5.10 of Chapter 5.

Having calculated the sliding coefficient of friction, it is now possible to calculate the sliding friction torque. Figure 7.10 shows the predicted values of the rolling (M'_{rr}) and sliding (M_{sl}) friction torques as function of the rotational speed. According to this figure, it is possible to verify that the weight of the rolling friction torque in the total friction torque will be small when compared to the sliding friction torque, specially at low entrainment speeds. The rolling friction torque increases with the increase of the rotational speed at constant temperature ($M'_{rr} \propto (\eta \cdot \nu)^{0.6}$), following the increase of the specific film thickness. As the temperature increases the rolling friction torque decreases, since it is now easier to push lubricant inside the contact. The polymer greases formulated with the same base oil, also show the same M'_{rr}, independently of the thickener content.

The experimental friction torque decreases as the rotational speed increases at constant operating temperature. Since the rolling torque increases, the sliding torque must decrease, as the lubricant film builds up. The sliding coefficient of friction is function of the optimized COF's μ_{bl} and μ_{ehd} and therefore, with the increase of the rotational speed, the weight of the COF μ_{bl} starts to decrease as the lubrication regime approaches mixed lubrication. On the other hand, the weight of the COF μ_{ehd} starts to increase.

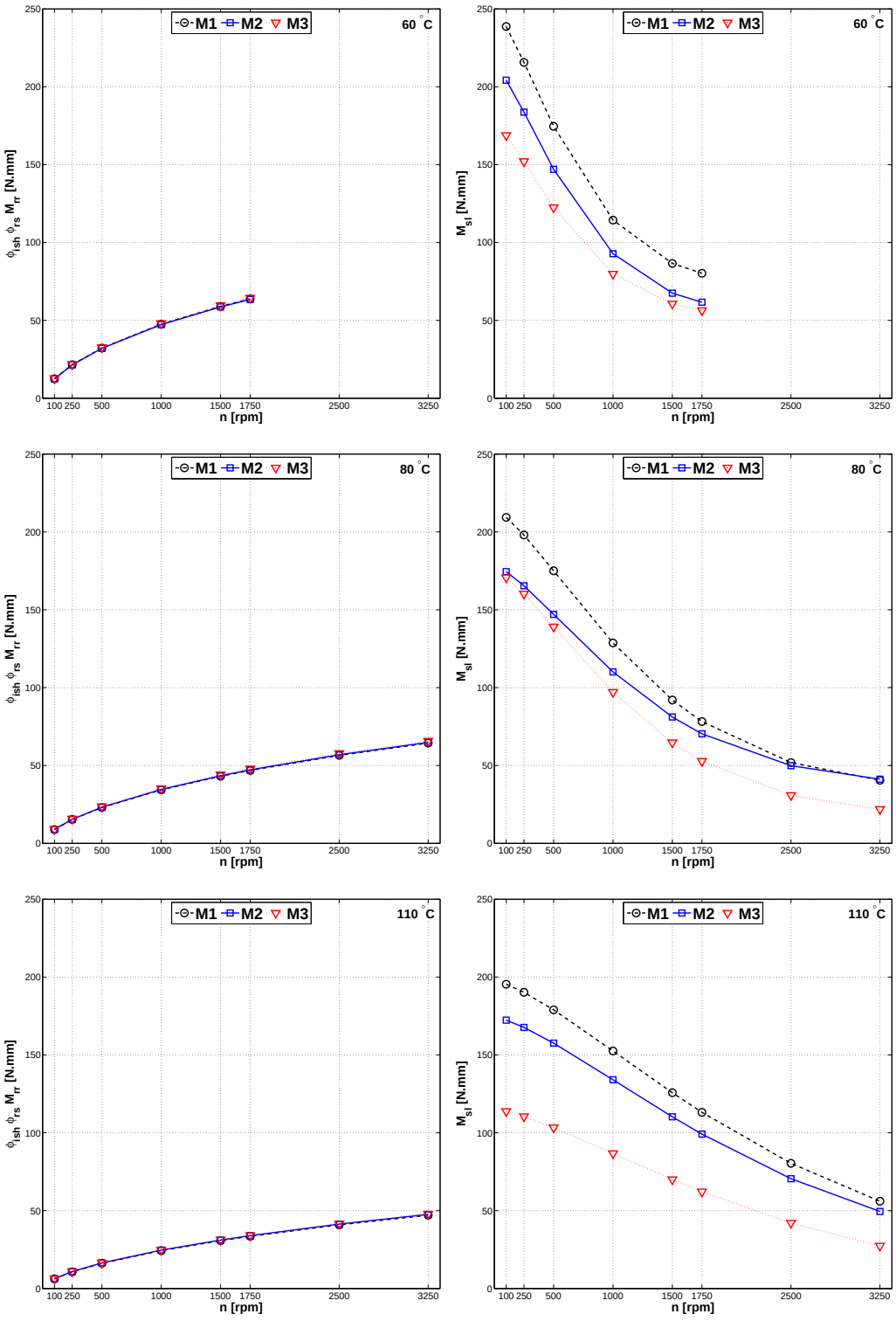

Figure 7.10: Rolling (M'_{rr}) and sliding (M_{sl}) friction torque calculated for the tested greases at the controlled temperatures of 60, 80 and 110 °C (respectively, from top to bottom).

Thus, taking for instance the value of M_{sl} at 1000 rpm, the following relationship can be found:

$$M1 > M2 > M3$$

which is valid for almost all the operating conditions, showing that, in the case of the polymer greases, the higher the thickener content, the lower should be the sliding friction torque.

It is interesting to notice that at low rotational speeds, the sliding torque is dominant regarding the rolling torque, relationship which decreases for higher speeds. Under low speeds, the difference between the sliding torque of the greases formulated with different thickener content is large. However, as the speed increases, and the lubricant film starts to be more relevant, the sliding friction torque generated by these greases gets closer.

7.5 Thrust roller bearings (TRB) friction torque

7.5.1 Specific film thickness inside the TRB

The specific film thickness of the TRB lubricated with greases M2, M5, MLi and MLiM is shown in Figure 7.11. The roller-raceway contact was considered to be linear (although it is strongly elliptic) and the film thickness predicted according to Equation 7.21 [179], considering already the inlet shear heating correction factor ϕ_T, as shown below:

$$h_{0c} = \phi_T \cdot 1.95 \cdot R_x \cdot U^{0.727} \cdot G^{0.727} \cdot W^{-0.091} \tag{7.21}$$

According to Figure 7.11, the TRB should all operate under mixed or boundary film lubrication. In the case of the TRB lubricated with greases M2 and M5, they should run only in boundary conditions given the low viscosity of its base oil. Those TRB lubricated with greases MLi and MLiM should reach mixed film lubrication for certain rotational speeds.

On the other hand, if the viscosity ratio k is considered instead, the lubrication regimes are similar. Figure 7.11 also shows the viscosity ratio calculated for greases M2, M5, MLi and MLiM. While the TRB lubricated with greases M2 and M5 continue to operate mainly under mixed ($\kappa > 1$) or boundary ($\kappa < 0.4$) film lubrication, the TRB lubricated with greases MLi and MLiM should operate mainly in the mixed film regime ($\kappa > 1$), only reaching boundary film for low rotational speeds.

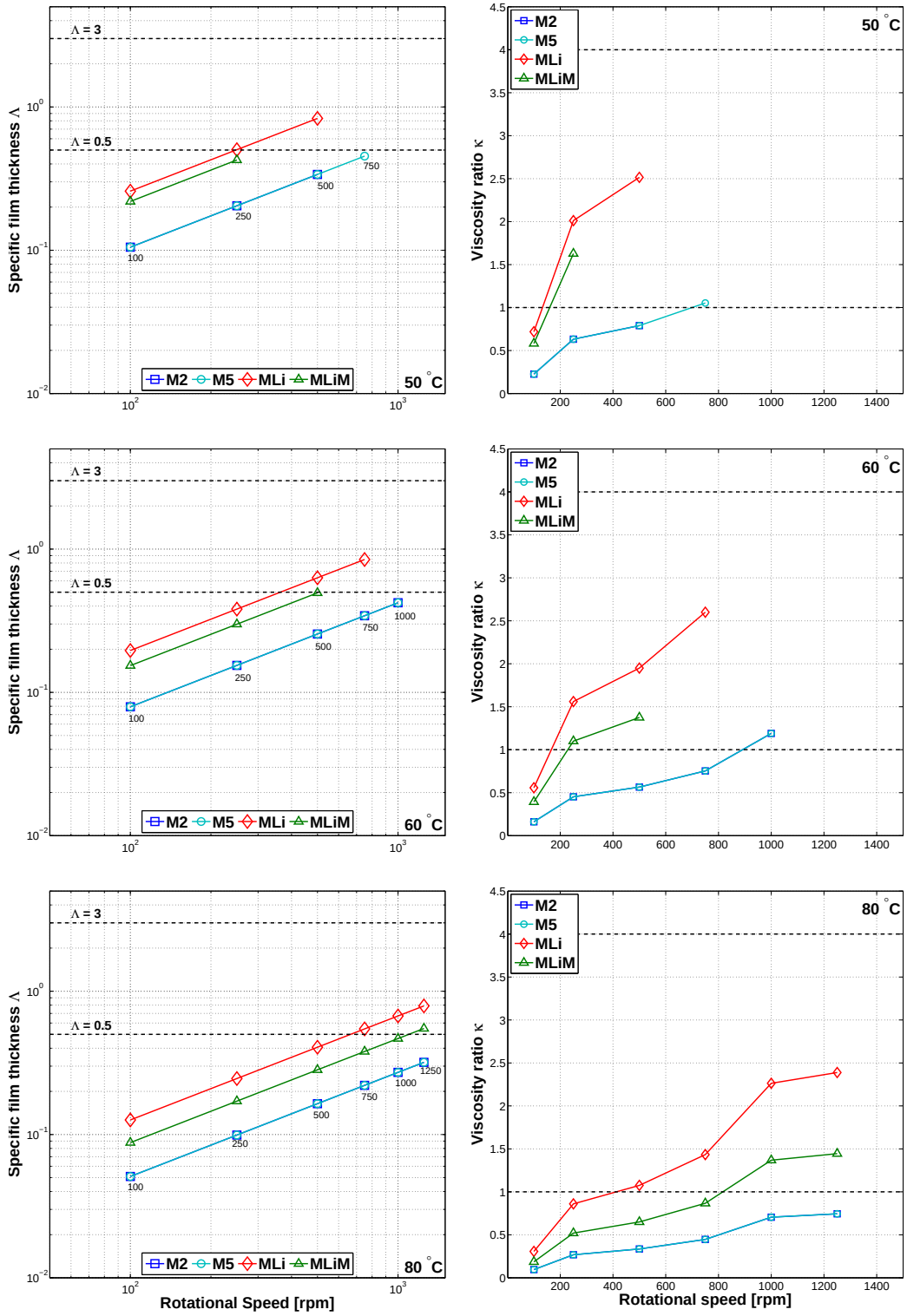

Figure 7.11: Figures to the left: Specific film thickness of a single roller-raceway contact of the TRB, considering the base oil as the active lubricant inside the contact. Figures to the right: SKF's viscosity ratio [42], considering the base oil as the active lubricant inside the contact.

7.5.2 Rolling bearings friction torque results

The friction torque results of the thrust roller bearings lubricated with greases M2, M5, MLi and MLiM, measured at controlled temperature of 50 , 60 and 80 °C, are shown in Figure 7.12. The standard deviation of the friction torque measurements is also shown for each data point, considering the 10 measurements performed at each speed step.

In general, the friction torque decreases with the increase of the rotational speed, although sometimes very slightly. It is also interesting to notice how the lithium thickened greases show higher friction torques, specially grease MLiM formulated with lithium complex thickener and a mineral based oil. Both polymer greases M2 and M5 show similar friction torques, although grease M5 generally shows lower torques.

Once again, the coefficients of friction under boundary and full film lubrication

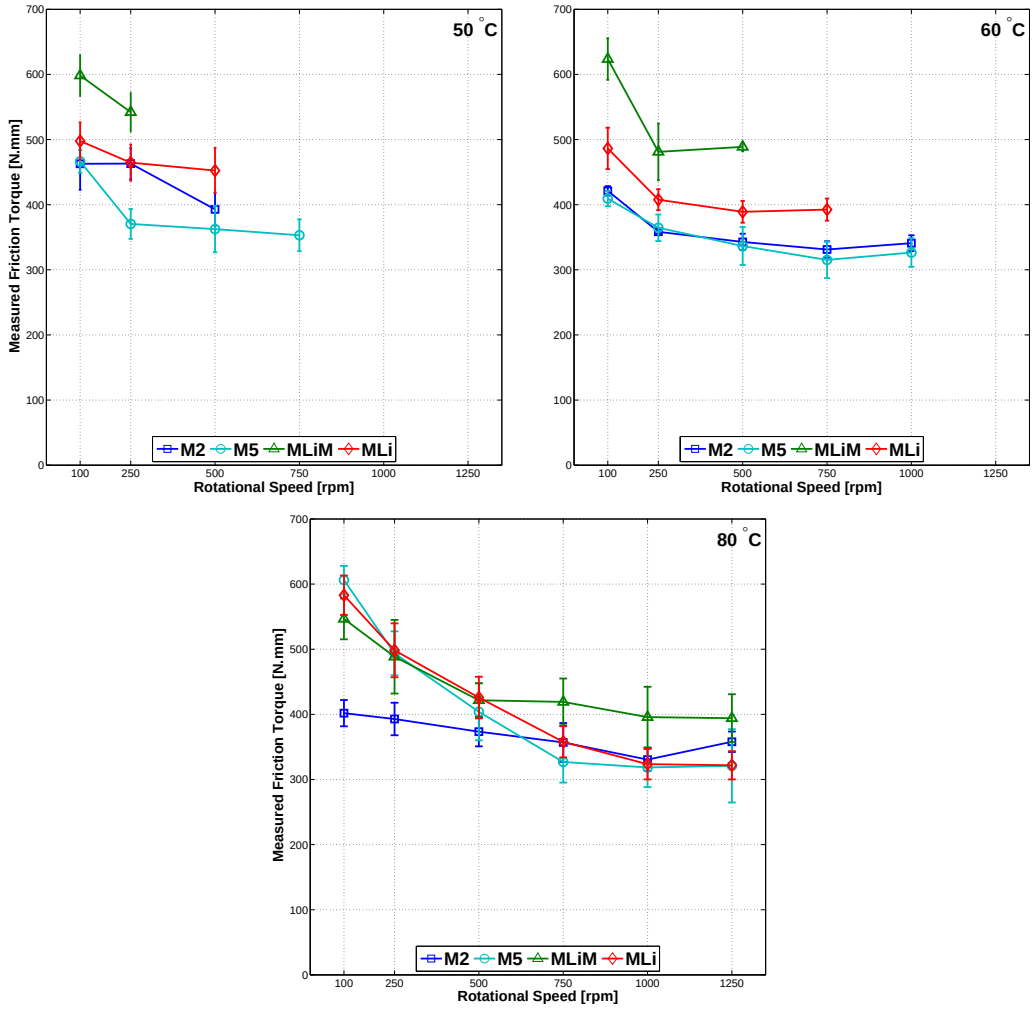

Figure 7.12: TRB friction torque measured for greases M2, M5, MLi and MLiM, at constant temperature of 50, 60 and 80 °C and constant load of ≈ 7 kN.

Table 7.7: Optimized values of COF under boundary film (μ_{bl}) and full film (μ_{ehd}) lubricating conditions. The average error of the optimization to the experimental results is also shown.

	μ_{bl}	μ_{ehd} 50 °C	Error [%]	μ_{ehd} 60 °C	Error [%]	μ_{ehd} 80 °C	Error [%]
M2	0.047	0.024	3.01	0.013	9.90	0.009	9.61
M5	0.045	0.019	5.75	0.013	8.08	0.008	10.81
MLi	0.058	0.031	2.82	0.024	3.00	0.019	6.49
MLiM	0.059	0.044	3.18	0.035	6.80	0.023	4.99

were optimized in order to match the SKF friction torque model to the experimental results. The optimized values of this coefficients are shown in Table 7.7. The optimization was performed for each grease considering the properties of the active lubricant inside the contact to be equal to the base oil's. The average error of the optimization regarding the experimental results is also shown in Table 7.7. This average error is generally small, being close or below 10 %, which shows a good approximation to the experimental results.

As shown in this table, the coefficient of friction under boundary film lubrication μ_{bl} is always higher than the coefficient of friction under full film lubrication μ_{ehd}, as expected. This difference becomes larger as the temperature increases and the system gets close to boundary film lubrication since the weight of the μ_{ehd} becomes smaller. It is also interesting to notice that the values of μ_{bl} are higher for the LiX thickened greases than for the PP greases.

From the values shown in Table 7.7, the sliding coefficient of friction μ_{sl} was calculated using SKF's weight distribution function ϕ_{bl}. The optimized μ_{sl} of each grease is shown in Figure 7.13, plotted as function of the Hersey modified parameter S_P (see Equation 5.4, in Chapter 5). The optimized μ_{sl} is compared at each temperature with the value of μ_{sl} expected from the experimental measurements. The deviation of the optimized values to the experimental results increases for higher temperatures, not only because the model struggles to correctly approximate the friction torque under boundary lubrication but also because the number of data points to approximate is larger. It is also possible to observe the evolution of the optimized μ_{sl} as the operating temperature increases: the curves move down and to the left, towards boundary film lubrication.

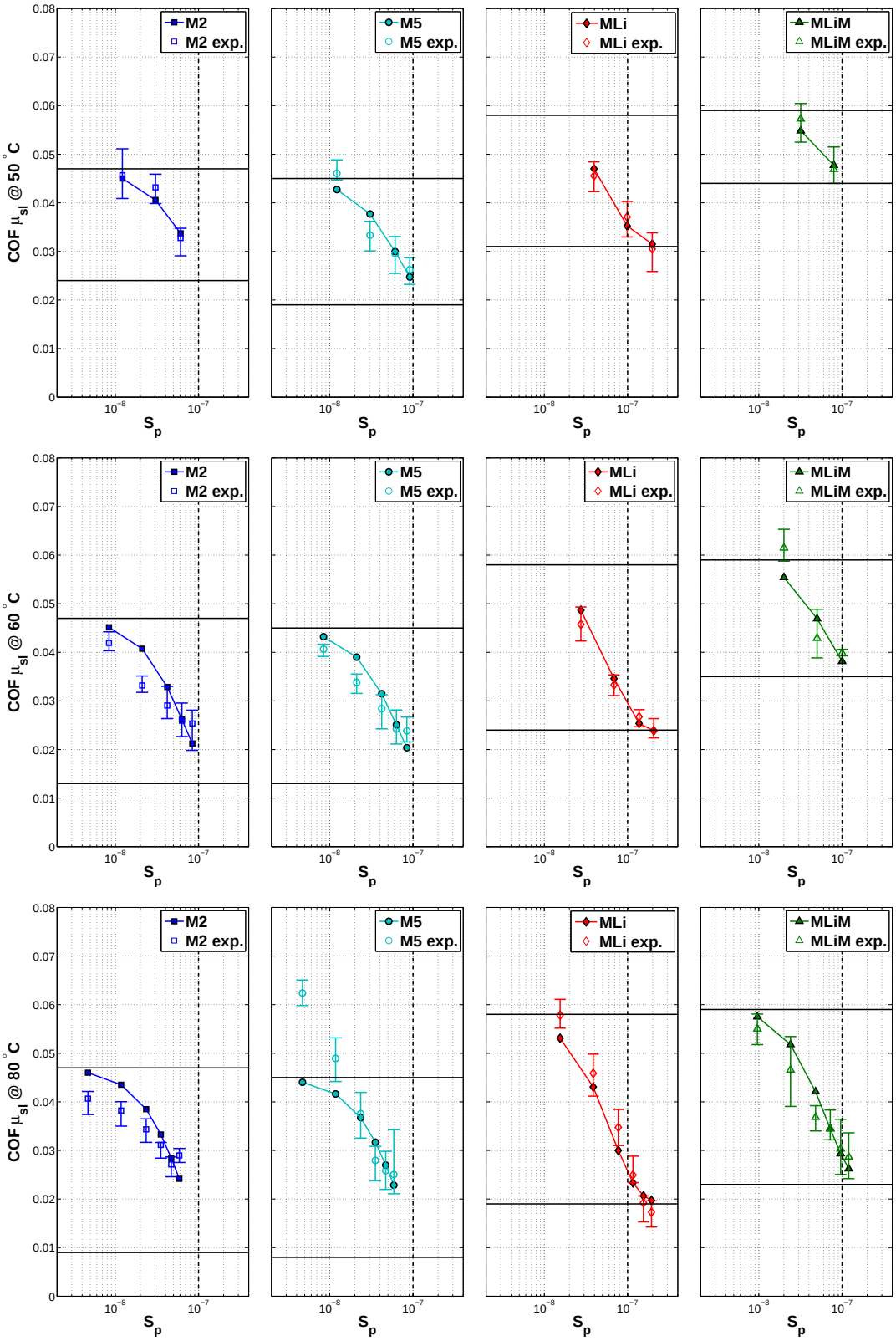

Figure 7.13: Experimental (exp) coefficient of friction and optimized coefficient of friction, calculated for the tested greases at the controlled temperatures of 50, 60 and 80 °C. The vertical dashed line represents the S_P value at which $\Lambda \approx 0.5$.

Comparing the value of μ_{sl} of different greases, it is interesting to observe that for the same S_P numbers and therefore same lubrication regime (similar film thickness despite different combination of speed and operating viscosity), grease MLi and MLiM always show higher values of μ_{sl} than greases M2 and M5. These results are in agreement with the results obtained in Chapter 5, despite the geometry, number of contacts and operating conditions being very different.

It is now possible to calculate the sliding friction torque, in order to compute the total friction torque. In Figure 7.14, the rolling (M'_{rr}) and sliding (M_{sl}) friction torques of each grease at different operating conditions are shown.

Since M'_{rr} depends highly on the lubricant's viscosity and speed $(n \cdot \upsilon)^{0.6}$, it shows a similar behaviour to the film thickness, increasing with both parameters. The higher the viscosity, the higher should be the rolling friction torque. Given that greases M2 and M5 were formulated with the same base oil, their rolling torques should be similar. Grease MLi generates the highest rolling torque because its base oil also shows the highest viscosity at each operating condition.

On the other hand, the sliding friction torque shows the opposite behaviour, decreasing with the entrainment speed, as the lubricant film builds up. The sliding friction torque, by influence of the optimized coefficients of friction, allows to distinguish different formulations (thickener content/type, base oil nature or additives), even if the base oil viscosity is similar at the same operating temperature. Grease MLiM, formulated with a blend of mineral based oils, shows smaller viscosity than the PAO blend oil used in the formulation of grease MLi but generates a much higher sliding torque. Grease M2 and M5 show very similar formulations except for the elastomer content and therefore, the sliding torque is also similar. However, the fact that grease M5 shows a slightly smaller sliding toque might be a reflection of the elastomer presence.

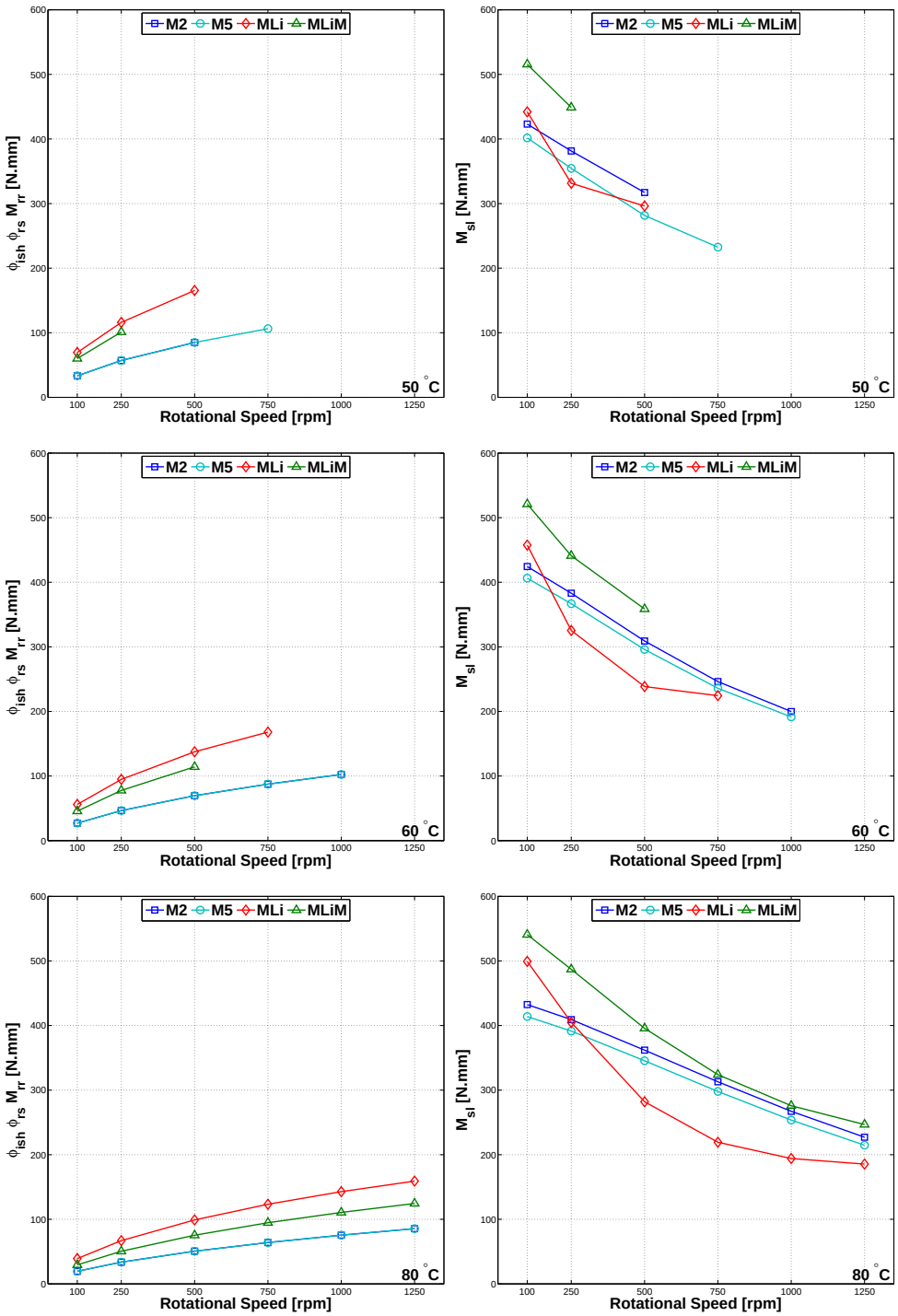

Figure 7.14: Rolling (M'_{rr}) and sliding (M_{sl}) friction torques at constant operating temperature of 50, 60 and 80 °C.

7.5.3 Grease vs Base oil vs Bleed oil

In the previous section, the friction torque of the rolling bearings lubricated with grease was predicted considering that the active lubricant shows similar properties to the base oil. However, it is frequent for the bleed-oil of some greases to show different properties than the base oil, as is the case of grease M5 and MLi. In this section, the measured friction torque of thrust roller bearings lubricated with base oil and bleed-oil will be shown, compared to the previously shown results for the greases.

Figure 7.15 shows the TRB friction torque as function of the rotational speed for the operating temperatures of 50, 60 and 80 °C, measured with each grease and the corresponding base oil and bleed-oil. It is possible to observe how the friction torque behaviour of the base and bleed-oil relate to the grease's. In the case of greases M2 and MLiM, the base oil and bleed-oil show not only similar FTIR spectra between them, but also very close dynamic viscosities (as shown in Chapter 3). Moreover, its film thickness under fully flooded conditions is also similar, despite being inferior to the grease's (as shown in Chapter 4). In the case of the friction torque, the conclusions are similar. The base oil and bleed-oil of these greases generate similar friction torque at any of the tested conditions, although it is higher than the friction torque generated by the greases.

On the other hand, the bleed-oils extracted from greases M5 and MLi show different properties than the corresponding base oils. Although the difference could not be observed on the FTIR spectra, the measured dynamic viscosities are quite different: the bleed-oil of M5 shows higher viscosity than the base oil (due to the elastomer), while the bleed-oil of MLi shows smaller viscosity. Furthermore, the bleed-oil of grease M5 shows shear-thinning behaviour which was not observed for the base oil, at least under the same shear rate range. Additionally, both the bleed-oils of greases M5 and MLi produce a higher film thickness than the corresponding base oils. Regarding the friction torque, the base oil and bleed-oil show different behaviour from each other for both greases. However, it seems that the base oils show a better correlation to the grease behaviour than the bleed-oils, specially in the case of grease MLi.

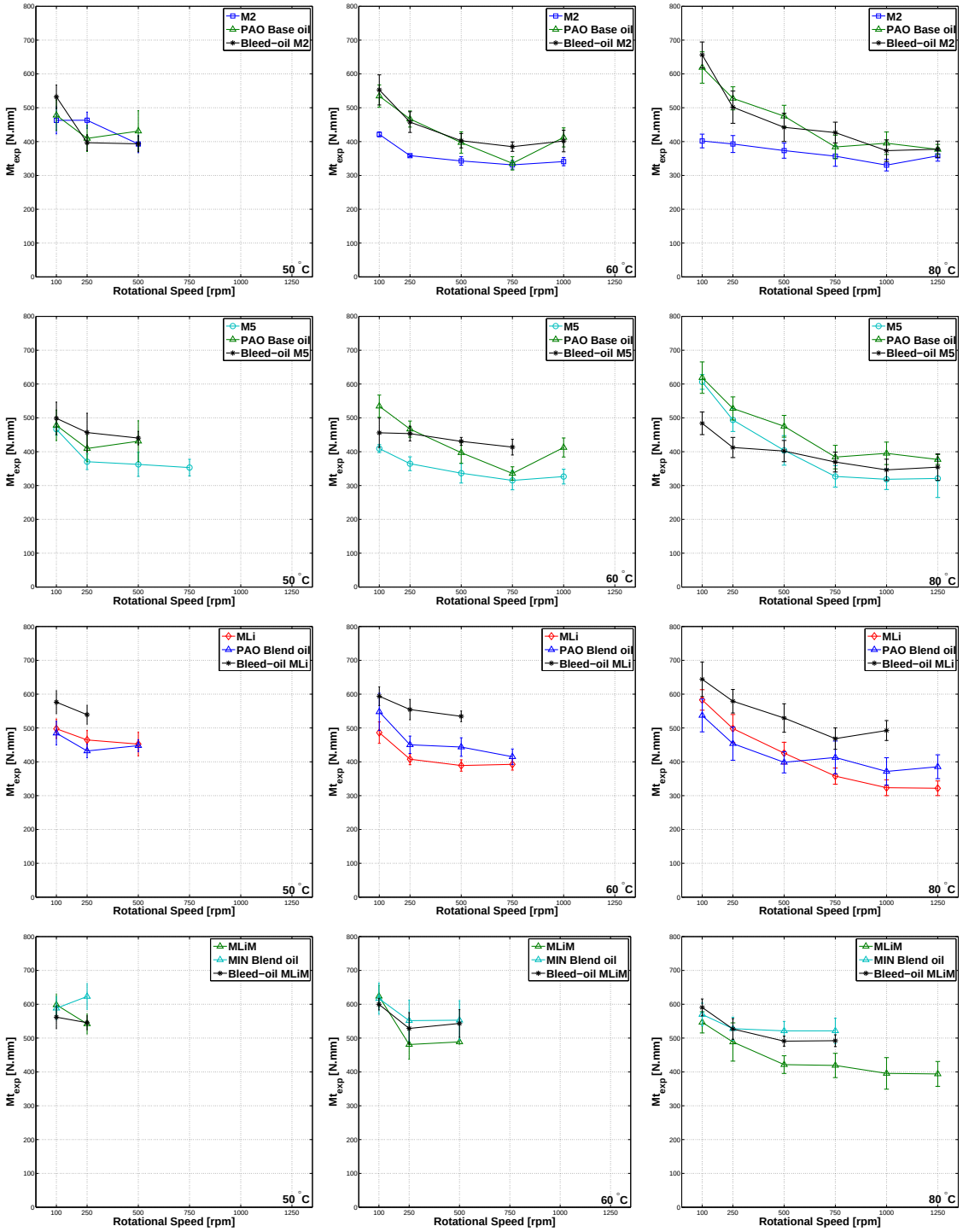

Figure 7.15: Friction torque of the TRB lubricated with each grease and the corresponding base oil and bleed-oil, measured at constant operating temperatures of 50, 60 and 80 °C and constant load of ≈ 7 kN.

7.6 Closure

The lubricating greases presented in Chapter 3 were submitted to rolling bearings friction torque measurements in two different types of rolling bearings: TBB and TRB. Although they are both axial thrust open bearings, the raceways and rolling elements are quite different. Furthermore, and despite it was not the scope of this work, the experimental results clearly show that the rolling bearing geometry has a great influence on the friction and consequent power loss. The TRB generated higher friction torque than the TBB for the same operating conditions, even though, the contact pressure is twice higher for the latter.

Regarding the different grease formulations substantial differences were found. First, in the tests performed on TBB lubricated with polymer greases formulated with the same base oil but different thickener content (M1, M2 and M3), it was found that the higher the thickener content, the lower is the friction torque, specially under low rotational speeds. If this fact is due to the different rheological properties of the greases (higher thickener content leads to higher consistency) or to the fact that more thickener material enters the contact, it is unknown. However, the same relationship was found in the ball-on-disc testes reported in Chapter 5.

Second, and comparing the TRB's friction torque generated by each grease (M2, M5, MLi and MLiM) with its base oil and its bleed-oil in controlled temperature tests, it was found that the base and bleed-oil might generate different friction torques if their properties are also different. When they are not, the friction torque behaviour is very similar, although different from the grease's. As a general conclusion, the friction torque generated by the base and bleed-oil is higher than the friction torque generated by the grease.

Finally, comparing the TRB's friction torque results and the optimized values of the sliding coefficient of friction for differently formulated greases (M2, M5, MLi and MLiM), it was found that the lithium thickened greases generally produced higher friction than the polymer greases tested. While this could be due to the higher viscosity of their base oils, the differences were found for the same values of the Hersey modified parameter S_P and therefore similar film thickness, which suggests that the differences are due to the thickener type and base oil nature. Hence, grease MLiM, formulated with LiX thickener and mineral based oil, was the one generating the highest friction, followed by grease MLi and then by the polymer greases M2 and M5, which show very similar coefficient of friction.

8 Thermal degradation of lubricating greases

8.1 Introduction

Grease aging in rolling bearings is characterized by permanent changes in its properties. According to Cann *et al.* [68], these changes depend mostly on the grease formulation (base oil viscosity and nature, and thickener type), on the bearing geometry, material and type, on the bearing house and also on the rolling bearing operating conditions (mainly speed and temperature) and running time. Wear debris and water contamination have also been reported to promote grease aging [33, 46, 67, 70].

It is known that quite frequently a large majority of the rolling bearings fail primarily due to lubricant failure than by surface fatigue [2]. However, it is still very hard to accurately estimate grease life based only on the properties of fresh greases.

Different aging mechanisms are known to occur with grease when lubricating a rolling bearing, depending on the operating conditions. The aging can generally be grouped in mechanical and chemical changes. The mechanical aging, which is not the scope of this work, promotes oil separation and deterioration of the grease thickener matrix [2]. The balance between the oil loss and the degradation of thickener material by shear can lead to grease softening or hardening (reduction or increase in consistency, respectively). On the other hand, the chemical/thermal aging of greases is still poorly studied. It is known that during operation at high temperatures the grease is continuously stressed thermally and mechanically, leading to chemical and physical changes. The oxidation of both thickener and oil can happen and it was found that this type of aging can also lead to grease softening or hardening depending on the grease formulation (thickener nature, base oil viscosity/nature) [71]. The oxidation is known to promote reaction/consumption of additives, acid formation, thermo-oxidative degradation of thickeners and base oils, polymerization of base oils and also to promote the formation of varnish and sludge [2, 71, 72]. However, the way these changes affect the lubricity, the capacity to maintain a lubricating film and the overall tribological behaviour are still unknown.

8.2 Aging process and evaluation methods

A sample of each fresh grease was subjected to an artificial aging procedure. The sample was manually spread over a steel disk forming a layer thickness of approximately 1 mm, as shown in Figure 8.1. The process was intended to replicate the aging in a grease lubricated rolling bearing and the grease interaction with the steel surfaces. Despite the layer thickness could have a considerable influence on the overall aging of the grease sample, it was found that for the aging time and temperature tested in this work, 1 mm was enough to obtain an homogeneous sample of aged grease. Similar aging methods have been used by other authors [67, 72, 180], using grease layers of different thickness.

Both the PP and the LiX thickened greases were thermally aged in the oven for 5 (120 h) and 10 (240 h) consecutive days at 120 °C which is the maximum working temperature of the PP thickened greases, indicated by the manufacturer for

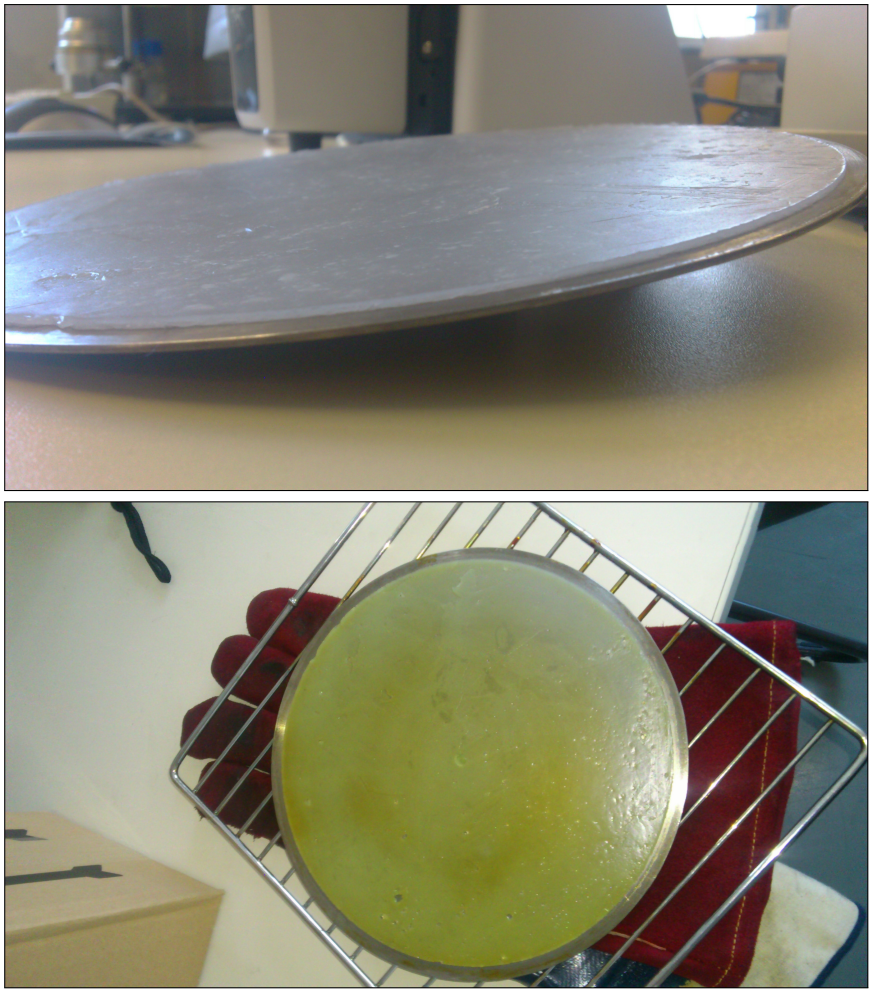

Figure 8.1: Photographs of grease M2, spread across the steel disc with a layer thickness of 1 mm, before and after the aging process.

continuous use (the corresponding temperature for the LiX thickened greases is 150 °C). The temperature of the oven was adjusted manually through a potentiometer, using a thermometer for the atmosphere temperature evaluation. Although there was no forced convection mechanism, the oven had a breathing hole on the top, allowing the chamber atmosphere to be refreshed. Care was taken to keep the temperature constant at all times.

After the aging process, the disc was removed from the oven to the room temperature and the grease was immediately collected in a container to avoid further aging. These samples were evaluated through FTIR and rheological measurements. The thickener morphology was also investigated through scanning electron microscopy (SEM). For more information regarding the methods used to characterize the aged grease samples, please refer to Chapter 3.

From here on, the aged samples will be referred to with the suffix "a" for aged (eg. M2 - fresh grease, M2a - grease sample aged for 5 or 10 days).

8.3 Introductory Notes

This chapter results from a series of tests performed alongside the main tests performed for this project. The focus was to study the grease degradation in rolling bearings while developing an artificial method to study the late stages of grease life without the need to perform full rolling bearing tests upon failure, which are very time consuming. Moreover, grease life tests not only take much time but their repeatability is often low, that is why the rolling bearings service life is frequently treated statistically.

In the beginning it was intended to study both the mechanical and thermal aging, but given the huge amount of testing needed and the fact that the mechanically aging requires not only time but specific equipment to severely shear the grease, in the end only thermal aging was evaluated.

Still, even thermal aging presented a few challenges. The fact that different base oil natures or different thickener types allow different maximum operating temperatures, makes it very hard to define an aging temperature which suites every grease, making the direct comparison of their aging almost impossible. Furthermore, it is hard to obtain a repeatable thermal aging procedure, given the number of variables involved. The thickness of the grease layer during the aging process is important and should be very small to assure the homogeneity of the aged sample time but as a consequence, it narrows the amount of grease that can be aged at a given time. Additionally, the substrate were the lubricant is deposited might also influence the end

result given the different thickeners' affinity with the substrate material. Moreover, the chamber temperature, the air convection rate and the oxygen content are other very important variables which were not even controlled.

Associated with these variables, the aging time is of the utmost importance. The aging time was defined from a single rolling bearing test lubricated with grease M2 and operating for 5 days at 100 °C and 1000 rpm. The FTIR spectrum taken from the worked sample showed severe oxidation regarding the fresh grease and therefore, a duration of 5 days at 120 °C was established for the artificial aging procedure.

However, after the chemical and rheological characterization of the samples aged for 5 days at the same aging temperature, some greases showed no oxidation while others were already severely aged, depending on their formulation. Hence, a second test of longer duration (10 days) was necessary in order to be able to see relevant changes in the properties of all the aged greases. However, due to logistic issues, it takes a long time to produce significant amounts of aged grease samples that could be characterized by several different methods (rheology, oil loss, SEM, bleed-rate, etc.) and tested tribologically in ball-on-disc and rolling bearing tests. Therefore, of these characterization methods, a few of them were only performed to the samples which were aged for 5 days. Additionally, some greases were only included in the work-flow later on and thus, were only aged for 10 days and characterized/tested for that aging time only.

8.4 Scanning electron microscopy

The SEM images of the thickener structure of each grease sample, before and after the artificial aging procedure are shown in Figure 8.2. Only the samples aged for 10 days were evaluated.

Regarding the polymer greases, the previously short and thick polypropylene elements discussed in Chapter 3 are now very hard to distinguish individually and it looks like they were melted with each other and their size increased. The matrix also looks much denser. It is not possible to estimate the elements' size with accuracy.

On the other hand, the morphology of the thickener elements obtained from the lithium complex thickened greases MLi and MLiM, remained the same after the artificial aging process. The fibres show a well defined shape and similar diameter and length to the fresh samples' fibres.

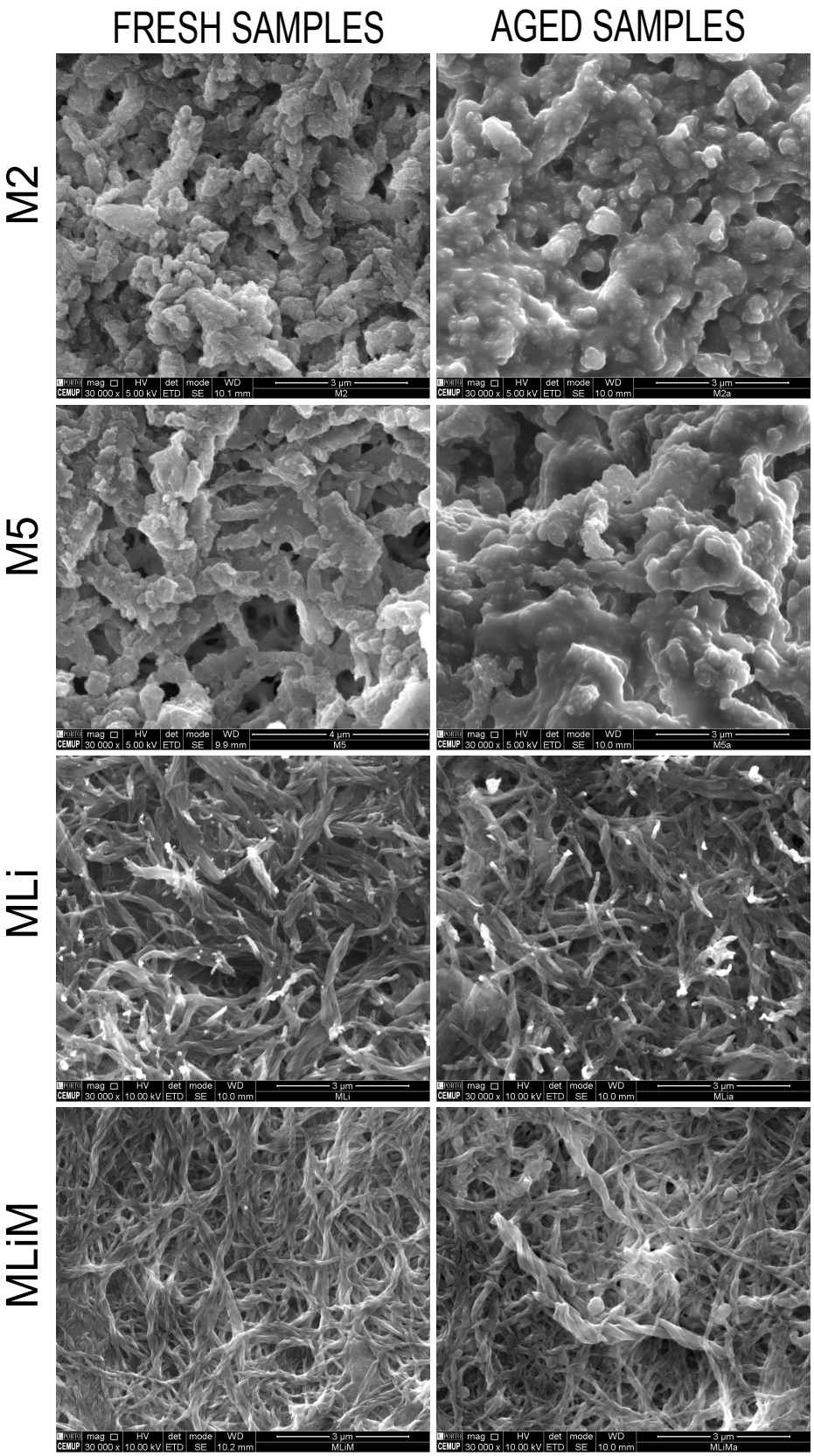

Figure 8.2: SEM images of the greases' thickener morphology, before and after 10 days of aging time.

8.5 Fourier transform infrared spectroscopy

Both the fresh and aged spectra of grease M5 after 5 and 10 days of aging time, can be observed in Figure 8.3. The bleed-oil and thickener spectra separated from each sample presented the same trends, following the same peak height order. The most relevant differences between fresh and aged samples are highlighted in four distinct areas, represented in Figure 8.3, as:

Area A - Hydroxyl compounds (O-H stretch), absorption bands from ≈3000 to 3500 cm^{-1}: alcohol species from the oxidation reaction and water absorption, observed as a baseline rise or offset [181, 182];

Area B - CH_2 and CH_3 Symmetric and asymmetric stretch, absorption bands from ≈2800 to 3000 cm^{-1}: the height reduction of the peaks at 2922 and 2855 cm^{-1} is simultaneously connected to evaporation of short chain volatile hydrocarbons of the base oil and the destruction of some C-H and C-C chains [183, 184] since both the bleed-oil and the thickener spectra showed reduction in these peaks' height. The slight increase in the peak at 2951 cm^{-1} for the aged grease spectrum can once again be associated with oil loss and evaporation, since this peak's absorbance is higher on the thickener spectrum;

Area C - Carbonyl compounds (C=O stretch), absorption bands from ≈1650 to 1800 cm^{-1}: high absorption bands due to the formation of the following oxidation products: ester (at 1733 cm^{-1}), lactone (at 1718 cm^{-1}), carboxylic acids and

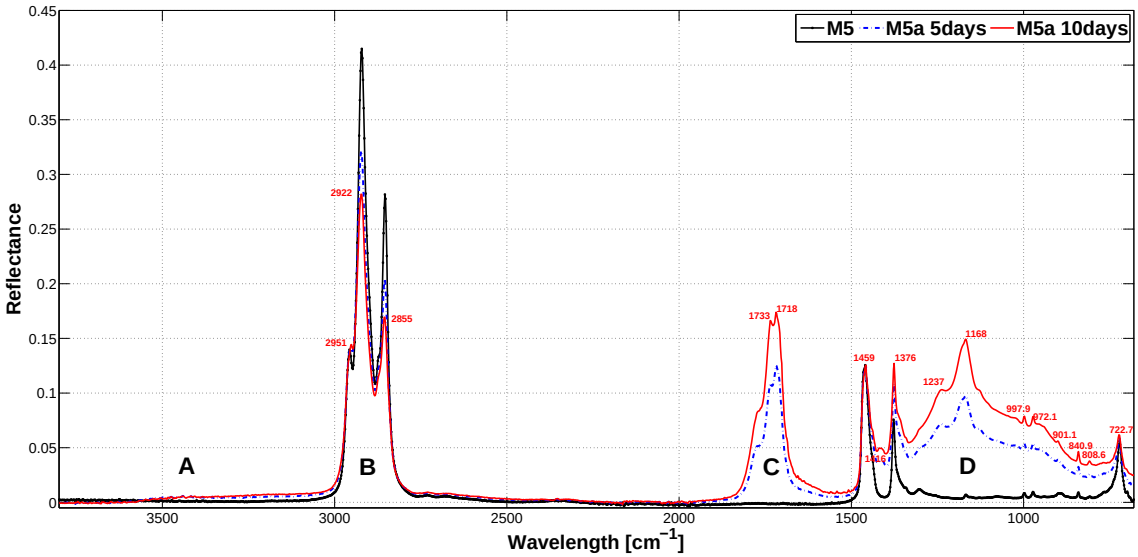

Figure 8.3: FTIR spectra of the thermally aged samples of grease M5 after 5 and 10 days of aging time.

other carbonyl species [65, 70, 181–184]. Although these products were found on both thickener and bleed-oil separate spectra, they might result from the degradation of only one of them;

Area D - Fingerprint region, absorption bands from 650 to ≈1500 cm^{-1}: this area includes the CH_2 and CH_3 deformation stretch (from the base oil and the thickener) and the products from the oxidation of grease, resulting in carbon-oxygen compounds (C-H and C-OH): carbonyl, hydroxy and other ester and ether compounds [65]. The ratio CH_3/CH_2 increased significantly after the aging since the peak at 1376 cm^{-1} increased considerably. This is due to chain-breaking reactions [72] in the oil molecules. Additionally, a new small peak appears at 1416 cm^{-1} probably from the degradation of the oil since the thickener showed no peak at this wavelength.

Grease M2 showed a very similar behaviour to grease M5. After 5 days it was already possible to observe severe differences from the fresh grease spectrum. Associated with these changes, there was also a remarkable darkening in the colour of all the aged samples, independently of thickener type or base oil nature, even for the lithium thickened greases. The LiX thickened greases MLi and MLiM, did not show any alteration in their spectra, there were no oxidation peaks or changes in the absorption intensities after 5 days of aging time at 120 °C. After 10 days however, it was already possible to observe relevant changes regarding the fresh grease spectrum, showing clear signs of oxidation. Furthermore, for this aging time, the darkening of the grease samples was clearly visible, as shown in Figure 8.4.

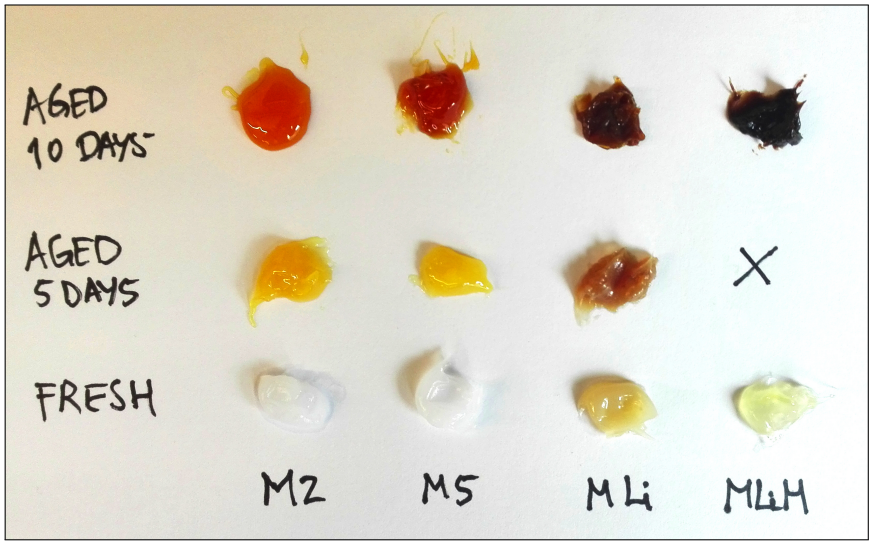

Figure 8.4: Picture showing the darkening of the aged grease samples as the aging time increases.

In Figure 8.6, the FTIR spectra of both the fresh and aged samples of each lubricating grease after 10 days of aging time are shown. It is possible to observe that all aged samples show different spectra from their fresh greases. As previously analysed, the differences observed are related to oxidation and to the formation of certain compounds (esters, ketones, etc.).

According to the FTIR results, the spectra of all the aged samples show signs of oxidation after 10 days of aging time. However, depending on the grease formulation, this oxidation was more or less severe. The aged PP thickened greases M2a and M5a showed higher oxidation peaks, followed by grease MLia and then by MLiMa which showed much less oxidation.

The rise of the peaks at around 1700 and 1150 cm^{-1} is very often associated with oxidation and a clear indication of the different oxidation resistance of the PP thickened greases regarding the LiX thickened greases, as shown in Figure 8.5 at the fingerprint region. Furthermore, the thermal aging is also responsible for the loss of oil through evaporation, which is very relevant for grease M2 and M5 through the reduction of the peaks at 2920 and 2850 cm^{-1} and also the relative increase of the peak at 1376 cm^{-1} regarding the peak at 1460 cm^{-1}. Regarding the peaks' height at 1700 and 1150 cm^{-1} (see Figure 8.5), the following relationship can be established:

$$M5a > M2a >> MLia > MLiMa$$

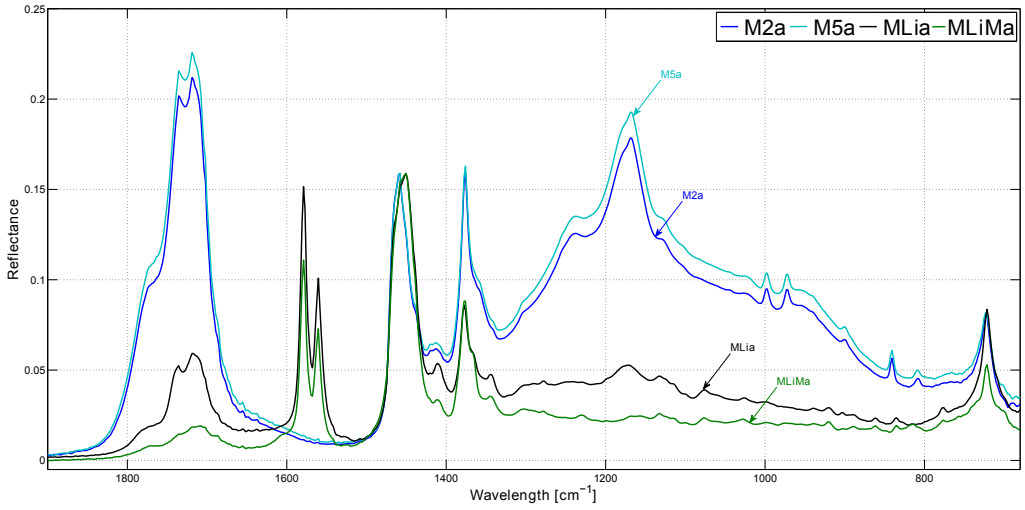

Figure 8.5: FTIR spectra of the fresh versus thermally aged grease samples after 10 days.

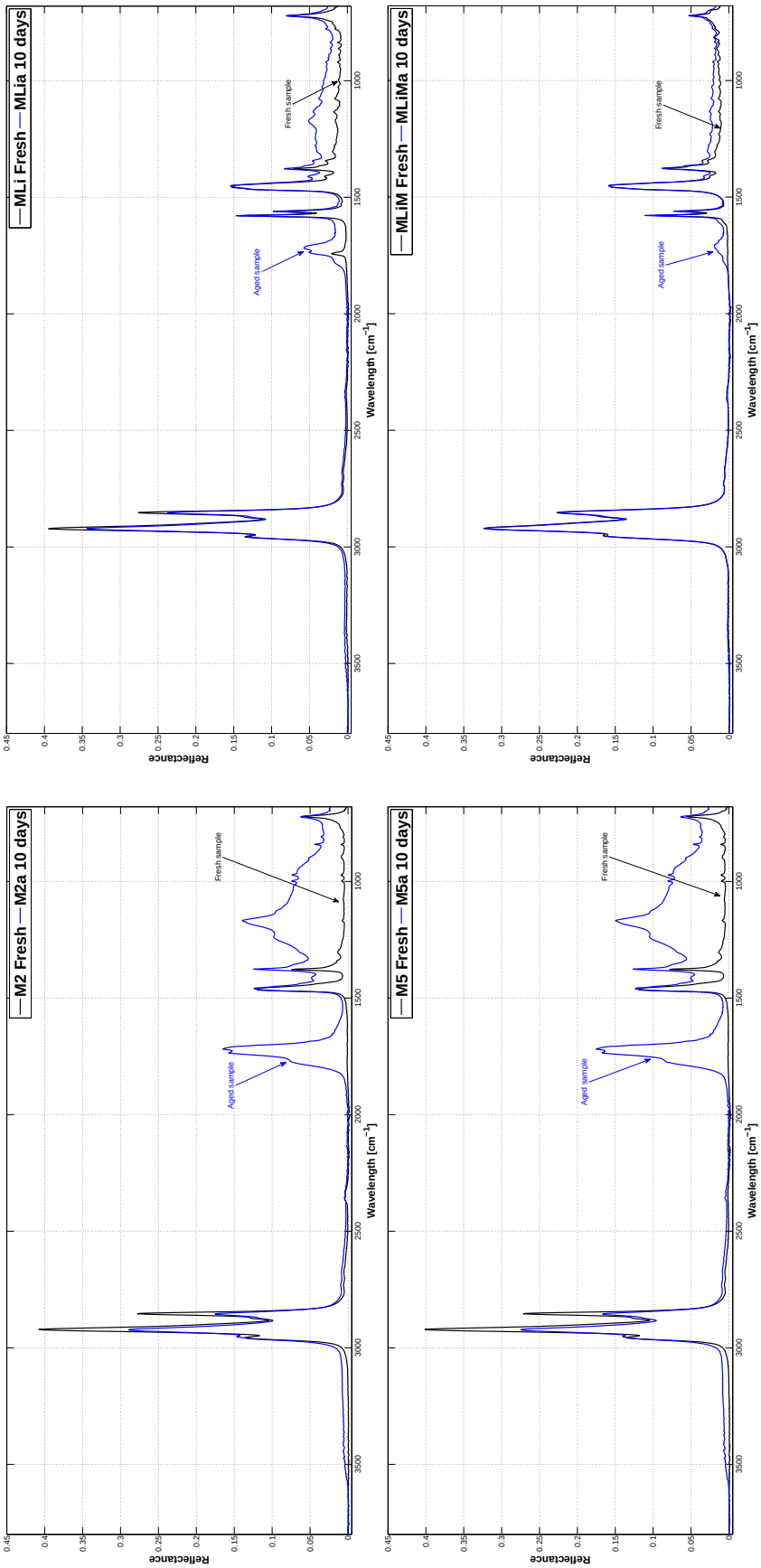

Figure 8.6: FTIR spectra of the thermally aged grease samples after 10 days.

This might indicate that the oxidation is very dependent on the nature of the thickener, i.e., the LiX thickened greases present a better oxidation resistance than the polymer greases at a given aging temperature. The reason behind it should also be related to the fact that the maximum working temperature of the PP thickener is 120 °C while the LiX thickener can work up to 150 °C. Besides this, greases M2 and M5 were formulated with a base oil of lower viscosity and therefore, more prone to be released from the grease and to evaporate. Furthermore, the differences observed should also be due, in part, to the fact that greases MLi and MLiM were formulated with base oils of different viscosity grades and nature.

To further investigate this issue, a new test was performed. A small sample of greases M2 and MLi and their base oils was taken to the oven in a Petri dish with a sample thickness of about 2 mm, for 5 days at 120 °C. These greases were chosen not only because their base oils are of the same nature (PAO) but also because no elastomer was used in its formulation. After the test, the mass loss of each sample was evaluated. The bleed-oil was extracted from each grease's sample and its spectrum compared to the aged base oil.

The results, presented in Figure 8.7, point out that the aged base oils show similar oxidation between them, with the base oil of grease M2 showing higher oxidation peaks. When compared to the bleed oils extracted from the greases, the aged base oils also show higher oxidation. This proves that in fact, for the same aging temperature, both thickeners protect or retard the oxidation of the oil, as expected. However, it seems clear that the LiX soap has a stronger protective action than the PP thickener against oxidation since the difference between the aged base and bleed oil is much smaller for grease M2. Moreover, according to the results shown in Table 8.1, despite both greases show smaller mass loss than the base oils, the LiX thickened grease also shows smaller mass loss than grease M2.

According to the manufacturer[1] of the greases tested in this work, this difference in oxidation at 120 °C might also be explained by the excess of LiOH in grease MLi. It

[1]Personal communication with Johan Leckner and René Westbroek from Axel Christiernsson.

Table 8.1: Mass loss of the grease and base oil samples tested.

	Start (g)	End (g)	Diff. (%)
Base oil M2	15.874	15.243	-4.0
Grease M2	15.427	15.127	-1.9
Blend oil MLi	15.924	15.461	-2.9
Grease MLi	16.076	15.896	-1.1

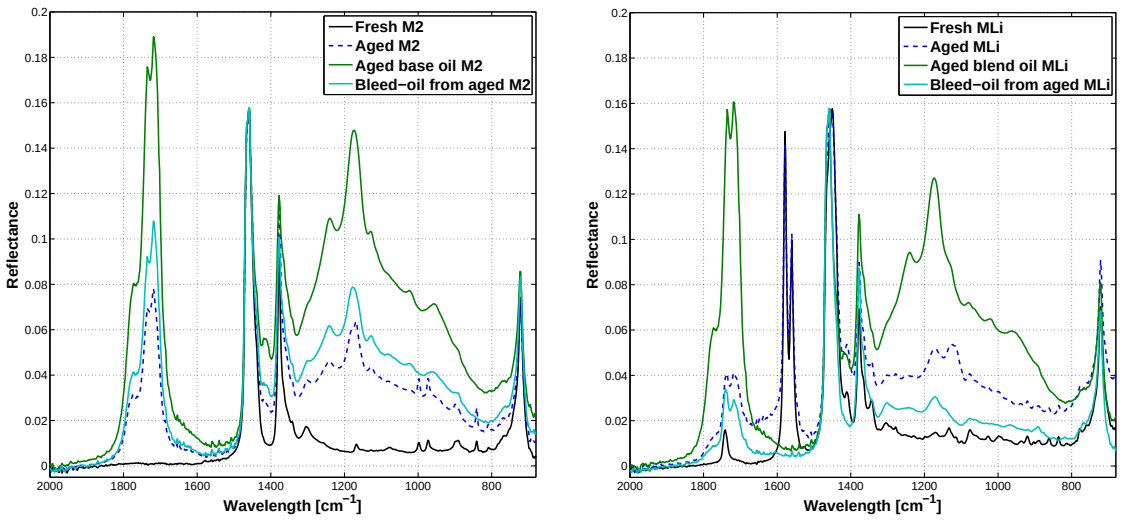

Figure 8.7: FTIR spectra of grease M2 and MLi, its base oil and corresponding bleed oil, after the aging procedure of 5 days.

is common for these LiX thickened greases to be formulated with an excess of LiOH which, might provide oxidation preventing properties, most likely by neutralizing reactive peroxide species [185–187].

8.6 Oil loss evaluation

The thickener content and corresponding oil loss were calculated through a filtration method. A sample of known mass of each grease was dissolved in petroleum ether by means of an ultrasonic device. Afterwards, the solution was filtered through an 8 μm mesh paper filter by the action of a vacuum pump, and then the filter was kept in the oven at ≈50 °C for at least 24h, just enough for the ether to evaporate from the filter. The thickener "powder" on the filter was weighed allowing the thickener/oil ratio to be estimated. Despite this is not a standard method, a satisfying repeatability (less than 5% variation) was found. More information regarding a very similar method can be found in [2].

The oil loss results after 5 and 10 days of aging time, can be seen in Table 8.2. According to this table, the longer is the aging time, the higher is the oil loss. However, depending on the grease formulation, the rate at which the oil is lost may be very different. Figure 8.8 shows the oil loss as function of the aging time measured for greases M2, M5, MLi and MLiM. It is possible to observe that the increase of the oil loss with the aging time is highly non-linear, specially for greases M2 and M5. It is clear that the polymer greases show higher oil loss after 5 or 10 days of aging time. The grease which shows the smaller oil loss is grease MLiM.

Table 8.2: Oil loss of the tested greases, after the aging process.

	Oil [%]	Thickener [%]	Oil loss [%]
M2	87	13	—
M2a 5 days	79.9	20.1	**7.1**
M2a 10 days	64.71	35.29	**22.29**
M5	87	13	—
M5a 5 days	79.11	20.89	**7.89**
M5a 10 days	57.78	42.22	**29.22**
MLi	83.4	16.6	—
MLia 5 days	82.8	17.2	**0.6**
MLia 10 days	75.93	24.07	**7.47**
MLiM	89.43	10.57	—
MLiMa 5 days	n.a.	n.a.	—
MLiMa 10 days	87.75	12.25	**1.68**

The observed differences should be related to the base oil viscosity. Greases M2 and M5 were formulated with a low viscosity base oil which is more prone to be released from the grease at high temperatures and then to evaporate. However, the oil bled by grease M5, should show very high viscosity due to the elastomer and therefore should not have lost oil so easily. On the other hand, the relationship between oil loss and oxidation is clear. The samples more heavily oxidized (M2a and M5a) are the ones which also lost more oil. MLiMa was the less oxidized sample and at the same time, the one who lost less oil.

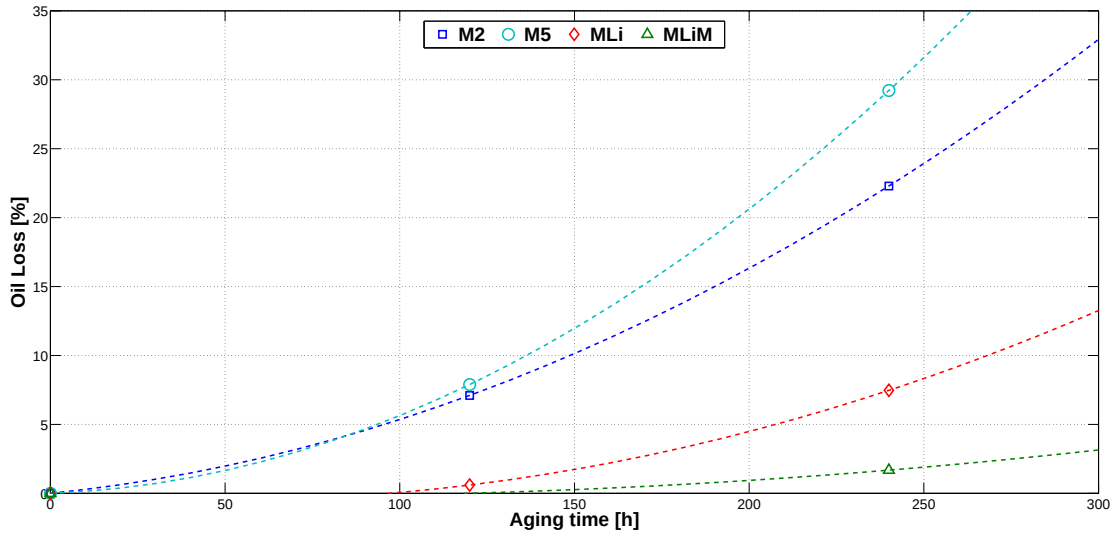

Figure 8.8: Oil loss as function of the thermal aging time, for differently formulated greases.

8.7 Rheology measurements

The storage and loss moduli of greases M2 and M2a (5 and 10 days) are shown in Figure 8.9, obtained through oscillatory measurements performed at 80 °C. According to Figure 8.9, the rheological properties of grease M2 decrease with increasing aging time. The storage and loss moduli, as well as the crossover and the yield stress, decrease as the aging time increases. This behaviour could also be observed for grease M5 and the other polymer greases tested for this work. However, in the case of the lithium thickened greases, the opposite behaviour was observed.

The rheological properties of the aged grease samples (after 5 and 10 days of aging time) are shown in Table 8.3. Comparing these values with the ones from the fresh greases shown in Chapter 3, it is possible to calculate the relative difference (Δ G' and Δ G") between the measured storage and loss moduli of the fresh and aged samples (as shown in Table 8.3).

Depending on the thickener type, two different behaviours were observed:

- the decrease of the moduli for the PP thickened greases - grease softening;
- the increase of the moduli for the Li thickened greases - grease stiffening.

Similar results had already been reported by other authors, for smaller aging times [99]. The storage and loss moduli of the aged samples after 10 days, measured at 80 °C, showed the following order:

$$G'^{MLiMa} > G'^{MLia} > G'^{M2a} > G'^{M5a}$$

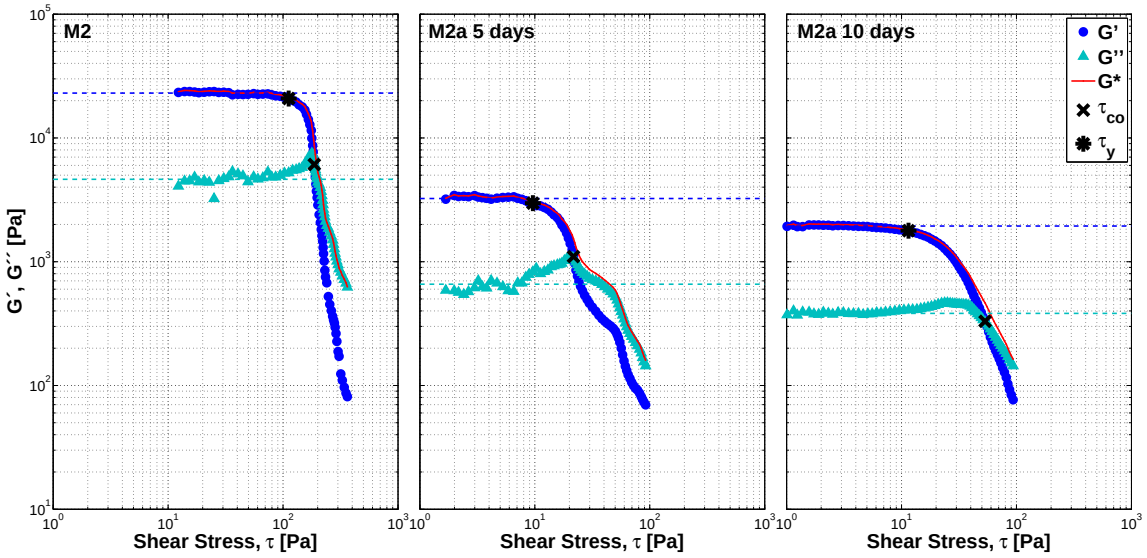

Figure 8.9: Viscoelastic properties of greases M2 and M2a, aged for 5 days and 10 days, measured at 80 °C.

Table 8.3: Properties of the thermally aged greases after 5 and 10 days of aging time.

	Grease Reference		M2a	M5a	MLia	MLiMa	Units
5 days	Storage Modulus G'	80 °C	3238	5467	50055	n.a.	Pa
	Loss Modulus G"		658	1247	14000	n.a.	Pa
	$\Delta = 100 \cdot \frac{aged-fresh}{fresh}$	Δ G'	-86.0	-67.7	+78.0	—	%
		Δ G"	-86.5	-74.6	+131.5	—	%
10 days	Storage Modulus G'	80 °C	1942	573	34870	48825	Pa
	Loss Modulus G"		382	256	8262	10618	Pa
	$\Delta = 100 \cdot \frac{aged-fresh}{fresh}$	Δ G'	-91.6	-96.6	+24.0	+189.9	%
		Δ G"	-92.2	-94.8	+36.6	+475.8	%

$$G"^{MLiMa} > G"^{MLia} > G"^{M2a} > G"^{M5a}$$

The fact that greases M2a and M5a showed much smaller storage and loss moduli indicates loss of mechanical stability - softening. The oxidation observed on the FTIR spectra contributes to the changes in the rheological properties. After the aging and given the high level of oxidation observed, the polymer greases show smaller G' and G''. This softening might indicate loss of structure and consequent drop in consistency. Although the polymer greases also showed higher thickener content after the aging, the oxidation of the base oil and its effect on the viscosity of the bleed-oil, lead to a decrease in the viscoelastic properties. Moreover, this decrease can also be coupled with the re-structuring of the PP-thickener matrix, leading to the softening of these greases. This re-structuring of the thickener (which could not be proved with the current tests) might also be due to the cooling rate, since after the aging process each sample was immediately removed from the oven at 120 °C to room temperature to be collected.

On the other hand, and although the LiX thickened greases did not show severe oxidation, the rheology also changed considerably. The viscoelastic properties of these greases increased as they got stiffer. This should reflect into reduced mobility.

Despite the same aging procedure was applied to greases with different types of thickeners, it should be noticed that the polymer and lithium complex thickened greases are very different in their nature. The fact that the soap thickened greases becomes stiffer after thermal aging while the polymer greases become softer, is a reflection of their very different natures. Furthermore, they also behave very differently in real applications and from the tests conducted so far, they work at very different temperatures as well. What often is noted is that the PP thickened greases generate lower stabilization temperatures than the LiX greases when lubricating rolling bearings operating under the same conditions. Similar reductions in running temperature

have been documented in industrial applications [2].

8.7.1 Bleed-oil viscosity

The kinematic viscosities, calculated from the measured values of dynamic viscosity averaged from the first Newtonian plateau, are show in Table 8.4 for the samples aged during 5 and 10 days. Information regarding the bleed-oil of greases M2a and M5a aged for 10 days could not be obtained since it was not possible to extract it using the same conditions used for the other samples. Grease MLiMa was only aged for 10 days and therefore the bleed-oil viscosity after 5 days was not be evaluated.

According the results shown in Table 8.4, it is possible to observe that the bleed-oil viscosities changed considerably after the aging. Three mechanisms are known to change the viscosity. Firstly chain breaking reactions which split heavy molecular weight compounds into smaller ones, leading to a decrease in viscosity. The chain breaking mechanism might be followed by evaporation of the new low molecular species, resulting in an increase of the bleed-oil viscosity [188]. Finally, the products resulting from the oxidation process (esters, ketones and aldehydes) might also reflect in an increase of the bleed-oil viscosity because they tend to form polymers and other high molecular weight condensations - polymerization [189] - leading in an ultimate extent to sludge and varnish, which do not lubricate [2]. The balance from these mechanisms might explain the differences obtained. Based on FTIR spectra shown

[2]Personal communication with Roger Persson, Volvo Group.

Table 8.4: Kinematic viscosities [cSt] of the bleed-oils extracted from the aged greases. The bleed-oil viscosity of the fresh greases is also shown for comparison.

Temperature [°C]	60	80	110
M2	23	13	7
M2a 5 days	447	173	62
M2a 10 days	could not be extracted		
M5	476	174	88
M5a 5 days	211	89	35
M5a 10 days	could not be extracted		
MLi	57	29	14
MLia 5 days	83	43	21
MLia 10 days	165	74	30
MLiM	58	27	13
MLiMa 5 days	sample not produced		
MLiMa 10 days	97	42	18

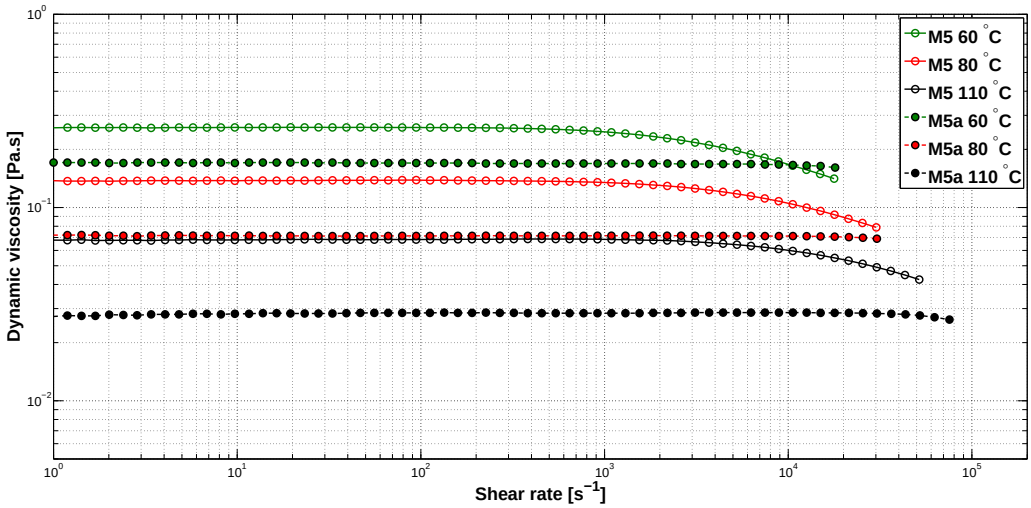

Figure 8.10: Dynamic viscosity of the bleed-oil of grease M5, fresh and aged for 5 days.

previously and the results shown in Table 8.4, it should be expected that the aging time leads to increased bleed-oil viscosity. Moreover, the longer the aging time, the higher should be the oxidation and consequently, the higher the bleed-oil viscosity increase.

In the case of grease M2, the fresh bleed-oil showed very similar viscosity to the PAO base oil but after 5 days of aging time, the viscosity greatly increased. In the case of grease M5, the viscosity of the fresh bleed-oil was significantly higher than the base oil however, after 5 days of aging time the bleed-oil viscosity decreased even if high oxidation was observed. While the fresh bleed-oil showed high viscosity due to the elastomer, the aging process should have been responsible for the destruction of the elastomer or at least blocking its effect on the bleed-oil viscosity. This is also supported by the fact that the shear-thinning behaviour observed for the fresh bleed-oil was not present after the aging for the same test conditions. The comparison can be observed in Figure 8.10 .

Despite it was not possible to obtain bleed-oil from the aged greases M2a and M5a after 10 days, the viscosity of their bleed-oils is expected to have greatly increased based on the results of the samples aged for 5 days and given the very high oxidation observed in the FTIR spectra of the samples aged for 10 days. This very high viscosity should also be responsible for retarding the bleeding rate [60], justifying why it was not possible to obtain bleed-oil from the samples aged for 10 days.

Likewise, the bleed-oils extracted from greases MLi and MLia also showed an increased viscosity regarding the fresh bleed-oils although the increase was not so large as for the grease M2. Given that these greases did not show the same levels of oxidation as the polymer greases, this result was already expected.

8.8 Oil bleeding rate

In Figure 8.11, the bleed-rate results of greases M2, M5 and MLi before and after 5 days of thermal aging are shown. No aged sample of grease MLiM was produced after 5 days, that is why it is absent from Figure 8.11. However, a similar behaviour should be expected.

Comparing the fresh and aged polymer greases it seems clear that the aging affects very significantly the oil bleeding rate. The mechanisms behind these differences should be related not only to the oxidation observed in the FTIR analysis, but also due to the fact that all greases lost oil during the thermal aging procedure. Caused by the oil loss, the thickener matrix is now denser which retards the oil bleeding rate. Furthermore, since the viscosity of the bleed-oils increased due to oxidation, it is also more difficult for this thicker oil to escape. The aged greases show much lower oil bleeding rates, while the relation between the oil bled and time seems more linear than the fresh greases for the duration of this test. Instead of releasing a greater amount of oil in just the first hours, the oxidized samples bleed oil more evenly over time. However, in a real rolling bearing application, the aged samples should in fact be greases which have already released a considerable amount of oil, before severe oxidation even takes place which makes this phenomenon particularly important.

Grease MLia showed lower oil bleed rate, even though the FTIR spectrum did not show severe oxidation peaks after five days of thermal aging. However, the bleed-oil viscosity increased. On the other hand, the polymer greases showed higher oil losses and lower bleed-rates, associated with increased bleed-oil viscosity due to severe oxidation. Given the lower oil content of the aged greases and the lower oil bleed

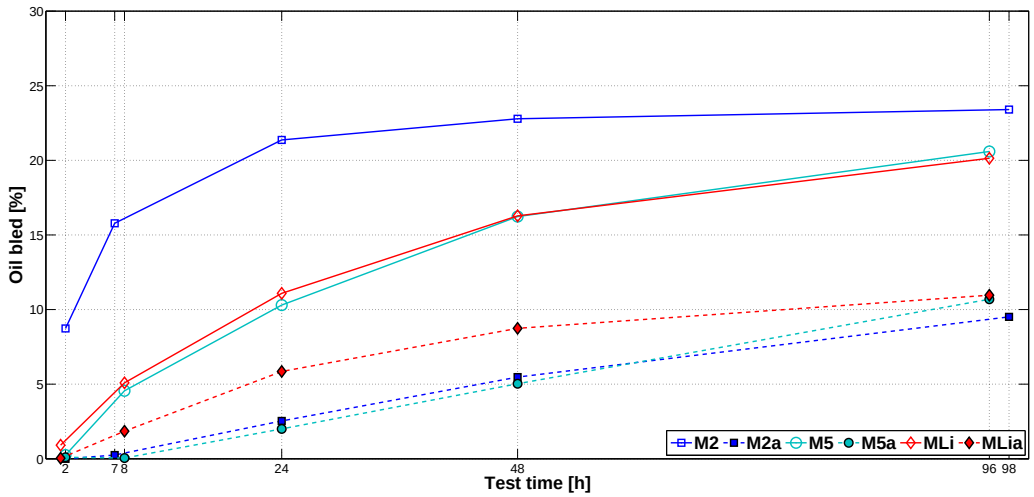

Figure 8.11: Oil bleeding rate of grease M2, M5 and MLi before and after the thermal aging procedure of 5 days.

rate, one should expect that these greases might not feed the contact so effectively, conditioning the contact replenishment and hydrodynamic film formation.

8.9 Film thickness results

The film thickness variation with the entrainment speed for the fresh and aged greases in fully flooded conditions, is shown in Figure 8.12, at the operating temperatures of 60, 80 and 110 °C (only the aged samples obtained after 10 days of thermal aging are shown). For the fresh greases, as previously stated in Chapter 4, it is possible to observe that the film thickness increases at a rate of $U^{0.67}$, under moderate to high speeds.

After the thermal aging and following the chemical and physical changes of the greases, several differences were found. Under full film conditions, all aged samples produced higher film thickness, supporting the theory that the active lubricant inside the contact is now of much higher viscosity. This increase was particularly important for the aged polymer greases. It is also interesting to notice that the film thickness plateau at low speeds was not found for the aged samples M2a and M5a. The inflexion on the film thickness curve might continue to exist but it should now happen at much lower speed.

For some of the measurements it was also possible to observe thermal effects. The very high viscosity of the aged lubricant, associated with high entrainment speeds at the contact inlet, promotes shear heating of the lubricant which results in a non-linear increase of the film thickness with the entrainment speed, in logarithmic scale. This effect is specially important at 60 °C and high speeds.

Although the film thickness increased for all tested greases, such increase was smaller for the LiX thickened greases. This result was already expected since these greases were less affected by the thermal aging than the polymer greases. In the case of grease MLi and MLiM, the inflection marking the thickener contribution to the film thickness was still found after the aging. However, the transition now occurs at higher speeds and for higher film thickness values.

After the aging, the film thickness under fully flooded condition and moderate to high speeds (U > u_{tr}), follows the order:

$$h_{0c}^{M5a} > h_{0c}^{M2a} > h_{0c}^{MLia} > h_{0c}^{MLiMa}.$$

It should be stressed that these tests were performed assuring fully flooded conditions. The behaviour under starved lubrication might be considerably different.

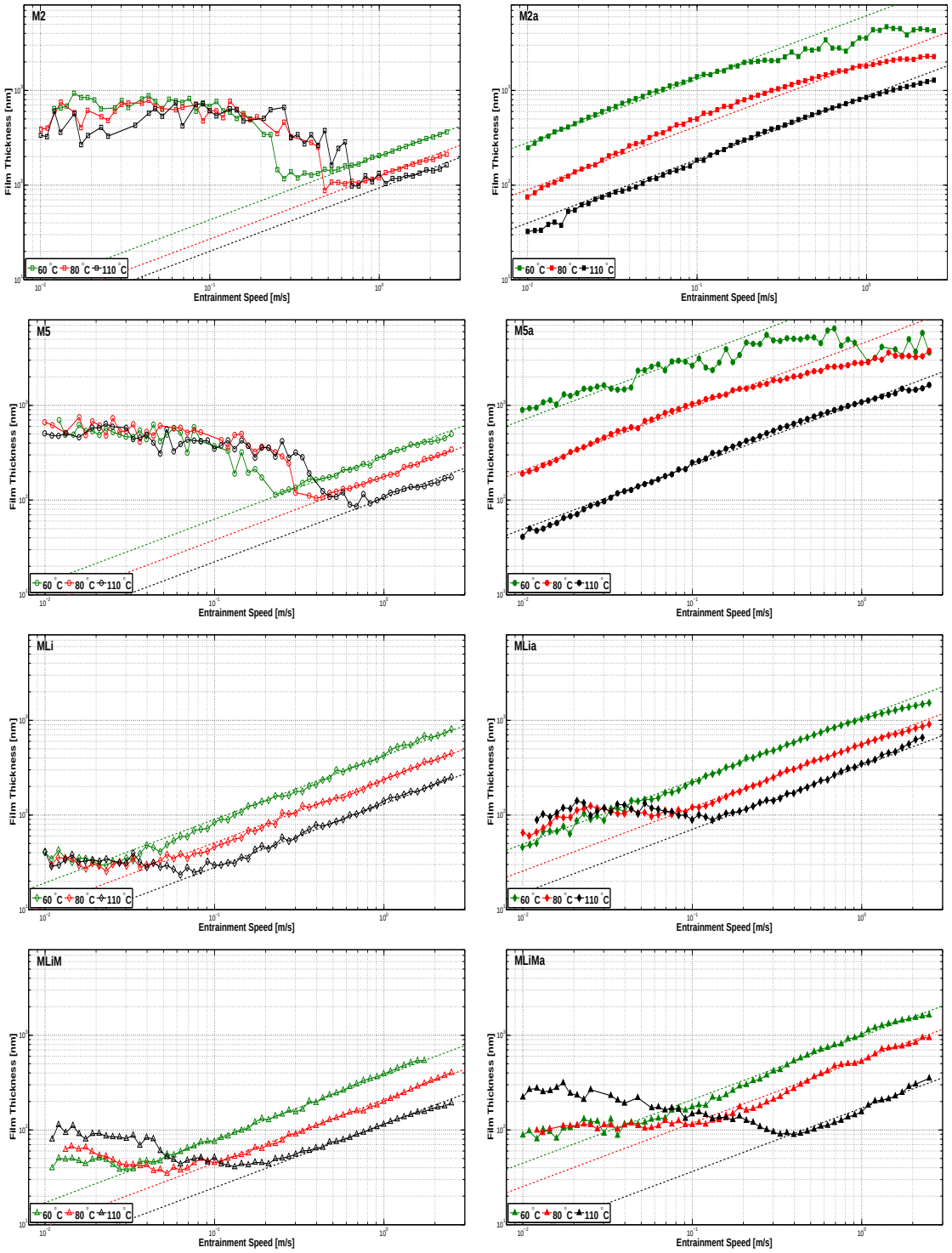

Figure 8.12: Film Thickness curves of the fresh greases (figures to the left) and thermally aged greases (figures to the right), measured at different operating temperatures, over the same entrainment speed range. The aged greases shown were subjected to 10 days of aging time.

8.10 Traction curves

The traction curves shown in Figure 8.13 were performed at 80 °C, with fresh and aged greases. Only the samples aged for 10 days were tested.

The measurement procedure was the same discussed in Chapter 5, using a ball-on-smooth disc contact. Once again, for this SRR range of values, no traction coefficient plateau or thermo-viscous behaviour was observed. The expected lubrication regime for these tests is mixed and full film lubrication given the very low surface roughness of both disc and ball.

Figure 8.13 shows that the traction coefficient of the aged greases is generally higher than for the fresh greases. This is specially true for the severely aged polymer greases but can also be seen for the less oxidized greases MLi and MLiM, under certain operating conditions. The differences between the aged and fresh greases is less evident for the lithium thickened greases which is in line with other previously shown results, indicating that the aging procedure affected these greases much less. At 0.9 m/s, the traction coefficient μ of the aged greases follows this order:

$$\mu^{MLiMa} > \mu^{M2a} > \mu^{M5a} > \mu^{MLia}$$

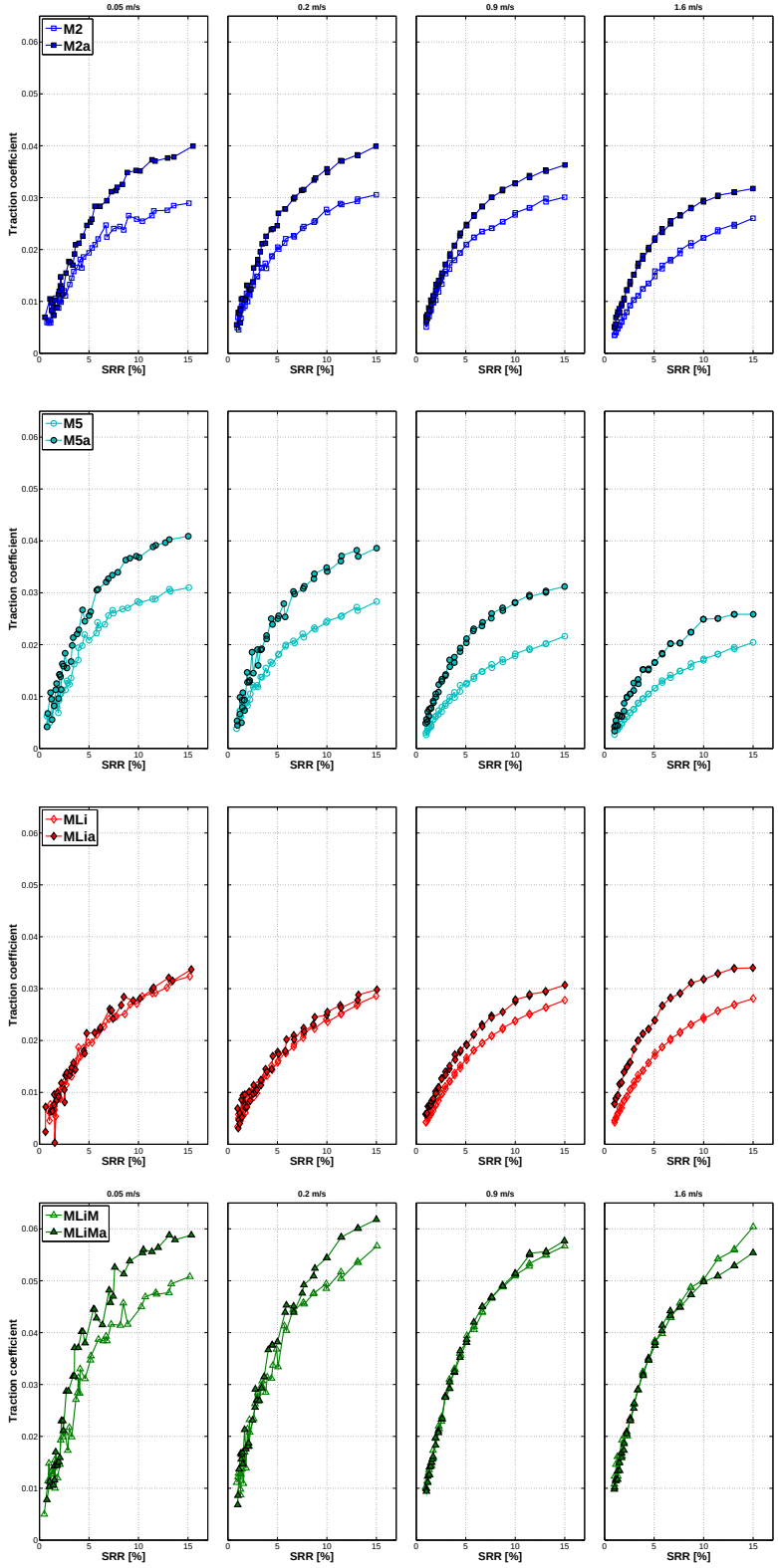

Figure 8.13: Traction curves at 80 °C of fresh and aged greases (10 days).

8.11 Stribeck curves

The friction behaviour of each grease was studied at two different temperatures and also different SRR values, through the measurement of Stribeck curves. The measurement procedure was the same discussed in Chapter 5, using a ball on rough disc contact.

For this purpose, the S_p parameter developed by Brandão *et al.* [127] was used again, according to Equation 5.4. Despite the values of η and α being generally attributed to the base oil properties of the greases, given that the properties of the greases changed considerably with the aging process, the base oils should no longer be representative of their behaviour. Furthermore, the bleed-oils extracted from the aged samples show significantly different properties from the original base oils and even the original bleed-oil. Moreover, it was not even possible to obtain the bleed-oil for some of the grease samples, aged for 10 days. Therefore, the same procedure used in Chapter 5 was applied in order to calculate the Hersey modified parameter.

Using the measured values of film thickness at moderate to high speeds (U > u_{tr}) shown in Figure 8.12 and the Hamrock and Dowson's equation [104] to predict the film thickness in this region (h_{oc}), it is possible to quickly estimate the product $\eta^{0.67} \cdot \alpha^{0.53}$, as shown in Equation 8.1.

$$h_{oc} = h_{exp} \rightarrow h_{oc} = f(\eta, \alpha) = K \cdot \eta^{0.67} \cdot \alpha^{0.53} \tag{8.1}$$

After calculating the $\eta^{0.67} \cdot \alpha^{0.53}$ product, it is now possible to separately calculate the (η, α) parameters using Gold's equation [77] for the pressure-viscosity, shown in Equation 3.7. This procedure assumes that the lubricant nature did not change after the aging process, which of course is a rough estimation since severe oxidation was observed. The density ρ was considered to decrease linearly with temperature and to be unchanged by the aging procedure. However, this was also not investigated.

The resulting η and α parameters are shown in Table 8.5. Since these parameters are calculated from the measured film thickness curves and Gold's equation, the effect of the operating temperature is taken into account and that is why both η and α decrease with temperature, following the film thickness decrease. It is now possible to calculate the η and α parameters for any operating temperature. From the analysis of Table 8.5 it is also possible to observe that the viscosity and pressure-viscosity increased with the aging procedure, supporting the theory that the viscosity of the active lubricant increased, as expected.

Table 8.5: Calculated results for (η, α) parameters.

Grease	T [°C]	η [Pa.s]	α [GPa^{-1}]	$\eta^{0.67} \cdot \alpha^{0.53}$
M2	60	0.078	5.4	7.519E-06
	80	0.042	5.0	4.722E-06
	110	0.028	4.7	3.504E-06
M2a	60	7.908	10.0	2.302E-04
	80	1.806	8.2	7.716E-05
	110	0.572	7.1	3.296E-05
M5	60	0.131	5.8	1.102E-05
	80	0.066	5.3	6.633E-06
	110	0.032	4.8	3.900E-06
M5a	60	27.237	11.8	5.753E-04
	80	4.400	9.3	1.492E-04
	110	0.753	7.4	4.041E-05
MLi	60	0.212	6.1	1.574E-05
	80	0.099	5.6	8.937E-06
	110	0.044	5.0	4.887E-06
MLia	60	0.759	7.3	4.043E-05
	80	0.313	6.5	2.100E-05
	110	0.146	5.9	1.200E-05
MLiM	60	0.147	7.8	1.400E-05
	80	0.067	7.0	7.822E-06
	110	0.030	6.3	4.313E-06
MLiMa	60	0.535	9.4	3.655E-05
	80	0.243	8.4	2.031E-05
	110	0.051	6.9	6.371E-06

Despite the dynamic viscosity and the pressure-viscosity are calculated with this method, the idea behind the procedure is not to determine the lubricant properties with accuracy but only to calculate parameters which allow to plot the COF curve of different lubricants over a common abscissa, reflecting the lubrication regime of each curve. This would allow for the COF of lubricants with different viscosities and natures to be directly compared for the same operating conditions (load, entrainment speed, SRR and same surface geometry, material and roughness).

After calculating the $\eta^{0.67} \cdot \alpha^{0.53}$ product from the film thickness measurements, it is now possible calculate the specific film thickness for the operating conditions of the friction measurements, according to Equation 4.7. The composite roughness of the surfaces σ was calculated through Equation 4.8.

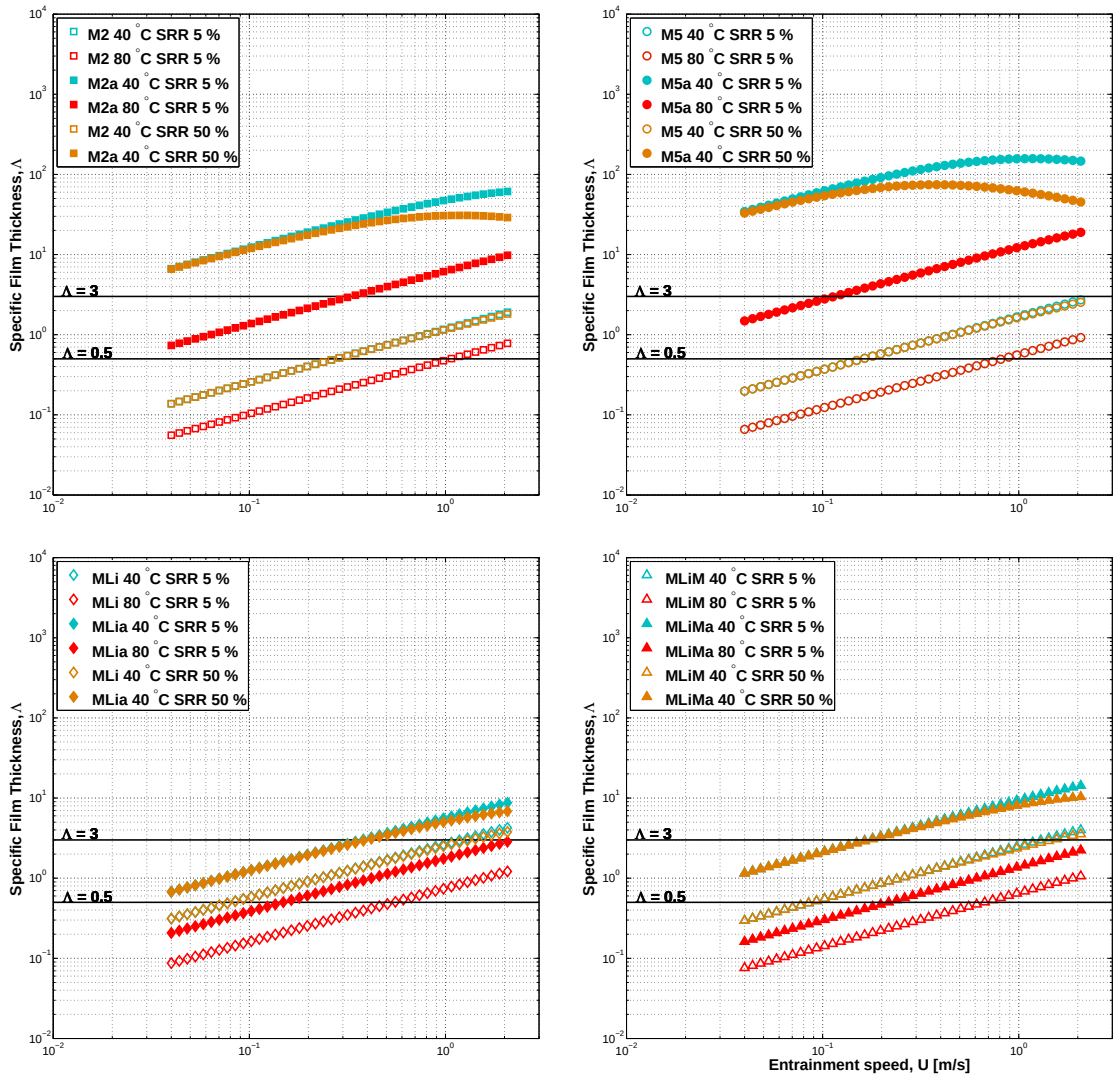

Figure 8.14: Specific film thickness curves of the tested greases, calculated for different operating conditions.

The results for each grease at different operating conditions are shown in Figure 8.14. These specific film thickness curves are not representative of the real grease behaviour since they do not contemplate the film thickness plateau at low speeds discussed in Chapter 4. However, they should represent well the behaviour at moderate to high speeds, because they are based on real film thickness measurements performed using the same contact geometry and operating conditions.

In Figure 8.15, the measured Stribeck curves of fresh and aged greases are shown, plotted against S_p. The S_p values which correspond to the transitions between lubrication regimes [117] were previously defined in Chapter 5 and are still valid for these curves.

After the aging, the greases show a very different behaviour from the fresh state. Given the previously shown film thickness increase, it is expected that the

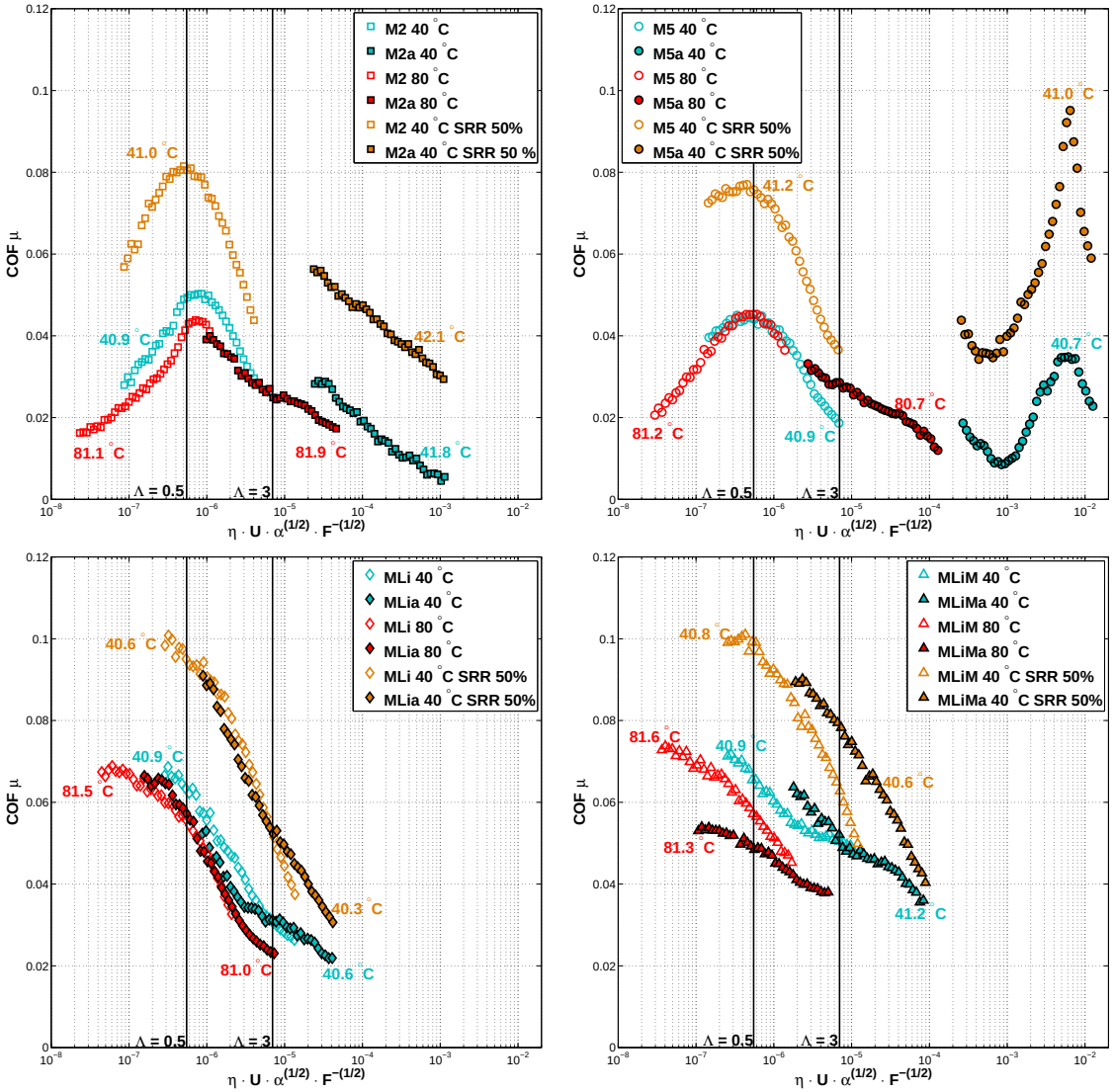

Figure 8.15: Stribeck curves of the fresh and thermally aged greases (10 days) at different operating conditions.

(η, α) values also increased and therefore, the COF curves of all greases are now at higher S_p numbers.

As it happened with the film thickness curves, the Stribeck curves of grease MLi and MLiM did not change considerably after the thermal aging procedure. The curves moved down and to the right (towards higher S_p numbers), following the increase of the film thickness, but the COF behaviour is very similar, supporting the results which showed that the thermal aging at 120 °C was not very effective in quickly degrading these greases.

While the curve's behaviour of greases MLia and MLiMa did not show much differences, in the case of greases M2a and M5a, the curve behaviour is now much different. Once again, the largest differences were found for the aged polymer greases

which, for the same operating conditions, now do not reach boundary lubrication and therefore, the inflexion observed on the COF curve of the fresh greases M2 and M5 was not found for the aged samples. These greases, under fully flooded conditions now seem to run mainly under full film lubrication, only reaching mixed film lubrication at higher temperatures.

The COF of grease M2a, measured under the same operating conditions, increases with the decrease of the entrainment speed as it goes from full film up to almost mixed film lubrication. The inflection previously observed for the fresh greases and attributed to thickener lumps crossing the contact, was not found.

On the other hand, grease sample M5a shows an even more different behaviour. At 40 °C and under a SRR of 5% or 50%, the COF decreases with the increase of the entrainment speed under full film lubrication until it reaches a minimum value. After this point, the COF starts to increase again at a very high rate, as the lubricant film keeps rising. Given the combination of high lubricant viscosity and high speeds, the COF quickly rises by the increase of viscous friction.

At a certain entrainment speed, the shear heating effect at the inlet decreases the lubricant viscosity which, associated with possible starvation, promotes a quick film thickness decrease and a sudden drop in the COF shown by the inflexion on the curves at high S_p values.

At 80 °C, the consistency and viscosity of the grease are lower and therefore, both the inlet shear heating and starvation are less likely to occur, explaining why the inflexion was not observed at this temperature.

The fact that after the aging each grease seems to be operating under different lubricating regimes, makes it hard to compare their COF as function of S_p. Figure 8.16 shows the Stribeck curves at 40 °C and 5 % of SRR, plotted over the entrainment speed, instead. This result shows that, even after the aging, the polymer greases seem to generally show lower COF values than the lithium thickened greases, specially at low entrainment speeds.

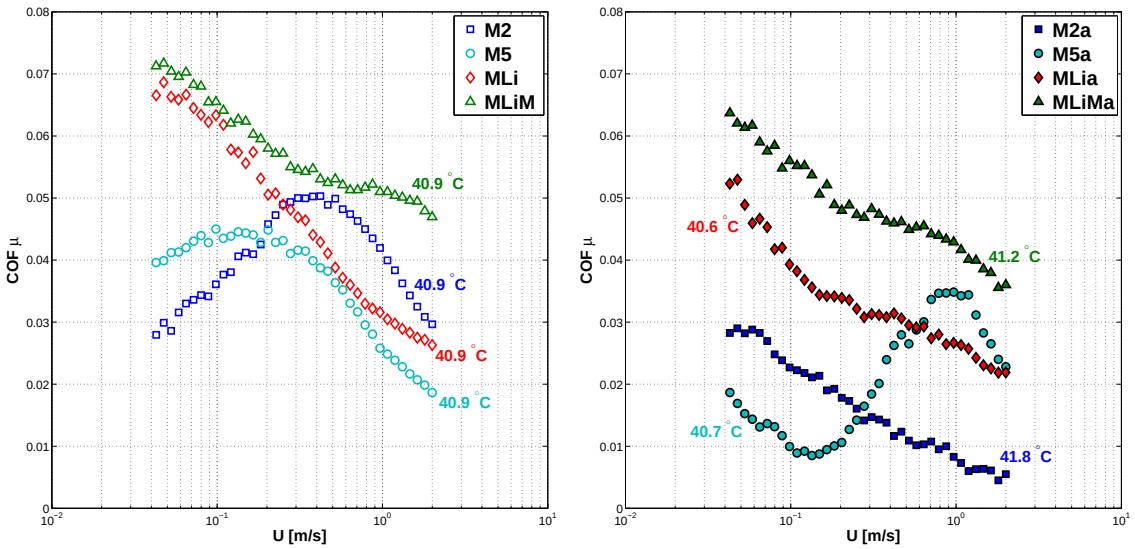

Figure 8.16: Stribeck curves of the fresh and thermally aged greases (10 days) at constant operating temperature of 40 °C and 5 % of SRR.

8.12 Rolling bearings friction torque

The friction torque of rolling bearings lubricated with fresh and aged greases was measured according to the procedure described in Chapter 7. The grease samples aged for 5 days were tested in thrust ball bearings (TBB) and those samples aged for 10 days were tested in thrust roller bearings (TRB). Grease MLiM was only tested in TRB.

The analysis procedure was the same reported in Chapter 7, whenever justifiable. The specific film thickness and the viscosity ratio are calculated to identify the lubrication regime and then the SKF friction torque model is approximated to the experimental results in order to obtain the sliding coefficient of friction, describing the evolution of the COF as the operating conditions change.

8.12.1 Thrust ball bearings

The specific film thickness of each fresh and aged grease (5 days) is shown in Figure 8.17, at 80 and 110 °C. After the aging procedure, the base oil properties should not be representative of the active lubricant any more. Therefore, the properties of the oil released by the aged greases - bleed-oil - were used instead. In the case of the fresh greases, the base oil properties were used, as before. It is important to notice that the nature of the bleed-oil was considered unchanged, i. e., it was assumed that the aging procedure did not change the nature of the lubricant. However, given the formation of several oxidation products (see Figure 8.5), this assumption might be misleading.

According to Figure 8.17, the film thickness increased following the increase of the bleed-oil's viscosity. The increase was specially important for the aged polymer greases, given the severe degradation they showed. The lubrication regime clearly changed and the aged greases M2a and M5a should now be running mainly under mixed film lubrication, even at 110 °C. The bleed-oil's viscosity of grease MLia did not increase considerably and therefore, only a slight increase in the film thickness is to be expected.

Figure 8.18 shows the TBB's friction torque, measured at 80 and 110 °C with fresh and aged greases. The friction torque generate by the fresh grease MLi and aged sample MLia is very similar, demonstrating once again that 5 days of aging time were not sufficient to considerable degrade this grease and change its behaviour. In the case of the polymer greases M2a and M5a, the differences are much more evident. When compared to the fresh greases, the aged samples M2a and M5a generate higher friction torque under high entrainment speeds and smaller friction torque under low entrainment speeds. However, considering the specific film thickness results shown in Figure 8.17, the friction mechanisms responsible for these differences should have changed.

To better understand the observed differences, the SKF model was applied and optimized to match the experimental results. The optimized coefficients of friction

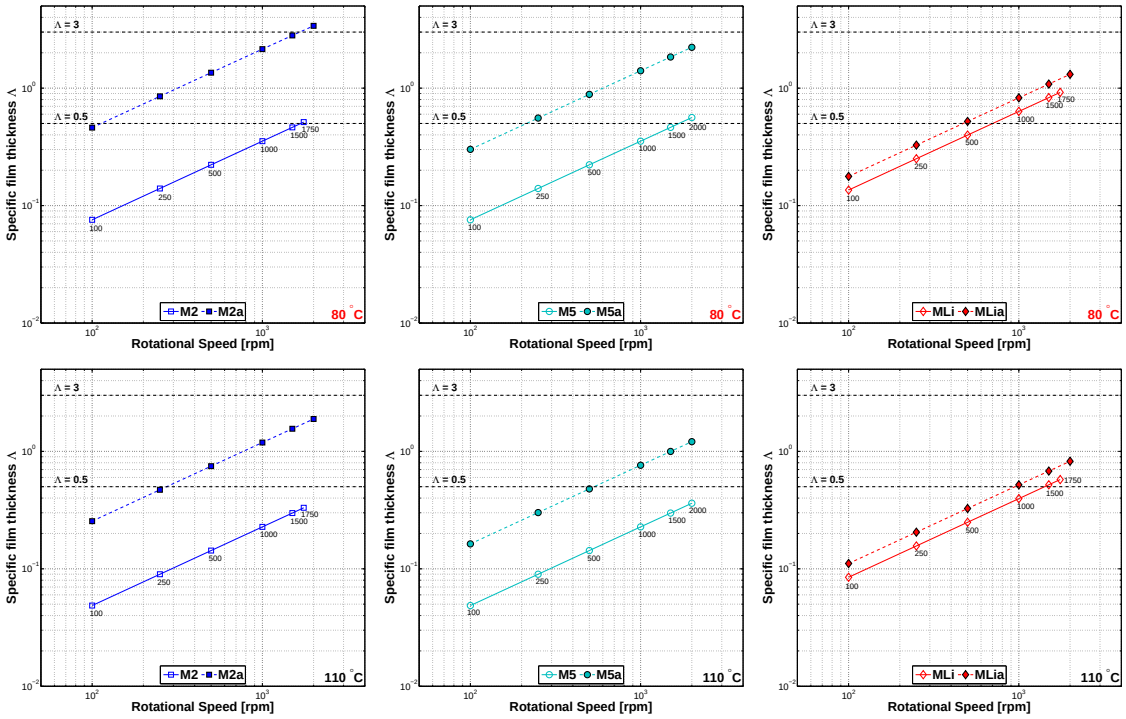

Figure 8.17: Calculated specific film thickness of TBB lubricated with fresh and aged (5 days) greases at 80 and 110 °C.

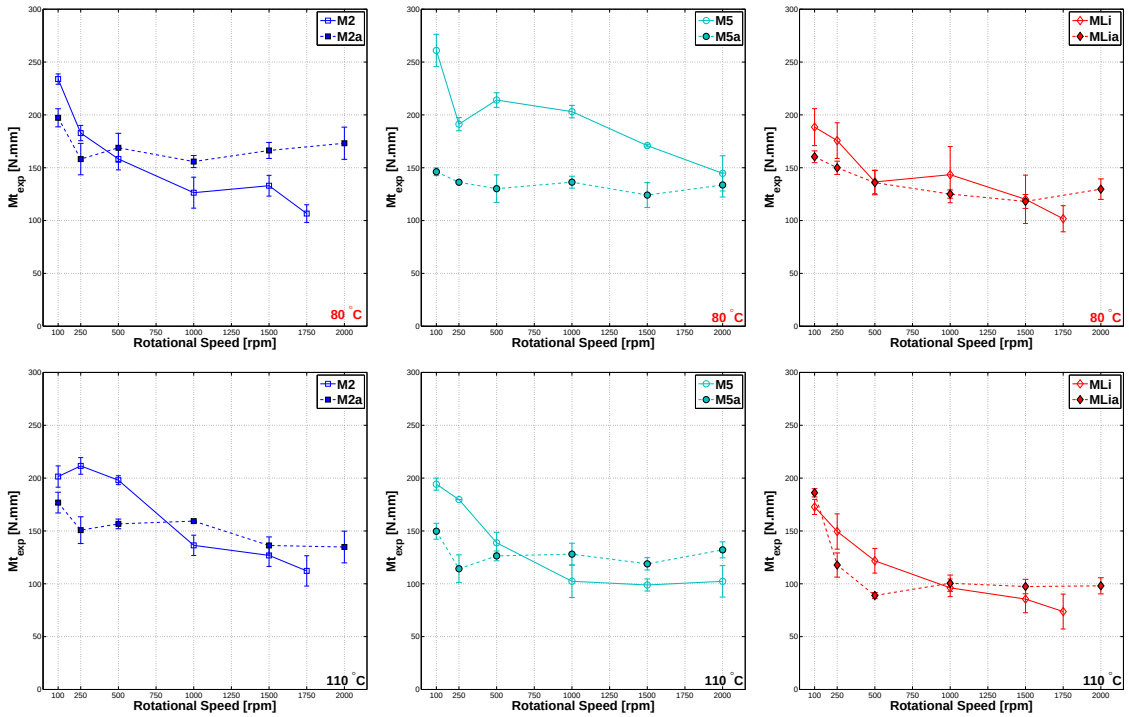

Figure 8.18: TBB's friction torque, lubricated with fresh and aged (5 days) greases, measured at 80 and 110 °C and constant load of ≈ 7 kN..

μ_{bl} and μ_{ehd} and the average error of the approximation are shown in Table 8.6. The average error is generally higher than 10 %. Given the high standard deviation of the experimental measurements and since the rolling bearings are lubricated with aged grease operating at high temperatures, the error was considered acceptable.

From the values of Table 8.6, the sliding coefficient of friction was calculated. The results are shown in Figure 8.19 plotted versus the Hersey modified parameter. The experimental sliding coefficient of friction is also shown graphically representing the average error shown in Table 8.6. According to Figure 8.19, the differences between the fresh and aged results are evident. The change in the lubrication regime

Table 8.6: Optimized coefficients of friction μ_{bl} and μ_{ehd}.

	μ_{bl}	μ_{ehd} 80 °C	Error [%]	μ_{ehd} 110 °C	Error [%]
M2	0.075	0.013	10.6	0.001	13.2
M2a	0.103	0.023	11.6	0.019	18.2
M5	0.071	0.038	12.4	0.001	24.5
M5a	0.059	0.015	12.6	0.018	7.5
MLi	0.071	0.017	6.7	0.001	16.1
MLia	0.055	0.019	9.4	0.008	16.6

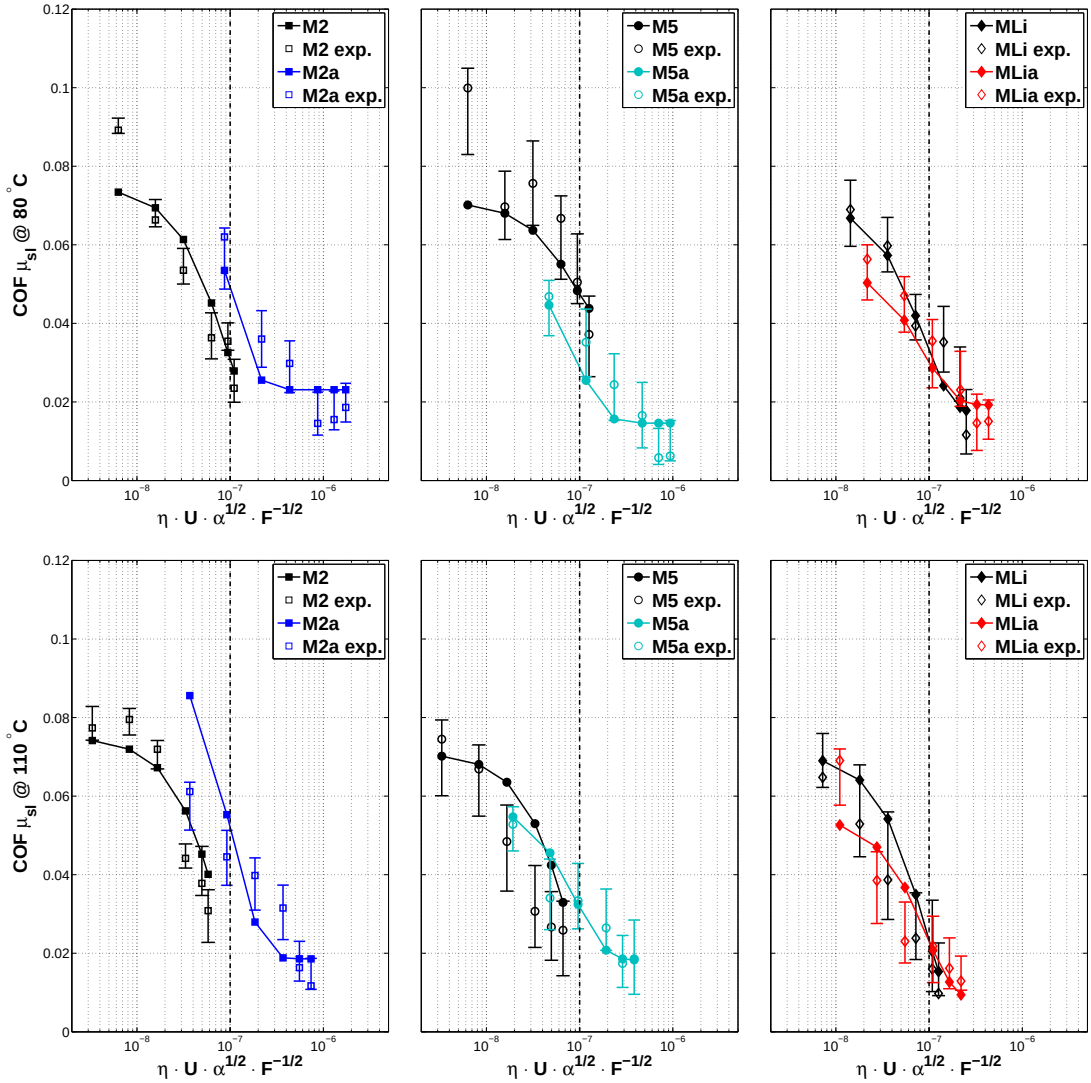

Figure 8.19: Optimized sliding coefficient of friction of fresh and aged (5 days) greases at 80 and 110 °C, plotted against the Hersey modified parameter S_P.
The vertical dashed line is referred to the S_P value at which the $\Lambda \approx 0.5$.

for the aged polymer greases is well represented in the COF, following the increase in the bleed-oil's viscosity.

It is now possible to calculate the rolling and sliding friction torques, the results are shown in Figure 8.20. These results show that the rolling friction torque is now the main source of friction for the aged polymer greases, opposite to what happened for the fresh greases. Furthermore, the sliding friction torque is now almost constant above 500 rpm. Since the viscosity of the bleed-oil increased, the film thickness should also have increased and therefore, the rolling friction torque overlaps the sliding friction torque. In the case of grease MLi, once again, no relevant changes were appreciated.

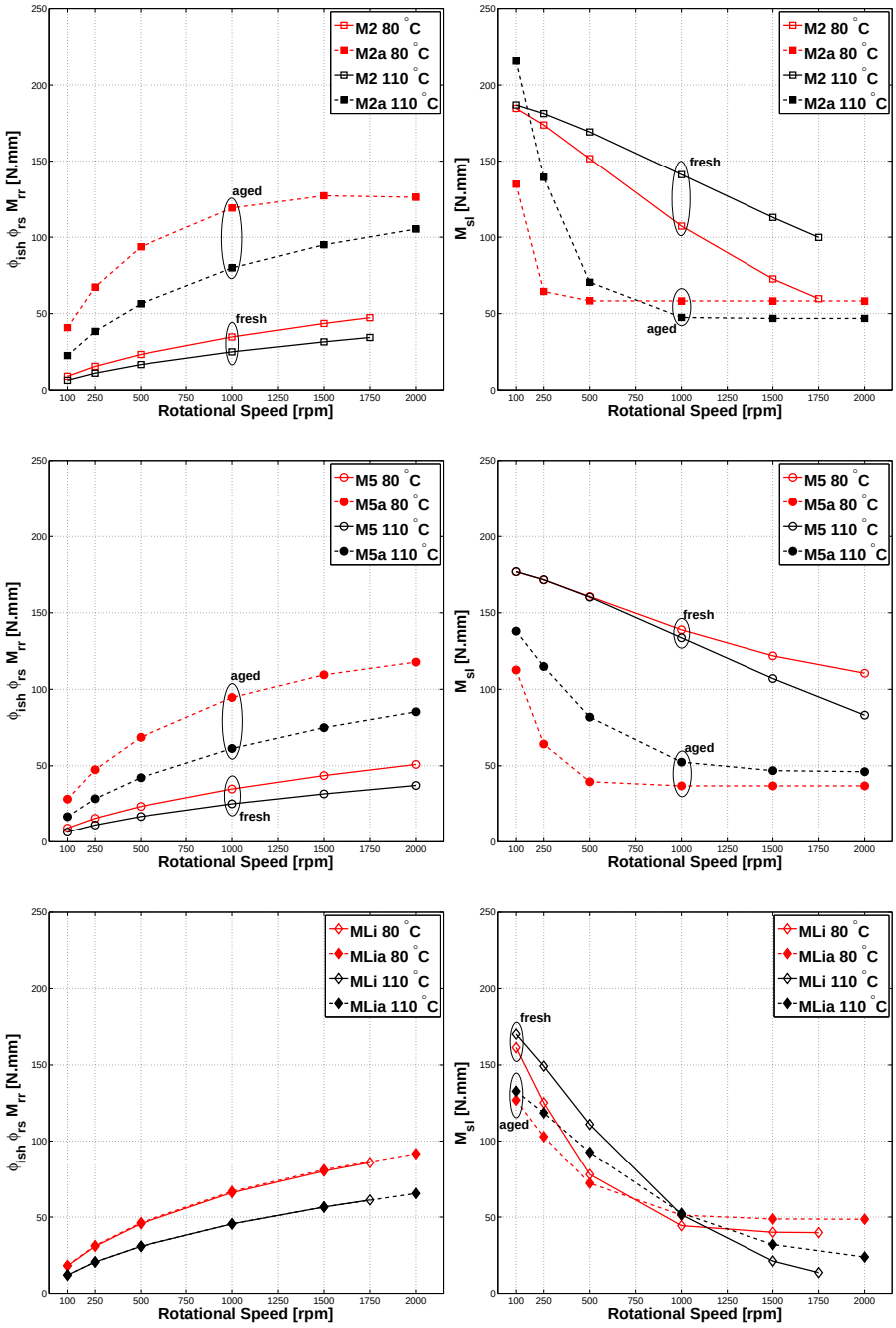

Figure 8.20: Rolling and sliding friction torques, calculated for fresh and aged greases at 80 and 110 °C.

8.12.2 Thrust roller bearings

The experimentally measured friction torque of the TRB lubricated with the grease samples aged for 10 days is shown in Figure 8.21 compared to the friction torque of the fresh greases (already discussed in Chapter 7). The measurement procedure was the same reported in the previous chapter, where the friction torque was to be measured at 50, 60 and 80 °C, with the entrainment speed increasing stepwise from 100 to 1250 rpm.

The first thing it should be noticed is that the aged greases' friction torque could not be tested at operating temperatures lower than 60 °C even if the operating speed was low, opposite to what happened with the fresh greases. This means that these aged greases generate higher friction and consequently, increased heat generation. Furthermore, even at 60 and 80 °C, the number of operating speeds that could be

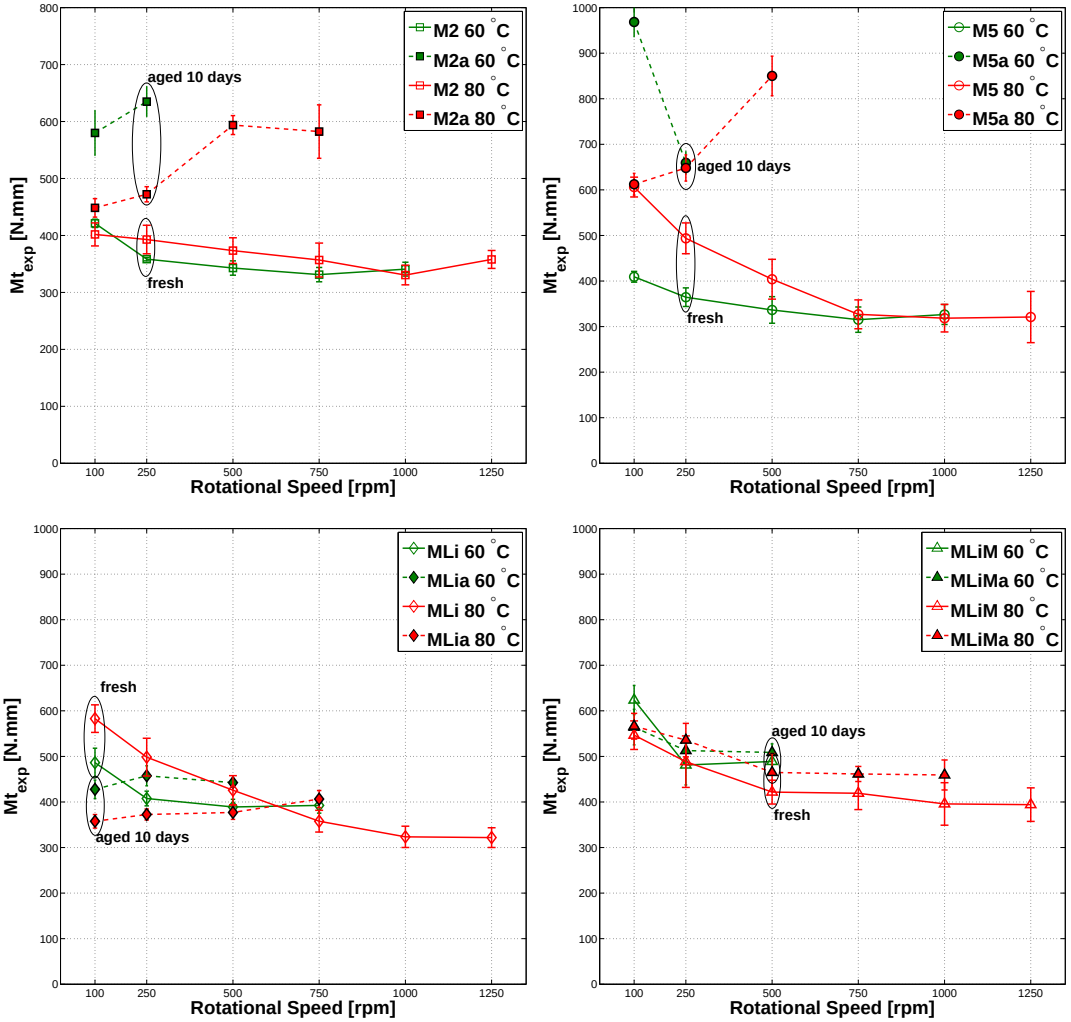

Figure 8.21: Friction torque of the TRB lubricated with fresh and thermally aged (10 days) greases, measured at 60 and 80 °C and constant load of ≈ 7 kN.

tested at constant temperature is much lower than those tested for the fresh greases, as it can be seen in Figure 8.21. This phenomenon was observed for all aged greases, independently of the formulation. However, it was much more relevant for the severely aged polymer greases.

Secondly, the friction torque behaviour of the aged polymer greases is very irregular and much higher than the friction torque generated by the fresh greases. Moreover, it seems to increase with increasing rotational speed, contrary to the behaviour observed for the fresh greases. Once again, the friction torque generated by the TRB's lubricated with the Lithium thickened greases before and after the thermal aging was not greatly affected. They do generate higher friction and more heat, but the differences on the friction torque are much less relevant.

In the case of the greases aged for 10 days, the bleed-oil could not be obtained for some of the samples. Since the properties of the bleed-oils were not available and the properties of the fresh base oils are not representative of the aged greases, it would not make sense to apply the SKF model to the friction torque results, given that the properties of the active lubricant are unknown.

8.13 Closure

The thermal aging of lubricating greases is extremely complex. Not only because the greases are viscoelastic and therefore have very different behaviours depending on the operating conditions, but also because greases are in fact a stable and homogeneous mixture of two very different materials: thickener and oil. These materials have different functions and show different properties and hence, are also affected by the thermal aging very differently. Furthermore, there is a vast amount of different thickener types and different base oil natures (and also viscosity grades) which makes it very hard to define a procedure capable of delivering a representative and fair artificial aging procedure for all grease formulations.

However, if the objective is not to compare different formulations but only understand the mechanisms behind thermal aging, then the artificial aging procedure described in this work should be very straight forward and representative.

Differently formulated greases were thermally aged in the oven for 5 and 10 days at 120 °C. Most of the changes observed concern chemical changes and oil loss, and the consequent effects on the rheological properties. Depending on the grease formulation (mainly thickener type), the viscoelastic properties might increase - hardening - or decrease - softening. The PP thickened greases got softer, while the LiX thickened greases hardened. Exactly how these changes reflect in the film forming or friction

generating behaviour it could not be investigated. However, both changes might be inconvenient. While a hardened grease shows reduced mobility and therefore, less ability to flow and feed the contact, a very soft grease will easily flow increasing the churning and friction in one hand and more easily fleeing the contact in the other. It will mainly depend on the rolling bearing type, geometry and of course, operating conditions.

As a general rule, the thermal aging is responsible for oil loss, base oil oxidation and/or thickener degradation, polymerization and consequent increase in the bleed-oil viscosity. As a result of the oil loss and a bleed-oil of higher viscosity, the oil release rate also decreases and severe starvation should now be more likely since there is less oil available and it is harder for the grease and/or the thicker bleed-oil to return to the contact. The polymer greases were the most affected by all these mechanisms.

Regarding the tribological testing, the fact that the bleed-oil viscosity increased leads, in fully flooded conditions, to increased film thickness in ball-on-disc tests and a clear change in the lubrication regime. As a consequence, the viscous friction should be much higher and the coefficient of friction is also increased, even if the lubricating film is thicker.

In the case of the rolling bearings tests, the conclusions are similar. If the grease properties were severely affected by the thermal aging (as it was the case for the polymer greases), then so was the friction torque. Otherwise, the changes are subtle. It was verified that the aged greases, independently of their formulation, generated higher friction and therefore more heat than the fresh samples for both types of rolling bearings tested. The main source of friction is also expected to have changed following the increase of the active lubricant viscosity and hence, the viscous friction. As a consequence, the coefficient of friction might considerable change. From the optimization of the SKF's friction torque model to some of the experimental results and supposing that the greases are still able to release and replenish oil to the contact, the bleed-oil seems to be representative of the active lubricant and the use of its properties to predict the lubrication regime and the friction torque is satisfactory.

9 Conclusions and Future Work

9.1 Conclusions

Chapter 3 reports the main methods used to characterize the properties of differently formulated lubricating greases.

It was shown that the chemistry of the polypropylene and the lithium complex thickeners is quite different, as well as the nature of the mineral and poly-alpha-olefin base oils. It was also found that the bleed-oil does not show any of the thickener's characteristic peaks or at least its content is so low that it could not be evaluated through FTIR. The micro-structure of the different tested thickeners was evaluated by SEM and AFM, and found to be quite different.

The dynamic viscosity of base oils and bleed-oils was measured, showing that generally their properties are very much alike, as the FTIR had also shown. However, a few exceptions were found, for certain grease formulations.

The rheological properties of the greases were also evaluated showing that it is difficult to clearly identify different formulations based only on rheological data. However, a relationship between different thickener content and certain rheological parameters was found. It is still unknown how these properties might correlat to grease performance in tribological testing.

In **Chapter 4**, the results of film thickness measurements performed in a ball-on-disc device are reported. The tests were performed under different operating conditions in order to better evaluate the different grease lubrication mechanisms in the early stages of grease life, where fully flooded conditions are observed.

It was found that under low entrainment speeds the thickener contributes to the film formation. Depending on the thickener properties, the film thickness in this region can be considerable different. It was observed that the PP greases generate a much thicker film than the LiX greases. A relationship between film thickness and PP content for this region was also found.

Above a certain transition speed, the film thickness increases at the typical rate of $U^{0.67}$. This behaviour was found for all greases independently of their formulation. This transition speed was found to increase with the thickener content for the polymer

greases tested. In this region at higher speeds, the greases' film thickness shows a very similar behaviour to its base oil and bleed-oil. However, the greases show film thickness values in fully flooded conditions which higher than the corresponding oils. Nevertheless, the higher the base oil viscosity, the higher is the film thickness of the grease.

Chapter 5 reports the traction and Stribeck curves measured in a ball-on-disc device using steel discs of different surface finishing. Once again, fully flooded conditions were imposed for both tests.

It was found that the traction coefficient is highly influenced by the base oil nature and viscosity, specially under operating conditions which promote high specific film thickness values. No thickener content dependence was found for these tests.

The Stribeck curves were measured with a rough disc in order to obtain low specific film thickness values and boundary film lubrication. In these conditions, the thickener contribution to the coefficient of friction was addressed. It was found that the COF of grease and base oil show similar behaviours under mixed film lubrication but, as the speed is reduced and the lubrication regime approaches boundary film, the COF of the grease becomes much lower than the values found for the base oil. This difference was attributed to thickener material entering the contact, increasing the lubricant film, and consequently decreasing the coefficient of friction. This phenomenon was observed for all greases independently of thickener type and/or base oil nature.

However, in the case of the polymer thickened greases, the COF not only is smaller than the COF of the corresponding base oil, but it actually decreases along with entrainment speed. The maximum value of COF is very similar between different operating temperatures, although the speed at which it occurs - transition speed - actually increases with temperature. Furthermore, it was found that the maximum value of COF increases as the thickener content decreases, while on the other hand, the transition speed decreases. These results are in agreement with the results found for the film thickness measurements.

The COF of the lithium greases is higher than the COF of polymer greases when compared for the same value of the modified Hersey parameter. This result shows that, under the same lubrication regime, the lithium greases produce higher friction than the polymer greases.

The tests reported in **Chapter 6** were performed to study the grease behaviour under starvation. Once again, the tests were performed in a ball-on-disc device.

Initially, the amount of grease available is very big and therefore, the results are

similar or even higher than those found for fully flooded conditions. With increasing speed or test duration, the film thickness drops quickly, as starvation is reached. After a while, the lubricant film tends to stabilize. In this situation the lubricant supply is reduced and the measured films are very thin. These films should be formed by a very small amount of oil which is slowly released by grease in the vicinity of the contact.

These thin films are constantly, but briefly, increased by thickener lumps crossing the contact ever so often. This was observed for all the tested greases. However, this phenomenon is more frequent for the polymer greases and the film thickness increments are also bigger. In starved conditions the polymer greases tend to show thicker films and smaller friction than the lithium greases.

Chapter 7 showed that a simple rolling bearings friction torque test is an interesting procedure to evaluate and differentiate different lubricants.

The friction torque measuring system is sensible to different grease formulations and, coupled with the SKF's rolling bearing friction torque model, it allows to calculate the coefficient of friction under different operating conditions, as function of the rolling bearing's rotational speed.

When compared to the coefficient of friction results obtained in single ball-on-disc tests, a parallelism can be made, although its absolute value cannot be compared. Nevertheless, it was found that the lithium thickened greases generally produced higher friction than the polymer greases tested, and a friction torque dependence on the polypropylene content of the polymer greases was also found.

In Chapter 8 the thermal aging of lubricating greases operating in rolling bearings was approached. Fresh grease samples were artificially aged and then characterized by comparison with the fresh greases' properties.

The aged grease samples showed significant changes in their physico-chemical properties: severe oxidation, significant oil loss, slower bleed rate and increased bleed-oil viscosity. The rheological parameters also changed considerably, the polymer thickened greases became softer while the lithium thickened greases became stiffer. These changes might contribute to restrict the oil supply to the contact, reducing the hydrodynamic film thickness and consequently, increasing the severity of the contact. However, this could not be investigated directly.

The tribological tests performed in the ball-on-disc machine showed that the film thickness in fully flooded conditions increased for all the aged grease samples. The increase was specially high for the polymer thickened greases, the most affected by the thermal aging. The friction behaviour also changed considerably for these

greases.

It is difficult to understand if the grease lubrication mechanisms changed. However, given the increase of the film thickness, coupled with considerable changes to the rheological properties, it is possible that the contact is now mainly lubricated by an enhanced viscous film of degraded thickener and oxidized bleed-oil.

How these changes affect the replenishment when the contact is starved was not investigated. Nevertheless, the tests performed in rolling bearings lubricated with aged grease samples showed that the friction torque is also affected, generally increasing as consequence of the increased viscous friction. Moreover, the main friction generation mechanism also changed and a higher heat generation was observed, although the calculated sliding coefficient of friction was found to be smaller for the same operating conditions.

9.2 Future Work

According to the conclusions drawn from this work, it would be interesting to further develop studies on:

A. Film thickness measurements and predictions in point contacts:

A.1 - Accurately determine the thickener dimensions, through SEM and AFM techniques;

A.2 - Develop analytical expressions to estimate grease film thickness, considering the thickener properties and base oil film thickness, under fully flooded and starved contacts;

B. COF prediction in point contacts:

B.1 - Develop a model for COF prediction, considering grease film thickness and its properties, under fully flooded and starved contacts;

C. Grease aging:

C.1 - Couple the thermal and mechanical aging of grease and study its influence on the grease bleeding phase;

D. Film thickness and COF measurements/prediction in line contacts.

Bibliography

[1] P. M. Cann and A. A. Lubrecht, "An analysis of the mechanisms of grease lubrication in rolling element bearings," *Lubrication Science*, vol. 11, no. 3, pp. 227–245, 1999.

[2] P. M. Lugt, *Grease Lubrication in Rolling Bearings*. WILEY, 2013.

[3] P. M. Lugt, "Modern Advancements in Lubricating Grease Technology," *Tribology International*, vol. 97, pp. 467–477, 2016.

[4] Z. Yang and X. Qian, "A solution to grease lubricated EHD Film thickness in an Elliptical rolling contact," *ImechE Conference Publication*, 1987.

[5] D. Dong and X. Qian, "A theory of elastohydrodynamic grease-lubricated line contact based on a refined rheological model," *Tribology International*, vol. 21, pp. 261–267, oct 1988.

[6] P. M. Cann, B. P. Williamson, R. C. Coy, and H. A. Spikes, "The behaviour of greases in elastohydrodynamic contacts," *Journal of Physics D: Applied Physics*, vol. 25, pp. A124–A132, jan 1992.

[7] S. Catalogue, "6000 EN," *SKF, November*, 2005.

[8] I. N. A. FAG, "Bearinx - online Easy Friction," tech. rep., Shaeffler Group, 2011.

[9] D. Dowson, *History of Tribology, 2nd Edition - TRIBOLOGY*. 1979.

[10] B. Bhushan, *Introduction to Tribology*. John Wiley & Sons, 2002.

[11] W. Madius, C.; Smets, *Grease Fundamentals*. Axel Christiernsson.

[12] W. Parish, "Lubricants," *Encyclopedia Britannica*, no. 14th ed., p. p. 453., 1929.

[13] W. J. Bartz, "History of Tribology - The bridge between the classical antiquity and the 21st Century," 2001.

[14] I. M. Hutchings, "Leonardo da Vinci's studies of friction," *Wear*, vol. 360-361, pp. 51–66, 2016.

[15] N. Partridge, "British Patent," 1835.

[16] J. Lewkowitsch, *Chemical technology and analysis of oils, fats, and waxes*. 1904.

[17] W. Little, "British patent 12571," 1849.

[18] H. Hertz, "Ueber die Berührung fester elastischer Körper," *Journal für die reine und angewandte Mathematik*, vol. 92, pp. 156–171, 1896.

[19] O. Reynolds, "On the Theory of Lubrication and Its Application to Mr. Beauchamp Tower's Experiments, Including an Experimental Determination of the Viscosity of Olive Oil.," *Proc. R. Soc. Lond.*, vol. 177, no. 40, pp. 191–203, 1886.

[20] R. Stribeck and M. Schröter, *Die wesentlichen Eigenschaften der Gleit-und Rollenlager: Untersuchung einer Tandem-Verbundmaschine von 1000 PS*. Springer, 1903.

[21] R. Holm, "The friction force over the real area of contact," *Wiss. Veroff. Siemens-Werk*, 1938.

[22] F. P. Bowden and D. Tabor, "Friction, lubrication and wear: a survey of work during the last decade," *British Journal of Applied Physics*, vol. 17, pp. 1521–1544, dec 1966.

[23] D. Meijer and H. Lankamp, "Polymer thickened lubricating grease," mar 1996.

[24] D. Meijer and H. Lankamp, "Polymer thickened lubricating grease," feb 1999.

[25] "ASTM-D288 — Definition of Terms Relating To Petroleum," 1961.

[26] "A new ELGI (European Lubricating Grease Institute) Publication: The Rheology of Lubricating Grease," *Industrial Lubrication and Tribology*, vol. 52, no. 4, p. null, 2000.

[27] P. M. Lugt, "A Review on Grease Lubrication in Rolling Bearings," *Tribology Transactions*, vol. 52, pp. 470–480, jun 2009.

[28] S. Y. Poon, "An Experimental Study of Grease in Elastohydrodynamic Lubrication," *Journal of Lubrication Technology*, vol. 94, p. 27, jan 1972.

[29] A. R. Wilson, "The Relative Thickness of Grease and Oil Films in Rolling Bearings," *Proceedings of the Institution of Mechanical Engineers*, vol. 193, no. 1, pp. 185–192, 1979.

[30] H. Åström, O. Isaksson, and E. Höglund, "Video recordings of an EHD point contact lubricated with grease," *Tribology International*, vol. 24, pp. 179–184, jun 1991.

[31] M. Kaneta, T. Ogata, Y. Takubo, and M. Naka, "Effects of a thickener structure on grease elastohydrodynamic lubrication films," *Proceedings of the Institution of Mechanical Engineers, Part J: Journal of Engineering Tribology*, vol. 214, pp. 327–336, jan 2000.

[32] B. P. Williamson, D. R. Kendall, and P. M. Cann, "The influence of grease composition on film thickness in EHD contacts," *NLGI spokesman*, vol. 57, no. 8, pp. 13–18.

[33] E. R. Booser and D. F. Wilcock, "Minimum oil requirements of ball bearings," *Lubrication Engineering*, 1953.

[34] P. M. Cann and H. A. Spikes, "Film thickness measurements of lubricating greases under normally starved conditions," *NLGI spokesman*, vol. 56, no. 2, pp. 21–27.

[35] S. Hurley and P. M. Cann, "IR Spectroscopic Analysis of Grease Lubricant Films in Rolling Contacts," in *Lubrication at the Frontier The Role of the Interface and Surface Layers in the Thin Film and Boundary Regime Proceedings of the 25th LeedsLyon Symposium on Tribology*, vol. Volume 36, pp. 589–600, 1999.

[36] P. M. Cann, *Understanding grease lubrication*, vol. 31 of *Tribology Series*. Elsevier, 1996.

[37] I. Couronné, P. Vergne, D. Mazuyer, N. Truong-Dinh, and D. Girodin, "Effects of Grease Composition and Structure on Film Thickness in Rolling Contact," *Tribology Transactions*, vol. 46, pp. 31–36, jan 2003.

[38] P.-O. Larsson-Kråik, "Lubricant replenishment in the vicinity of an EHD contact," 1996.

[39] T. Cousseau, M. Björling, B. Graça, A. Campos, J. H. O. Seabra, and R. Larsson, "Film thickness in a ball-on-disc contact lubricated with greases, bleed oils and base oils," *Tribology International*, vol. 53, pp. 53–60, sep 2012.

[40] T. Cousseau, B. Graça, A. Campos, and J. Seabra, "Friction and wear in thrust ball bearings lubricated with biodegradable greases," *Proceedings of the Institution of Mechanical Engineers, Part J: Journal of Engineering Tribology*, vol. 225, no. 7, pp. 627–639, 2011.

[41] M. T. van Zoelen, C. H. Venner, and P. M. Lugt, "Prediction of film thickness decay in starved elasto-hydrodynamically lubricated contacts using a thin layer flow model," *Proceedings of the Institution of Mechanical Engineers, Part J: Journal of Engineering Tribology*, vol. 223, pp. 541 –552, may 2009.

[42] *SKF General Catalogue 6000 EN*. SKF.

[43] V. Wikström and B. Jacobson, "Loss of lubricant from oil-lubricated near-starved spherical roller bearings," *Proceedings of the Institution of Mechanical Engineers, Part J: Journal of Engineering Tribology*, vol. 211, pp. 51–66, jan 1997.

[44] W. Dresel and R. P. Heckler, *Ullmann's Encyclopedia of Industrial Chemistry*. Wiley, 2000.

[45] W. H. Bauer, A. P. Finkelstein, and S. E. Wiberley, "Flow Properties of Lithium Stearate-Oil Model Greases as Functions of Soap Concentration and Temperature," *A S L E Transactions*, vol. 3, pp. 215–224, jan 1960.

[46] S. Hurley, "Fundamental studies of grease lubrication in elastohydrodynamic contacts.," 2001.

[47] T. Mang and W. Dresel, *Lubricants and Lubrication*. Wiley, 2007.

[48] M. A. Delgado, M. Sánchez, C. Valencia, J. Franco, and C. Gallegos, "Relationship Among Microstructure, Rheology and Processing of a Lithium Lubricating Grease," *Chemical Engineering Research and Design*, vol. 83, no. 9, pp. 1085–1092, 2005.

[49] B. Mitacek, "Grease," tech. rep., 1969.

[50] S. Dodson and R. Newman, "Grease composition," nov 1974.

[51] D. Meijer and R. Pasaribu, "Polymer thickened grease compositions with improved low friction properties," aug 2012.

[52] S. Bair and F. Qureshi, "The high pressure rheology of polymer-oil solutions," *Tribology International*, vol. 36, pp. 637–645, 2003.

[53] J. E. Martín-Alfonso, C. Valencia, M. C. Sánchez, J. M. Franco, and C. Gallegos, "Evaluation of different polyolefins as rheology modifier additives in lubricating grease formulations," *Materials Chemistry and Physics*, vol. 128, pp. 530–538, aug 2011.

[54] W. C. Ward Jr and F. Qureshi, "The Impact of Polymers Blended to a Target Viscosity Range Upon Base Grease Properties," *NLGI Spokesman*, 2008.

[55] J. E. Martín-Alfonso, C. Valencia, M. C. Sánchez, J. M. Franco, and C. Gallegos, "Rheological Modification of Lubricating Greases with Recycled Polymers from Different Plastics Waste," *Industrial & Engineering Chemistry Research*, vol. 48, pp. 4136–4144, apr 2009.

[56] J. E. Martín-Alfonso, C. Valencia, J. F. Arteaga, M. J. Díaz, and J. M. Franco, "Design of lubricating grease formulations using recycled polypropylene from postconsumer films as thickener agent," *Journal of Applied Polymer Science*, vol. 127, pp. 1369–1376, jan 2013.

[57] J. E. Martín-Alfonso, C. Valencia, and J. Franco, "Effect of amorphous/recycled polypropylene ratio on thermo-mechanical properties of blends for lubricant applications," *Polymer Testing*, vol. 32, pp. 516–524, may 2013.

[58] J. E. Martín-Alfonso and J. Franco, "Influence of polymer reprocessing cycles on the microstructure and rheological behavior of polypropylene/mineral oil oleogels," *Polymer Testing*, vol. 45, pp. 12–19, aug 2015.

[59] N. A. Scarlett, "Use of grease in rolling bearings," *ARCHIVE: Proceedings of the Institution of Mechanical Engineers, Conference Proceedings 1964-1970 (vols 178-184), Various titles labelled Volumes A to S*, vol. 182, pp. 585–624, sep 1967.

[60] P. Baart, B. van der Vorst, P. M. Lugt, and R. a.J. van Ostayen, "Oil-Bleeding Model for Lubricating Grease Based on Viscous Flow Through a Porous Microstructure," *Tribology Transactions*, vol. 53, no. 3, pp. 340–348, 2010.

[61] I. G. Fuks, T. V. Medvedeva, and Y. L. Ishchuk, "Application of IR spectroscopy in studying grease composition and properties (review)," *Chemistry and Technology of Fuels and Oils*, vol. 8, no. 2, pp. 152–156, 1972.

[62] P. M. Cann and H. A. Spikes, "In Lubro Studies of Lubricants in EHD Contacts Using FTIR Absorption Spectroscopy," *Tribology Transactions*, vol. 34, pp. 248–256, mar 1991.

[63] K. Takahashi, Y. Shitara, and S. Mori, "Direct Observation of Thermo-Reversible Gel-Lubricants in EHL by FT-IR Micro-Spectroscopy," *Tribology Online*, vol. 3, no. 2, pp. 131–136, 2008.

[64] F. Higgins, "On-Site Additive Depletion Monitoring in Turbine Oils by FT-IR Spectroscopy," tech. rep., Polytec, Germany.

[65] J. P. Coates and L. C. Setti, "Infrared Spectroscopic Methods for the Study of Lubricant Oxidation Products," *A S L E Transactions*, vol. 29, no. 3, pp. 394–401, 1986.

[66] N. Robinson, "Monitoring oil degradation with infrared spectroscopy," *Wearcheck Tech. Bull*, pp. 1–8, 1998.

[67] S. Hurley, P. M. Cann, and H. A. Spikes, "Lubrication and Reflow Properties of Thermally Aged Greases," *Tribology Transactions*, vol. 43, no. 2, pp. 221–228, 2000.

[68] P. M. Cann, J. P. Doner, M. N. Webster, and V. Wikström, "Grease Degradation in Rolling Element Bearings," *Tribology Transactions*, vol. 44, no. 3, pp. 399–404, 2001.

[69] M. S. Stark, J. J. Wilkinson, P. M. Lee, J. R. L. Smith, M. Priest, R. I. Taylor, and S. Chung, "The degradation of lubricants in gasoline engines: Lubricant flow and degradation in the piston assembly," 2005.

[70] P. M. Cann, M. N. Webster, J. P. Doner, V. Wikström, and P. M. Lugt, "Grease Degradation in R0F Bearing Tests," *Tribology Transactions*, vol. 50, no. 2, pp. 187–197, 2007.

[71] T. Cousseau, B. Graça, A. Campos, and J. H. O. Seabra, "Grease Aging Effects on Film Formation under Fully-Flooded and Starved Lubrication," *Lubricants*, vol. 3, pp. 197–221, apr 2015.

[72] S. Hurley, P. M. Cann, and H. A. Spikes, "Thermal Degradation of Greases and the Effect on Lubrication Performance," *Proceedings of the 24th Leeds-Lyon Symposium on Tribology*, vol. 34, pp. 75–83, 1998.

[73] P. Katyal and P. Kumar, "Central film thickness formula for shear thinning lubricants in EHL point contacts under pure rolling," *Tribology International*, vol. 48, pp. 113–121, apr 2012.

[74] P. M. Lugt and G. E. Morales-Espejel, "A Review of Elasto-Hydrodynamic Lubrication Theory," *Tribology Transactions*, vol. 54, no. 3, pp. 470–496, 2011.

[75] C. Barus, "Isothermals, isopiestics and isometrics relative to viscosity," *American Journal of Science*, 1893.

[76] B. J. Hamrock, S. R. Schmid, and B. O. Jacobson, *Fundamentals of fluid film lubrication*. McGraw-Hill series in mechanical engineering, McGraw-Hill Higher Education, 1994.

[77] P. W. Gold, A. Schmidt, H. Dicke, J. Loos, and C. Assmann, "Viscosity–pressure–temperature behaviour of mineral and synthetic oils," *Journal of Synthetic Lubrication*, vol. 18, pp. 51–79, apr 2001.

[78] D. Dowson and G. R. Higginson, *Elasto-hydrodynamic lubrication: the fundamentals of roller and gear lubrication*. The Commonwealth and international library, Pergamon Press, 1966.

[79] H. A. Barnes, "A review of the slip (wall depletion) of polymer solutions, emulsions and particle suspensions in viscometers: its cause, character, and cure," 1996.

[80] H. A. Barnes, "Thixotropy—a review," *Journal of Non-Newtonian Fluid Mechanics*, vol. 70, no. 1-2, pp. 1–33, 1997.

[81] H. J. Walls, S. B. Caines, A. M. Sanchez, and S. A. Khan, "Yield stress and wall slip phenomena in colloidal silica gels," *Journal of Rheology*, vol. 47, p. 847, jun 2003.

[82] G. a. Davies and J. R. Stokes, "Thin film and high shear rheology of multiphase complex fluids," *Journal of Non-Newtonian Fluid Mechanics*, vol. 148, no. 1-3, pp. 73–87, 2008.

[83] G. Chang, J. Koo, and K. Song, "Wall slip of vaseline in steady shear rheometry," *Korea-Australia Rheology*, vol. 15, no. 2, pp. 55–61, 2003.

[84] H. A. Barnes, "A handbook of elementary rheology, Institute of Non-Newtonian Fluid Mechanics," *University of Wales*, 2000.

[85] S. K. Yeong, P. F. Luckham, and T. F. Tadros, "Steady flow and viscoelastic properties of lubricating grease containing various thickener concentrations," *Journal of Colloid and Interface Science*, vol. 274, no. 1, pp. 285–293, 2004.

[86] I. Couronné, G. Blettner, and P. Vergne, "Rheological Behavior of Greases: Part I—Effects of Composition and Structure," *Tribology Transactions*, vol. 43, pp. 619–626, jan 2000.

[87] H. A. Barnes, J. F. Hutton, and K. Walters, *An Introduction to Rheology*. 1989.

[88] H. A. Barnes, "The yield stress - a review or 'panta roi' - everything flows?," *Journal of Non-Newtonian Fluid Mechanics*, vol. 81, no. 1-2, pp. 133–178, 1999.

[89] I. Couronné, P. Vergne, L. Ponsonnet, N. Truong-Dinh, and D. Girodin, "Influence of grease composition on its structure and its rheological behaviour," *Tribology Series*, vol. 38, pp. 425–432, 2000.

[90] J. M. Franco, M. A. Delgado, C. Valencia, M. C. Sánchez, and C. Gallegos, "Mixing rheometry for studying the manufacture of lubricating greases," *Chemical Engineering Science*, vol. 60, no. 8-9 SPEC. ISS., pp. 2409–2418, 2005.

[91] J. Palacios and M. Palacios, "Rheological properties of greases in ehd contacts," *Tribology International*, vol. 17, pp. 167–171, jun 1984.

[92] P. M. Cann, "Starved Grease Lubrication of Rolling Contacts," *Tribology Transactions*, vol. 42, no. 4, pp. 867–873, 1999.

[93] J. M. Madiedo, J. M. Franco, C. Valencia, and C. Gallegos, "Modeling of the Non-Linear Rheological Behavior of a Lubricating Grease at Low-Shear Rates," *Journal of Tribology*, vol. 122, no. 3, p. 590, 2000.

[94] M. M. Cross, "Rheology of non-Newtonian fluids: A new flow equation for pseudoplastic systems," *Journal of Colloid Science*, vol. 20, pp. 417–437, jun 1965.

[95] P. J. Carreau, D. D. Kee, and R. P. Chhabra, *Rheology of Polymeric Systems: Principles and Applications*. 1997.

[96] P. O. Larsson, R. Larsson, A. Jolkin, and O. Marklund, "Pressure fluctuations as grease soaps pass through an EHL contact," *Tribology International*, vol. 33, pp. 211–216, apr 2000.

[97] J. J. Kauzlarich and J. A. Greenwood, "Elastohydrodynamic Lubrication With Herschel-Bulkley Model Greases," *A S L E Transactions*, vol. 15, no. 4, pp. 269–277, 1972.

[98] I. Couronné, P. Vergne, D. Mazuyer, N. Truong-Dinh, and D. Girodin, "Nature and Properties of the Lubricating Phase in Grease Lubricated Contact," *Tribology Transactions*, vol. 46, pp. 37–43, jan 2003.

[99] T. Cousseau, "Film thickness and friction in grease lubricated contacts. Application to rolling bearing torque loss," *Departamento De Engenharia Mecanica E Gestao Industrial*, vol. PhD, 2013.

[100] H. Cen, P. M. Lugt, and G. E. Morales-Espejel, "Film Thickness of Mechanically Worked Lubricating Grease at Very Low Speeds," *Tribology Transactions*, vol. 2004, no. May 2015, pp. 00–00, 2014.

[101] H. Cen, P. M. Lugt, and G. E. Morales-Espejel, "On the film thickness of grease lubricated contacts at low speeds," *Tribology Transactions*, vol. 2004, no. May 2015, pp. 00–00, 2014.

[102] H. S. Cheng, "A Numerical Solution of the Elastohydrodynamic Film Thickness in an Elliptical Contact," *Journal of Lubrication Technology*, vol. 92, no. 1, p. 155, 1970.

[103] L. D. Wedeven, D. Evans, and A. Cameron, "Optical Analysis of Ball Bearing Starvation," *Journal of Lubrication Technology*, vol. 93, p. 349, jul 1971.

[104] B. J. Hamrock and D. Dowson, "Isothermal Elastohydrodynamic Lubrication of Point Contacts: Part III—Fully Flooded Results," *Journal of Lubrication Technology*, vol. 99, no. 2, p. 264, 1977.

[105] R. J. Chittenden, D. Dowson, J. F. Dunn, and C. M. Taylor, "A Theoretical Analysis of the Isothermal Elastohydrodynamic Lubrication of Concentrated Contacts. II. General Case, with Lubricant Entrainment along Either Principal Axis of the Hertzian Contact Ellipse or at Some Intermediate Angle," *Proceedings of the Royal Society A: Mathematical, Physical and Engineering Sciences*, vol. 397, no. 1813, pp. 271–294, 1985.

[106] C. H. Venner and W. Napel, "Multilevel solution of the elastohydrodynamically lubricated circular contact problem part 2: Smooth surface results," *Wear*, vol. 152, pp. 369–381, jan 1992.

[107] S. Bair and P. Kottke, "Pressure-Viscosity Relationships for Elastohydrodynamics," *Tribology Transactions*, vol. 46, no. June 2015, pp. 289–295, 2003.

[108] D. Dowson and G. R. Higginson, *Elasto-Hydrodynamic Lubrication: International Series on Materials Science and Technology*. Elsevier, 2014.

[109] P. K. Gupta, H. S. Cheng, D. Zhu, N. H. Forster, and J. B. Schrand, "Viscoelastic Effects in MIL-L-7808-Type Lubricant, Part I: Analytical Formulation," *Tribology Transactions*, vol. 35, pp. 269–274, mar 1992.

[110] B. J. Hamrock and D. Dowson, *Ball bearing lubrication*. John Wiley & Sons, jan 1981.

[111] L. Bordenet, G. Dalmaz, J.-P. Chaomleffel, and F. Vergne, "A study of grease film thicknesses in elastorheodynamic rolling point contacts," *Lubrication Science*, vol. 2, pp. 273–284, jul 1990.

[112] P. M. Cann, "Starvation and reflow in a grease-lubricated elastohydrodynamic contact," *Tribology transactions*, vol. 39, no. 3, pp. 698–704.

[113] S. Hurley and P. M. Cann, "Grease composition and film thickness in rolling contacts," *NLGI spokesman*, 1999.

[114] Y. Kimura, T. Endo, and D. Dong, "EHL with Grease at Low Speeds," *Advanced Tribology*, 2010.

[115] G. E. Morales-Espejel, P. M. Lugt, H. R. Pasaribu, and H. Cen, "Film thickness in grease lubricated slow rotating rolling bearings," *Tribology International*, vol. 74, pp. 7–19, 2014.

[116] T. E. Tallian, "On Competing Failure Modes in Rolling Contact," *A S L E Transactions*, vol. 10, no. 4, pp. 418–439, 1967.

[117] H. A. Spikes, "Mixed lubrication—an overview," *Lubrication Science*, vol. 00, no. May, pp. 221–253, 1997.

[118] P. M. Cann, H. A. Spikes, and J. Hutchinson, "The Development of a Spacer Layer Imaging Method (SLIM) for Mapping Elastohydrodynamic Contacts," *Tribology Transactions*, vol. 39, pp. 915–921, jan 1996.

[119] H. van Leeuwen and H. van Leeuwen, "The determination of the pressure-viscosity coefficient of a lubricant through an accurate film thickness formula and accurate film thickness measurements," *Proceedings of the Institution of Mechanical Engineers, Part J: Journal of Engineering Tribology*, vol. 223, pp. 1143–1163, dec 2009.

[120] H. van Leeuwen, "The determination of the pressure-viscosity coefficient of a lubricant through an accurate film thickness formula and accurate film thickness

measurements. Part 2: high L values," *Proceedings of the Institution of Mechanical Engineers, Part J: Journal of Engineering Tribology*, vol. 225, pp. 449–464, jun 2011.

[121] I. I. Kudish, P. Kumar, M. M. Khonsari, and S. Bair, "Scale Effects in Generalized Newtonian Elastohydrodynamic Films," *Journal of Tribology*, vol. 130, no. October, p. 041504, 2008.

[122] I. Krupka, S. Bair, P. Kumar, M. M. Khonsari, and M. Hartl, "An Experimental Validation of the Recently Discovered Scale Effect in Generalized Newtonian EHL," *Tribology Letters*, vol. 33, no. 2, pp. 127–135, 2009.

[123] J. M. Palacios, a. Cameron, and L. Arizmendi, "Film Thickness of Grease in Rolling Contacts," *A S L E Transactions*, vol. 24, no. 4, pp. 474–478, 1981.

[124] S. Z. Wen and T. N. Ying, "A Theoretical and Experimental Study of EHL Lubricated With Grease," *Journal of Tribology*, vol. 110, no. 1, p. 38, 1988.

[125] N. Fang, L. Chang, M. N. Webster, and A. Jackson, "A non-averaging method of determining the rheological properties of traction fluids," *Tribology International*, vol. 33, pp. 751–760, nov 2000.

[126] G. E. Morales-Espejel and A. W. Wemekamp, "An engineering approach on sliding friction in full-film, heavily loaded lubricated contacts," *Proceedings of the Institution of Mechanical Engineers, Part J: Journal of Engineering Tribology*, vol. 218, pp. 513–527, jan 2004.

[127] J. A. Brandão, M. Meheux, F. Ville, J. H. Seabra, and J. Castro, "Comparative overview of five gear oils in mixed and boundary film lubrication," *Tribology International*, vol. 47, pp. 50–61, mar 2012.

[128] C. M. C. G. Fernandes, P. M. Marques, R. C. Martins, and J. H. O. Seabra, "Film thickness and traction curves of wind turbine gear oils," *Tribology International*, vol. 86, pp. 1–9, 2015.

[129] H. A. Spikes and Z. Jie, "History, Origins and Prediction of Elastohydrodynamic Friction," *Tribology Letters*, vol. 56, no. 1, pp. 1–25, 2014.

[130] S. Bair, P. Vergne, P. Kumar, G. Poll, I. Krupka, M. Hartl, W. Habchi, and R. Larsson, "Comment on "History, Origins and Prediction of Elastohydrodynamic Friction" by Spikes and Jie," *Tribology Letters*, vol. 58, no. 1, 2015.

[131] H. A. Spikes and J. Zhang, "Reply to the Comment by Scott Bair, Philippe Vergne, Punit Kumar, Gerhard Poll, Ivan Krupka, Martin Hartl, Wassim Habchi, Roland Larson on "History, Origins and Prediction of Elastohydrodynamic Friction" by Spikes and Jie in Tribology Letters," *Tribology Letters*, vol. 58, no. 1, 2015.

[132] K. L. Johnson and J. L. Tevaarwerk, "Shear Behaviour of Elastohydrodynamic Oil Films," *Proceedings of the Royal Society A: Mathematical, Physical and Engineering Sciences*, vol. 356, pp. 215–236, aug 1977.

[133] W. Hirst and A. J. Moore, "Elastohydrodynamic Lubrication at High Pressures," *Proceedings of the Royal Society A: Mathematical, Physical and Engineering Sciences*, vol. 360, pp. 403–425, apr 1978.

[134] M. Björling, W. Habchi, S. Bair, R. Larsson, and P. Marklund, "Towards the true prediction of EHL friction," *Tribology International*, vol. 66, pp. 19–26, oct 2013.

[135] S. Bair and W. O. Winer, "A Rheological Model for Elastohydrodynamic Contacts Based on Primary Laboratory Data," *Journal of Lubrication Technology*, vol. 101, p. 258, jul 1979.

[136] S. Bair and W. O. Winer, "Shear Strength Measurements of Lubricants at High Pressure," *Journal of Lubrication Technology*, vol. 101, p. 251, jul 1979.

[137] M. Yamanaka, K. Kumagai, K. Inoue, and H. Hata, "Evaluation of Property Difference between Traction Oil and Traction Grease," *Journal of Advanced Mechanical Design, Systems, and Manufacturing*, vol. 3, pp. 366–377, dec 2009.

[138] N. De Laurentis, A. Kadiric, P. M. Lugt, and P. M. Cann, "The Influence of Bearing Grease Composition on Friction in Rolling/Sliding Concentrated Contacts," *Tribology International*, vol. 94, pp. 624–632, 2015.

[139] Y. P. Chiu, "An Analysis and Prediction of Lubricant Film Starvation in Rolling Contact Systems," *A S L E Transactions*, vol. 17, pp. 22–35, mar 2008.

[140] J. Pemberton and A. Cameron, "A mechanism of fluid replenishment in elastohydrodynamic contacts," *Wear*, vol. 37, pp. 185–190, apr 1976.

[141] J. Chen, H. Tanaka, and J. Sugimura, "Experimental Study of Starvation and Flow Behavior in Grease-Lubricated EHD Contact," *Tribology Online*, vol. 10, pp. 48–55, 2015.

[142] S. Aihara and D. Dowson, "A study of film thickness in grease lubricated elasto-hydrodynamic contacts," *Proc. 5th Leeds-Lyon Symposium on Tribology*, 1978.

[143] H. Åström, J. O. Östensen, and E. Höglund, "Lubricating Grease Replenishment in an Elastohydrodynamic Point Contact," *Journal of Tribology*, vol. 115, p. 501, jul 1993.

[144] J.-S. Mérieux, S. Hurley, A. A. Lubrecht, and P. M. Cann, "Shear-degradation of grease and base oil availability in starved EHL lubrication," 2000.

[145] M. T. van Zoelen, C. H. Venner, and P. M. Lugt, "The prediction of contact pressure-induced film thickness decay in starved lubricated rolling bearings," *Tribology Transactions*, vol. 53, no. 6, pp. 831–841, 2010.

[146] P. M. Lugt, S. Velickov, and J. H. Tripp, "On the Chaotic Behavior of Grease Lubrication in Rolling Bearings," *Tribology Transactions*, vol. 52, no. 5, pp. 581–590, 2009.

[147] C. Attila and M. Kozma, "Influence of the oil churning, the bearing and the tooth friction losses on the efficiency of planetary gears," *Journal of Mechanical Engineering*, vol. 56, pp. 245–252, 2010.

[148] E. C. Cabello, "Advantages of modified polyalphaolefines for gearboxes in wind power industry," in *LUBMAT*.

[149] R. Koschabek, C. Wincierz, M. Müller, M. P. Kettunen, and S. Dörr, "New Approaches to Wind Turbine Gear Oil Formulation," in *18th International Colloquium Tribology Industrial and Automotive Lubrication*, 2012.

[150] Klüber, "Special lubricants for wind turbines," *Product selection*, vol. (2014), 2014.

[151] H. Siebert and A.-P. Holm, "Protecting Gears in Wind Power Applications," *Gear Solutions*, vol. March, pp. 39–44, 2009.

[152] M. Weigand, "Lubrication of Rolling Bearings - Technical Solutions for Critical Running Conditions," *Machinery Lubrication*, 2006.

[153] P. M. Cann, "Grease lubrication of rolling element bearings — role of the grease thickener," *Lubrication Science*, vol. 19, pp. 183–196, jul 2007.

[154] V. Paleu, S. Cretu, and D. Nelias, "Friction Moment in Oil and Kerosene Mist Lubricated All-Steel and Hybrid Ball Bearings," in *16th International Colloquium Tribology*, 2008.

[155] L. Houpert, "Ball Bearing and Tapered Roller Bearing Torque: Analytical, Numerical and Experimental Results," *Tribology Transactions*, vol. 45, no. 3, pp. 345–353, 2002.

[156] T. Cousseau, B. Graça, A. Campos, and J. Seabra, "Experimental measuring procedure for the friction torque in rolling bearings," *Lubrication Science*, vol. Volume 22,, pp. 133–147, apr 2010.

[157] S. Cretu and I. Damian, "A more accurate evaluation of the frictional torque in angular contact ball bearings," in *8th International Tribology Conference*, 2003.

[158] J. Takabi and M. M. Khonsari, "Experimental testing and thermal analysis of ball bearings," *Tribology International*, vol. 60, no. 0, pp. 93–103, 2013.

[159] M. Bercea and M. Bercea, "Friction reduction in rolling bearing by using polymer additives," *Lubrication Science*, vol. 21, no. 8, pp. 321–330, 2009.

[160] S. Iqbal, F. Al-Bender, J. Croes, B. Pluymers, and W. Desmet, "Frictional power loss in solid-grease-lubricated needle roller bearing," *Lubrication Science*, vol. 25, no. 5, pp. 351–367, 2013.

[161] T. Hatazawa and T. Kawaguchi, "Frictional Torque of Needle Roller Thrust Bearings," *Tribology Transactions*, vol. 52, no. 1, pp. 127–132, 2008.

[162] M. R. D. Balan, V. C. Stamate, L. Houpert, and D. N. Olaru, "The influence of the lubricant viscosity on the rolling friction torque," *Tribology International*, vol. 72, no. 0, pp. 1–12, 2014.

[163] J. J. Blake and C. E. Truman, "Measurement of running torque of tapered roller bearings," *Proceedings of the Institution of Mechanical Engineers, Part J: Journal of Engineering Tribology*, vol. 218, no. 4, pp. 239–250, 2004.

[164] Y. Yang, S. Danyluk, and M. Hoeprich, "Rolling Element Skew in Tapered Roller Bearings," *Tribology Transactions*, vol. 43, no. 3, pp. 564–568, 2000.

[165] V. Paleu, S. Cretu, D. Dragan, and R. Balan, "Test Rig for friction torque measurement in rolling bearings," in *The Annals of University "DUNAREA DE JOS" of Galati*.

[166] R. S. Zhou and M. R. Hoeprich, "Torque of Tapered Roller Bearings," *Journal of Tribology*, vol. 113, no. 3, pp. 590–597, 1991.

[167] P. Eschmann, L. Hasbargen, K. Weigand, and E. H. Weigand, *Ball and Roller Bearings - Theory, Design, and Application*. John Wiley and Sons, 1985.

[168] N. T. N. NTN, "Rolling Bearings Handbook," pp. 5–7.

[169] NSK, "E728g," technical report cat. no. e728g.

[170] A. Palmgren, *Ball and roller bearing engineering*. SKF Industries, 1959.

[171] C. M. C. G. Fernandes, P. M. P. Amaro, R. C. Martins, and J. H. O. Seabra, "Torque loss in cylindrical roller thrust bearings lubricated with wind turbine gear oils at constant temperature," *Tribology International*, vol. 67, no. 0, pp. 72–80, 2013.

[172] C. M. C. G. Fernandes, R. C. Martins, and J. H. O. Seabra, "Friction torque of thrust ball bearings lubricated with wind turbine gear oils," *Tribology International*, vol. 58, no. 0, pp. 47–54, 2013.

[173] C. M. C. G. Fernandes, R. C. Martins, and J. H. O. Seabra, "Friction torque of cylindrical roller thrust bearings lubricated with wind turbine gear oils," *Tribology International*, vol. 59, no. 0, pp. 121–128, 2013.

[174] C. M. C. G. Fernandes, P. M. P. Amaro, R. C. Martins, and J. H. O. Seabra, "Torque loss in thrust ball bearings lubricated with wind turbine gear oils at constant temperature," *Tribology International*, vol. 66, no. 0, pp. 194–202, 2013.

[175] I. Standard, "ISO 281: Rolling bearings - dynamic load rating and rating life," 2007.

[176] G. E. Morales-Espejel, A. Gabelli, and E. Ioannides, "Micro-geometry lubrication and life ratings of rolling bearings," *Proceedings of the Institution of Mechanical Engineers, Part C: Journal of Mechanical Engineering Science*, vol. 224, no. 12, pp. 2610–2626, 2010.

[177] P. M. Cann, E. Ioannides, B. Jacobson, and A. A. Lubrecht, "The lambda ratio - a critical re-examination," *Wear*, vol. 175, no. 1–2, pp. 177–188, 1994.

[178] R. Heemskerk, "EHD lubrication in rolling bearings - review of theory and influence on fatigue life," *Stratto da Tribologia e Lubrificazione*, vol. 4, pp. 3–7, 1980.

[179] D. Dowson and G. R. Higginson, *Elasto-hydrodynamic Lubrication*. University of Michigan: Pergamon Press, si ed., 1977.

[180] I. Couronné and P. Vergne, "Rheological Behavior of Greases: Part II—Effect of Thermal Aging, Correlation with Physico-Chemical Changes," *Tribology Transactions*, vol. 43, pp. 788–794, jan 2000.

[181] D. J. Carré, R. Bauer, and P. D. Fleischauer, "Chemical Analysis of Hydrocarbon Grease from Spin Bearing Tests," *A S L E Transactions*, vol. 26, pp. 475–480, mar 2008.

[182] A. Toms, J. Powell, and J. Dixon, "The utilization of FT-IR for Army oil condition monitoring," 1998.

[183] Q. Li, H. Zhong, P. Wei, and P. Jiang, "Thermal degradation behaviors of polypropylene with novel silicon-containing intumescent flame retardant," *Journal of Applied Polymer Science*, vol. 98, no. 6, pp. 2487–2492, 2005.

[184] P. M. Cann, "Grease degradation in a bearing simulation device," *Tribology International*, vol. 39, no. 12, pp. 1698–1706, 2006.

[185] S. D. Hollis, "Antioxidants and lithium ion," 1985.

[186] C. Zimmerman, Amy, J. Deppa, Debra, A. O'toole, Deborah, and R. Mayne, James, "Topical skin compositions, their preparation and their use," aug 2002.

[187] N. Canter, "Grease additives: important contributors not to be overlooked," *Society of Tribologists and Lubrication Engineers*, vol. Tribology, no. 68.12, pp. 28–32,34–38.

[188] S. Naidu, E. Klaus, and J. Duda, "Kinetic Model for High-Temperature Oxidation of Lubricants," *Industrial & Engineering Chemistry Product Research and Development*, vol. 25, pp. 596–603, dec 1986.

[189] M. Doi and S. F. Edwards, *The Theory of Polymer Dynamics*. Clarendon Press, 1988.